

FEASIBILITY STUDY
30 WATTS PER POUND
ROLLUP SOLAR ARRAY

Quarterly Report
Contract No. 951971

REPORT NO. 40067-1 10 NOVEMBER 1967

RYAN
■■■■

FACILITY FORM 602

N68-12939	
(ACCESSION NUMBER)	(THR)
339	1
(PAGES)	(CODE)
CR-91445	03
(NASA CR OR TMX OR AD NUMBER)	(CATEGORY)

FEASIBILITY STUDY
30 WATTS PER POUND
ROLLUP SOLAR ARRAY

Quarterly Report
Contract No. 951971

REPORT NO. 40067-1 10 NOVEMBER 1967

This work was performed for the Jet Propulsion
Laboratory, California Institute of Technology,
as sponsored by the National Aeronautics and
Space Administration under Contract NAS 7-100.

This report contains information prepared by the Ryan Aeronautical Company under JPL subcontract. Its content is not necessarily endorsed by the Jet Propulsion Laboratory, California Institute of Technology, or the National Aeronautics and Space Administration.

ABSTRACT

Work began with re-examination of the proposed solar array concept with reference to specification requirements and contract objectives. Sub-elements of the array were studied for more efficient use of material (lowest weight) versus function. Alternate designs of structural and mechanical arrangements were performed, substantiated by analysis. Solar cell layouts, materials and circuitry were selected for evaluation. Values for power per unit area and power per weight of electrical installation were developed for various solar cell designs, sizes and cover-glass use. Supporting technical analyses and studies included dynamics, thermal, stress, reliability and weights. The majority of work performed was directed to tradeoff studies. Manufacturing feasibility was investigated wherever gross size, foil gage fabrication techniques, or a unique process might present constraints. Design verification testing was performed on adhesives and film type plastics. Results of concept studies and design tradeoffs were summarized and a configuration selected for a more detailed preliminary design effort. This design is estimated to produce 31.3 watts per pound of weight, an estimate developed by conservative analysis, and allowing for design growth and contingency for normal tolerances. The concept, the materials and processes involved, are all considered to be within bounds of feasibility and state-of-the-art capability.

PRECEDING PAGE BLANK NOT FILMED.

CONTENTS

<u>SECTION</u>	<u>PAGE</u>
1.0 GLOSSARY	1
2.0 INTRODUCTION	3
3.0 TECHNICAL DISCUSSION	5
3.1 Applicable Documents	5
3.2 Fabrication Feasibility	5
3.2.1 Investigation of Array Structure	5
3.2.2 Investigation of Mechanisms	11
3.2.3 Investigation of Electrical Designs	13
3.2.4 Investigation of Materials and Processes	21
3.2.5 Manufacturing Restraints	27
3.3 Preliminary Design and Analysis	29
3.3.1 Design Criteria	29
3.3.2 Studies and Analyses	30
3.3.2.1 Panel Aspect Ratio Studies	30
3.3.2.2 Substrate Attachment	33
3.3.2.3 Deployment Beam Studies	45
3.3.2.4 Beam Tip Intercoastal Studies	59
3.3.2.5 Wrap Drum Studies	74
3.3.2.6 Effects of Dynamics of Space- craft Mount on Design	81
3.3.2.7 Torque Tube Studies	88
3.3.2.8 Wrapped Substrate Layer Separation Medium Studies	90
3.3.2.9 Thermal Studies	100
3.3.2.10 Solar Cell Installation Studies	115
3.3.2.11 Weight Analysis	132
3.3.2.12 Reliability Considerations	142
3.3.2.13 Handling Provisions & Ground Support Equipment	152

CONTENTS (Continued)

<u>SECTION</u>	<u>PAGE</u>
3.3.3 Test Data	154
3.3.3.1 Adhesive Evaluations — Environmental	154
3.3.3.2 Peel Strength of Cell Bonding Adhesives	157
3.3.3.3 Screening Tests on Kapton Bonding	158
3.3.3.4 Substrate Attachment Pull Test	163
3.3.3.5 Solar Cell Interconnection Test	176
3.3.3.6 Test Procedures — Solar Cell Installation	179
3.3.3.7 Design Development Tests	181
4.0 CONCLUSIONS	185
4.1 Array Structure and Mechanisms	189
4.2 Solar Cell Array and Power Transmission System	191
4.3 Array Sequence of Operation	194
5.0 RECOMMENDATIONS	197
6.0 NEW TECHNOLOGY	199
7.0 REFERENCES	201
8.0 APPENDIX DATA	205
8.1 Dynamic Considerations of Proposed Spacecraft Mount	205
8.2 Dynamic Considerations of Redesigned Spacecraft Mount	217
8.2.1 Titanium Box Structure	217
8.2.2 Aluminum Box Structure	224
8.3 Dynamic Considerations of Beam Guide Mount	227
8.4 Considerations in Using Torque Tube as Drum Support	239
8.4.1 No Torque Tube Snubber at Center	239
8.4.2 With Center Snubber	247
8.4.3 Conclusions	250

CONTENTS (Continued)

<u>SECTION</u>	<u>PAGE</u>
8.5 Drum End-On Solar Flux Considerations	251
8.6 Performance of Very Thin Silicon Solar Cells	271
8.7 Fracture of Solar Cells	293
8.8 Log Sheets - Thermal Vacuum Test	296
8.9 Drawings	300

PRECEDING PAGE BLANK NOT FILMED.

LIST OF FIGURES

<u>FIGURE</u>		<u>PAGE</u>
1	Drum/Beam Mounting Concepts	6
2	Array-to-Vehicle Attachment Concepts	8
3	Wrap Drum Concepts	10
4	Beam Deployment Mechanism Concepts	12
5	Motor Drive Concepts	14
6	Typical Solaflex [®] Interconnections for 2 x 2 cm Bar Contact, Solar Cells	16
7	Typical Solaflex [®] Interconnections	17
8	Typical Dart Contact Solar Cell and Interconnect Arrangement	18
9	Electrical Transmission - Solar Cells to Wrap-Drum Connectors	20
10	Wrap Drum Length Considerations	31
11	Aspect Ratio as Related to Influential Weight Variables and to Power/Weight Objectives	34
12	Schematic Thermal Model of Deployable Solar Array Support Beam	51
13	Thermal Distortion Versus Weight for Various Beams	58
14	Wrap-Drum Optimization	80
15	Effect of Increased Spacecraft Mount Cross-Section	84
16	Drum Snubber at Center of Drum Length	87
17	Typical Static Stress-Strain Curve for Flexible Polyurethane Cushion at Room Temperature	93
18	Polyurethane Weight vs. Frequency	97
19	Silicone Weight vs. Frequency	97
20	Thermal Model Section - Outer Solar Cell Wrap	101
21	Thermal Model Section - Inner Solar Cell Wrap	102
22	Isothermal Nodes - Outer Cell Wrap	103
23	Nodal Temperatures - Inner Solar Cell Wrap	105
24	Nodal Temperatures - Outer Solar Cell Wrap	106
25	Power Output per Cell Thickness (Watts/Ft. ²) 2 x 2 cm Corner Dart Contact	118
26	Power Output per Cell Thickness Watts/Ft. ²) 2 x cm Bar Contact	119
27	Weight/Area vs. Cell Thickness, 2 x 2 cm, Corner Dart Contact, Various Coverglass Thicknesses and Systems	122

LIST OF FIGURES (Continued)

<u>FIGURE</u>		<u>PAGE</u>
28	Specific Power Output per Cell Thickness, 2 ohm cm, Dart Contact Cell	123
29	Specific Power Output per Cell Thickness, 2 ohm cm, Bar Contact Cell	124
30	Specific Power Output per Cell Thickness, 2 ohm cm, Bar Contact, 2 x 6 cm Cell	125
31	Spectrolab Drawing SK-0007	127
32	Power/Weight Monitor	141
33	Test Results of Substrate Attachment	165
34	Drum Assembly - Vibration Test, Model 400	183
A-1	End-On Solar Flux Consideration, Hot End Nodal Points	252
A-2	End-On Solar Flux Considerations, Hot End of Drum and Support, Nodal Points	253
A-3	End-On Solar Flux Considerations, Cold End Nodal Points	254
A-4	End-On Solar Flux Considerations, Cold End of Drum and Support, Nodal Points	255
A-5	Solar Cells and Fracture Characteristics	295
A-6	Roll-Up Assembly - 250 Square Foot (Sheet 1 of 2)	301
A-6	Roll-Up Assembly - 250 Square Foot (Sheet 2 of 2)	303
A-7	Model 400 - Drum/Beam Mounting, Fixed Drum and Pivoting Guide, Concept 1a.	305
A-8	Model 400 - Drum/Beam Mounting, Floating Drum and Fixed Guides, Concept 1b.	307
A-9	Model 400 - Mounting to Vehicle, Tubular Mounting, Concept 2a.	309
A-10	Model 400 - Mounting to Vehicle, Box Mounting, Concept 2c.	311
A-11	Model 400 - Mounting to Vehicle, Mounting with Shock Mounts, Concept 2d.	313
A-12	Model 400 - Beam Design, Concept 4	315
A-13	Model 400 - Drum Assembly, Concept 5	317
A-14	Model 400 - Mechanical Drive System, Concept 6.	319
A-15	Model 400 - Electrical Lead-Out, Coiled Continuous Harness, Concept 7a.	321
A-16	Model 400 - Electrical Lead-Out, External Disc Slip Rings, Concept 7b.	322
A-17	Model 400 - Electrical Lead-Out, Internal Sleeve Slip Rings, Concept 7c.	323
A-18	Model 400 - Motor Drive, Single Gear Motor, Concept 8a.	325
A-19	Model 400 - Motor Drive, Double Gear Motor, Concept 8b.	327

LIST OF TABLES

<u>TABLE</u>	<u>PAGE</u>
1 Computed Titanium Beam Temperatures and Gradients	52
2 Computed Fiberglass Beam Temperatures and Gradients	53
3 Computed Beryllium-Copper Beam Temperatures and Gradients	54
4 Beam Surface Characteristics	55
5 Properties of Beam Materials	55
6 Materials and Their Properties Considered in Thermal Analysis	104
7 Drum Support and Guide Sleeve Mount Assembly	133
8 Beam Guide Sleeves	134
9 Wrap Drum Assembly	135
10 Spacecraft Mount Assembly	136
11 Substrate Installation Weight	137
12 Deployment/Retraction System	138
13 Weight Summary	139
14 Splicing Adhesives	159
15 Cell Bonding Adhesives	159
16 Peel Test Data — 0.001 Inch Kapton to Aluminum	160
17 Peel Test Data — 0.001 Inch Kapton to Solar Cells	161
18 Lap Shear Test Data Kapton to Kapton — 0.001 Inch Thick	161
19 Lap Shear Test Data Kapton to Kapton — 0.005 Inch Thick	161
20 Peel Data — 0.001 Inch Kapton to 0.005 Inch Kapton	162
21 Trade Study Summary	187

1.0 GLOSSARY

AMO	Air Mass Zero
AR	Anti-Reflective
AU	Astronomical Unit
GSE	Ground Support Equipment
I-V	Current-Voltage
RFQ	Request For Quotation
UV	Ultra-Violet



PRECEDING PAGE BLANK NOT FILMED.

2.0 INTRODUCTION

This, the first Quarterly Report, is submitted by the Ryan Aeronautical Company to the Jet Propulsion Laboratory in accordance with Article I, item (a)(2)(iv) and Article II, item (a)(5) of Contract No. 951971. The report presents a summary of work accomplished from date of contract through 31 October 1967. The reporting period was extended from 30 September 1967 in order to conclude design trade-off studies and report the additional data. The request was made when it was apparent that the extension would allow inclusion of the results of the studies.

The discussion presented herein is a composite report of work performed by Ryan and its associate contractor, Spectrolab Division of Textron Electronics, Inc. It deals principally with preliminary design investigations, engineering trade-offs and manufacturing considerations.

From these studies a configuration has been selected for the follow-on task of performing a preliminary engineering design of the solar array assembly.



3.0 TECHNICAL DISCUSSION

3.1 APPLICABLE DOCUMENTS

System Specification No. SS501407, Rev. A, dated 4 January 1967, titled: ROLL UP SOLAR CELL ARRAY, 30 WATTS PER POUND, DETAIL REQUIREMENTS FOR.

Contract No. 951971, dated 26 June 1967, California Institute of Technology, Jet Propulsion Laboratory, for FEASIBILITY STUDY, 30 WATTS PER POUND, ROLL UP SOLAR ARRAY.

3.2 FABRICATION FEASIBILITY

While preparing Ryan's response to its pre-contract Request For Proposal, several design concepts were studied which suggested good feasibility of meeting specified program objectives. From these studies a configuration was selected and proposed that is very similar in concept to the Ryan design for a 50 square foot roll-up solar array (Reference 1) which is currently undergoing physical and environmental testing.

All developments and technical progress to date on the 30 watt/pound concept tend to corroborate the selection. Consequently the discussion which follows concerns itself with detail investigations of subelements of the selected concept and with descriptions of the various structural, mechanical and electrical design approaches which were studied.

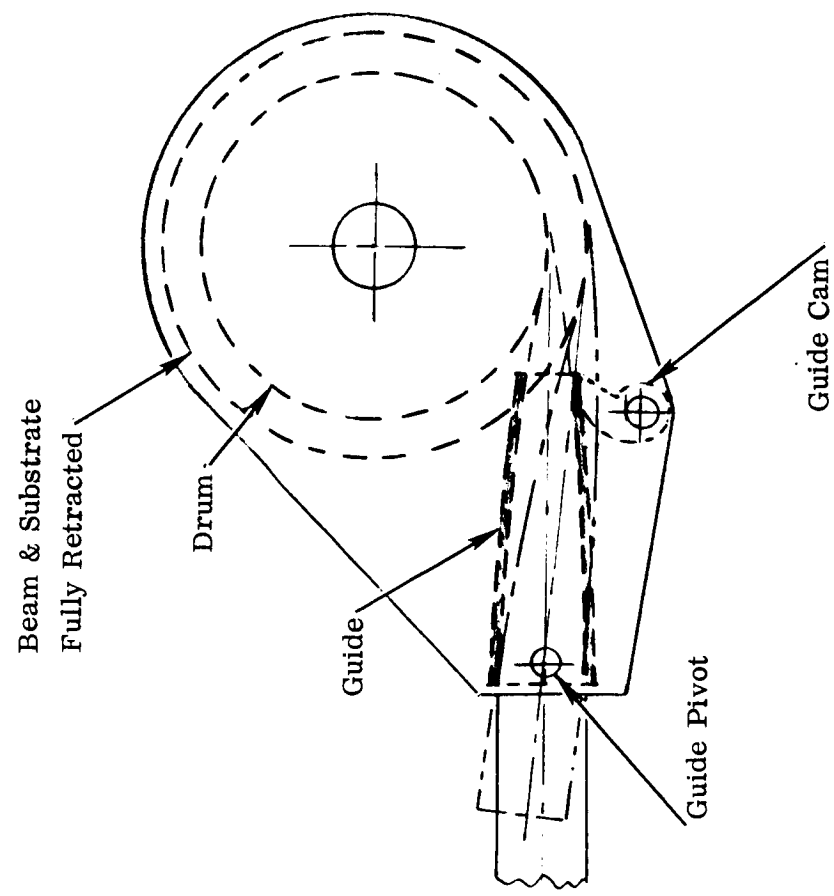
3.2.1 Investigation of Array Structure

3.2.1.1 Drum/Beam Mounting

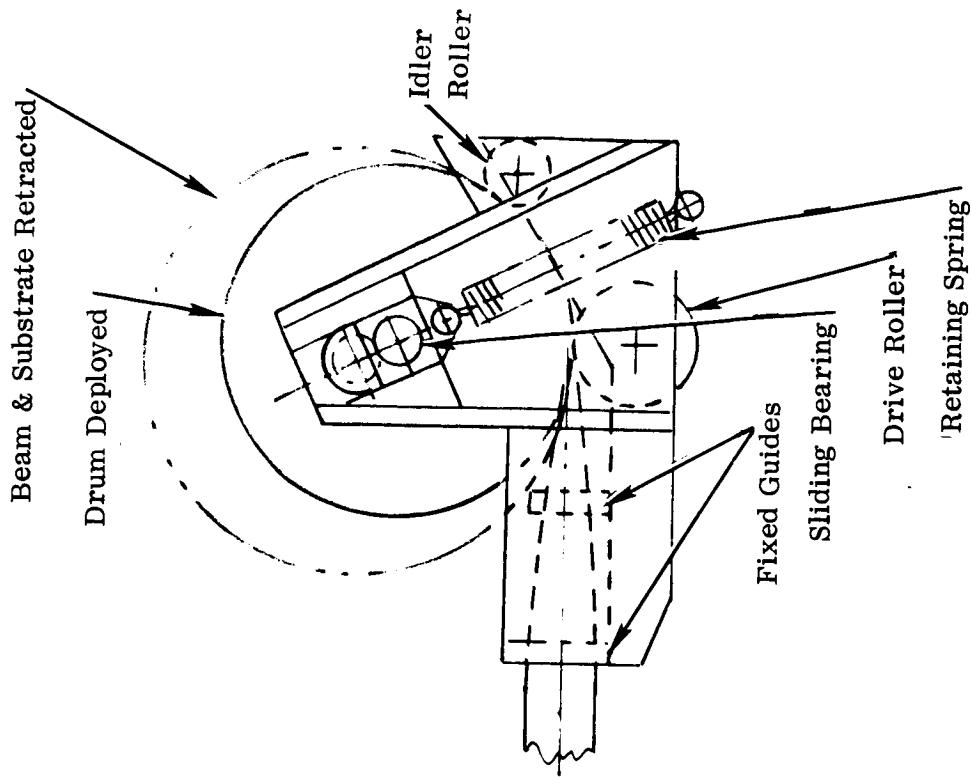
Studies included basic concepts for the mechanical compensation arrangement necessary to adjust for a diameter change in the wrapped substrate during deployment or retraction, (See Figure 1) as follows:

1. A fixed drum with a pivoting guide. This system was used on the JPL model 208¹. The beam guide is pivoted at its forward end and driven by a cam mechanism at the rear in such a manner that it follows the increasing or decreasing diameter of the drum.

Note: Superscript numbers apply to Section 7.0, References.



FIXED DRUM & PIVOTING GUIDE



FLOATING DRUM & FIXED GUIDES

Figure 1. Drum/Beam Mounting Concepts

2. Floating drum and fixed guides. In this scheme the drum rests on fixed drive and idler rollers. The drum center bearings work in slides on the fixed support structure. Heavy tension springs keep the drum in contact with the rollers. As the drum substrate increases or decreases in diameter the drum center rises or falls in the slide.

In the fully wrapped configuration, stops are provided to prevent dynamic loads being transmitted through the tension springs or through the wrapped beam via the rollers.

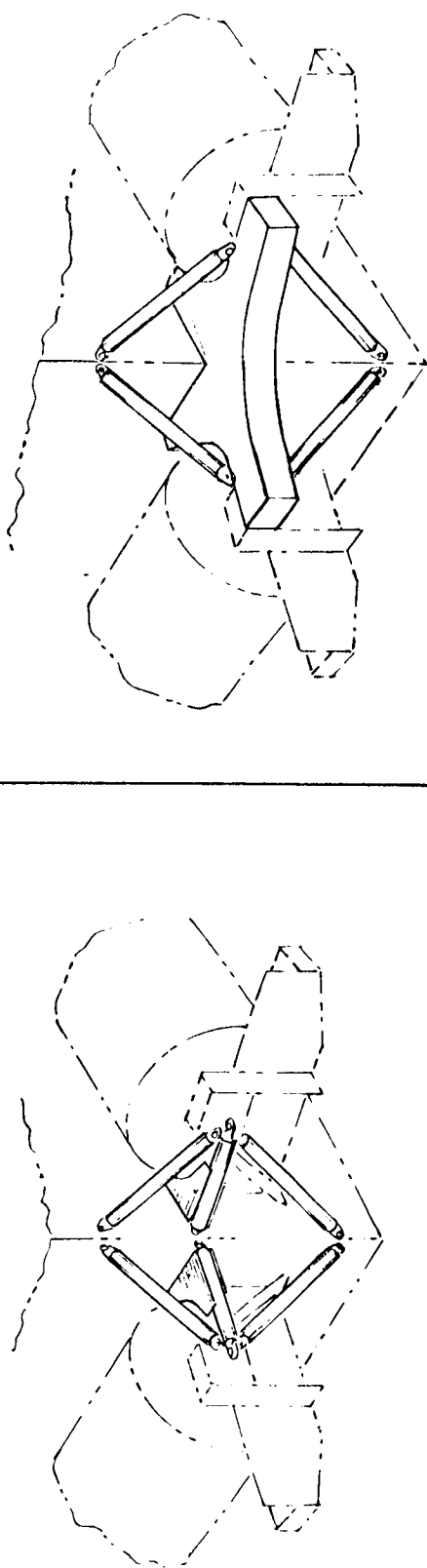
3.2.1.2 Array-to-Vehicle Attachment

Four schemes were investigated for the type of structure that would mount upon the spacecraft and support the array assembly, (See Figure 2):

- a. A tubular mounting arrangement representing a truss made up of tubes that are pin-jointed at intersections.
- b. An X-frame design for an array with edge beams on 90.0-inch centers. It consists of an aluminum box structure in the form of an "X" which provides a common mounting for the end of one roll-up unit and the opposite end of the adjacent unit. The structure is braced by tube struts for loads in the vertical plane.
- c. A box-mount arrangement for an array with edge beams on 82.0-inch centers. The structure mounts to the corner of the spacecraft and provides a common support for two roll-up units similar to the X-frame design. It also uses tubular braces to react vertical loads.
- d. A support structure with resilient-type shock mounts. This support method is also a structural box which attaches to the corner of the spacecraft utilizing shock mounts between the box member and the roll-up unit. This scheme was the only concept investigated involving application of a mechanical dampener device.

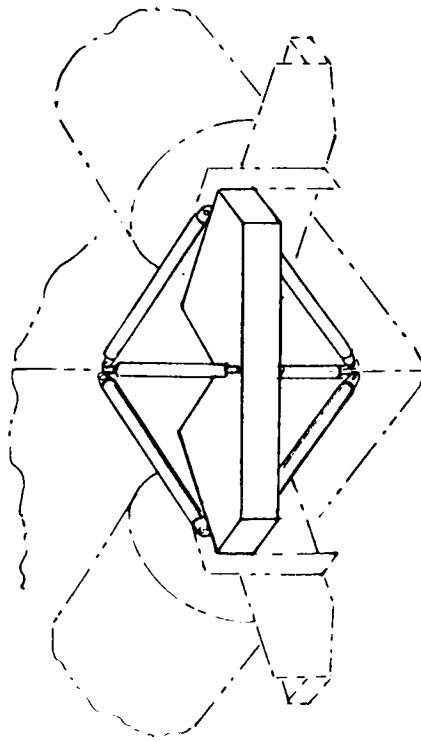
3.2.1.3 Substrate

Substrate studies have concentrated on investigation of three candidate materials; that is, a thin fiberglass laminate and two thin film materials,

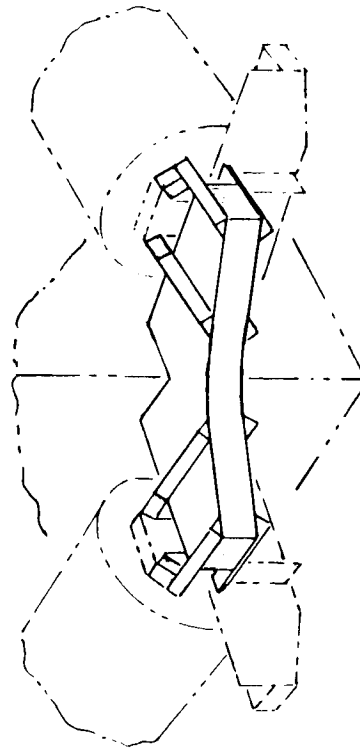


a. Tubular Mounting

b. "X" Form Mounting



c. Box Mounting



d. Shock Mounts

Figure 2. Array-to-Vehicle Attachment Concepts

Mylar and Kapton. Various materials and installation arrangements were studied that would act as interlayer dampeners when the rolled up substrate is subjected to launch accelerations and other dynamic inputs and steady state loads that occur in the boost phase. The results of materials studies are discussed in detail in Paragraph 3.2.4. Applied loads and stress analyses are discussed in Paragraph 3.3.2.

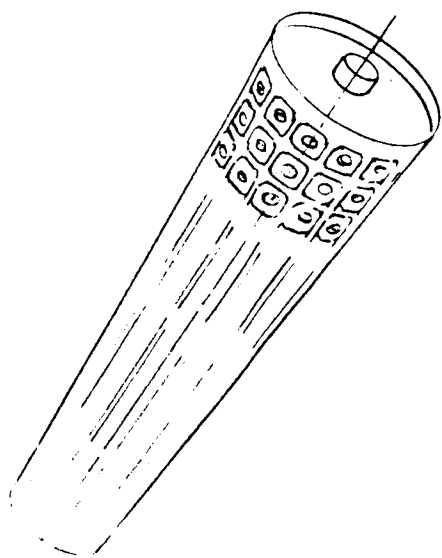
3.2.1.4 Extendible Beam

The extendible beam configuration for deploying and supporting an array of solar cells is similar in concept to the beam arrangement on the 50-square-foot rollout array.¹ Three types of materials were investigated; i.e., titanium, beryllium-copper, and stainless steel. Beam design studies considered that diameter and material thickness were the same regardless of material for each case that was analyzed. It is interesting to note that in the final analysis, diameter and material thickness selections were fixed on the basis of manufacturing feasibility minimums and handling characteristics.

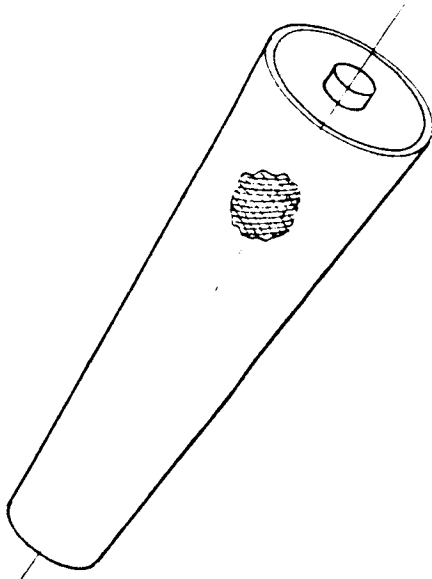
3.2.1.5 Wrap Drum

A wrap drum diameter of 12 inches was adopted on the basis of packaging and dynamic characteristics. Using this diameter as a standard base line four concepts of manufacturing the drum assembly were investigated (See Figure 3):

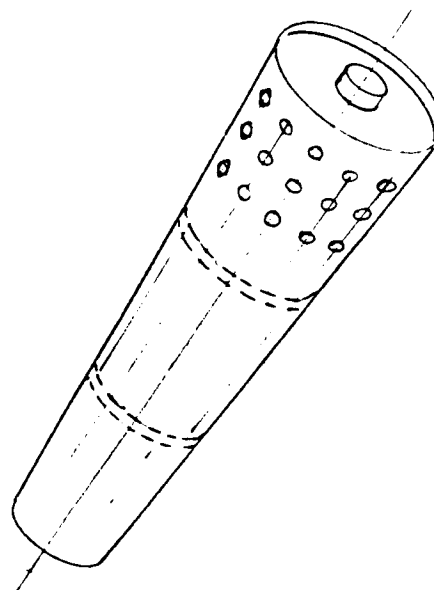
- a. A wrap drum made from magnesium, the cylindrical shell pierced with lightening holes and pocketed by chemical milling to reduce weight
- b. A wrap drum made from honeycomb reinforced skins, a composite of aluminum core and fiberglass facing skins; without any internal stiffening of the drum shell
- c. A wrap drum made from beryllium, the cylindrical shell pierced with lightening holes (unflanged edges) and stiffened with internal members
- d. A wrap drum made from magnesium, the cylindrical shell pierced with flanged lightening holes, and stiffened with internal rings



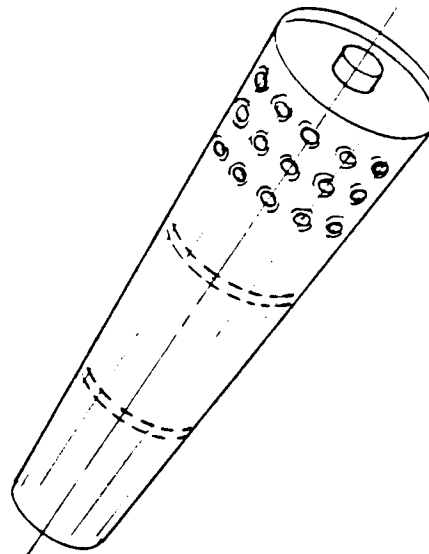
a. Chem Milled Magnesium Skin



b. Aluminum Honeycomb Fiberglass Skins



c. Beryllium Skin & Stiffeners



d. Magnesium Skin With Flanged Lightness Holes

Figure 3. Wrap Drum Concepts

3.2.2 Investigation of Mechanisms

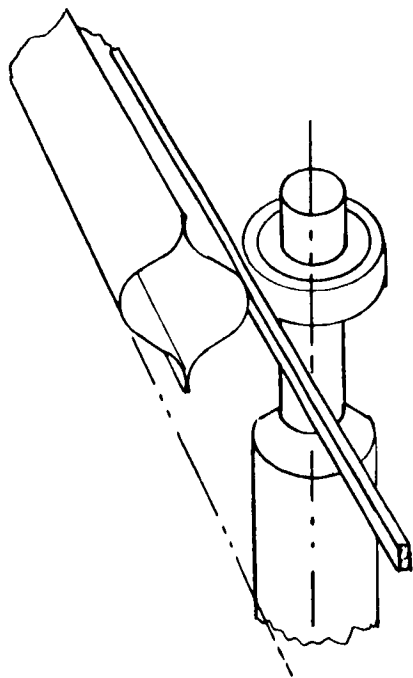
3.2.2.1 Mechanical Drive System

The mechanical drive system consists of the devices by which the beams and substrate assembly are deployed or wound onto the drum, and the method by which the movement of one beam is synchronized with the movement of the other. The simplest and lightest method of synchronizing beam movements was found to be a torque tube extending from one end of the unit to the other.

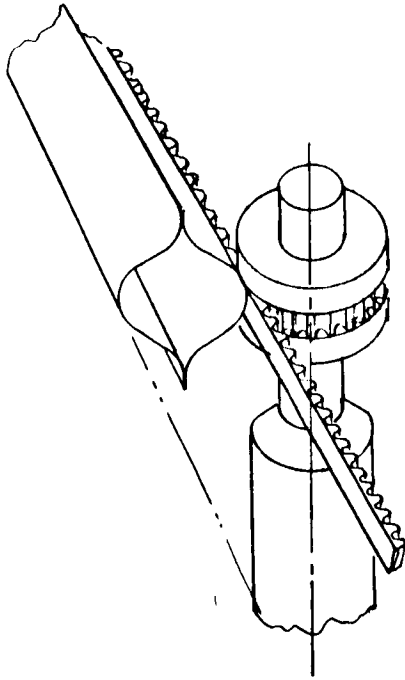
A drum tensioning system employs an elastic belt drive to a pulley on the drum center, working through a slip clutch, and a one-way drive clutch that maintains tension on the substrate during retraction. This concept supercedes the separate tensioning motor described in the pre-contract proposal.

Four designs for the beam deployment system were investigated (Figure 4) as follows:

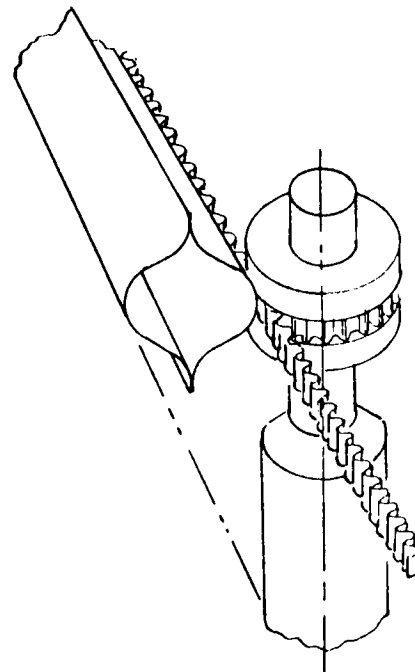
1. A friction drive whereby a silicone rubber-faced drive wheel engages a rubber strip on the center of the beam.
2. A toothed rack on the beam. This design is a rack and pinion type drive; the rack being a silicone rubber strip with a gear tooth form bonded to the center of the beam. The rubber strip also acts as the beam spacer required to compensate for the difference in combined substrate and damper pad thickness and the flattened beam. A mating pinion with a matching tooth form engages the rubber strip and drives the beams. An alternate arrangement would be to have the toothed strip formed or cut from polyurethane plastic.
3. Toothed rack on beam (formed titanium strip). This design is basically the same as the preceding approach except the silicone-toothed strip is replaced by a tooth form titanium strip, spot welded to the centers of the beams.
4. Sprocket drive. A toothed sprocket wheel would engage matching holes punched in the extendible beams.



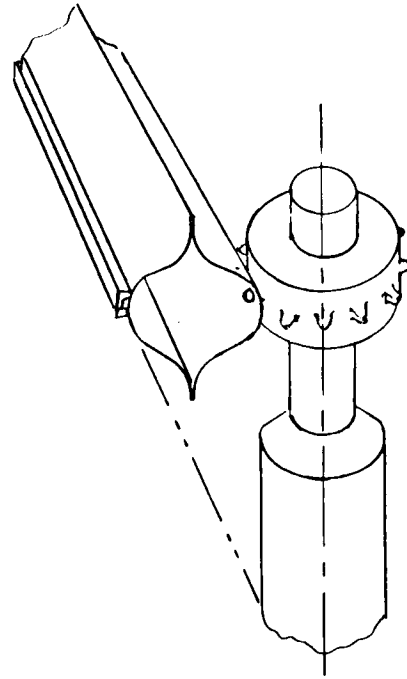
a. Silicone To Silicone Friction Drive



b. Formed Silicone or Polyurethane Rack on Beam



c. Toothed Rack - Formed Titanium Strip



d. Toothed Sprocket, Matching Holes in Beam

Figure 4. Beam Deployment Mechanism Concepts

3.2.2.2 Motor Drive

The motor drive is the arrangement by which the array is deployed or retracted. Two design concepts were investigated, as shown in Figure 5.

- a. Single gear motor drive. This method consists of a single gear motor driving the end of the drive shaft. The rollup array is locked in a precise position when the motor is stopped because of the high gear reduction ratio.
- b. Double gear motor (redundant drive). This method would provide two gear motors coupled into a small differential gear box, the output end of the differential being attached to the array drive shaft. In normal operation both motors would drive through the differential to provide power to the drive system. Failure of any one motor will reduce the speed of operation to half of normal speed. With both motors stopped the array is locked as positioned by the power-off command.

3.2.2.3 Limit Switch-Motor Drive

The limit switch controls the power to the motor drive and stops power when the array has reached either deployment or retraction position. It incorporates a microswitch unit operating on a rotary tumbler-type action. The tumblers actuate microswitches after a given number of revolutions and are adjustable over a broad range.

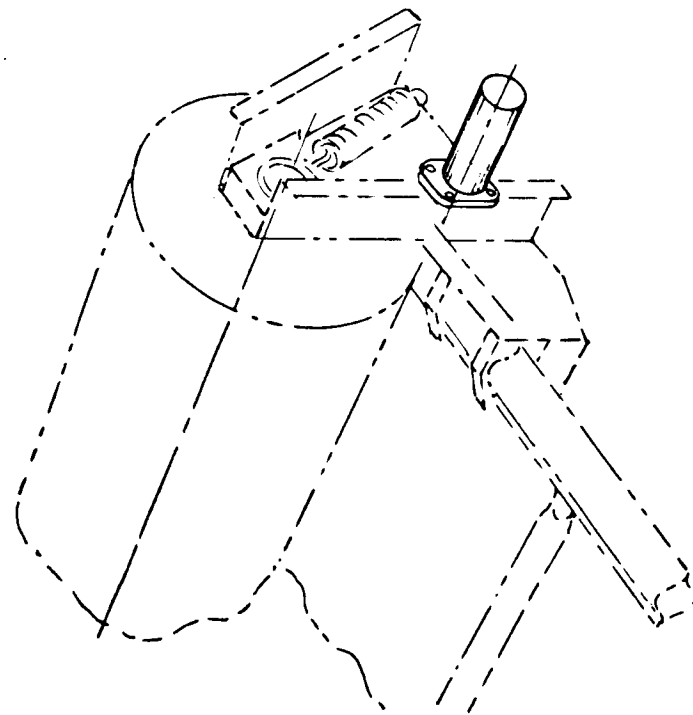
The unit is mounted in an accessible position on the array assembly and is positively driven by a miniature cog belt from the drive shaft.

3.2.3 Investigation of Electrical Designs

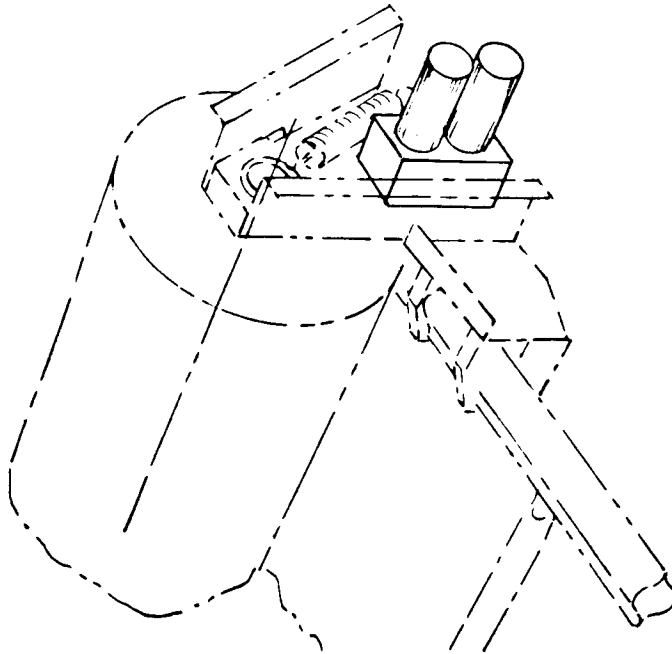
3.2.3.1 Solar Cell Layout

Various solar cell layouts (i. e. , module sizes, arrangements, and circuitry) were studied to determine the most satisfactory design. Many considerations entered in to the evaluations which are discussed in detail in Section 3.3 Preliminary Design and Analysis. Prime attention was given to (1) cell layout per available area, (2) circuit-module designs, (3) interconnect configurations and (4) general suitability of the solar cell installation for thin film, flexible substrate.

Layouts were investigated using the conventional 2x2 CM cells or the newer, large area, 2x6 CM cells. Use of 2x6 CM cells portend



SINGLE GEARMOTOR DRIVE



DOUBLE GEARMOTOR & DIFFERENTIAL GEARBOX
(Redundant Drive)

Figure 5. Motor Drive Concepts

attractive gains in electrical output and also results in more efficient use of available substrate area.

Interconnect concepts and solar cell contact designs were objects of intensive study. Examples of typical arrangements are illustrated in Figures 6, 7 and 8.

Probable arrangement of the best solar cell installation is shown in Spectrolab drawing number SK-0007. (See Figure 31.)

3.2.3.2 Coverslides

In view of the nonspecified radiation environment, it has been assumed that no unusual radiation spectrum is anticipated. With this assumption, the best coverslides, in terms of overall cell output, cost and handling would be microsheet with an AR coating. The initial higher output of this configuration, when corrected for expected UV radiation degradation, will then produce a higher output after maximum radiation damage than samples with selective blue filters.

3.2.3.3 Solar Cells

Solar Cell designs and electrical characteristics that are applicable to the subject contract are elaborated upon in Paragraph 8.6, and report entitled, "Performance of Very Thin Silicon Solar Cells". There will be repeated reference to this data in subsequent analytical discussion regarding the solar cell installation.

3.2.3.4 Conductor Leads

Study was devoted to various material composites and manufacturing techniques for conductor leads which would be used to collect series-connected cells into parallel circuitry (transversely across the array) and connect with flexible longitudinal leads bringing collected power into the inboard end of the array. Conductor designs were considered which would be made from plastic shielded wire and/or ribbon, conductive metal foil, a bimetallic composite or plated base metal. Redundancy is assured in the array by providing primary power transmission bus bars along both longitudinal edges of the array and connecting transverse module leads to both sides.

No connectors in the cell layout are planned for the array configuration. The two longitudinal transmission bus bars will be terminated on terminal boards incorporated on the inboard end of the deployable substrate assembly.

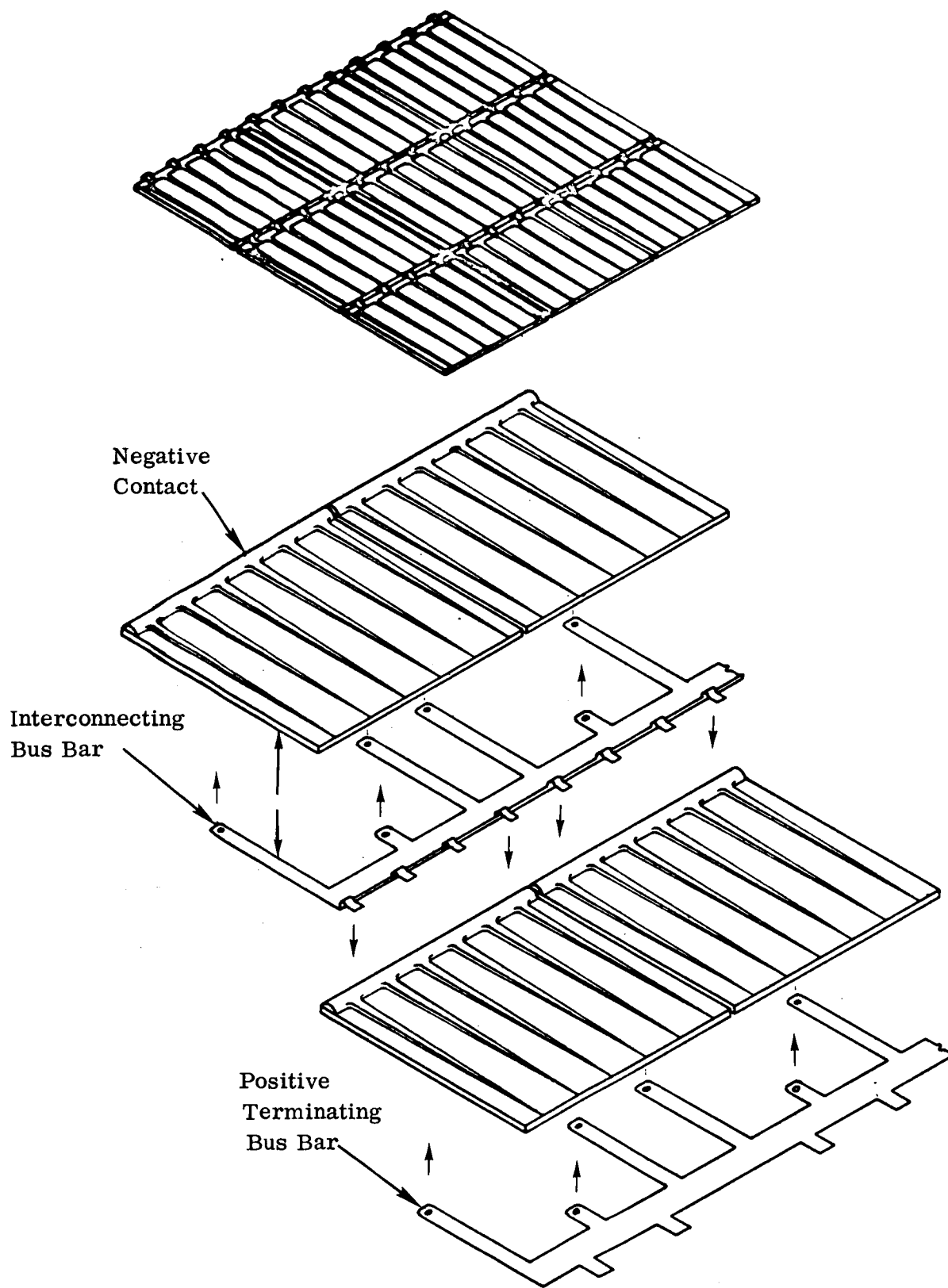


Figure 6. Typical Solaflex[®] Interconnections for 2 x 2 cm Bar Contact, Solar Cells

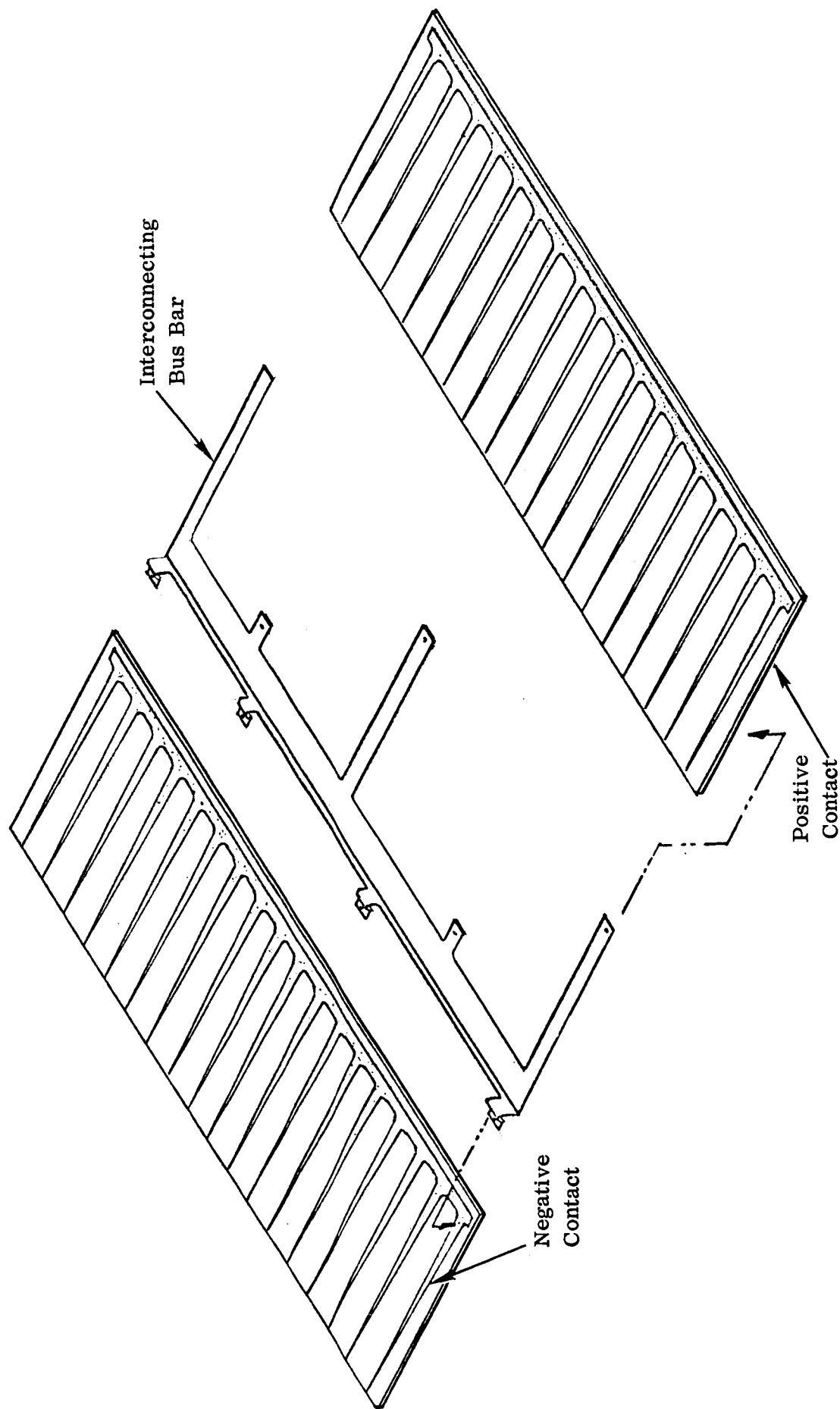


Figure 7. Typical Solaflex[®] Interconnections

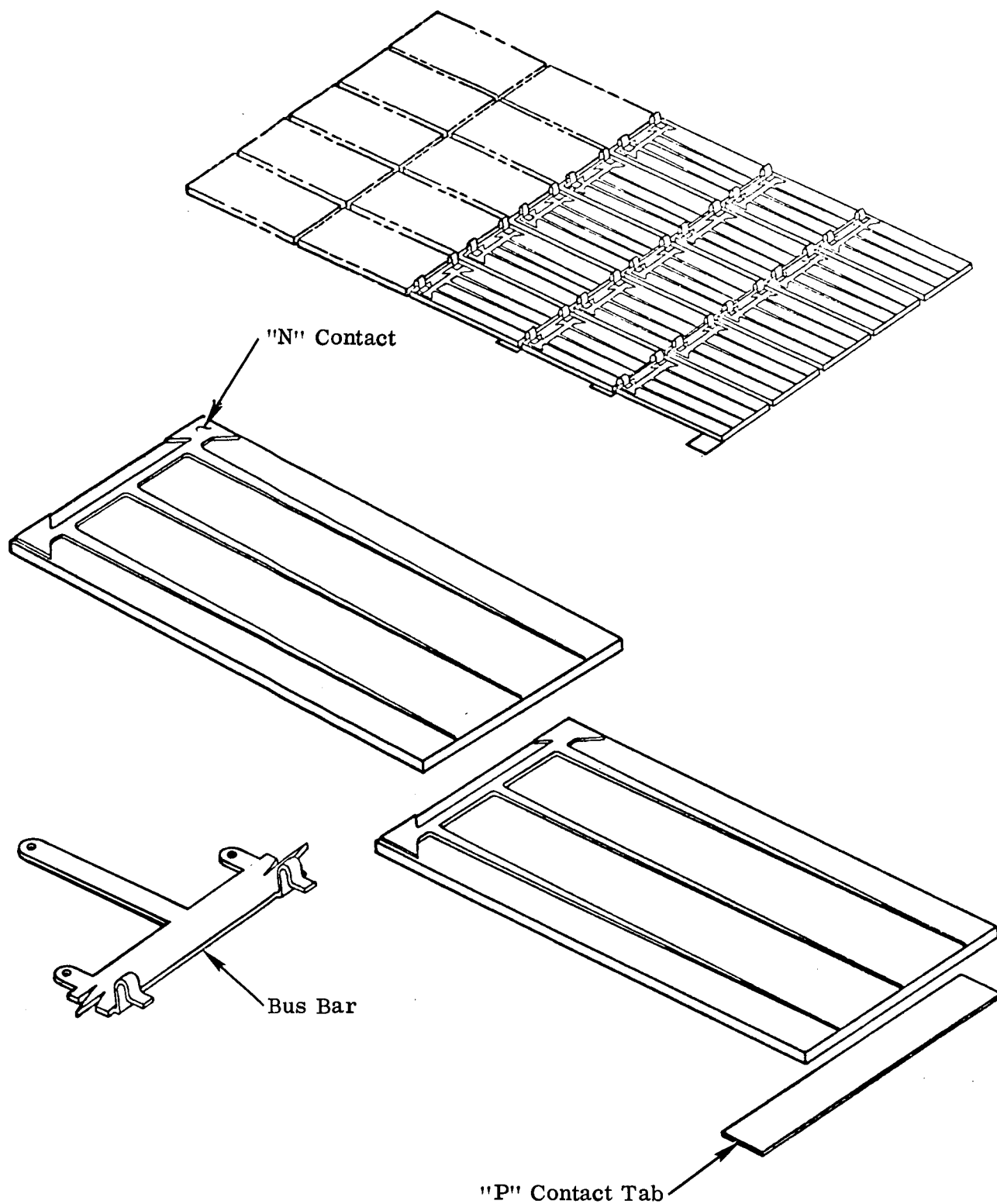


Figure 8. Typical Dart Contact Solar Cell and Interconnect Arrangement

3.2.3.5 Solar Cell-Substrate Interface

Mylar, Kapton H, and Kapton HF (Kapton H with Teflon) were considered in Spectrolab investigations. Initially, bonding difficulty was encountered with Kapton H. However, this was satisfactorily remedied through an adhesive testing program with chromic acid etching of the Kapton. The Kapton HF has a disadvantage of greater weight than Kapton H without any advantages. The Mylar proved unsuitable because of its extremely fragile characteristics. In view of the flexibility necessary for the array substrate this would make the Mylar impractical.

The 1.5-mil fiberglass exhibited a rather poor resistance to point impact and would fracture at the impact point. Radial fracture lines would be generated which were prone to fracture during handling. Bondability was excellent, and consequently this material should be retained for further review from the standpoint of solar cell installation.

3.2.3.6 Diodes

Requirements for blocking diodes were studied but there appears to be no foundation for their use. Chief reasons for not using diodes are:

- The substrate is a nonconductive material and not subject to the short circuit hazards associated with use of metallic, rigid substrate.
- The fact that shadow effects are assumed to approach a complete eclipse of the array rather than local, concentrated area shadows.

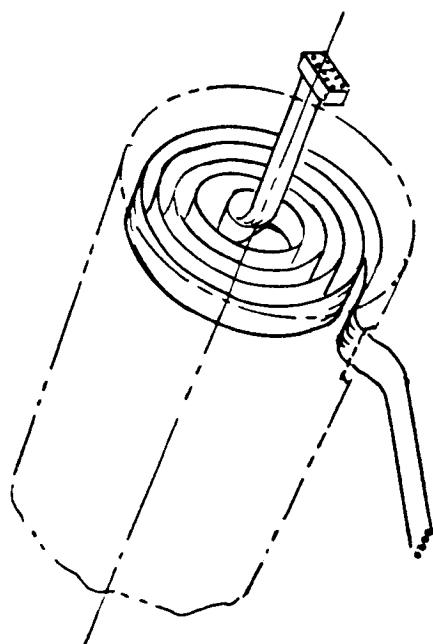
Further discussion is presented in Paragraph 3.3.2.10.5.

3.2.3.7 Electrical Transmission-Array to Vehicle

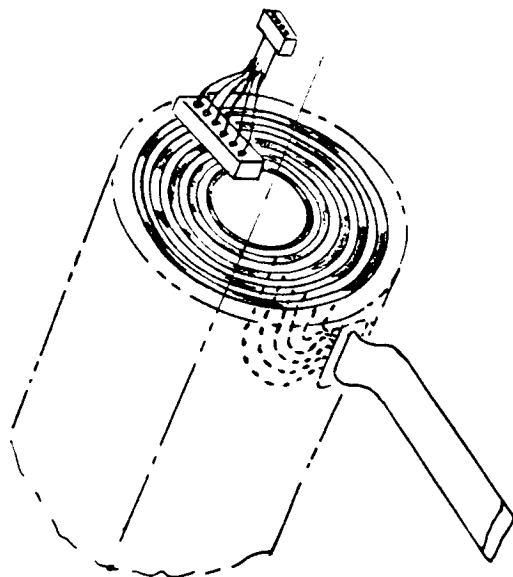
This system transmits current generated by the solar cells from the deployed array to the spacecraft electrical system. The design must accept rotation of the wrap drum and consequently the harness and/or rotating conductor must be compatible with wrap drum operation.

Three designs were investigated, (see Figure 9):

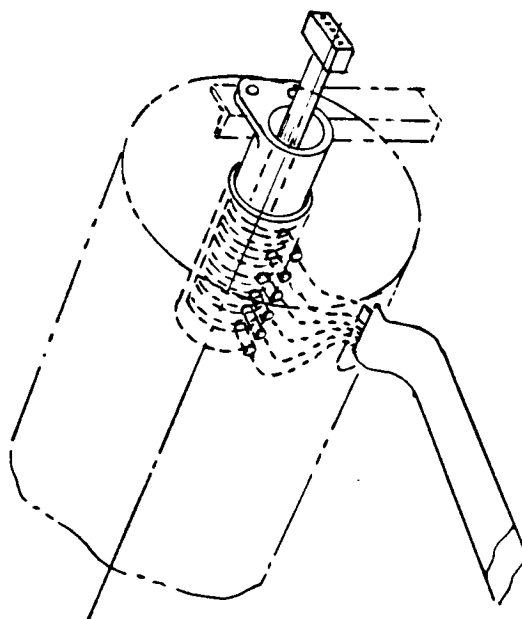
- A continuous coiled harness. This configuration is similar to the concept used on the 50-square-foot array¹. The continuous coil is formed so that during retraction the coil winds up and will unwind on deployment.



a. Continuous Coiled Harness



b. External Disc Slip Rings



c. Internal Sleeve Slip Rings

Figure 9. Electrical Transmission - Solar Cells to Wrap-Drum Connectors

- External disc slip rings. Several conductor discs are separated by insulating strips and fixed to the end of the drum so that they rotate with the drum. Spring loaded, stationary pickup brushes mount to the array support structure and conduct current from the drum.
- Internal slip rings. This method uses a series of slip rings and pickup brushes within the rotating shaft of the drum. The contacts are a series of rings inside the shaft that rotate with the drum. The pickup brushes are stationary, being fixed to outside structure and are inserted inside the rotating shaft.

3.2.4 Investigation of Materials and Processes

Introduction

The evaluation of materials to be used in the deployable solar array panel has been based on functional and environmental requirements specified in Section 3.0 of JPL Specification SS501407A. In approaching this particular design, materials evaluations need consider not only functional requirements and flight environments but also methods of fabrication, assembly, and ground handling.

The program objectives require that weight of structural components be held to a minimum level. In many cases, the lower limit of design weight is determined by feasibility of processing and handling rather than by design load requirements. For this reason, special attention in the trade-off study has been given to, (1) fabrication feasibility, (2) minimum practical gauges and (3) densities of materials that were considered.

There are many suitable materials available for use in the specified space environment. Several candidate materials have been evaluated for each component of the design. Evaluations were based on data in the literature, manufacturers' data, and prior work conducted in the 50-square-foot rollup solar array program (Reference 1). Where necessary, special tests were conducted to obtain materials properties information.

Beam

Materials considered for the support beams include titanium, beryllium-copper, stainless steel and glass fiber reinforced plastic. Each of these candidate materials can be fabricated successfully into the beam configuration to meet functional and environmental requirements. Selection of metallic materials must be limited to nonmagnetic metals with high yield

strength in order to satisfy functional requirements. The metals present no radiation damage problems; Reference 2. The selection of reinforced plastic composite is more critical. Radiation resistance is dependent on the resin system used with phenolic and epoxy systems which are preferred for maximum resistance (Reference 2). Also temperature resistance and creep properties are critical in selecting a reinforced plastic. These factors were considered in the beam development for the 50-square-foot solar array. A phenyl-silane composite (Narmco 534) and two epoxy anhydrides (EPON 1031-NMA and Scotch-ply 1007) were found satisfactory in creep tests at 295°F (Reference 3).

Fabrication methods vary with the material used. Forming of annealed titanium can be accomplished at up to 1,350°F without affecting mechanical properties. This allows a closed-section beam to be welded prior to forming. Reinforced plastic, beryllium-copper, and stainless steel beams should be formed prior to joining, which presents additional welding and bonding problems.

The desired thermal radiative properties of the beam surfaces can be achieved by special coatings or controlled natural finishes. To minimize weight, the use of paints should be avoided. Also the effect of flattening and wrapping the beam on surface finish can be a significant problem. In order to reduce thermal gradients, the inside surface of the closed beam section should exhibit high emittance. For the reinforced plastic beam, the natural surface has an emittance of $\epsilon = 0.9$. Beryllium-copper can be treated with a coating such as Elvanol C to increase emittance to $\epsilon = 0.9$. Titanium surface properties have been controlled by dust blasting the surfaces and oxidizing during forming to obtain $\epsilon = 0.6$.

The feasibility of forming beams 40 feet long has also been considered. Titanium beams of 20 feet long have been formed in a full length heat treat fixture. Longer beams can be fabricated by, (1) extending the size of tooling fixtures and furnaces, (2) by using a continuous forming process, or (3) by incorporating splice joints in the beam. The use of splice joints is readily applicable. Several titanium beam test sections have been spliced by welding to produce a satisfactory joint. This method is also applicable to beryllium-copper and steel.

Equipment limitations oppose the use of larger tooling fixtures to produce beams 40 feet long. Continuous forming appears to be feasible with considerable promise but requires tooling development. Continuous forming would not be applicable to the reinforced plastic beams.

Final selection of the beam material depends on ability to meet functional and environmental requirements with minimum weight. Titanium is preferred to beryllium-copper or steel because of its lower density and higher specific yield strength. The limiting factor on material choice is the minimum practical gauge for fabrication and handling. This limit appears to be about 0.002 to 0.003 inch. The metals are preferred to reinforced plastic because of superior wrapping characteristics and resistance to the environmental conditions.

Substrate

Candidate materials for the substrate include Kapton, Mylar, and fiberglass reinforced plastic. Each of these materials have good mechanical and dielectric properties required for substrate application. Because of the integral relationship between the substrate and the solar cell array, particular attention to this interface is required.

These materials are considered because of availability in thin sheet, and suitability for space environment. Silicone rubber or teflon films are substantially heavier than the candidates. Both Kapton and Mylar are available in gauges ranging downward to 0.0005 inch thick. Molded Fiberglass sheet is not readily available in less than 0.002-inch thickness but 0.001-inch cloth is available and can be impregnated with a suitable resin.

A fiberglass-epoxy resin substrate had been previously selected for the 50-square-foot solar array design (Reference 1) in order to meet deployment and midcourse maneuver requirements. However, in this design, the reduced load requirements and weight objectives suggest consideration of very thin films.

The radiation resistance of Kapton film and glass reinforced EPON 828 is somewhat better than Mylar, with standing gamma ray doses as high as 5×10^8 rad.; Reference 2. The limiting dose for Mylar is 10^8 rad. Ultraviolet stability of Kapton is superior to Mylar which discolors and becomes brittle (Reference 2). Also, the broader service temperature range (-250 to $+400^\circ\text{C}$) makes Kapton a preferred choice over Mylar (-70 to $+165^\circ\text{C}$) (Reference 4). The EPON 828-RP7A glass cloth reinforced plastic system has good stability in vacuum over a temperature range of -240 to $+140^\circ\text{C}$ (Reference 5).

Analytical studies indicate that a 0.001-inch thick film of Kapton is adequate to meet load requirements. In order to determine the feasibility of producing a fiberglass reinforced film of 0.001-inch thickness, sample

sheets of two epoxy resin systems were prepared using type 108 glass cloth (0.001-inch thick) for reinforcement. Sheets of Stanpreg 5103, an epoxy-amide prepreg, were produced with a thickness range from 0.002 to 0.004 inch. Difficulties in removing excess resin from the prepreg material prevented achievement of lower uniform thickness. The second resin system tried was EPON 828 with D10NRP-7A, an aromatic amine system, which was impregnated as a wet layup between two sheets of Tedlar film. Uniform sheets of 0.001-inch thickness were produced.

Edge attachment tests were conducted on Kapton, Mylar, and EPON 828-RP7A sheets with satisfactory results for each material. These tests are reported in Paragraph 3.3.3 and following. It should be noted that the Kapton film has a lower weight for the same thickness because of its lower density ($\rho = 1.4$) compared to fiberglass sheet ($\rho = 1.8$).

The Kapton film has better handling characteristics than the fiberglass sheet because of its lower modulus of elasticity. The fiberglass must be handled with more care to prevent folds or wrinkles which cause the material to tear or crack. The initial tear strength of Kapton is greater than fiberglass sheet. However, the propagating tear strength of the Kapton is lower. This propagation tear strength (8 grams/mil) is so low that provision must be made in the design to preclude the start of any tears.

A major consideration in evaluation of Kapton film was the need to determine reliable adhesive systems and methods for joining the film, bonding the solar cells, and repairing defects. Problems in bonding of cells to Kapton using common adhesives such as RTV 40 have been reported in the literature (Reference 6) and were experienced in earlier work at Spectrolab.

The concept of a substrate-solar cell array with integrated conductors also requires that a bonding method be determined for the conductor to Kapton bond. The adhesives considered are discussed below and test results are reported in Paragraph 3.3.3 and following. The tests were limited to Kapton adhesive systems. Adhesive bonding to the fiberglass-epoxy substrate presents no unusual problem and there are many satisfactory systems which can be used such as RTV 40 (General Electric), EPON 934 (Shell Chemical Company) and FM-1044 (American Cyanamid) (References 2, 3, 4, and 5).

Adhesives

Several adhesive systems were evaluated for use in the array. Structural adhesives considered include FM-1000, FM-1044R, and FM 96U (American Cyanamid); Narmco 225 and Narmco 329 (Whittaker Corporation); EPON 934 and EPON 956 (Shell Chemical Company); TR150-25 (Thermo Resist, Inc.); RTV 3145, Silastic 140 (Dow Corning), and GT100 (Schjeldahl).

For solar cell adhesives the following were considered: RTV108, RTV41, RTV511, RTV577, RTV602 (General Electric); Sylgard 182 and 92-024 (Dow Corning).

These materials are generally acceptable to the specified environment with the epoxy and polyimide types being more resistant than the silicones (References 2 and 6).

Because of a need to establish an ability to bond to Kapton, sample tests were conducted to establish methods and strength values for bonding Kapton to Kapton; solar cells to Kapton, and aluminum to Kapton. These tests are reported in detail in Paragraph 3.3.3 and following.

Test results indicate that both TR150-25 (Polyamide-imide) and FM 1044R (epoxy-amide) produce good bonds of Kapton to itself and are preferred for splicing and application of doublers.

Satisfactory bonds of solar cells to Kapton were achieved using Silicone adhesives RTV41, RTV511, RTV577 and RTV3145.

An evaluation of solar cell adhesives (to measure effects of thermal cycling between -195 and +140°C at 10^{-7} Torr) was conducted and is reported in Paragraph 3.3.3 and following. Materials tested included RTV602, Sylgard 182, RTV41, RTV511, RTV577; Silastic 140 and Schjeldahl GT-100.

Cushioning Materials

In order to protect the solar cells in the stowed position during launch, a cushion or pad arrangement must be provided. Silicone foam materials having a density of 10 to 20 pounds/cubic foot have been investigated and found suitable for sterilization, launch and space environment (Reference 3). In this design, lower foam densities are desirable to meet weight objectives. Therefore, flexible polyurethane foam was evaluated because of its more uniform properties at densities as low as 2.0 pounds/cubic foot. Except for its weight disadvantage, the flexible silicone foam has

preferred environmental resistance. The service temperature range of silicone foam is -90°C to $+315^{\circ}\text{C}$ compared with -55°C to $+150^{\circ}\text{C}$ for polyurethane (Reference 4). At the lower temperature limits the flexible foams become rigid. However, the critical damping requirement exists at launch when temperature is not a factor.

Metallic Components

Nonmagnetic materials are used throughout the structure assembly, except for the drive motor. Metals considered in the design include aluminum, beryllium, beryllium-copper, magnesium, corrosion resistant steel, and titanium. All of these metals are space qualified and present no significant environmental problems.

Nonmetallic Components

The nonmetallic components considered for the design include adhesives, substrate, insulation, damping pads, guide sleeves, coatings, and lubricants. The evaluation and selection of materials for substrate, adhesives, and damping pads were discussed previously.

Thermal control paints which have been considered includes IIT S-13, methyl silicone-zinc oxide white, Fuller 517-W-1 white and Cat-A-Lac epoxy white and Cat-A-Lac 463-1-8 epoxy black. These materials have been found resistant to the space environment and suitable for thermal control (References 3 and 4).

The use of teflon (TFE) for the beam guide sleeves provides a low friction, temperature-resistant support. The range of useful properties extends from -200°C to $+320^{\circ}\text{C}$ (Reference 4). Under the relatively light loads and low speeds of beam travel, the wear resistance of the unmodified Teflon is adequate. Radiation stability in vacuum is somewhat inferior to other polymers such as phenolic, epoxy or polyimide with some loss of ductility occurring at 10^6 rads (Reference 2). However, this effect is not significant in this application.

Versilube G-300 (General Electric) has been considered for lubrication of the drive motor and gears. This material is a silicone grease with good stability in the flight environment recommended for fine pitch gears and gear trains, (Reference 2) and previously used in the 50-square-foot deployable array design (Reference 1).

3.2.5 Manufacturing Restraints

Ryan's experience in manufacturing and assembling components for a 50-square-foot rollout array has provided baptismal experience in applicable fabrication techniques and processes. Comparing to the subject program it is anticipated that the most significant difference will be problems concerned with the fivefold increase in array area. Also, a corresponding increase in risk involved in working with higher cost accumulation components.

A design that must be constructed, tested, and demonstrated repeatedly in a one-G environment and yet weigh, in aggregate, no more than a third of a pound per square foot of exposed substrate surface area, is going to be sensitive to tolerances in materials and workmanship and in day-to-day handling requirements.

Where possible, designs for subelements of the array should be sized to a practical minimum consistent with such general considerations as:

- A major component should be designed to be mechanically assembled and conversely, removable in the event of damage. Examples: the wrap drum, support structure, individual beams, incremental elements of the substrate, if possible, etc.
- Electrical circuitry should be designed for convenient access to connector terminals points. Circuitry should be so arranged as to permit frequent in-process inspection to assure that functions and tolerances can be electrically checked as often as necessary or prudent; also to facilitate precise disconnect and re-solder operations when repairs are necessary.
- Suitable unit strength; i. e. , designed as modular assemblies with sufficient strength and durability in identifiable handling and pickup areas as to facilitate controlled movement and manipulation without crippling effects.

However, no design is to be penalized with excess material (and weight) for added strength if an improvement in handling fixture concept is the more responsible answer.

Materials studies have been concerned not only with physical properties and environmental suitability but also with availability and the fabrication technology that would be involved in manufacture of components. As an

example, beryllium was not considered for array support structure because of the probable complexity in construction of this item. The alloy did receive consideration for use in the wrap drum where relatively simple fabrication methods are involved. A simple wrap drum was designed to be made from beryllium and the drawing and an RFQ submitted to several beryllium fabricators. All returned answers of "No quote." Bonded honeycomb sandwich construction was rated as secondary when compared to single thickness material, conventionally stiffened (doublers, brackets, etc.), because of incongruous quality control methods that are characteristic of composite sandwich materials. Film-type plastics for substrate material were rated as more desirable than a thin fiberglass laminate because of a tendency towards brittleness in resin-reinforced glass fibers. The substrate will be handled frequently in construction and in testing the array. The film-plastics are generally tough and quite flexible but they do have poor resistance to tear propagation. This is a known problem that can be resolved in the design by reinforcement provisions and in manufacture by process control in edge preparations.

Solar cell module assembly and installation on thin-film plastic substrates may present some new development requirements but this remains to be investigated in work which is to follow this reporting period. Sample investigations and tests, working with adhesive systems, cell-substrate compatibility and interconnect designs and materials have not disclosed any alarming problems. Future work will also be concerned with repair procedures. The language and intent of the contract limits materials and manufacturing processes to short term developments, preferably to the use only of state-of-the-art designs and materials. Therefore, all efforts to date have concentrated on applying proven solar cell technology and processing methods to the requirements. It is felt that current process controls, tolerances, soldering techniques, and handling procedures will be amendable to the general requirements of this program. The unique situations are expected to relate to substrate size and flexibility and there does not appear to be serious restraints that cannot be overcome with diligent effort and application of experience, and suitable shop aids.

Ryan anticipates applying its present manufacturing methods to the construction of the extendible beams. Splicing techniques have been developed to assure that increased beam length is not a constraint. An optimum process for making continuous lengths of a closed beam (one that can be coiled without permanent deformation) would require improved technology. The company is pursuing this objective for other purposes but beam designs and manufacturing concepts to be applied to the subject program are not dependent on such developments.

Manufacturing practicability and/or an intrinsic handling characteristics were judged to be the significant weighting factors in the configuration of the beams, substrate, and wrap drum.

Special care is necessary in arrangement of manufacturing facilities for large solar arrays. Layouts for workpiece and equipment arrangements must limit personnel traffic and part movement. Handling equipment designs must be cognizant of local bearing loads and possible creep loading circumstances. Foil gage materials will predominate in most subelement designs. Consequently, protective planning and measures will be an ever-dominant consideration.

No fabrication-type obstacles of consequence have developed in first quarter studies that would suggest abnormal lead time in manufacture preparations. If requirements develop for high quantity, production plating of molybdenum on solar cell bus bars, preplanning efforts should be directed to assure that there are adequate sources with qualified processes and controls. Development and qualification of a thirty-watt-per-pound capability solar array appears to be feasible within span times normally estimated for execution of a space program with multi-kilowatt electrical requirements.

3.3 PRELIMINARY DESIGN AND ANALYSIS

3.3.1 Design Criteria

Design requirements and tolerances, including performance and environmental criteria, are set forth in JPL Specification SS501407. More specifically, the following paragraphs and respective subparagraphs constitute the data that have been invoked:

3.2 DESIGN CONSIDERATIONS,

3.3 MATERIALS, PARTS AND PROCESSES,

3.4 ELECTRICAL POWER CRITERIA,

3.5 MECHANISM RESTRAINTS,

3.6 RELIABILITY,

3.7 INTERFACES,

3.8 MANUFACTURING RESTRAINTS,

3.9 ENVIRONMENTAL REQUIREMENTS, and those definitions and explanations presented in,

6.0 NOTES.

3.3.2 Studies and Analyses

3.3.2.1 Panel Aspect Ratio Studies

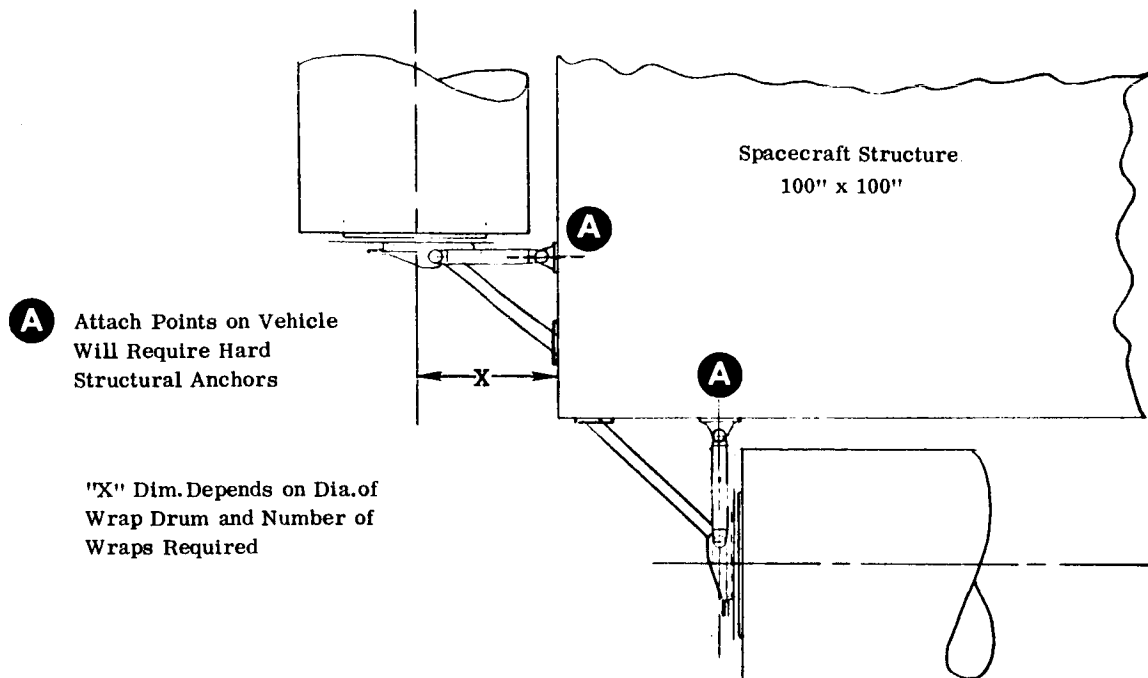
This study is conducted to determine the optimum deployed panel aspect ratio; a criterion considered to be analogous to minimum weight design for the solar cell area objective of this program. By performance of this study, the wrap drum and deployable beam lengths are established.

The study is reduced to simplicity by considering only those components whose weight will change, or effect an appreciable weight change in the total structure weight with a change in panel aspect ratio. These influencing components are, (a) wrap drum, (b) deployable beams, and (c) spacecraft mounts. Other components such as substrate, drive system, drum mount, and beam guides will not change enough, if any, to significantly affect the results of this study.

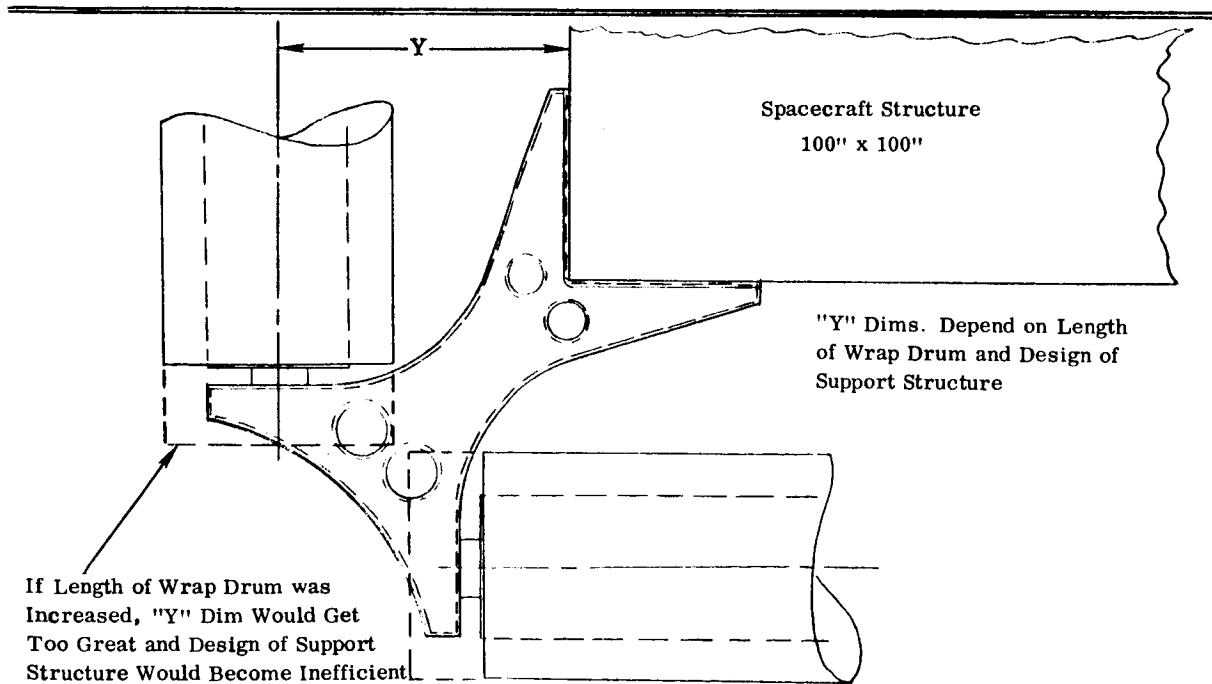
For the purposes of this study it will be considered that:

1. The wrap drum dynamic deflection remains constant (approximately 0.2 inch single amplitude) with a change in drum length by varying skin thickness, t , and holding drum diameter constant at 12 inches. For comparison, six-inch diameter magnesium drums and also six-inch diameter beryllium drums are considered, where total weight is affected only by the drum since the size of the spacecraft mount is a function of aspect ratio and not drum diameter; and
2. That the deployable beam weight will change in direct proportion to a change in length since it is considered that the proposed beam cross-section of 1.7-inch diameter x 0.003-inch thick titanium is minimum for fabrication and stability reasons in handling.

The wrap drum configuration suggested in the proposal, namely a magnesium ring-stiffened skin, is considered for this study, with a desired drum length bracketed between 90 and 96 inches (5.3 to 4.6 aspect ratio) for practical reasons (see Figure 10) in mounting to the hypothetical 100-inch sided square spacecraft bus shown in Figure 1, JPL Specification SS501407A.



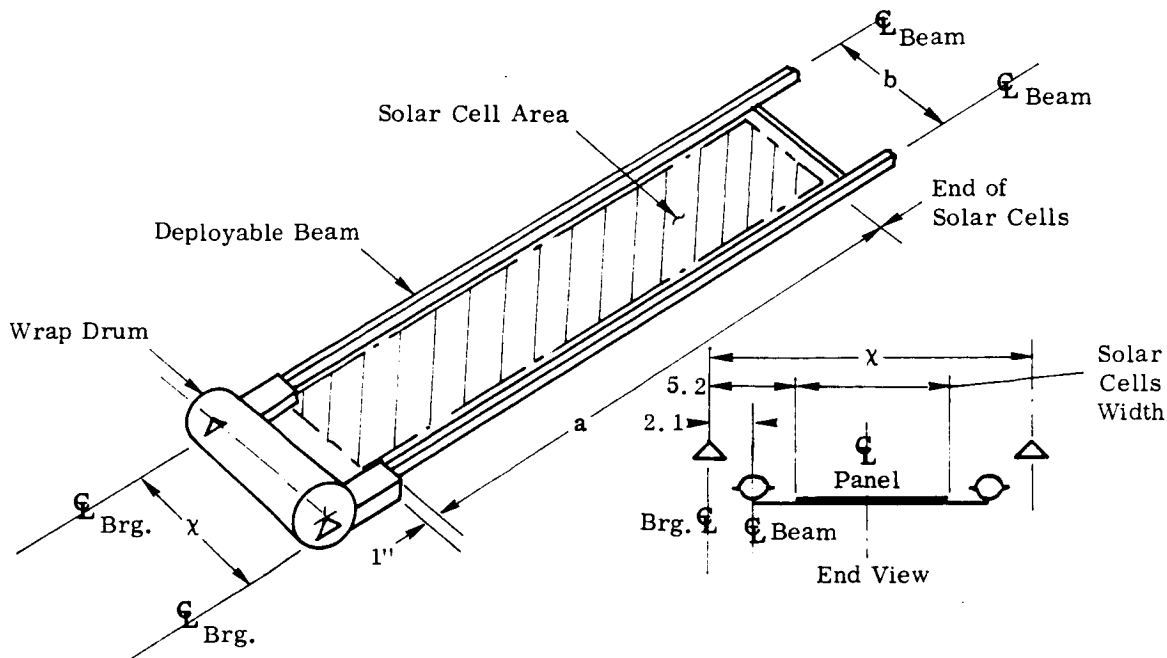
SPACECRAFT MOUNTINGS FOR DRUMS SHORTER THAN 90"



SPACECRAFT MOUNTINGS FOR DRUMS LONGER THAN 96"

Figure 10. Wrap Drum Length Considerations

For purposes of this study, the deployed panel aspect ratio (a/b), is a function of the variable dimensions a and b shown below. Relative weight is considered a function of (1) wrap drum skin based on support bracket center distance, X , and (2) that portion, a , of deployable beam length where deployable beam weight/inch is based on the proposal weight of 4.2×10^{-3} pounds/inch. Weight attributed to the spacecraft mount is based on a function of the 3.1 pounds given in the proposal.



X, in.	Solar Cell Area	Solar Cell Width (in.)	a in.	b in.	Aspect Ratio	Drum Skin t, in.			Drum Skin Weight, lbs.			Weight of (2) Beams (lbs.)	Space Craft Mount Wt./lbs.	Sum'y. Wt. of Items Concerned (lbs.)		
						12 in.	6 in.	6 in. Be	12 in.	6 in.	6 in. Be			12 in.	6 in.	6 in. Be
110		99.6	361.4	105.8	3.41	.071	.568	.092	13.40	53.6	8.68	3.04	6.2	22.6	62.8	17.9
96		85.6	420.6	91.8	4.58	.041	.328	.053	6.75	27.0	4.36	3.53	3.1	13.4	33.6	11.0
90	250 ft. ²	79.6	451.3	85.8	5.26	.032	.256	.042	4.93	19.72	3.24	3.79	3.1	11.8	26.6	10.1
80		69.6	516.2	75.8	6.81	.020	.160	.026	2.74	10.96	1.78	4.34	6.2	13.3	21.5	12.3
60		49.6	725.8	55.8	13.01	.020	.051		2.06	2.63		6.10	6.2	14.4	14.9	

$$\text{Solar cell width} = X - (2 \times 5.2) \quad t_{(12 \text{ in. Dia. Drum)} = \frac{X^4}{X_o^4} \cdot t_o,$$

Letting $t_o = 0.032''$

$$X_o = 90 \text{ in.}$$

$$a = \frac{\text{Solar Cell Area}}{\text{Solar Cell Width}}$$

$$b = X - (2 \times 2.1)$$

$$\text{Aspect Ratio} = \frac{a}{b} \quad t_{(6 \text{ in. Dia. Drum)} = \left(\frac{E_{12 \text{ in. Drum}}}{E_{6 \text{ in. Drum}}} \right) \cdot \left(\frac{12}{6} \right)^3 \cdot t_{(12 \text{ in. Dia. Drum)}$$

Conclusions

The curves presented in Figure 11 show the effect of aspect ratio change on weight of the solar panel. Even though it shows an optimum aspect ratio of 5.26, using a 12-inch diameter magnesium drum as was proposed, the design goal of 30 watts/pound could be met for ratios above 3.5. A design approximately equal in weight to a 12-inch diameter magnesium drum is possible by use of a 6-inch diameter beryllium wrap drum when small wrap drum diameters are desired. The curves show that as the wrap drum diameter decreases for a given material, the optimum aspect ratio increases, meaning that the drum length decreases with a decrease in diameter. Drums larger than 12-inch diameter are not considered here because (1) the weight of the drum mount increases as the drum moves further from the spacecraft bus and (2) the drum skin now becomes thicker for drum bending stability reasons thereby making the drum heavier.

3.3.2.2 Substrate Attachment

Analyses of the substrate attachment concept were performed for three design conditions:

- (a) 1 G, roller support,
- (b) 2 G, handling, and
- (c) 0.2 G, arbitrary cruise maneuver.

Conclusions are noted at the terminus of these notations. Development tests related to substrate attachment investigations are discussed in Paragraph 3.3.3 and following.

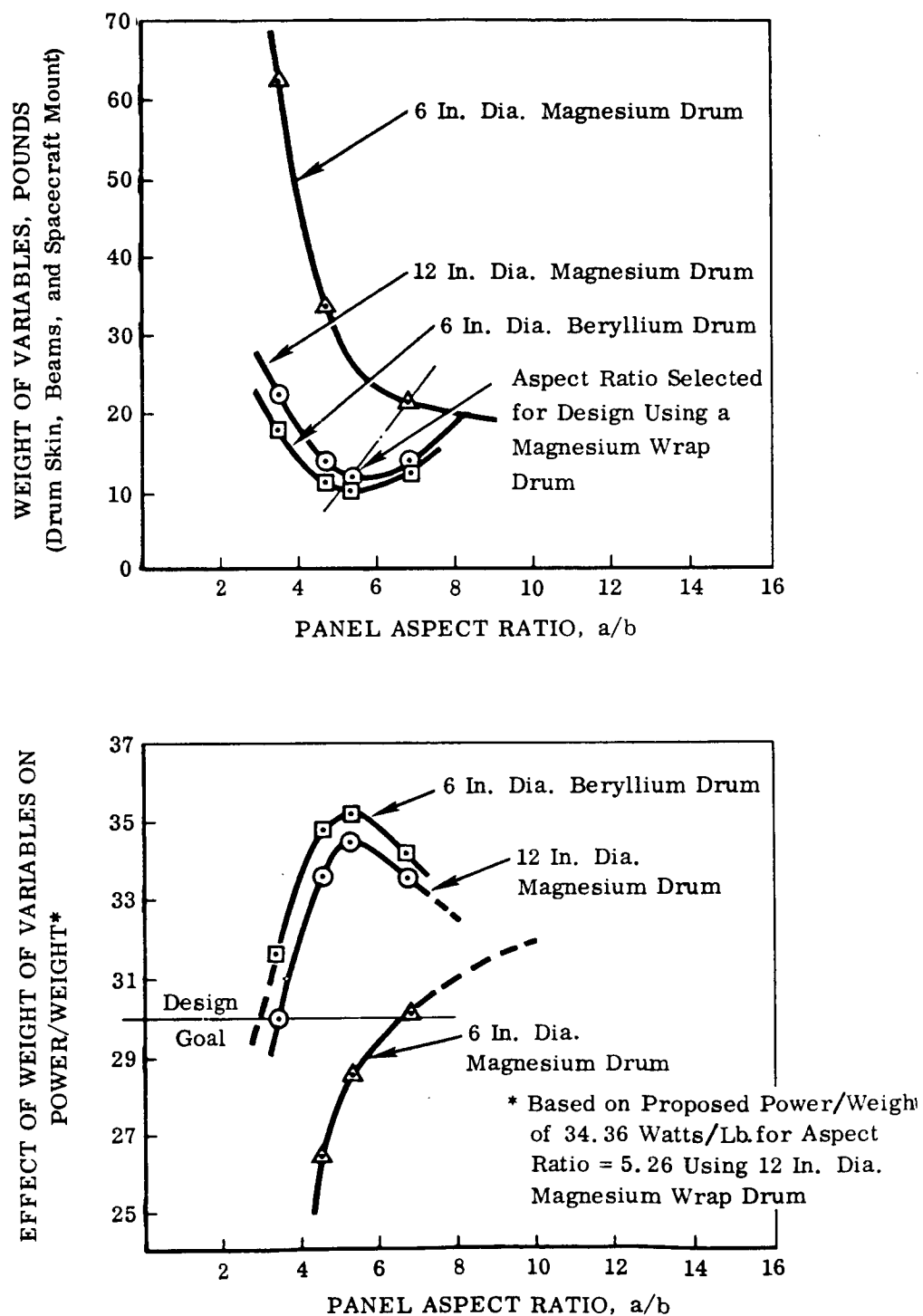
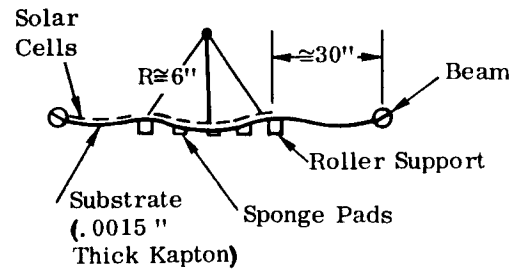
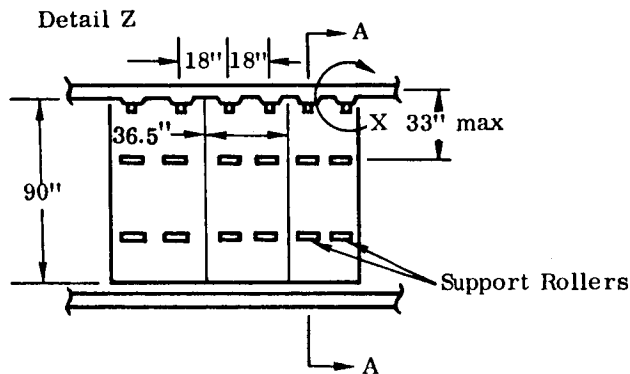
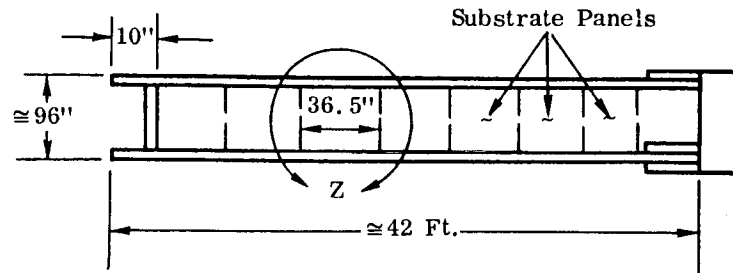


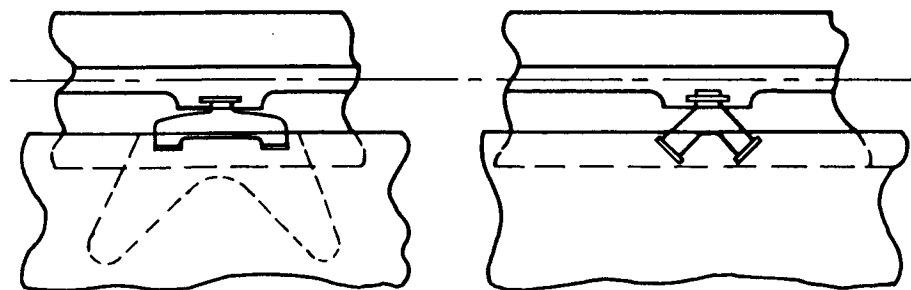
Figure 11. Aspect Ratio as Related to Influential Weight Variables and to Power/Weight Objectives

1G, Roller Support

Estimated weight of substrate, solar cells, sponge pads = 0.22 lb./ft.².
 Substrate material — 0.0015 in. Kapton. Design condition - 1G.
 supported by rollers, by simplified analysis.



SECTION A-A
 ROTATED COUNTERCLOCKWISE



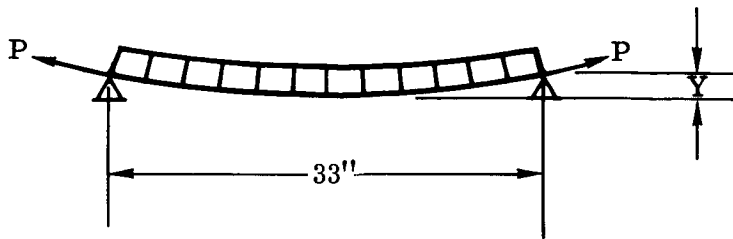
DETAIL X

Attach Clips

ALTERNATE METHOD

Assume Substrate Acts as a Cable:

(For 18" width)



$$w = \frac{18''(1)}{144} (.22)$$

$$= .0275 \text{ lb./in.}$$

$$W = w \ell$$

$$w = .0275(33)$$

$$= .908 \text{ lb.}$$

$$\text{MAX } Y = \ell \left(\frac{3w\ell}{64EA} \right)^{1/3}$$

$$= 33 \left[\frac{(3)(.908)}{64(4.3 \times 10^5)(.0015)(18)} \right]^{1/3}$$

$$Y = 33(.00000366)^{1/3} = 33(.0154) = \underline{.509 \text{ in.}}$$

$$P = \frac{1}{8} \frac{w\ell^2}{\text{MAX } Y} = \frac{1}{8} \frac{.0275(33)^2}{.509} = \underline{7.38 \text{ lb. LIMIT}}$$

$$= 9.22 \text{ lb. ULT @ 18 inch centers or @ 9 inch}$$

$$\text{centers } \underline{4.60 \text{ lb. ULT}}$$

$$\frac{P}{A} = \frac{7.38}{(.0015)(18)} = 273 \text{ psi}$$

Substrate: "KAPTON" Type H

$$E = 430,000 \text{ psi @ } + 25^\circ\text{C}$$

$$F_{TU} = 25,000 \text{ psi @ } + 25^\circ\text{C}$$

$$\text{YIELD PT}_1 = 10,000 \text{ psi @ } + 25^\circ\text{C}$$

5% Elongation @ 13,000 psi

Density 1.42 gm/cc

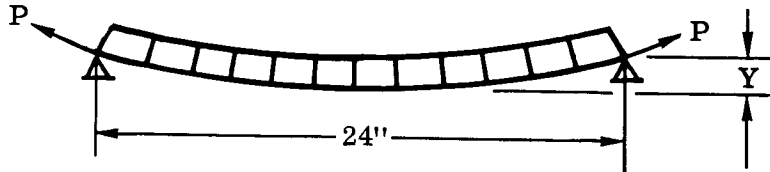
- Mylar

Density = 1.4 gm/cc

$F_{TU} = 25,000 \text{ psi}$

% Elongation at Break = 100%

At 1/4 panel width spacing for support rollers:



$$Y_{MAX} = 24 \left[\frac{3 \cdot (.0275)(24)}{64(4.3 \times 10^5)(.0015)(18)} \right]^{1/3}$$

$$= 24 \left[2.66 \times 10^{-5} \right]^{1/3}$$

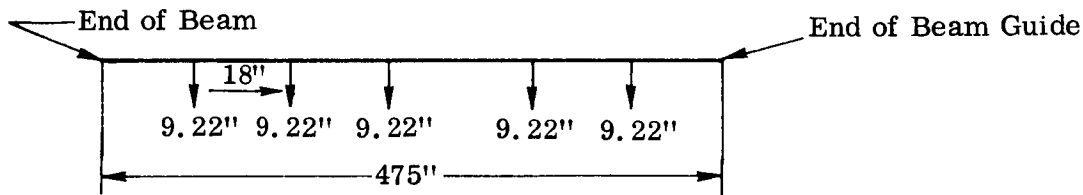
$$= 24 (.01385) = \underline{.332 \text{ INCH}}$$

$$P = \frac{1}{8} \frac{.0275(24)^2}{.332} = \underline{5.97 \text{ lb. LIMIT}}$$

$$= \underline{7.45 \text{ lb. ULT}} @ 18 \text{ in. Centers or } 3.73 \text{ lb. ULT}$$

@ 9 in. Centers

Lateral deflection considerations in beam:

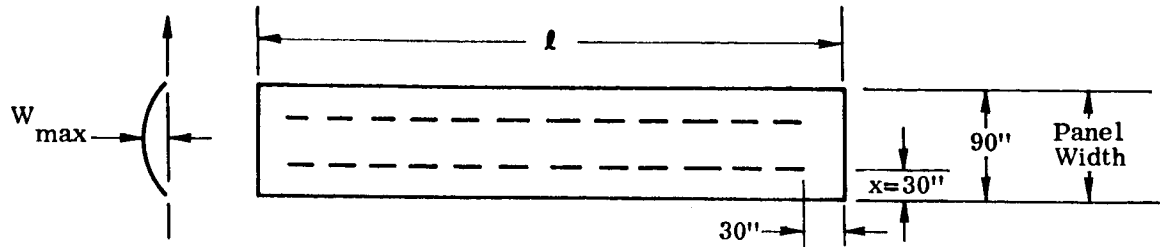


$$\delta = \frac{5WL^3}{384EI} = \frac{5(9.22)(475)(475)^3}{18(384)(16 \times 10^6)(2.43)(.003)}$$

= Deflection too great.

∴ We will restrain the beams from lateral deflection by rollers.

Substrate analysis for a thermal test condition of 1G at 250°F, supported by rollers at 1/3 panel width and with attachment clips at 6.0-inch spacing, (Kapton material-- f_{tu} @300°F = 17,000 psi).



Checking a 30-inch square section $\left(\frac{a}{b} = \frac{30}{30} = 1\right)$,

$$W_{MAX} = n_1 \cdot a \left(\frac{8a}{Et}\right)^{1/3}$$

$$= .318 (30) \left[\frac{.00191(1)(30)}{4.3 \times 10^5 (.0015)} \right]^{1/3} \quad n_1 = .318$$

$$n_2 = .356$$

$$= 9.55(.0000887)^{1/3} = 9.55(.0446) = .426 (1.1) = \underline{.47} \text{ inch}$$

$$S_{MAX} = n_2 \left[E \left(\frac{8a}{t}\right)^2 \right]^{1/3}$$

$$= .356 \left[4.3 \times 10^5 \left(\frac{.00191(1)(30)}{.0015} \right)^2 \right]^{1/3}$$

$$= .356 \left[4.3 \times 10^5 (1460) \right]^{1/3} = .356 \left[6.26 \times 10^8 \right]^{1/3}$$

$$= .356 \left[8.55 \times 10^2 \right] = \underline{304} \text{ psi ULT. M.S.} \rightarrow \underline{\text{HIGH}}$$

Clip load, $P = \underline{2.75} \text{ lbs/clip ULT.}$

If we consider a maximum distance between support rollers of 11 in. ,

$$W_{MAX} = .47 \left(\frac{11}{30} \right) \left(\frac{11}{30} \right)^{1/3} = \underline{.12} \text{ in.}$$

$$S_{MAX} = 304 \left[\left(\frac{11}{30} \right)^2 \right]^{1/3} = \underline{157} \text{ psi ULT.}$$

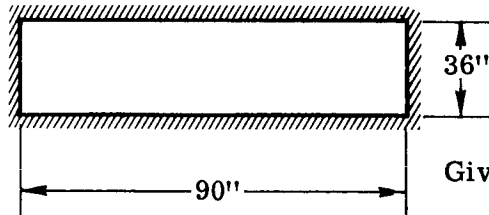
Clip load = 1.41 lbs. ultimate f 6" c-c, or, .94 lbs. ult. for

4" c-c

2G, Handling

Assume that substrate is so thin that clamped and fixed supports will not affect deflection or stress values. Check for 2G's at room temperature for manufactured element size, 90 in. by 36 in. panel, with uniform support and clamped edges,

a = Long Side
q = Lateral Press
t = Thickness
n = Dimensional Constant



Given:
Substrate Kapton
.0015 Inch
.006 " Doublers

Weight of substrate (total) .22 lb./ft. (in 1G field), or .00191 lb./in.²
ULT.

Assume held vertically; $36(90)(.00191)(2) = 12.4$ lbs. ULT.

$$\text{Stress} = \frac{12.4}{36(.0015)} = 2,290 \text{ psi}$$

$$\text{M.S.} = \frac{25,000}{2,290} - 1 \rightarrow \underline{\underline{\text{HIGH}}}$$

Assumed held horizontal during manufacture; (Ref. 7, p. A17.6)

$$\frac{a}{b} = \frac{90}{36} = 2.5$$

$$n_1 = .125$$

$$n_2 = .304$$

$$\begin{aligned} (\text{DEFL}) W_{\text{MAX}} &= n_1 a \left(\frac{qa}{Et} \right)^{1/3} \\ &= .125(90) \left[\frac{(.00191)(.2)(90)}{4.3 \times 10^5 (.0015)} \right]^{1/3} \end{aligned}$$

$$= 11.25(5.33 \times 10^{-4})^{1/3} = 11.25(.031) = .911(1.1) = \underline{\underline{1.0}} \text{ inch}$$

$$S_{MAX} = n_2 \left[E \left(\frac{qa}{t} \right)^2 \right]^{1/3}$$

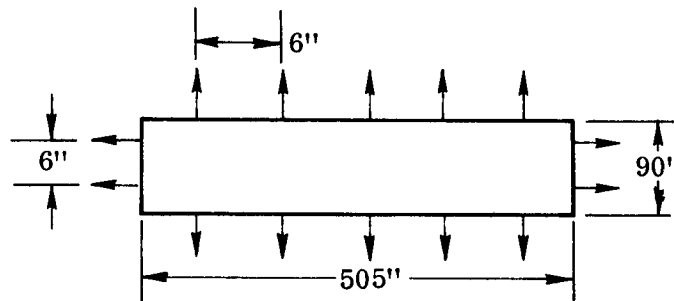
$$= .304 \left[4.3 \times 10^5 \left(\frac{.00191(2)90}{.0015} \right)^2 \right]^{1/3}$$

$$= .304 \left[4.3 \times 10^5 (5.25 \times 10^4) \right]^{1/3} = .304(22.6 \times 10^9)^{1/3}$$

$$= .304(2.82 \times 10^3) = \underline{\underline{856}} \text{ psi} \quad MS. = \frac{25,000}{856} - 1 \rightarrow \underline{\underline{HIGH}}$$

0.2G, Arbitrary Cruise Maneuver

An arbitrary 0.2G at 250°F cruise maneuver, simply supported by clips at 6 inch intervals,



$$\frac{a}{b} = \frac{505}{92} = 5.5$$

$$n_1 = .052$$

$$n_2 = .205$$

$$W_{MAX} = n_1 a \left(\frac{qa}{Et} \right)^{1/3} = .052(505) \left[\frac{(.00191)(.2)(505)}{4.3 \times 10^5 (.0015)} \right]^{1/3}$$

$$= 26.3 (3.0 \times 10^{-4})^{1/3} = 26.3 (.067) = 1.76(1.1)$$

$$= \underline{1.94} \text{ inch (neg. lateral beam bending)}$$

$$S_{MAX} = n_2 \left[E \left(\frac{qa}{t} \right)^2 \right]^{1/3}$$

$$= .205 \left[4.3 \times 10^5 \left(\frac{(.00191)(.2)505}{.0015} \right)^2 \right]^{1/3}$$

$$= .205 \left[4.3 \times 10^5 (165) \right]^{1/3} = .205 (7.08 \times 10^7)^{1/3}$$

$$= .205 (4.14 \times 10^2) = \underline{84.5} \text{ psi}$$

$$M.S. = \frac{17,000}{84.5} - 1 \rightarrow \underline{HIGH}$$

$$\text{Clip Loads} = 84.5(.0015)(6) = \underline{.764} \text{ lb./clip ULT}$$

Conclusions

Stresses in the sheet substrate are within acceptable limits for all loading conditions anticipated. Maximum pull loads at the beam-substrate attach clips occur in a 1G field with the substrate supported intermittently, by rollers. With distances between lines of rollers of 11 inches, clip loads are approximately 16 ounces ultimate with clips spaced at 4.0 inches. This appears to be a reasonable design load requirement and is compared with the actual capability of the attachment (see substrate attachment pull test), refer to Figure 33.

3.3.2.3 Deployment Beam Studies

This section presents the design approach taken in selecting the solar array beam configuration. Discussion includes the structural and thermal analysis of the various beam sections and the selection of the optimum beam through parametric evaluation of the beam configurations which were considered. It is felt that the most critical design constraints are:

1. Maintaining panel flatness under the most severe solar radiation environment (260 mw/ cm²)
2. Providing a stable support system under bending and torsional loads and whose natural frequencies are de-coupled from those of the spacecraft
3. Providing a platform that possesses growth potential; i. e. , increase in size and/or load capability
4. Provide a platform that with the failure of a single element will not result in the loss or degradation of the solar array.

Beam Configuration

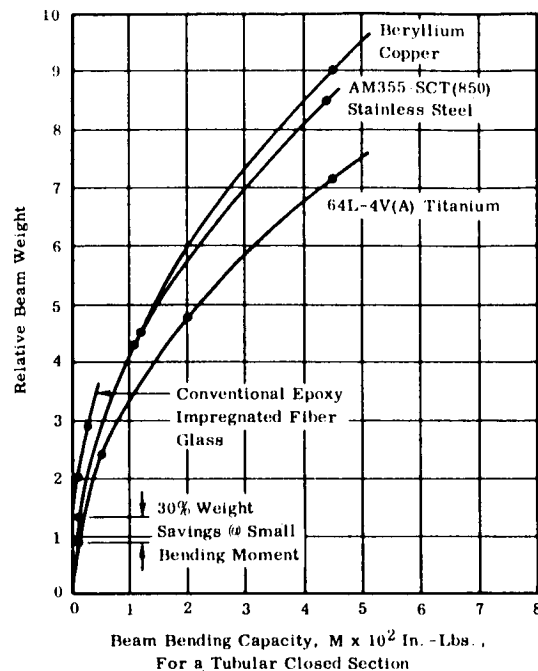
A beam cross-section was needed which, (1) could be stowed on a small diameter drum and (2) after deployment be most efficient in providing bending and torsional stability and in-plane panel requirements when subjected to severe thermal environments. These requirements indicated a closed section, tubular type beam. The materials considered for such a beam section should have a small E/ Fy ratio if a minimum storage package envelope is to result, and a high E/ P for elastic structural stability.

The candidate materials that possess these characteristics and were considered as possible beam materials are, 6 AL - 4 V (A) Titanium, AM 355 - SCT (850) Stainless steel, fiberglass and beryllium-copper. A plot of bending capability vs. relative weight for the proposed beam design configuration is based on the equation shown below,

$$M = \pi \cdot K \cdot E_c \cdot r \cdot t^2$$

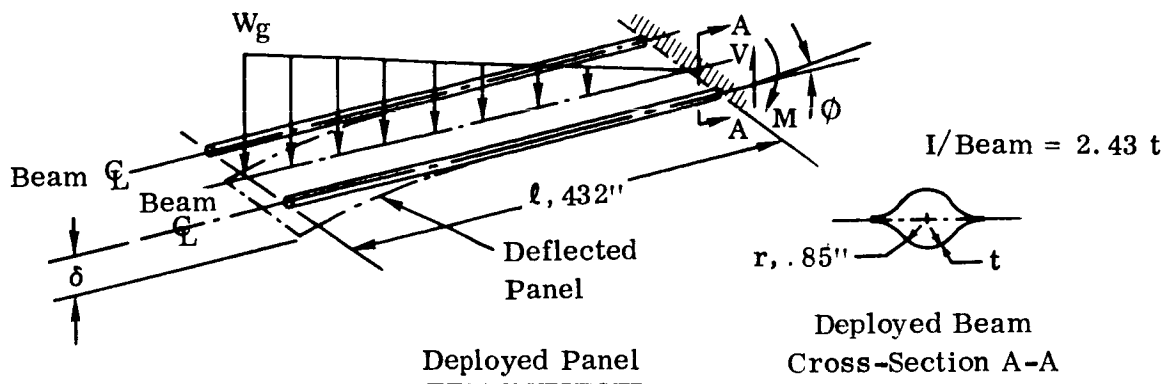
where buckling coefficient, K, vs. material modulus of elasticity, Ec, was determined empirically at Ryan by cantilevered bending tests. It should be noted that shear at the root of the cantilevered beam has negligible affect on the bending capacity for beams of this length. The

plot serves to show that titanium would be the selection for the beam material based solely on strength considerations; even for very low bending moments, a weight savings of approximately 30 percent is realized with respect to the nearest alternate.



Beam Bending

The deployed panel is analyzed for bending and deflections induced by acceleration impulses from the Spacecraft Guidance System. The angular acceleration impulse (square wave) of 2×10^{-5} radians/seconds² is of such time duration (13 seconds minimum) that it will be considered as steady state for this analysis. Beam temperatures are considered at 350 °F. Deflection analysis is made conservative by considering the beam stiffness as a function of cross-section A-A (Root Section) only.



Small deflection theory is considered valid for this analysis.

$$V = (wg)\ell = (.145 \times 2 \times 10^{-5}) \times 432 = \underline{1.25 \times 10^{-3} \text{ lbs.}}$$

limit, not critical

$$M = \frac{2}{3} V\ell = \frac{2}{3} \times 1.25 \times 10^{-3} \times 432 = .36 \text{ in. lbs. limit}$$

$$= .18 \text{ in. lbs. limit/beam}$$

$$= \underline{.23 \text{ in. lbs. ult./beam}}$$

$$M_{\text{Allow (Elastic buckling)}} = \pi K E r T^2$$

$$= \pi \times .25 \times 14.9 \times 10^6 \times .85 \times .003^2$$

$$= 90 \text{ in. lbs. M.S.} \rightarrow \text{HIGH}$$

$$\delta = \frac{1}{2} \left[\frac{11 (Wg) \cdot \ell^4}{120 EI_{\text{beam}}} \right], \text{ Reference 11, Page 101, Case 7}$$

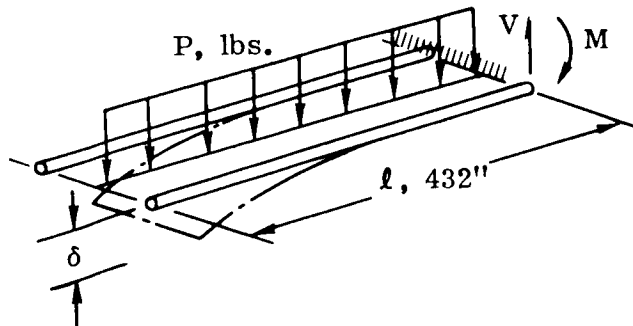
$$\delta = \frac{1}{2} \left[\frac{11 (.145 \times 2 \times 10^{-5}) \times 432^4}{120 \times 14.6 \times 10^6 \times 2.43 \times .003} \right] = \underline{4.4 \times 10^{-2} \text{ in.}}$$

$$\phi = \text{ARC TAN} \left(\frac{\delta}{\ell} \right) = \text{ARC TAN} \left(\frac{4.4 \times 10^{-2}}{432} \right)$$

$$= \text{ARC TAN } 1.01 \times 10^{-4}$$

$\phi < 0^\circ 1'$ which is well within Specification Requirements

For comparison, panel bending under solar radiation pressure is also shown to be extremely small.



$$\left[V = P = \text{Area} \cdot K \right] K = .892 \times 10^{-7} \text{ lbs./ft.}^2$$

Near earth (Reference 6)

If we assume a solar radiation pressure near Venus as twice that at earth

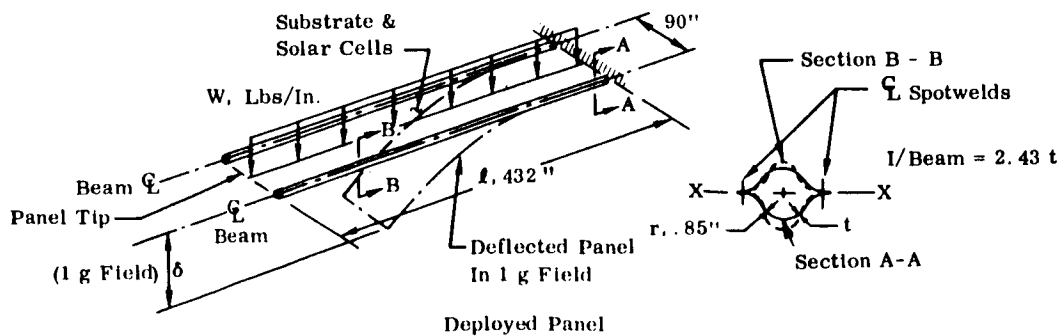
$$V = 2 (250 \times 892 \times 10^{-7}) = 4.4 \times 10^{-5} \text{ lbs. limit, not critical}$$

$$M = \frac{1}{2} V l = \frac{1}{2} \times 4.4 \times 10^{-5} \times 432 = 9.6 \times 10^{-3} \text{ in. lbs. limit}$$

$$= \underline{\underline{4.8 \times 10^{-3} \text{ in. lbs. limit/beam}}}$$

Cantilevered Panel Natural Frequency

The deployed beam temperature is considered at 350°F for near Venus conditions (260 mw/cm² solar flux) with a brown oxide or equivalent beam. Analysis is made conservative by considering the beam stiffness as a function of cross-section A-A (Root Section) only.



Tip deflection, δ , is determined from large deflection theory using Reference 8.

$$B = \left[\frac{2EI_{\text{(beam)}}}{1 - \mu^2} \right] \quad E = 14.6 \times 10^6 \text{ psi at } 350^\circ\text{F, Reference 12 for 6AL-4V(A) titanium}$$

$$= \frac{2 \times 14.6 \times 10^6 \times 2.43 \times .003}{1 - .29^2} = 232,413$$

$$\frac{Pl^2}{B} \quad \left[\text{where } P \text{ produces deflection, } \delta, \text{ equal to that produced by linear load, } W \right]$$

$$P = \frac{3Wl}{8} = \frac{3 \times .145 \times 432}{8}$$

$$P = 23.5 \text{ lbs.}$$

$$\frac{Pl^2}{B} = \frac{23.5 \times 432^2}{232,413} = 18.9$$

ITEM	W, LBS./IN.
Beams (2)	.011
Substrate (.003) Assume	.018
Solar Cells (.2 lbs./ft. ²)	.116
TOTAL	.145

And, from Reference 8,

$$\delta(\text{tip in } 1g) = .85l = .85 \times 432 = 367 \text{ in.}$$

Then,

$$f_n = 3.89 \left[\frac{1}{367} \right]^{1/2} = 3.89 \times 5.21 \times 10^{-2} = \underline{\underline{.20 \text{ Hz}}},$$

which is well within the JPL Specification requirements.

Thermal Analysis

This study has resulted in 34 separate computer nodal analyses of anticipated temperatures for the deployed boom in the vicinity of the planet Venus (solar flux = 260 mw/cm^2). The variations in boom configurations include three materials (Titanium, Fiberglass, and Beryllium-Copper), three boom diameters (.85, 1.7, and 2.6), and four material thicknesses (.002, .003, .0045, and .006).

In this analysis a ten inch section of the boom was considered, thereby minimizing the percentage loss of emitted radiation from the inside of the boom out the ends of the section. The diameter of the boom is represented in the analysis as a series of flat plates. The basic boom configuration and nodal breakdown is shown in Figure 12.

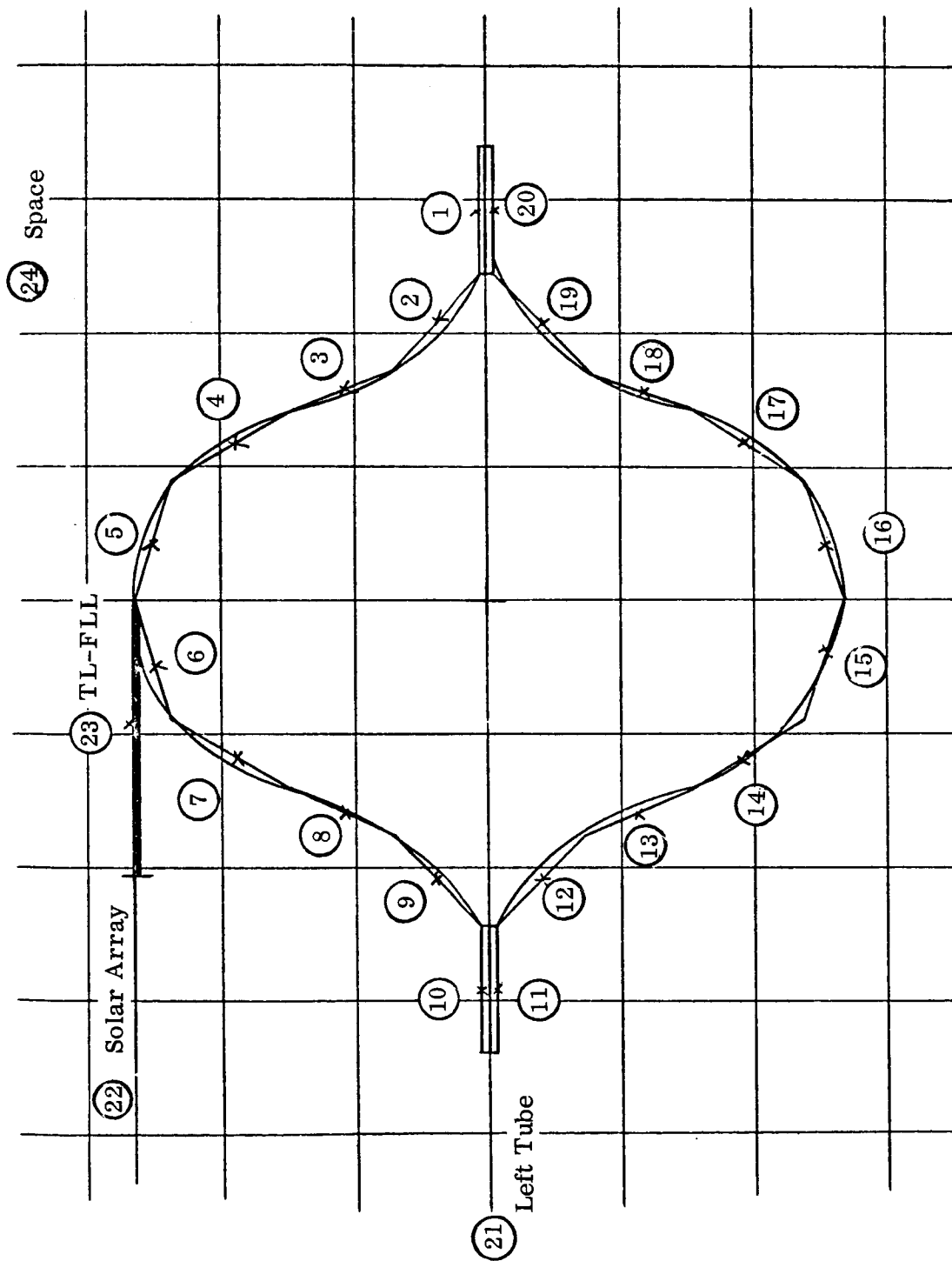
The variable parameters associated with each computer run and maximum temperature and temperature difference results are shown in Tables 1, 2, 3. These tables were compiled from computer runs.

Assumptions and Material Properties

It was assumed that the titanium coating would be obtained by the Ryan heat treatment oxidation process. For the fiberglass it was assumed that the material is untreated except for the exterior rear face which would be vacuum aluminized. The coatings for the beryllium-copper have yet to be developed, however, it seems likely that the basic absorptivity of the material can be retained by coating the front face with a transparent material, which would be emissive in the infra-red range of the spectrum. This same coating, perhaps a dip lacquer could be used on the inside and the rear face would be left uncoated to yield a low emittance. The values of emittance, absorptance, density, thermal conductivity and specific heat used in this analysis are given in Tables 4 and 5.

Beam Selection

The prime consideration (now that a beam cross-sectional configuration is established and other environmental effects have been shown to be small) for selecting the beam material, diameter and sheet thickness is that the beam under extreme thermal environment (260 mw/cm^2) will control distortion of the deployed solar panel to $\leq \pm 10^\circ$ with respect to a theoretical plane. Two considerations must be given in this regard; (a) the panel distortion induced by the deployed beams when a thermal gradient exists and (b) the possible effect the beam has on reducing substrate distortion, (natural radius of curvature the substrate assumes



Scale /cm = 2.111

Figure 12. Schematic Thermal Model of Deployable Solar Array Support Beam

TABLE 1

COMPUTED TITANIUM BEAM TEMPERATURES AND GRADIENTS

Beam Diam- eter	Thick- ness	Weight (lbs./ft.)	Nodal Weight	Maxi- mum Beam Temp.	Maxi- mum Beam ΔT	Nodes Between MAX. ΔT	ΔT^* Through Beam In Solar Flux Plane	Node 5 Temp.	R, $\frac{2r}{\Delta T}$
.85	.002	.01314	.00064	491	227	1, 10	124	458	1,268
	.003	.0197	.00096	477	201	1, 10	107	449	1,471
	.0045	.02955	.00144	462	175	1, 10	95	438	1,658
	.006	.0394	.00192	452	158	1, 10	86	430	1,830
1.7	.002	.02625	.00128	367	174	1, 10	105	336	3,000
	.003	.0394	.00192	358	160	1, 10	101	332	3,115
	.0045	.05910	.00288	350	142	1, 10	92	330	3,422
	.006	.0788	.00384	341	133	1, 10	93	324	3,385
2.6	.002	.0402	.00195	295	133	1, 17	96	268	5,020
	.003	.0603	.00293	290	122	1, 17	91	268	5,285
	.0045	.0904	.00439	288	105	1, 17	81	270	5,940
	.006	.1206	.00586	289	91	1, 14	70	273	6,880

α_1 in/in/°F	$3.9 \text{ to } 4.7 \times 10^{-6}$	4.8×10^{-6}	5.2×10^{-6}	5.4×10^{-6}
T_1 °F	-100 to 68°F	68 to 200°F	68 to 400	68 to 800

* ΔT Between Average (5-6) and Average (15-16)

TABLE 2

COMPUTED FIBERGLASS BEAM TEMPERATURES AND GRADIENTS

Beam Diam- eter	Thick- ness	Weight (lbs./ft.)	Nodal Weight	Maxi- mum Beam Temp.	Maxi- mum Beam ΔT	Nodes Between MAX. ΔT	ΔT^* Through Beam In Solar Flux Plane	Temp Node 5	$\frac{2r}{\alpha \Delta T}$
.85	.002	.00558	.00025	524	311	1, 11	60	436	5, 065
	.003	.00836	.00037	523	307	1, 11	60	435	5, 065
	.0045	.01910	.00055	521	301	1, 11	60	435	5, 065
	.006	.02550	.00074	519	294	1, 10	60	434	5, 065
1.7	.002	.01115	.00049	370	166	1, 11	45	305	13, 500
	.003	.01674	.00074	370	165	1, 11	44	305	13, 800
	.0045	.02510	.00110	369	163	1, 11	42	306	14, 450
	.006	.03350	.00147	369	158	1, 11	39	308	15, 580
2.6	.002	.01708	.00075	288	94	1, 8	35	238	26, 520
	.003	.02565	.00112	288	93	1, 4	33	239	28, 150
	.0045	.0384	.00168	289	108	1, 3	29	242	32, 000
	.006	.0512	.00225	290	104	1, 3	24	246	38, 650

α_1 in/in°F	Parallel To Warp	
	4.8×10^{-6}	2.8×10^{-6}
T_1 °F	-100 to 200	+300 to 600

TABLE 3

COMPUTED BERYLLIUM-COPPER BEAM TEMPERATURES AND GRADIENTS

Beam Diameter	Thickness	Weight (lbs./ft.)	Nodal Weight	Maximum Beam Temp.	Maximum Beam ΔT	Nodes Between MAX. ΔT	ΔT^* Through Beam In Solar Flux Plane	Temp Node 5	$\frac{2r}{\alpha \Delta T}$
.85	.002	.0244	.00119						
	.003	.0367	.00178						
	.0045	.0550	.00267	224	15	5, 14	13	224	7, 110
	.006	.07235	.00356	217	12	5, 14	11	217	8, 400
1.7	.002	.0488	.00238						
	.003	.07235	.00356	200	21	6, 15	20	199	9, 235
	.0045	.1100	.00535	195	15	6, 15	15	195	12, 870
	.006	.14470	.00713	192	11	6, 16	11	192	17, 550
2.6	.002	.0748	.00362	190	23	7, 15	14	178	20, 150
	.003	.1123	.00534	188	21	7, 15	13	179	21, 750
	.0045	.1682	.00815	187	15	7, 16	8	180	35, 300
	.006	.2245	.1087	186	12	7, 16	7	180	40, 300

α , in/in/°F	9.2×10^{-6}
T_1 °F	68 to 212°F

TABLE 4

BEAM SURFACE CHARACTERISTICS

	Titanium	Beryllium-Copper	Fiberglass
ϵ Front	.63	.63	.9
ϵ Read	.18	.10	.05
ϵ Inside	.63	.63	.85
αS	.835	.4	.1

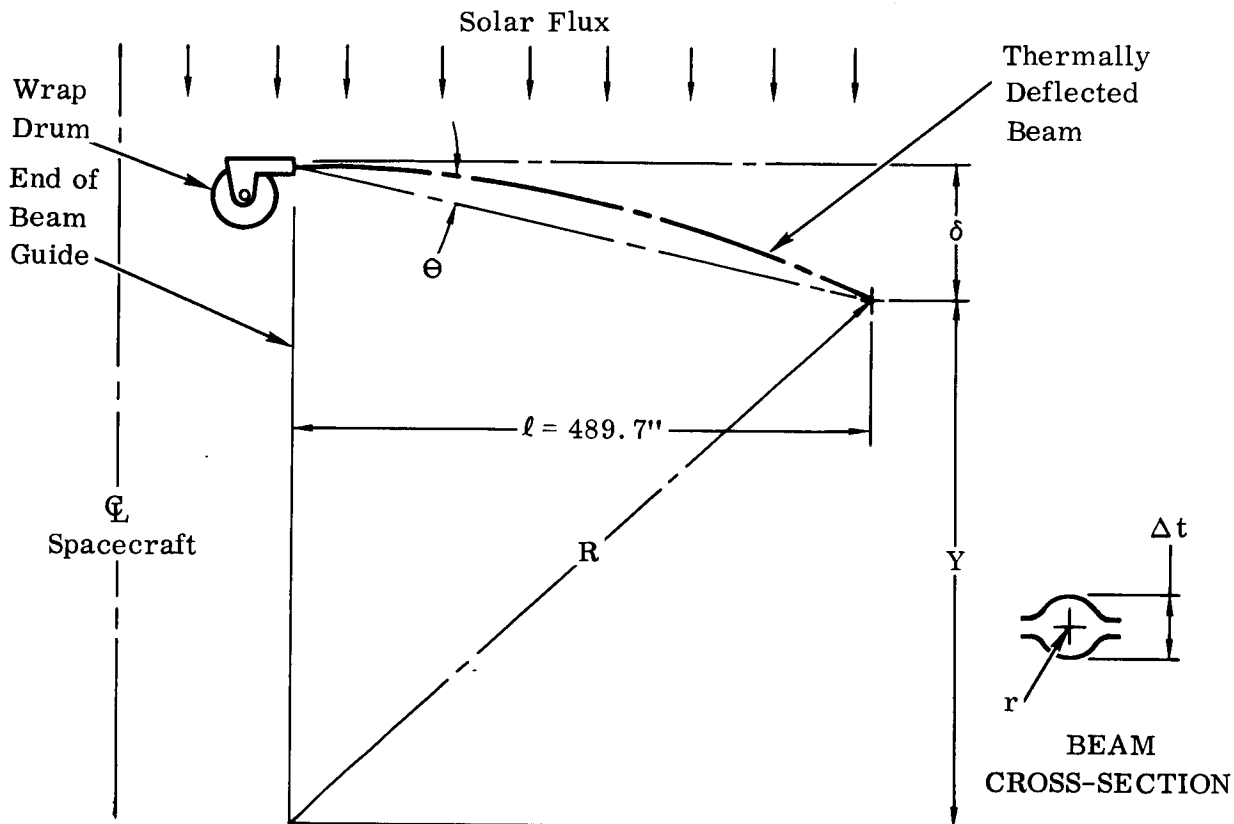
TABLE 5

PROPERTIES OF BEAM MATERIALS

	Titanium	Beryllium-Copper	Fiberglass
P	.16	.297	.06138
K	4.3	105.	.1
Cp	.135	.10	.31

	Symbols
ϵ	Emittance
α	Solar Absorptivity
P	Density lb/in ³
K	Thermal Conductivity BTU/hr°F ft.
Cp	Specific Heat BTU/lb°F

when a thermal gradient exists). Consideration of the latter requires a more detailed analysis than is performed in Section 3.3.2.9 of this report if normal-to-panel thermal gradients are to be obtained. For the parametric study performed in this section, therefore, an out-of-plane distortion constraint of $\pm 5^\circ$ for beam selection will be used. This assures that, when integrated with the selected substrate in the detailed analysis phase of the program, the constraint of $\leq \pm 10^\circ$ will be achieved. The out-of-plane angle, θ , that is referenced is shown in the following sketch.



Thermal deflection analysis is made using analogous stress-deflection theory for a beam with a uniform bending moment distribution along its length. This is based on the consideration that the temperature along the beam is nearly uniform and temperature gradients through the beam at any point along the beam are nearly equal. An example analysis is as follows:

$$R = \frac{EI}{M}$$

where,

$$M = \frac{(f_b) \cdot I}{r} = \frac{E \propto \cdot \frac{\Delta t}{2} \cdot I}{r} = \frac{E \propto \cdot \Delta t \cdot I}{2r}$$

Then,

$$R = \frac{EI \cdot 2r}{E \alpha \cdot \Delta t \cdot I} = \frac{2r}{\alpha \Delta t}$$

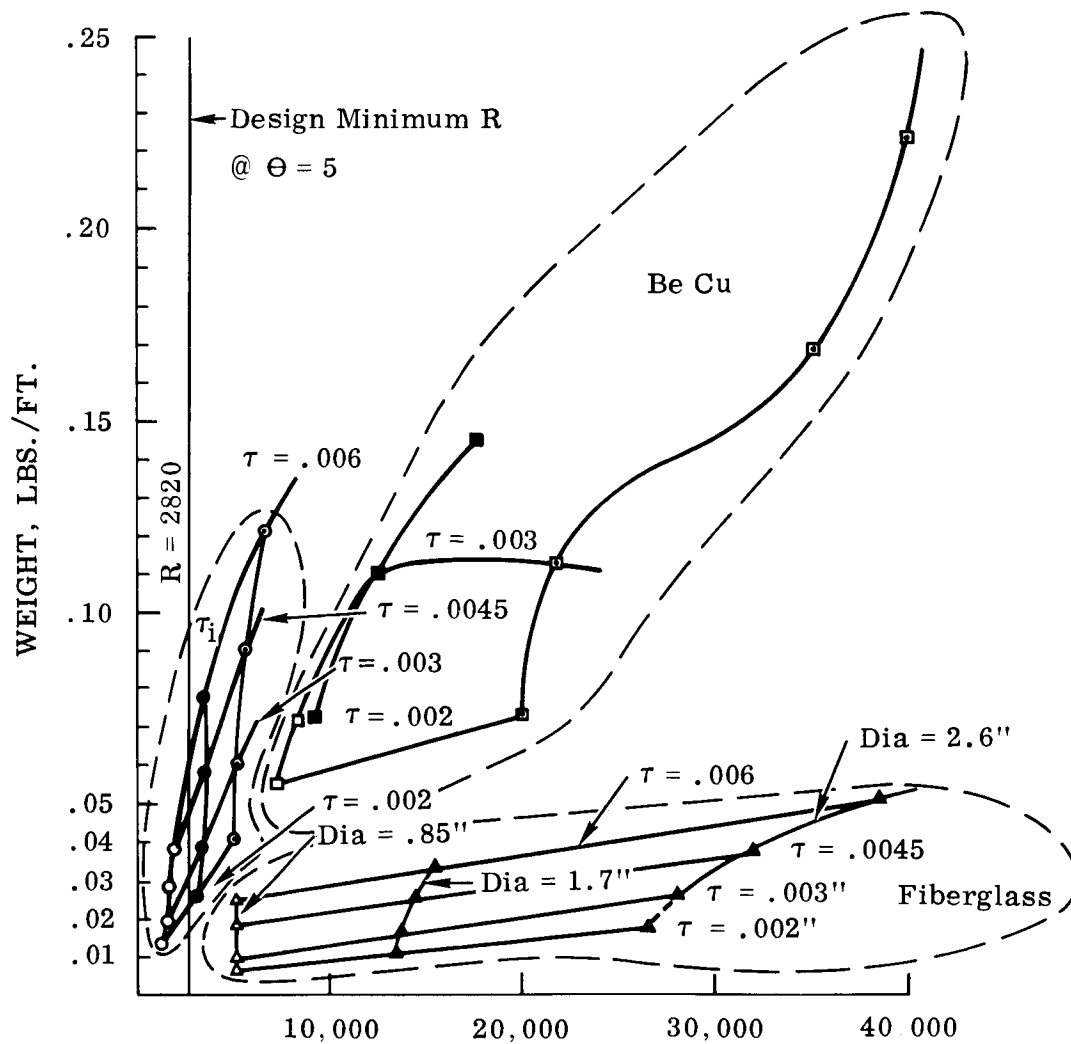
and,

$$\delta = R - Y = R - (R^2 - l^2)^{1/2}$$

$$\theta = \text{ARC TAN } \frac{\delta}{l}$$

Conclusions

Results of the beam thermal analysis were plotted in Figure 13 as a function of two critical parameters; (1) thermally distorted radius of curvature R and (2) weight in lbs./ft. of length. If we limit beam sheet thickness to .003 in. as a minimum for handling and fabrication reasons, the lightest beam to satisfy a thermal distortion constraint of $\theta = 5^\circ$ maximum ($R = 2820$ inches) would be of fiberglass and have a diameter of less than .85 in. This beam is not selected for use because, (a) it is structurally weak for demonstration of such a large panel area in a 1 g field and (b) its operating temperature is high (523°F) for fiberglass. The beam selected is 1.7 in. diameter and of 6AL-4V titanium material because, (a) temperature affects on this material are less critical ($T = 358^\circ\text{F}$), (b) it is more structurally compatible with a 1 g demonstration environment, (c) it meets the constraint requirement and (d) it is equal in weight to a fiberglass beam which would have to be approximately two inches diameter and would function at about 310°F . A beryllium-copper beam is not selected because it is heaviest.



THERMALLY DISTORTED RADIUS OF CURVATURE, $R = \frac{2r}{\alpha \Delta T}$, INCHES

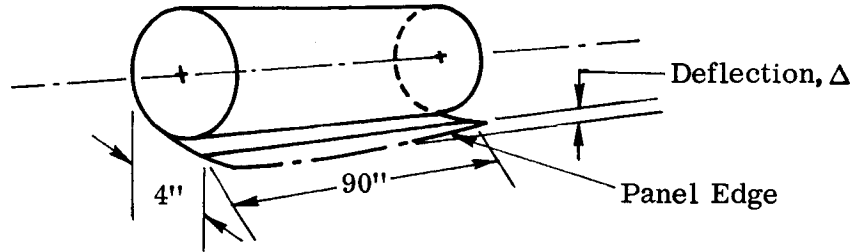
Titanium		Fiberglass		Beryllium Copper	
○	.85D	△	.85D	□	.85D
●	1.7D	▲	1.7D	■	1.7D
⊙	2.6D	▲	2.6D	▣	2.6D

Figure 13. Thermal Distortion Versus Weight for Various Beams

3.3.2.4 Beam Tip Intercostal Studies

Justification for Tip Intercostal

This study is made to determine the effects of launch vibration on the edge of the outer wrapped panel layer if the edge is not stabilized.



The natural frequency, F_n , is calculated as follows, assuming the 0.001 Kapton substrate to act as a catenary cable,

$$2\pi^4 EI_y + \frac{1}{8}\pi^4 EAY^3 = \frac{1}{2}wl^4$$

$$\therefore y(2\pi^4 EI) + y^3 \left(\frac{1}{8}\pi^4 EA \right) = \frac{1}{2}wl^4$$

$$y(2)(3.141)^4 (4.3 \times 10^5) (.282 \times 10^{-9}) + y^3 \left(\frac{3.141}{8} \right)^4 (4.3 \times 10^5) (.0015)$$

$$= \frac{.22(90)^4}{12(2)}$$

$$y(195.5)(4.3 \times 10^5) (.282 \times 10^{-9}) + y^3 (12.22)(4.3 \times 10^2)(1.5)$$

$$= 600,000$$

$$y(.0237) + y^3(789) = 600,000$$

$$\therefore y^3 789 \cong 600,000$$

$$y^3 = 760$$

$$y = 9.13 \text{ inch}$$

$$F_n = 3.53 \left(\frac{1}{\Delta_{ig}} \right)^{1/2} = 3.53 \left(\frac{1}{9.13} \right)^{1/2} = 3.53 \sqrt{.109} = 1.165 \text{ cps}$$

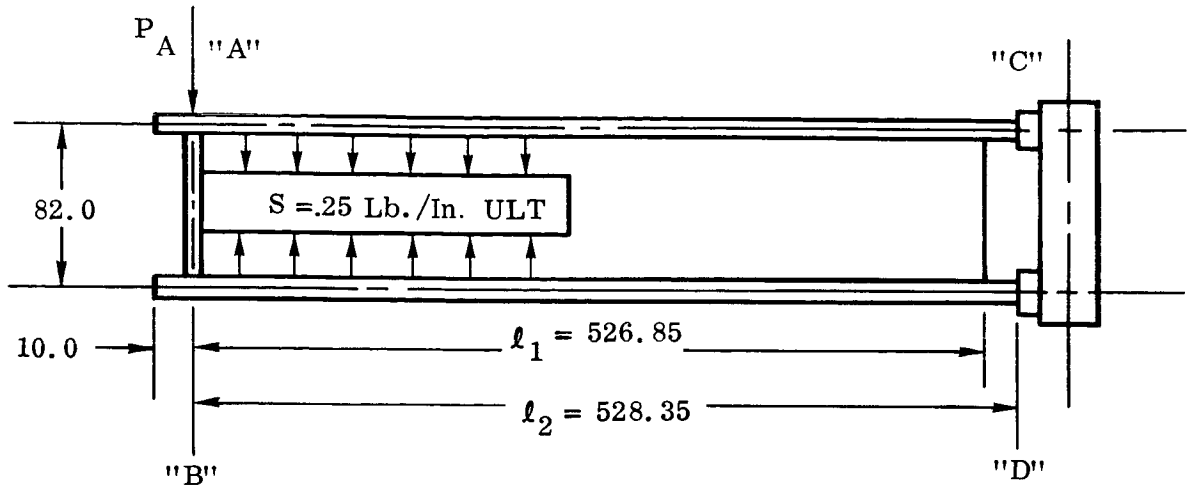
$$\Delta_{\text{DYN}} = \frac{386 (g_{\text{in}} \cdot Q)}{(2\pi f_n)^2} = \frac{386 (4) (10)}{[2 (3.141) (1.165)]^2} = \frac{15,400}{54.2}$$

$$\Delta_{\text{DYN}} = 285 \text{ inches}$$

This deflection is unrealistic but is indicative that an edge support is required to prevent excessive deflections and possible cell damage.

If we preload a sponge medium to 25% deflection this mode can be eliminated. It can be accomplished using a structural transverse member (tip intercostal) with a sponge silicone backing. The intercostal will also serve as a beam separation spacer with panel subject to normal plane loads when deployed.

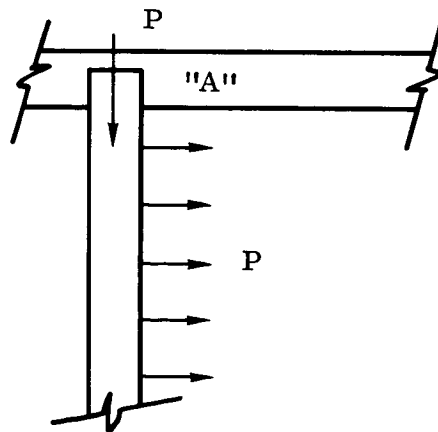
Configuration Studies



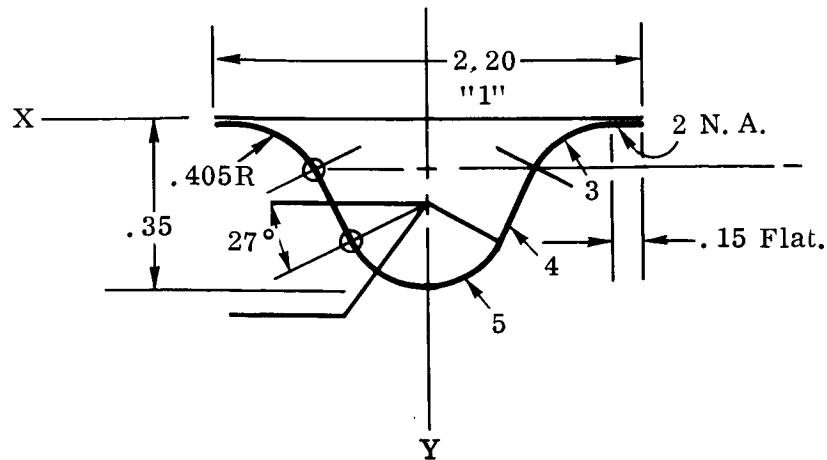
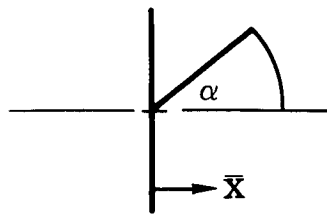
Side loading on beams "A-C" and "B-D" considering a 1 G roll out loading (in vacuum chamber): there is a 1.00 lb. (ULT) load at each of the clips, spaced on 4 in. ϕ to ϕ , $s = 1.00 \text{ lb.}/4.00 \text{ in.} = .25 \text{ lb./in. ULT}$.

Normal load on intercostal "A - B", $P = s\ell_1/2 = .25 (526.85)/2 = 65.87 \text{ lb. ULT}$.

Side loading on intercostal, $P = .05 \text{ lb./in.}$



Configuration (A) —



About "X-X" axis:

Elem	b	h	A	d	Ad	Ad ²	I _o
1	1.10	t	1.1000t	.002	.00220t	—	—
2	.15	t	.1500t	.006	.00090t	.00001t	—
3	—	—	.4453t	.085	.03785t	.00322t	.00165t
4	1.1223t	.40	.4489t	.420	.18854t	.07919t	.00599t
5	—	—	.4453t	.773	<u>.34422t</u>	<u>.26608t</u>	<u>.00165t</u>
$\Sigma 1/2$			2.5895t		.57371t	.3485t	.009292t
$2 \Sigma 1/2$			5.1790t		1.14742t	.6970t	.01858t

$$(4) \quad t' = t / \cos 27^\circ = t \sec 27^\circ = 1.1223t$$

$$(3) \quad A = \alpha r t = \left[(90 - 27) / 57.3 \right] (.405)t = .4453t$$

$$\bar{X} = r \sin \alpha / \alpha = .405 \sin 63^\circ / (63 / 57.3) = .405 (89101) / 1.0995$$

$$\bar{X} = .328$$

$$d = r - \bar{X} + .008 = .405 - .328 + .008 = .085''$$

$$I_o = I_{NA} = r^3 (t) \left[\alpha / 2 + (\sin 2\alpha) / 4 - (\sin^2 \alpha) / \alpha \right]$$

$$= (.405)^3 t \left[(1.0996 / 2) + (.78801 / 4) - (89101)^2 / 1.0996 \right]$$

$$I_{NA} = .00165t$$

$$(5) \quad d = .850 - r + \bar{X} = .850 - .405 + .328 = .773$$

$$(4) \quad I = bh^3/12 = 1.1223t(.4)^3/12 = .11223t(.4)^2/3 = .00599t$$

$$\bar{X}_{CG} = \Sigma Ad/\Sigma A = 1.14742t/5.179t = .2216'' = a$$

$$I_{NA} = .6970t + .01858t - .2216(1.14742)t = .4613t$$

$$P_{CR} = n^2 \pi^2 EI/L^2$$

$$I_{REQ} = PL^2/n^2 \pi^2 E = 68.87(82.0)^2/(1)^2 \pi^2 16(10^6)$$

$$I_{REQ} = .4613t = .463082/157.91 = .0029325$$

$$t_{REQ} = .0029325/.4613 = .00636$$

Letting $t = .007$,

$$j = \sqrt{EI/P} = \sqrt{16(10^6)(.4613)(.007)/(68.87)} = \sqrt{7.5019(10^2)}$$

$$j = 27.39$$

$$L/2j = 82.0/2(27.39) = 1.4969 \text{ Rad} = 85^\circ 46'$$

$$M_{L/2} = Pa \sec L/2j = 68.87(.2216)(13.575) = 207.18 \text{ in. lb. ULT.}$$

$$f_{bcx} = M_x C/I_x = 207.18(.2216)/.4613(.007) = 45.911/.003229$$

$$f_{bcx} = 14,218 \text{ psi ULT.}$$

$$f_{co} = P/A = 68.87/5.179(.007) = 1900 \text{ psi ULT}$$

$$M_{yL/2} = Wj_y^2 (\sec L/2j - i)$$

$$j_y^2 = EI/P = 16(10^6)(1.937)(.007)/68.87 = 3150.05$$

$$j = 56.12$$

$$L/2j = 82.0/2(56.12) = .7306 \text{ Rad} = 41^\circ 52'$$

$$M_{yL/2} = (.05)(3150.05)(1.3428) = 1211.49$$

$$f_{co_y} = M_u C/I_y = 1211.49(1.1)/1.937(.007) = 232.64/.013559$$

$$f_{bc_y} = 17,156 \text{ psi ULT.}$$

$$f_{c_{MAX}} = f_{bcy} + f_{co} = 17,156 + 1900 = 18,956 \text{ (t = .007)}$$

For flat element simply supported; Reference 9, p. 371,

$$F_{cr} = 3.6 E (t/b)^2 = 3.6(16) (10^6) (.007/1.90)^2$$

$$F_{cr} = 3.6(16) (7/1.9)^2 = 781.8 \text{ psi}$$

THIS CONFIGURATION NOT ADEQUATE.



Elem	b	h	n	A	d	Ad	Ad ²	I _O
1	1.30	t	1	1.3000t	.002	.0026t	.00001t	—
2	.40	t	2	.8000t	.006	.0048t	.00003t	—
3	t	.40	2	.8000t	.180	.1440t	.02592t	.01067t
4	—	—	1	.6283t	.145	.0911t	.01321t	.05027
5	t	.40	2	.8000t	.600	.4800t	.28800t	.01067t
6	—	—	2	1.2566t	1.055	1.3257t	1.39863t	.10053t
7	.50	t	1	<u>.5000t</u>	1.200	<u>.6000t</u>	<u>.30000t</u>	<u>—</u>
				6.0849t		2.6482t	2.0258t	.17214t

(4) 6) $A = n \alpha r t = n(\pi/2)(.4)t = .62832 \text{ nt}$

$$(4) \quad \bar{X} = .6366r \quad d = r(1 - .6366) = .4(.3634) = .145''$$

$$(6) \quad \bar{X} = .6366r \quad d = .8 + \bar{y} = .8 + (.4)(.6366) = 1.055$$

$$(4) \ 6) I_{NA} = n\pi r^3 t/4 = (.4)^3 \pi nt/4 = .050266t$$

$$\bar{y}_{CG} = \Sigma Ad / \Sigma A = 2.6482t / 6.0849t = .4352''$$

$$I_{CG} = 2.0258t + .17214t - .4352(2.6482)t$$

$$I_{CG} = 1.0454t$$

About "Y" axis:

Elem	b	h	n	A	d	Ad	Ad ²	I _O
1	t	1.3	1	1.3000t	1.050	1.36500t	1.43325t	.18308t
2	t	.8	1	.8000t	1.300	1.04000t	1.35200t	.04267t
3	.40	t	2	.8000t	1.300	1.04000t	1.35200t	—
4	—	—	2	1.2566t	.145	.18221t	.02642t	.10053t
5	.40	t	1	.4000t	0	—	—	—
6	—	—	1	1.6283t	1.155	.72568t	.83817t	.05027t
7	t	.5	1	.5000t	.650	.32500t	.21125t	.01042t
8	.40	t	1	.4000t	1.300	.52000t	.67600t	—
				6.0849t		5.1979t	5.8891t	.3870t

$$(6) \quad d = 1.3 - .4 + \bar{y} = .9 + .6366r = .9 + (.6366)(.4) = 1.155$$

$$(4) \quad d = r - X = r(1 - .6366) = .4(.3634) = .145$$

$$\bar{X} = \Sigma Ad / \Sigma A = 5.1979t / 6.0849t = .8542 \text{ in.}$$

$$I_{CGY} = 5.8891t + .3870t - (.8542)(5.1979t)$$

$$I_{CGY} = 1.836t \quad I_y = 1.937t$$

$$t = .004 \quad a = \bar{y}_{CG} = .4352 \quad W_x = 0$$

$$j = \sqrt{EI/P} = \sqrt{16(10^6)(1.0454)(.004)/68.87} = \sqrt{9.7148(10^2)}$$

$$j = 31.17$$

$$L/2j = 82/(2)(31.17) = 1.3154 \text{ rad} = 75^\circ 22'$$

$$P_{CR} = n^2 \pi^2 EI / L^2 = \pi^2 16(10^6)(1.0454)(.004) / 82.0^2$$

$$P_{CR} = .660335(10^6) / 6724 = 98.2 \text{ lb.}$$

$$\sec L/2j = 3.9583$$

$$M = Pa \sec L/2j = 68.87(.4352)(3.9583)$$

$$M_{L/2} = 116.84 \text{ in. lb. ULT}$$

$$(X) \quad f_{bcx} = MC/I = 116.84(4.352)/1.0454(.004) \\ = 116.84(.4352)/.0041816 = 12,160 \text{ psi ULT}$$

$$f_{co} = P/A = 68.87/6.0849(.004) = 68.87/02434$$

$$f_{co} = 2,829 \text{ psi ULT}$$

Due to side load $p = .05 \text{ lb./in.}$

$$(Y) \quad f_{bc} = MC/I_y = M_y \bar{Y}/I_y = M(.8542)/1.937(.004) = 110.25 M_y$$

$$M_y = Wj^2 \left[\sec L/2j - 1 \right]$$

$$j_y = \sqrt{EI_y/P} = \sqrt{16(10^6)1.937(.004)/68.87} = \sqrt{18.10^2}$$

$$j_y = 42.49$$

$$L/2j = 82.0/2(42.49) = .9649 \text{ rad} = 55^\circ 17'$$

$$M_y = .05(1800)(1.7559 - 1) = 68.03 \text{ in. lb. ULT}$$

$$f_{bcy} = 110.25 M_y = 110.25(68.03) = 7,500 \text{ psi ULT}$$

$$f_{cMAX} = f_{bcx} + f_{co} = 12,160 + 2,829 = 14,989 \text{ psi ULT at } P_T \text{ "A"}$$

$$(t = .004)$$

Crippling allowable in intercostal,

$$b_2 = bf_2 + 1.07 R = .4 + 1.07(.4) = .828$$

$b/t = .828/.004 = 207$; Reference 10, for flat simply supported plate; Reference 9, p. 371,

$$F_{CR} = 3.62 E (t/b)^2 = 3.62(16)(10^6)/(207)^2$$

$$F_{CR} = 57.92(10^2)/4.2849 = 1,352 \text{ psi ULT}$$

This is for simply supported edges and an infinitely long sheet.

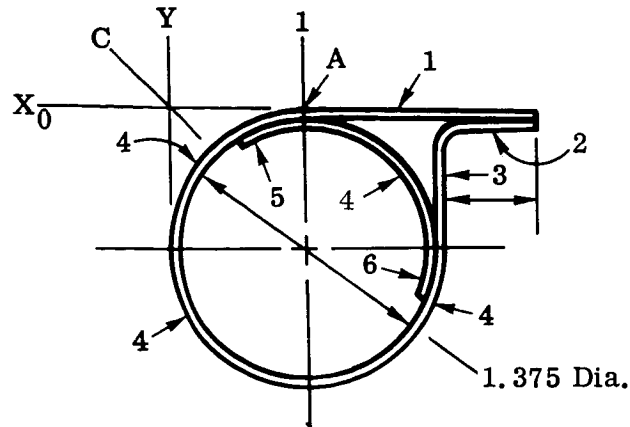
For curved corner elements,

$$F_{c_{cr}} = (.30) E (t/R) = (.606) (16) (10^6) (.004 / .4)$$

$$F_{c_{cr}} = (.30) (16) (.01) 10^6 = 48,000 \text{ psi}$$

THIS CONFIGURATION NOT ADEQUATE.

Configuration (C) —



About "X" Axis:

Elem	b	h	A	d	Ad	Ad ²	I _O
1	1.19	t	1.190t	.002	.0024t	—	—
2	.50	t	.500t	.004	.0020t	—	—
3	t	.69	.690t	.360	.2484t	.0894t	.0274t
4	—	—	4.300t	.688	2.9563t	2.0324t	1.0209t
5	.32	t	.320t	.010	.0320t	—	—
6	t	.32	.320t	.850	.2720t	.2312t	.0027t
			7.320t		3.5131t	2.3530t	1.0510t

$$4) 7) \quad A = \pi Dt = \pi(1.375)t = 4.320t$$

$$I = \pi D^3 t / 8 = \pi(1.375)^3 t / 8 = 1.0209t$$

$$y_{NA} = \Sigma Ad / \Sigma A = 3.5131t / 7.320t = .4799'' = a$$

$$I_{NA} = 2.3530t + 1.0510t - (.4799)(3.5131) = 1.718t$$

About "Y_o" Axis:

Elem	b	h	A	d	Ad	Ad ²	I _o
1	t	1.19	1.190t	1.283	1.5268t	1.9588t	.1404t
2	t	.50	.500t	1.625	.8125t	1.3203t	.0274t
3	.69	t	.690t	1.375	.9488t	1.3045t	—
4	—	—	4.300t	.690	2.9670t	2.0472t	1.0209t
5	t	.32	.320t	.530	.1696t	.0899t	.0027t
6	.32	t	.320t	1.365	.4368t	.5962t	—
Σ			7.320t		6.8615t	7.3169t	1.1914t

$$\bar{X}_{CG} = \Sigma Ad / \Sigma A = 6.8615t / 7.320t = .9374$$

$$I_{CG} = 7.3169t + 1.1914t - (.9374)(6.8615) = 2.0763t$$

a) $t = .004$ $a = \bar{y}_{CG} = 1.718t$ $W_x = 0$ $P = 65.87$

$$j_x = \sqrt{EI/P} = \sqrt{16(10^6)1.718(.004)(65.87)} = \sqrt{1669.23}$$

$$j_x = 40.86$$

$$L/2j_x = 82.0/2(40.86) = 1.00343 \text{ rad} = 57^\circ 30'$$

$$\sec L/2j_x = 1.8612$$

$$M_{L/2} = Pa \sec L/2j = 65.87(.4799)(1.8612) = 58.83 \text{ in. lbs. ULT}$$

$$f_{bcx} = Mc/I = 58.83(.4799)/1.718(.004) = 58.83(.4799)/.006872$$

$$f_{bcx} = 4,108 \text{ psi ULT at Point "A"}$$

$$f_{co} = P/A = 65.87/7.320(.004) = 65.87/.02928$$

$$f_{co} = 2,250 \text{ psi ULT at Points "A" and "B"}$$

Side load due to $W_y = .05$:

$$j_y = \sqrt{10^6(16)(2.0763)(.004)/65.87} = \sqrt{2017.35} = 44.92$$

$$L/2j_y = 41/44.92 = .9127 \text{ rad} = 52^\circ 18'$$

$$M_{L/2y} = Wj^2 (\sec L/2j_y - 1) = .05 (2017.35) (1.6353 - 1)$$

$$M_{L/2y} = 64.08 \text{ in. lbs. ULT}$$

$$f_{bcy} = MC/I_y = 64.08 (.9374)/2.0763 (.004) = 64.08 (9374)/.0083052$$

$$f_{bcy} = 7,233 \text{ psi ULT (This is MAX stress and occurs at Point "B".)}$$

$$f_{C\text{MAX}} = f_{bcy} + f_{co} = 7,233 + 2,250 = 9483 \text{ psi ULT at Point "B".}$$

At point C, (45°),

$$C_x = Y_{CG} - (r - r \cos 45^\circ) = .4799 - 1.375 (1 - 70711)/2 =$$

$$C_x = .4799 - .2014 = .2785$$

$$C_y = \bar{X}_{CG} - (r - r \cos 45^\circ) = .9374 - .2784 = .6590$$

$$f_{bcx} = M_x C_x / I_x = 58.83 (.2785) / .006872 = 2384 \text{ psi ULT}$$

$$f_{bcy} = M_y C_y / I_y = 64.08 (.6590) / .0083052 = \underline{5,085}$$

$$f_{bcxy} = 2,384 + 5,085 = 7469$$

$$f_{C\text{MAX}} = f_{bcxy} + f_{co} = 7,469 + 2250 = 9719 \text{ psi ULT}$$

For tubular section,

$$R/t = D/2t = 1.375/2(.004) = 172$$

$$Z = (L^2/rt)(1 - N^2)^{1/2} = \left[(82.0)^2 / (1/2) (1.375) (.004) \right] (1 - .3^2)^{1/2}$$

$$Z = (82.0)^2 (.954) / (.00275) = 2.333 (10^6)$$

This is in the very long tube range \therefore use,

$$F_{CCR} = (.3)Et/R = (.3) 16 (10^6) (.004) (2) / 1.375$$

$$F_{CCR} = 300 (16) (8) / 1.375 = 27,927 \text{ psi}$$

$$P_{CR} = n^2 \pi^2 EI / L^2 = \pi^2 (16) (10^6) (.006872) / (82.0)^2$$

$$P_{CR} = 1.0852 (10^6) / 6724 = 161.39 \text{ lb.}$$

$$R_{c_{cr}} = f_c / F_{CCR} = 9,719 / 27,927 = .348$$

$$R_{C_o} = P / P_{CR} = 65.87 / 161.39 = .408$$

$$M.S. = 1 / (R_{c_{cr}} + R_{C_o}) - 1 = 1 / (.348 + .408) - 1$$

$$M.S. = 1 / (.756) - 1 = \underline{.32} \text{ at } \underline{Q} \text{ beam.}$$

This was not combined with torsion since MAX torsion is at beam supports and is zero at beam \underline{Q} .

Torsion,

$$T = W(L/2)r = (.05)(82.0/2)(1.375/2) \text{ at beam end}$$

$$T = 1.409 \text{ in. lbs. ULT}$$

$$f_s = Tc/5 = (1.405)(1.375)/(2)(2)(1.0209)(.004)$$

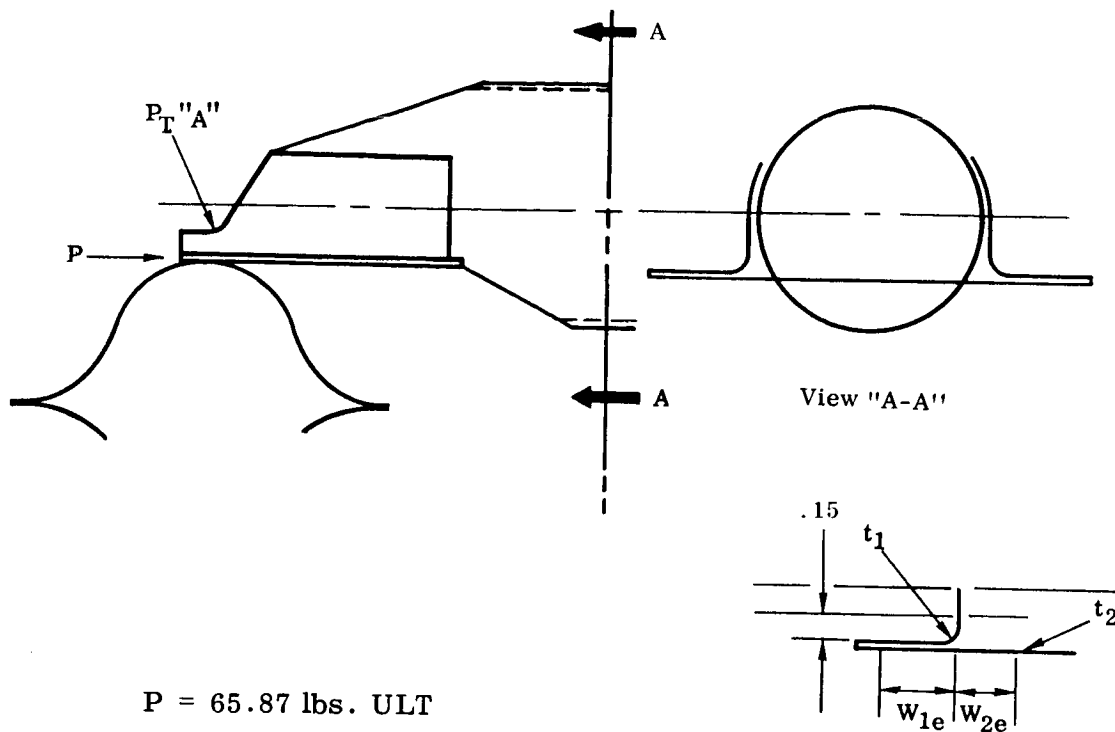
$$f_s = (1.405)(1.375)/.0163344 = 1183 \text{ psi ULT}$$

$$\begin{aligned} F_{s_{cr}} &= .272 E(t/r)^{3/2} / (i - \mu^2)^{3/4}; \text{ Reference 11, p. 353,} \\ &= (.272)(16)(10^6) \left[.004 / (1.37512) \right]^{3/2} / (.91)^{3/4} \\ &= 43.52 (10^6) (10^{-2})^{3/2} (.5818)^{3/2} / (.9316) \\ &= 43.52 (10^3) (.4438) / .9316 \end{aligned}$$

$$F_{s_{CR}} = 20,732 \text{ psi}$$

This is in the circular portion of the tip intercostal, at the attachment transition.

Transition attach area



$$P = 65.87 \text{ lbs. ULT}$$

for $t_1 = t_2 = .004$ and at Point "A".

letting $W_{1e} = .60$ full effective

$W_{2e} = .75$ full effective

$$A = 2(.60)t + .75t + .15t$$

$$A = (1.2 + .75 + .15)t = 2.00t = 2.00(.004) = .008$$

$$f_c = D/2A = 65.87/(2)(.008) = 65.68/.016 = 4,105 \text{ psi ULT}$$

$$b/t = .30/.004 = 75$$

For simply supported plate $b = 2W_{2e} = 1.5$

$$F_{CCR} = 3.62 E(t/b)^2 = 3.62 (16) (10^6) (.004/1.5)^2; \text{ Reference 9, P. 371,}$$

$$F_{CCR} = 3.62 (16) (8/3)^2 = 412 \text{ psi ULT}$$

Increasing $t_2 = .008$,

$$A = (.60 + .15)t_1 + 1.35t_2 = .75(.004) + 1.35(.008) = .01380$$

$$f_c = 65.87/2(.0138) = 65.87/ (.0276) = 2,387 \text{ psi ULT}$$

$$F_{c_{cr}} = 3.62(16)(10^6)(.008/1.5)^2 = 4(412) = 1648 \text{ psi}$$

$$\text{Assume } W_{2e} = .50 \quad b = 2W_{2c} = 1.00$$

$$F_{c_{cr}} = 3.62(16)(10^6)(.008)^2 = 3,707 \text{ psi}$$

$$A = (.60 + .15)t_1 + (.60 + .50)t_2 = .75(.004) + 1.10(.008) = .0118$$

$$f_c = 65.87/2(.0118) = 2,791 \text{ psi, adequate in crippling.}$$

3.3.2.5 Wrap Drum Studies

The method of approach used for the wrap drum analysis is presented first for review. At the end of this section a graph showing the results of analysis in depth for the ring stiffened concept is given. Conclusions are then drawn from that graph.

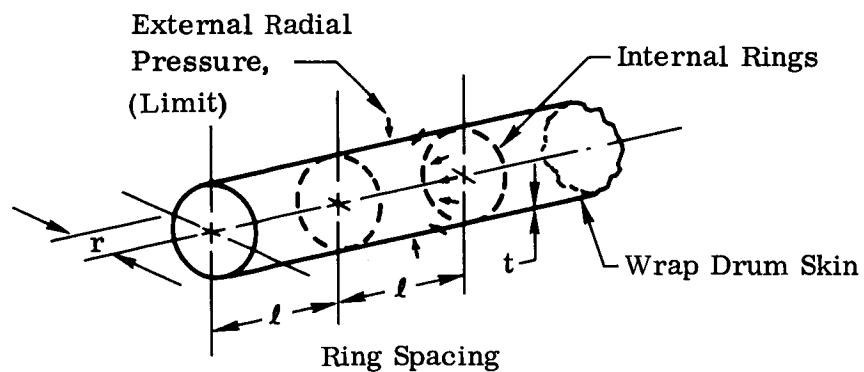
The basic considerations in structural design of the wrap drum are (1) minimum torsion deflection during actuation if driving the opposite beam through the drum; (2) sufficient longitudinal bending stiffness to withstand launch vibration excitations; and (3) sufficient radial elastic stability to withstand radial pressures induced during launch if the array layers are excited in a radial "breathing" mode of vibration. Since this design drives through an auxiliary torque tube and the fact that torsion considerations are less severe than bending considerations, torsion will not be considered here.

Two design concepts are given consideration: (1) ring-stiffened magnesium with lightening holes and (2) bonded honeycomb construction consisting of fiberglass skin and aluminum honeycomb. Wrap drum temperatures during launch are considered not to exceed 75 °F. The prime constraints set forth here for use in selecting the optimum drum are (1) minimum weight, and (2) dynamic deflection limited to 0.25 inch, act as a constraint to minimize the possibilities of structure damage to the solar cell installation and to minimize the clearance required between drum and adjacent structure. The 0.25-inch dynamic deflection may be a conservative number but will be verified later in the vibration test.

Ring-Stiffened Concept Considerations

The ring spacing is selected to prevent radial elastic instability with loads induced if a radial "breathing" mode of vibration is excited. The spacing is largely a function of drum radius, r , and skin sheet thickness, t . The controlling equation for a unit length of drum is a function of,

$$\text{Allowable Radial Pressure} = f\left(\frac{t}{r}\right)^3 \quad (\text{Ref. 7, Pg. C.B. 11})$$



which shows that t should be maximized while r is minimized. This holds true for longitudinal bending capability as well, so long as natural longitudinal vibration frequency is not critical. A suggested way to reduce weight and yet maximize t is to add numerous small lightening holes

(30 percent area reduction feasible) in the skin. Holes would not be considered if torsional stiffness requirements were more critical. For example, if we consider a minimum wrap drum radius of six inches, the skin thickness and ring spacing, ℓ , relationship to prevent radial elastic instability is calculated using Roark, (Reference 11) page 318, Case Q.

$$P_{CR} = 1.25P = .807 \frac{Et^2}{\ell r} \left[\left(\frac{1}{1 - \mu^2} \right)^3 \cdot \frac{t^2}{r^2} \right]^{1/4}$$

$$1.25P = .807 \frac{E}{r} \left(\frac{t^{5/2}}{\ell} \right) \left[\left(\frac{1}{1 - \mu^2} \right)^3 \cdot \frac{1}{r^2} \right]^{1/4}$$

$$\left(\frac{\ell}{t^{5/2}} \right) = .646 \cdot \frac{E}{pr} \left[\left(\frac{1}{1 - \mu^2} \right)^3 \cdot \frac{1}{r^2} \right]^{1/4} \quad \begin{array}{l} E = 6.5 \times 10^6 \text{ psi} \\ \mu = .35, \text{ for} \\ \text{AZ31B-H24} \\ \text{Magnesium at R.T.,} \\ \text{Reference 12} \end{array}$$

For $r = 6 \text{ in.}$, and $p = .61 \text{ lbs/in}^2$ (O-Peak) Dynamic Load based on 50 g response accel. at Resonance if 2/3 of wraps vibrate in a radial breathing mode.,

$$\left(\frac{\ell}{t^{5/2}} \right) = .646 \cdot \frac{6.5 \cdot 10^6}{.61 \cdot 6} \left[\left(\frac{1}{1 - .35^2} \right)^3 \cdot \frac{1}{6^2} \right]^{1/4}$$

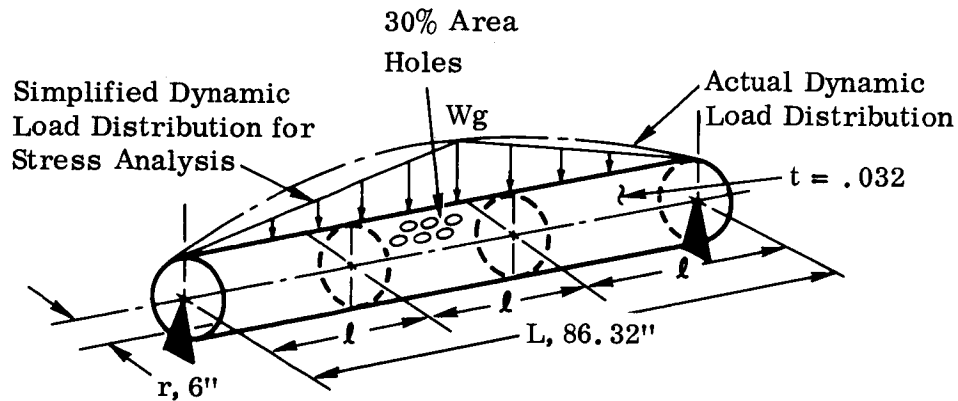
$$= .646 \cdot \frac{6.5 \cdot 10^6}{.61 \cdot 6} \cdot .45$$

$$\left(\frac{\ell}{t^{5/2}} \right) = 5.16 \cdot 10^5$$

t	t, 30 PERCENT LIGHTENING HOLES	RING SPACING, ℓ	NUMBER OF INTERMEDI- RINGS	t EFFECTIVE FOR 86.32 IN. DRUM
.025	.017	19.5	3	.0174
.030	.020	29.3	2	.0203
.032	.021	33.2	2	.0213
.036	.024	46.2	1	.0242
.036	.024	46.2	2	.0243

*Note small difference in effective t when adding one more intermediate ring.

For the example case, we will consider a 0.032 inch skin drum with two intermediate rings and analyze for bending induced if the wrap drum is excited by sinusoidal vibration at its fundamental longitudinal frequency during launch. The effect of end moment restraint is considered negligible. All panel wraps are considered to vibrate in phase at 50 g's response acceleration for this vibration mode.



Let $W = 0.68$ pound/inch to include wrap drum, and wrapped panel with a solar cell installation weight of 0.19 pound/square foot.

$$f_b = \frac{Mr}{I} = \frac{Mr}{\pi r^3 t_e} = \frac{(Wg) \cdot L^2}{12\pi r^2 t_e}$$

$$f_b = \frac{(.68 \times 50) \times 86.32^2}{12\pi \times 6^2 \times .021} = 8889 \text{ psi limit}$$

11111 psi ULT.

$$F_{b_{cR}} = 1.3 \text{ CE } \frac{t}{r} \quad \left[\begin{array}{l} C = .3, \text{ Reference 13, Figure 5.4.2,} \end{array} \right]$$

$$= 1.3 \times 3 \times 6.5 \times 10^6 \times \frac{.032}{6}$$

$$F_{b_{cR}} = 13520 \text{ psi}$$

$$\text{M.S.} = \frac{F_{b_{cR}}}{f_b} - 1 = \frac{13520}{11111} - 1 = +.22 \text{ ULT.}$$

The fundamental bending frequency is calculated as,

$$f_n = 3.53 \left(\frac{1}{\delta_{1g}} \right)^{1/2}$$

$$\delta_{1g} = \frac{\delta W l^4}{384 E(I)}, \text{ Reference 5, Page 102, Case 13}$$

$$\delta_{1g} = \frac{5 \times .68 \times 86.32^4}{384 \times 6.5 \times 10^6 (\pi \times 6^3 \times .7 \times .032)} = .005 \text{ in.}$$

$$f_n = 3.53 \left(\frac{1}{.005} \right)^{1/2} = \underline{49.9} \text{ cps}$$

Maximum deflection at fundamental bending frequency is calculated from the equation for sinusoidal vibration:

$$\delta_{(\text{dynamic})} = \frac{386 (\text{g response})}{(2\pi f_n)^2} = \frac{386 (50)}{(2\pi \times 49.9)^2}$$

$$\delta_{(\text{dynamic})} = \underline{.20 \text{ in.}} \text{ Single Amplitude}$$

The above weight, f_n , and dynamic deflection of the drums analyzed are plotted in Figure 14 to facilitate selection of the optimum drum.

Honeycomb Concept Considerations:

Considerations are given to a honeycomb concept for the reasons that (1) providing the core density is low, it would be more efficient for radial breathing mode external pressures because of the greater effective section thickness. If we consider a 0.125-inch thick aluminum honeycomb section with bonded facings of fiberglass, the facing thickness for a weight savings of only one percent compared to the magnesium ring-stiffened concept used in the example is calculated as follows:

$$t = \frac{1}{2} \cdot \frac{(.99 t_{\text{eff}} \rho_{\text{mag.}} - \text{core WT/in.}^2 - \text{adhesive WT/in.}^2)}{\rho_{\text{fiberglass}}}$$

$$t = \frac{1}{2} \cdot \frac{(.99 \times .0213 \times .0639 - 2.24 \times 10^{-4} - 3.47 \times 10^{-4})}{.065}$$

$$t = .0060 \text{ in.}$$

For the longitudinal bending mode of vibration, the facing elastic dimpling and working stresses are calculated, respectively, as follows, neglecting solar cell stabilization effects,

$$\sigma_{\text{cR}} = 2 \frac{E}{(1 - \mu^2)} \left(\frac{t}{s} \right)^2 \quad \left| \text{Reference 14} \right.$$

$$\sigma_{\text{cR}} = 2 \times \frac{5 \times 10^6}{(1 - .12^2)} \cdot \left(\frac{.006}{.125} \right)^2 = 23377 \text{ psi}$$

$$f_{\text{bc}} : f_{\text{bc}(\text{ring-stiffened})} \cdot \left(\frac{t_{\text{ring-stiffened}}}{2t_{\text{fiberglass}}} \right) = 11111 \left(\frac{.021}{2 \times .006} \right)$$

$$= 19444 \text{ psi ULT.}$$

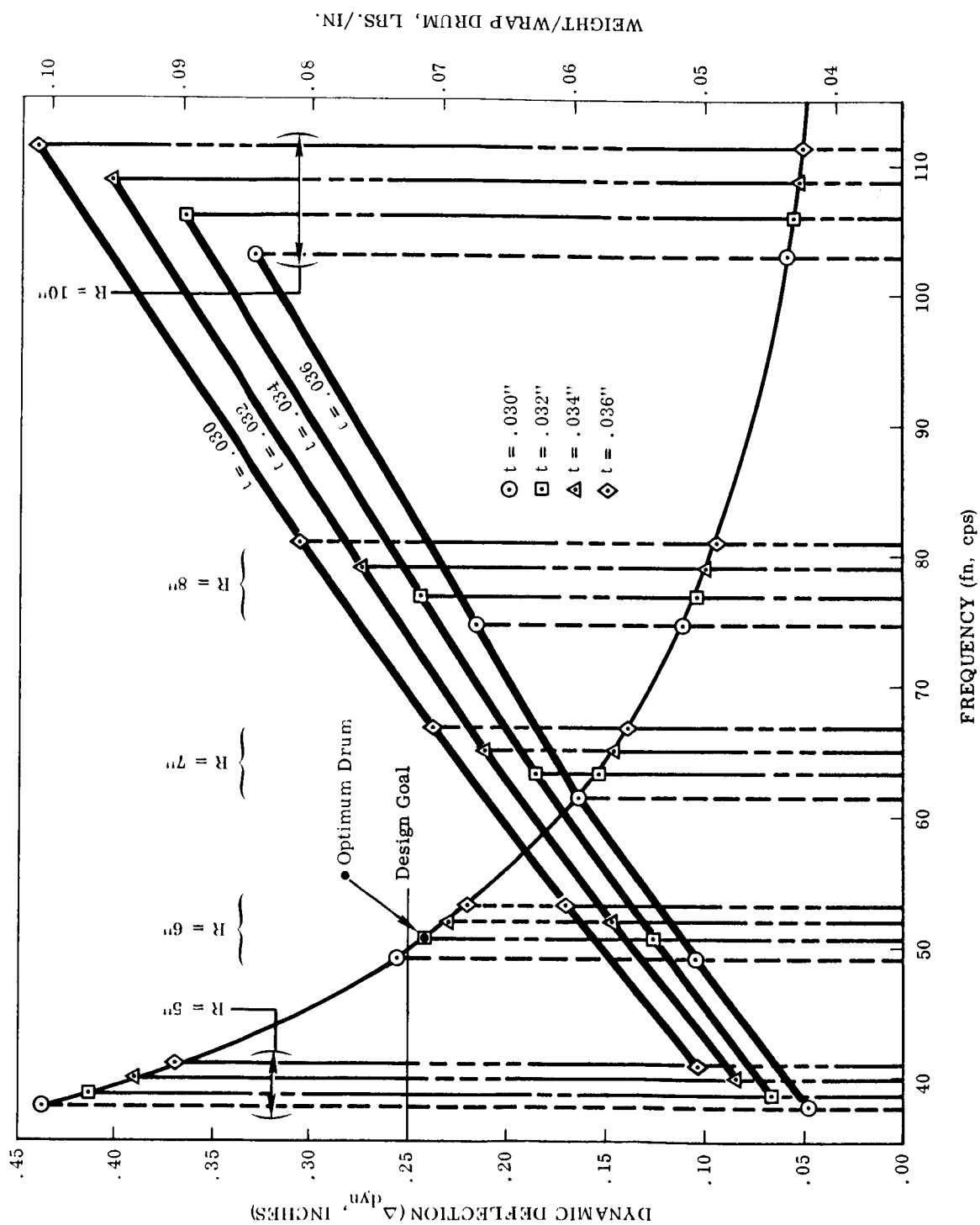


Figure 14. Wrap-Drum Optimization

$$M.S. = \frac{G_c R}{f_{bc}} - 1 = \frac{23377}{19444} - 1 = \underline{+.20} \text{ on ULT.}$$

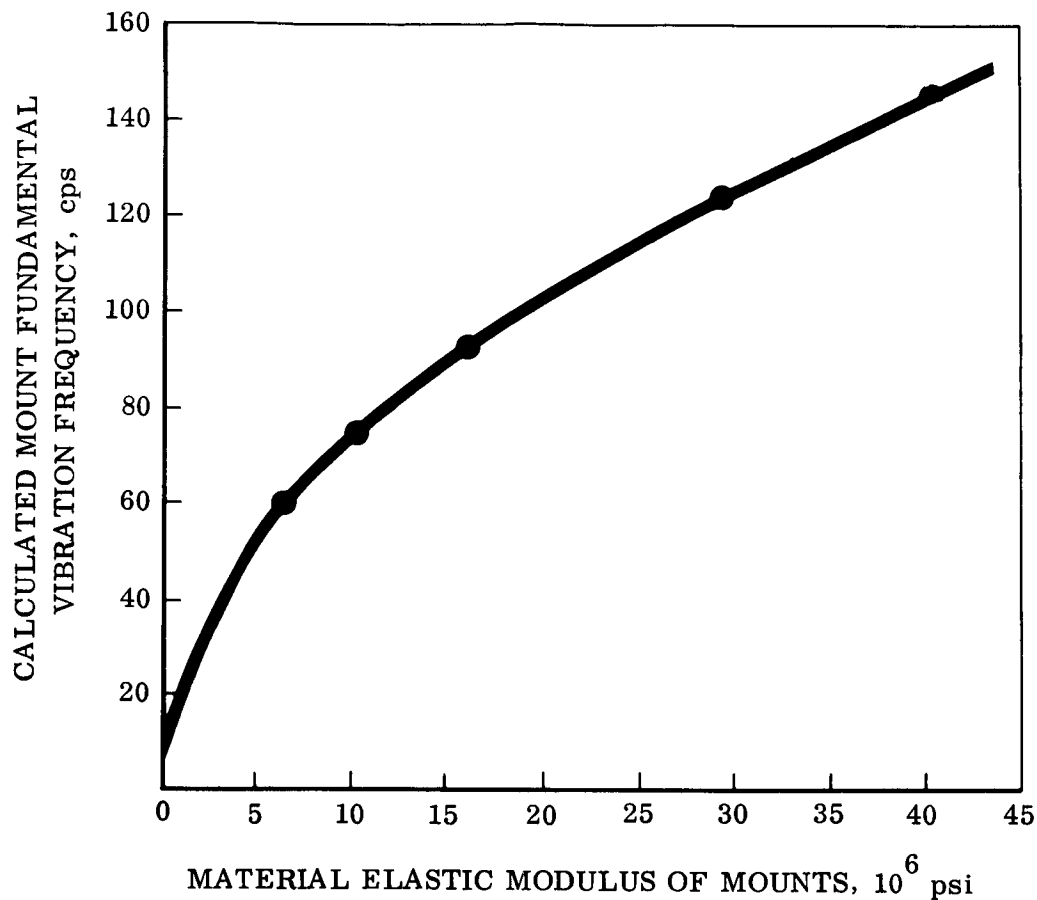
Therefore, a weight savings using the honeycomb wrap drum in place of the magnesium ring-stiffened drum would be about one percent; the longitudinal bending frequency would be lowered to about 38 cps with a resulting increase in dynamic deflection to about 0.35 inch, which is higher than desired for protection of the stowed solar cells. Based on an equal deflection basis, the honeycomb concept would weigh more than the magnesium ring-stiffened concept by an amount equal to the weight of honeycomb core and facing adhesives.

Conclusions

The study shows that the optimum wrap drum is the magnesium ring-stiffened concept. The drum is approximately six inches in radius with a 0.032-inch thick skin with flanged lightening holes.

3.3.2.6 Effects of Dynamics of Spacecraft Mount on Design

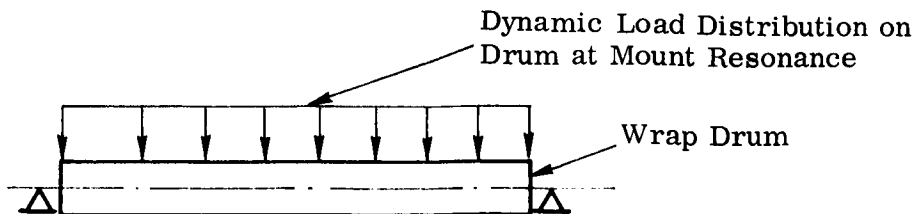
The dynamic analysis of the rollup panel mounts shows that the proposed mount using magnesium is not sufficiently rigid, ≥ 150 cps ($200/\sqrt{2}$) natural frequency, to limit the dynamic response to $\cong 50$ G in the drum. The mount should be made of a higher modulus material such as beryllium. See graph on next page. With mount resonance critical, and for a mount damping ratio of 0.03 (realistic for metallic structure) there are two critical conditions to be considered for the proposed magnesium drum.



Wrap Drum Considerations

Dynamic excitation to the rollup array at mount resonance will be approximately 66.8 G (0-peak) when the excitation to the mount is 4 G (0-peak).

The dynamic transmissability in the wrap drum (with drum vibrating as a simple beam) for a dynamic ratio of 0.05 (considered best possible with wrapped substrate acting as a damping medium) and a mount resonance frequency to drum natural frequency ratio of 1.2 (60/50), will be approximately 1. The resulting load distribution for this condition is nearly uniform with load distribution proportional to G , ($G = 66.8 \times 1 = 66.8$ G 0-peak), and resulting induced bending factor in the middle of



the wrap drum of 1.61 as compared to 1.0 for the best drum of magnesium; the magnesium drum will fail or deflect more than desired (0.25 inch) causing possible solar cell damage. By considering the use of beryllium drum skin (of equal thickness and weight) for its higher modulus, the increased load could be carried and deflections minimized.

Actually, the beryllium natural drum frequency will increase to approach 149 cps resulting in a transmissability of 0.120 in the drum rather than 1.0. If we increase the magnesium drum bending capacity by increasing skin thickness, the drum natural frequency increases in proportion to $\Delta(t)^{1/2}$, dynamic loads increase exponentially, and bending capacity increases linearly. If we consider an increase in t from 0.032 to 0.050 using magnesium, the increase in bending capacity is 56%, but the resulting dynamic transmissability in the drum at mount resonance is increased by a factor of 5; drum failure will still occur and we have increased weight of the rollup panel by 2.9 pounds. Therefore, a more effective means of reducing loads and deflection in the drum is required if beryllium is not used for drum skin. The possibilities are:

- a. Increase mount stiffness. Stiffness increase by increasing section depth $\cong 80\%$ is required using aluminum. This forces a decrease in wrap drum length (See Figure 15) approximately 9.5% (small effect on required skin thickness) and therefore an increase in deployable beam length of 10.5 percent (area required = constant). The resulting increase in weight would be negligible (including additional wiring) using aluminum mounts. No increase in weight would be reflected using a beryllium mount of proposed configuration.
- b. An intentional shortening of the drum would have results given in a above.
- c. Use viscoelastic shear damping medium between mount and drum to reduce effect of dynamic transmissability into drum (at mount resonance) from 16.7 G to approximately 12 G or less.

Since the bending factor in drum at mount resonance (using 0.032 magnesium drum skin and 0.025 magnesium mount) is 2.5 times that at drum resonance, the damping medium should have a dynamic transmissability $1/2.5 = 0.4$ or less. From the transmissability curve (assuming a damping ratio of 1.0 for the damping medium) the forcing frequency/natural frequency ratio is about 4 for a transmissability of 0.4, which gives a natural frequency of

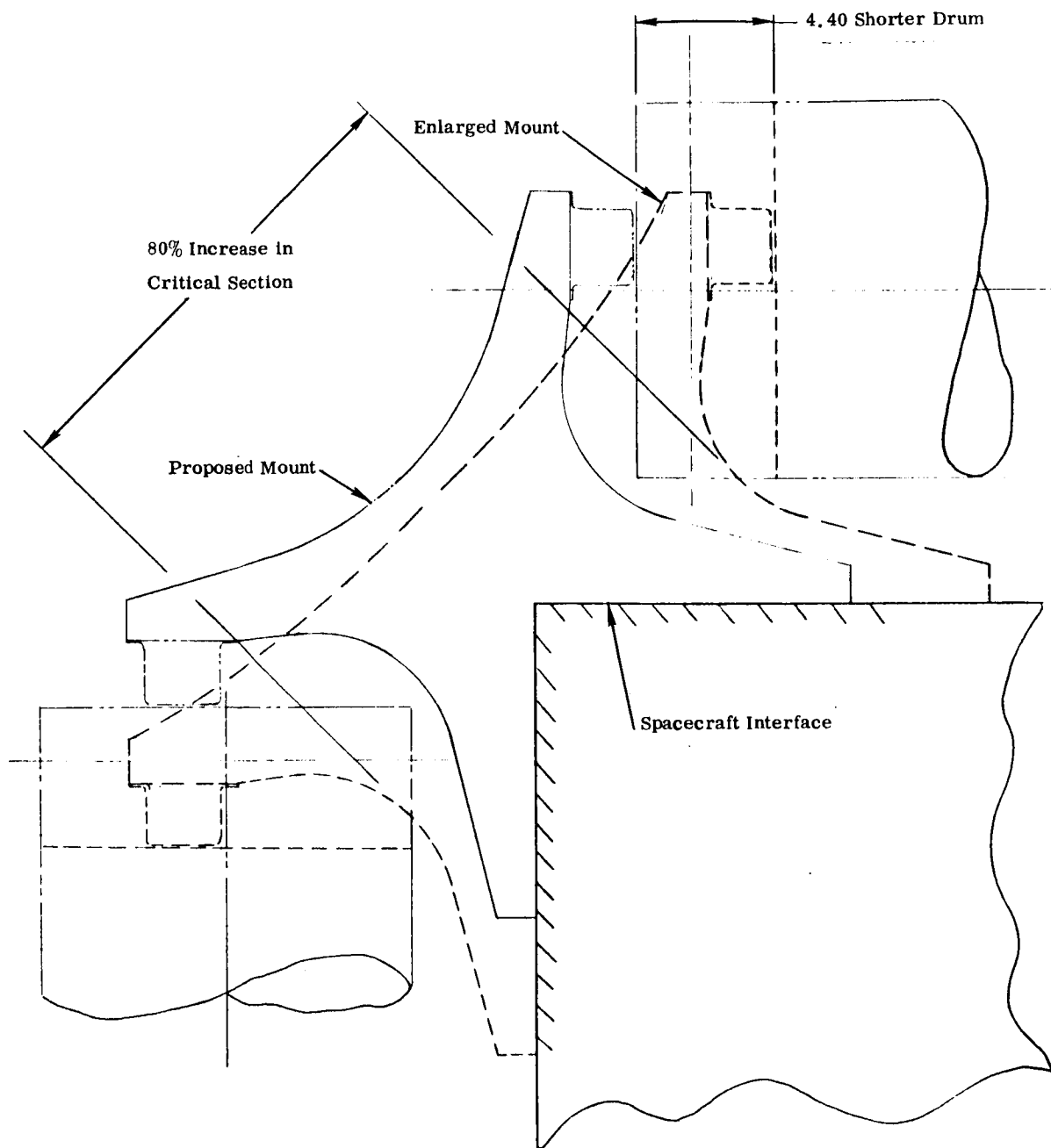
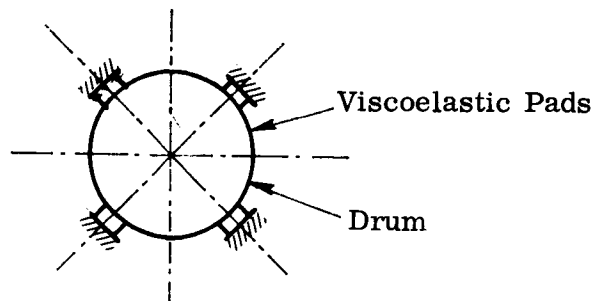


Figure 15. Effect of Increased Spacecraft Mount Cross-Section

damping medium,

$$f_n = \frac{60}{4} = 15 \text{ cps. For mount resonance.}$$

If the drum is supported at each end to spacecraft mount by four viscoelastic pads (as illustrated), the spring constant, K, required for a frequency of 15 cps is calculated from



$$f_n = \frac{1}{2\pi} \left(\frac{k}{m} \right)^{1/2}$$

m, that portion of mass of 1/2 of stowed drum and array at each

$$\text{Pad} = \frac{\frac{1}{4} \left(\frac{65}{2} \right)}{G} = 8.1/G$$

$$K_{(\text{Req'd.})} = (2\pi \cdot f_n)^2 \cdot \frac{W}{G} = (2\pi \times 15)^2 \times \frac{8.1}{386.4}$$

$$K_{(\text{Req'd.})} = 186.2 \text{ lbs/in.}$$

and deflection of Pad at Mount Resonance is Calculated as,

$$\begin{aligned} \frac{\text{Load on Pad From Drum}}{K} &= \frac{(W)(G_{in} \times Q)}{K} = \frac{(8.1)(4 \times 16.7 \times .48 \times 1)}{186.2} \\ &= 1.39 \text{ in.} \end{aligned}$$

If we consider the above viscoelastic pads when the drum resonates, dynamic transmissibility, Q , in the mount is 2.5; dynamic transmissibility in the pads is 0.6, and for a Q of 10 in the drum, maximum acceleration at the center of drum is,

$$G_{(in)}(\Sigma Q) = 4 (2.5 \times .6 \times 10) = \underline{\underline{60 G's}} \text{ (O-Peak)}$$

which exceeds the buckling allowable of the drum (pads will bottom out) by a factor of 1.2 based on ultimate loads (limit $\times 1.25$), or gives a 5 percent margin of safety based on limit loads. The added weight for silicone pads would be about 1 pound.

- d. Use of snubber (Figure 16) at center of wrap drum to effectively reduce drum to two shorter drums which can carry higher bending loads. The effective weight addition per rollup panel would be approximately 2.0 pounds.

The solar cells would be protected by 100 percent silicone sponge support in this local area. Snubber reaction vectors 120 degrees apart are suggested for effectiveness in snubbing against vibration in all directions in a plane normal to drum axis.

Wrapped Panel Considerations

None of the above possible solutions, however, will eliminate the second critical condition, which occurs when the substrate mode is excited (i.e., loose wrapped substrate).

It will be necessary to support the wrapped substrate in a manner compatible with the minimum weight such that the separation distance of wrapped layers is sufficient to prevent contact during vibration induced during launch. This aspect is given consideration in Paragraph 3.3.2.8.

Justification for Concept Selection of Solution 'a' Using Aluminum Mounts

1. Does not require use of beryllium.
2. Added weight is negligible.
3. Is a definite solution to the problem in lieu of test data whereas use of viscoelastic damping material between mount and drum would require additional testing in trade-off study phase.

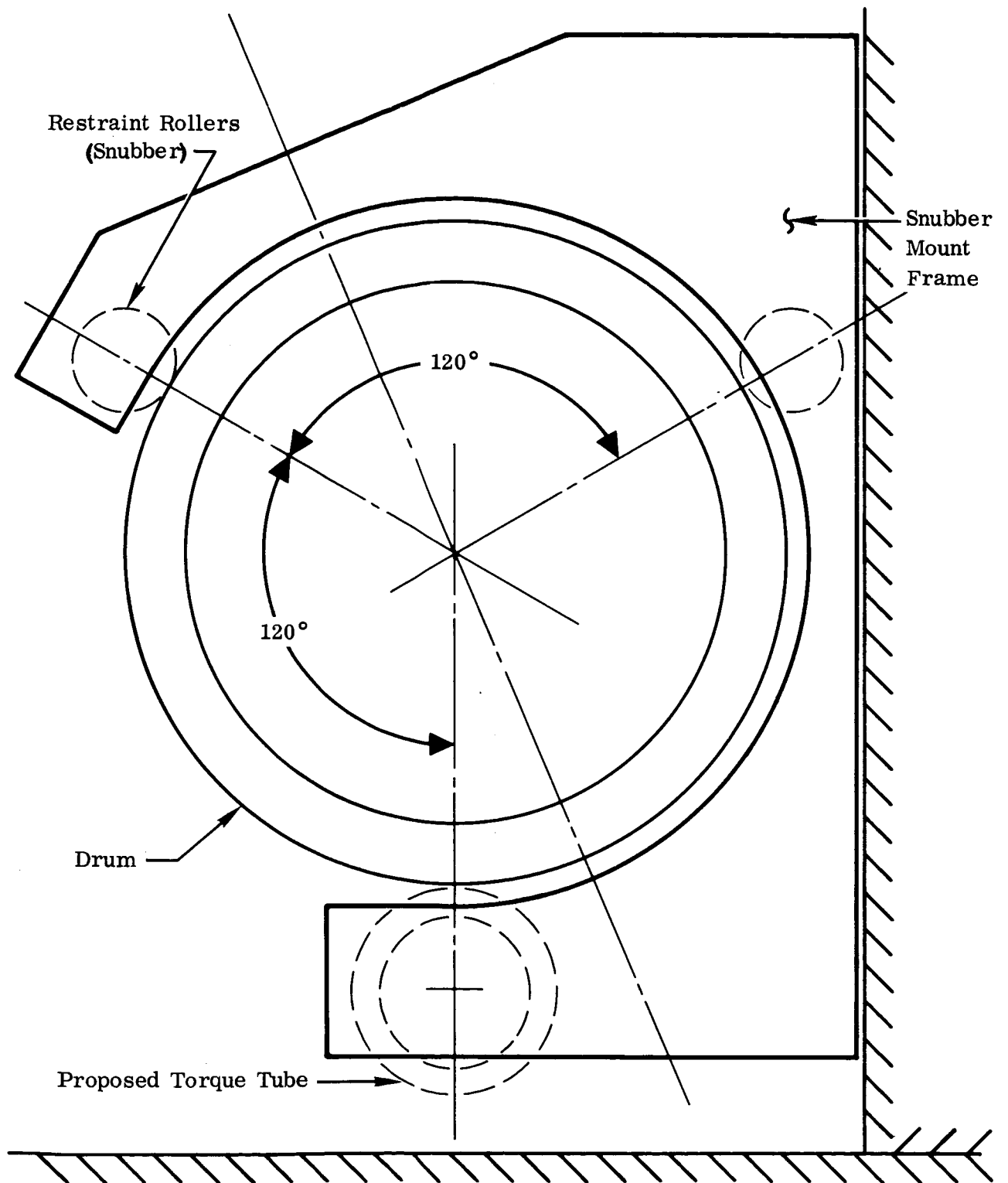


Figure 16. Drum Snubber at Center of Drum Length

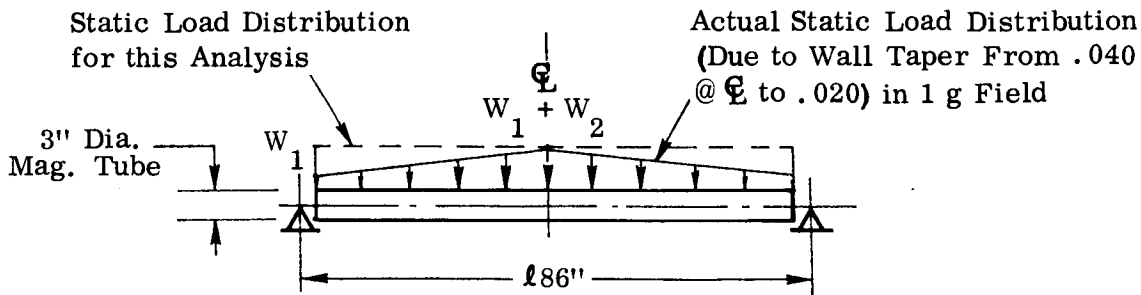
4. Change in Panel Aspect Ratio from 5.25 to 6.4 has negligible effect on total array power/weight ratio.
5. Design goal of 30 watts/pound can still be met.

3.3.2.7 Torque Tube Studies

Comparison is made here between (1) a torque tube which must carry its own load at resonance in a sinusoidal vibration environment, and (2) a torque tube which is snubbed at its midspan.

Pin-Ended Torque Tube

The torque tube, without midspan snubber, is considered to vibrate in its lowest mode as a pin-ended beam. Holes in the surface of the tube for weight reduction are not suggested since torsional deflection must be minimized. Rather, a tube of tapered wall thickness will be considered for minimizing weight. The torque tube suggested is analyzed conservatively for its fundamental vibration frequency as follows, assuming here that it is a uniform tube of uniform stiffness.



$$f_n = 3.53 \left(\frac{1}{\delta_{\text{static}}} \right)^{1/2}$$

$$\delta_{\text{(static in 1 g)}} = \frac{5(W_1 + W_2) \ell^4}{384 EI} = \frac{5(.024)86^4}{384 \times 6.5 \times 10^6 \times .424} = .0062 \text{ in.}$$

$$f_n = 3.53 \left(\frac{1}{.0062} \right)^{1/2} = 44.8 \text{ cps.}$$

Dynamic deflection at f_n when excited in the direction towards the wrap drum is calculated as,

$$\delta_{\text{dyn.}} = \frac{386.4 (g_{\text{at tube}} \cdot Q)}{(2\pi f_n)^2}$$

$g_{\text{at tube}} = 1.05 \times 4$ for a ratio of f_n / spacecraft mount freq.

$$= \frac{44.8}{160} = .28$$

Q in the tube = 16.7 at f_n based on a damping ratio in tube of .03.

$$\delta_{\text{dyn.}} = \frac{386.4(1.05 \times 4 \times 16.7)}{(2\pi \times 44.8)^2} = .34 \text{ in. Single Amplitude}$$

Bending stress at tube center for $\delta_{\text{dyn}} = \underline{0.34}$ inch is calculated as,

$$f_b = \frac{M}{\pi r^2 t}$$

M , for Triangular Load Distribution,

$$= \frac{10 EI \cdot \delta}{l^2} = \frac{10 \times 6.5 \times 10^6 \times .424 \times .34}{86^2}$$

$M = 1260 \text{ in} - \text{lbs}$

$$f_b = \frac{1260}{\pi \times 1.5^2 \times .040} = 4452 \text{ psi.}$$

$$F_{\text{cr (elastic backing)}} = 1.3 KE \frac{t}{r} = 1.3 \times .3 \times 6.5 \times 10^6 \times \frac{.040}{1.5}$$

$$= 67574 \text{ psi.}$$

M.S. \rightarrow High

Spacing required between wrap drum and torque tube to prevent contact will be approximately δ drum + δ torque tube = 0.25 + 0.34 = 0.59 inch. A reduction in dynamic deflection inversely proportional to the Δ Dia.³ · t or Δ E with no change in weight would result in a considerable change in stiffness of the torque tube by increasing diameter or by using beryllium. However, this is not necessary from a strength reason and would only increase size and weight of drive sprockets required.

Torque Tube Snubbed at Center

If we consider snubbing at midspan, the torque tube wall could be made uniform in thickness (0.030 inch) rather than tapered, resulting in an equal weight tube. It is not suggested that any weight reduction be considered for this case since torsional rigidity would then be sacrificed.

Conclusions

If we consider the possibility of a wrapped substrate build-up of an additional 0.28 to 0.57 inch of radius (depending on thickness of separation medium of 0.125 to 0.15 inch, respectively) due to the probability that the low modulus substrate does not have the capacity to induce a preload in the wrapped panel layer separation medium, the required spacing between torque tube and wrapped panel, allowing .123 minimum clearance, becomes 1.0 to 1.29 inch. To prevent contact of outer wrapped panel layer and torque tube at torque tube resonance, the possibilities are (1) to increase spacing by increasing torque tube drive sprocket diameter, or (2) to add a thin metal band snubber at center of torque tube and attach it to the spacecraft bus. The required spacing reduces to 0.66 to 0.95-inch minimum based on 1/8 inch between layers. The suggestion (1) forces an excessive increase in length of four guide sleeve mount members which would require additional weight for stiffness to prevent excessive deflection of the guide sleeves at vibration resonance. Suggestion (2) appears to be the more positive solution and will add the least weight.

3.3.2.8 Wrapped Substrate Layer Separation Medium Studies

Constraints

The primary reason for the use of a medium between the wrapped substrate layers is to prevent vibration-induced buffeting of solar cells. This separation medium should be (1) of low density to minimize weight and (2) have the proper spring rate to allow for some energy absorption and yet prevent excessive deflection (possibly causing solar cell contact and breakage) at vibration resonances. Also of importance is the

vibration damping provided by this medium when considering the wrap drum design. Since many variances of the wrapped panel affect the amount of damping, (such as substrate material, solar cell adhesive and thickness, solar cell interconnects, damping medium, percent of damping medium contacted, and percent of solar cell bonded area) a damping ratio of 0.05 will be considered until the wrap drum vibration test has been conducted and the actual ratio determined.

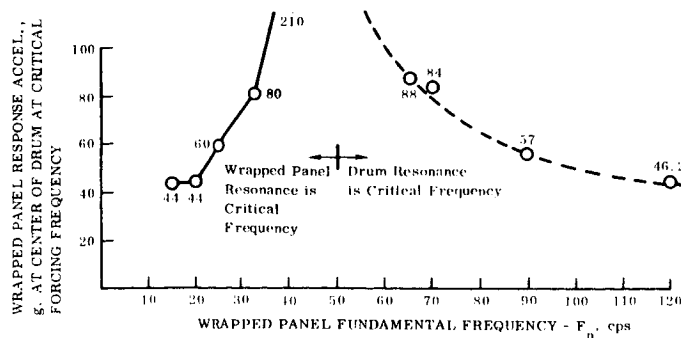
Induced sinusoidal vibration environment is treated here as the more critical design environment. Steady state environment (magnitudes of which are given in the JPL Specification; considered maximum and not to occur simultaneously with maximum vibration environment), is shown to be less severe than sinusoidal vibration excitations when it is considered that it takes only a vibration transmissibility, Q , of 3.3 at resonance in the launch axis and Q of 1.5 normal to launch axis to equal the steady state environment. Random Gaussian vibration is shown to be less severe than sinusoidal by considering that a minimum sinusoidal response at resonance would be about 40 G, 0-peak ($G_{in} \cdot Q = 4 \times 10$); random response would be less, calculated as follows:

$$\ddot{Y}_{(0\text{-peak})} = 1.414 \left[\frac{\pi}{2} (F_n) (\text{Spectral Density}) (Q \text{ at Sin. Response}) \right]^{1/2}$$

for resonances as high as 200 cps,

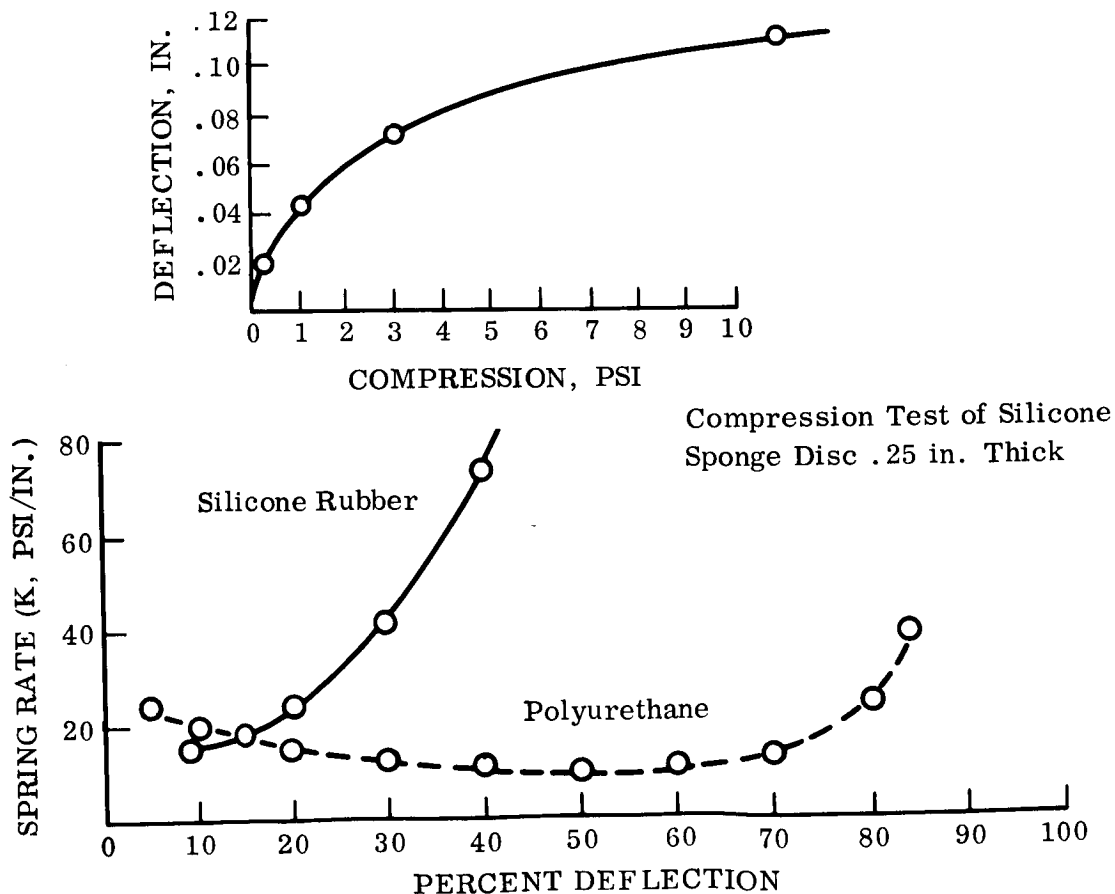
$$\ddot{Y}_{(0\text{-peak})} = 1.414 \left[\frac{\pi}{2} (200) (.1) (10) \right]^{1/2} = 25 \text{ G.}$$

An integration of dynamic transmissibility, Q , between spacecraft mount interface and wrapped panel at maximum excursion area (center of wrap drum) for respective wrapped panel response accelerations as shown based on (1) a wrap drum fundamental frequency of 50 cps and Q of 10, (2) a spacecraft mount fundamental frequency of 160 cps and Q of 16.7, and (3) a wrapped panel Q of 10:



If the substrate were wrapped with sufficient precision, unstressed in tension, such that all layers contacted the separator medium, the resulting minimum dynamic radial pressure (based on a solar cell and substrate weight of 1.53×10^{-3} pounds/square inch and a fundamental frequency of 20 cps) would be 0.067 pounds/square inch, 0-peak at the outer layer and, if all layers were vibrating in phase, 0.87 pound/square inch, 0-peak at the inner layer. This inner layer radial pressure is probably conservative, since the layers do not wrap with such precision and, therefore, not all will resonate at the same frequency. For analysis, however, the conservative approach will be considered.

Selection of the optimum separation medium design for a sinusoidal vibration system on a minimum weight basis is made from a plot of weight versus frequency for various configurations. These configurations vary in medium thickness, and where the medium is less than a full blanket (local disc pads) the variables are pad diameter and center distances. A medium spring rate is based on silicone sponge density of 0.008 pound/cubic inch (which is about the minimum obtainable). Comparison is made with separating medium configurations using 0.00116 pound/cubic inch polyurethane foam. The spring rate is obtainable from the Ryan test curves shown below and in Figure 17.



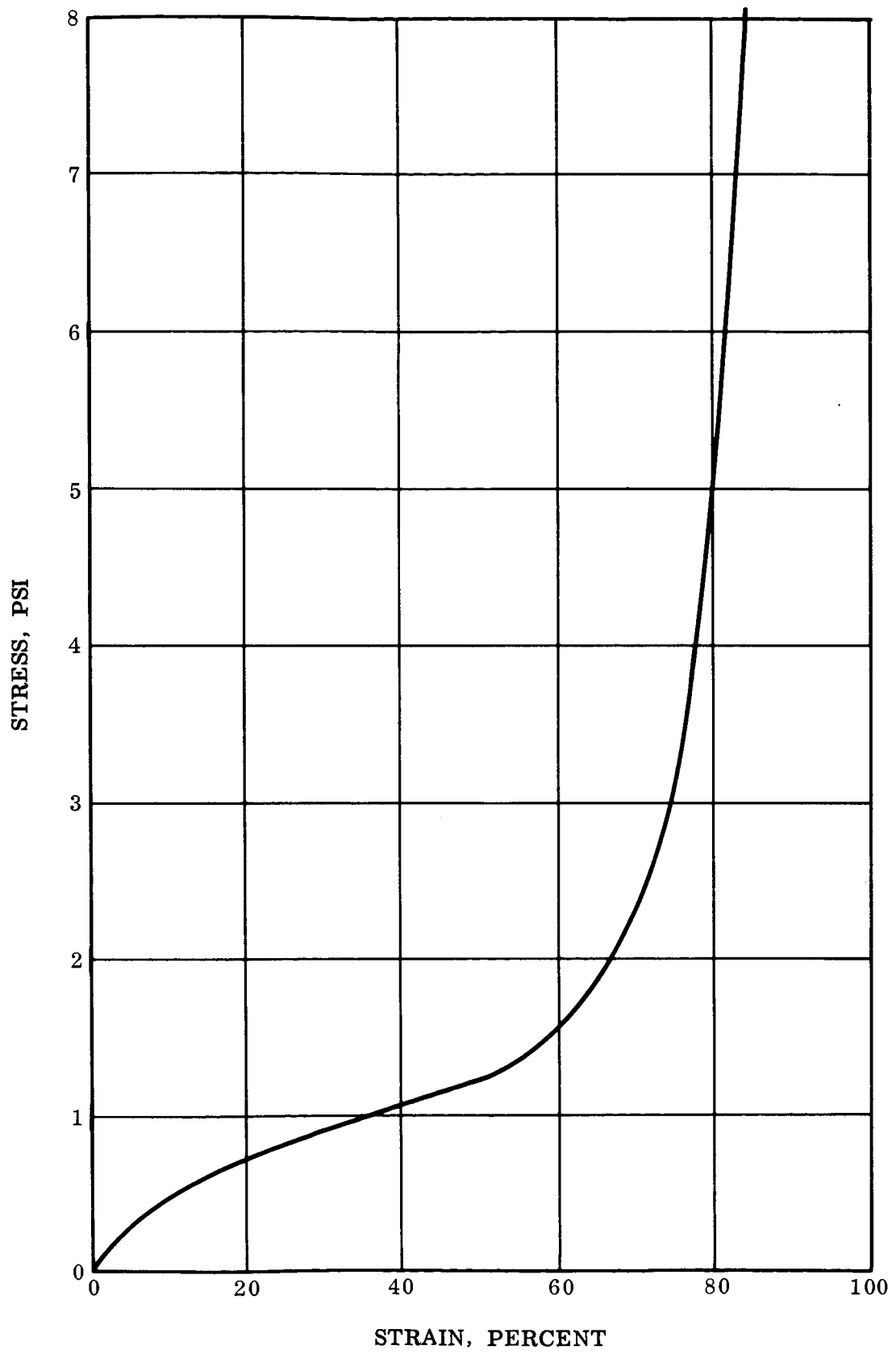
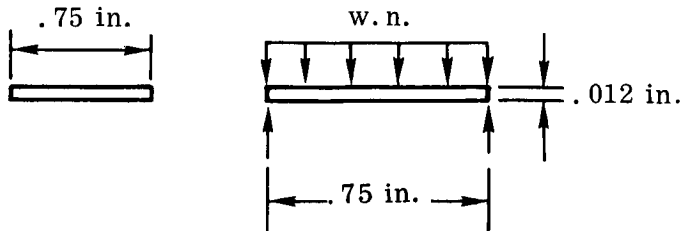
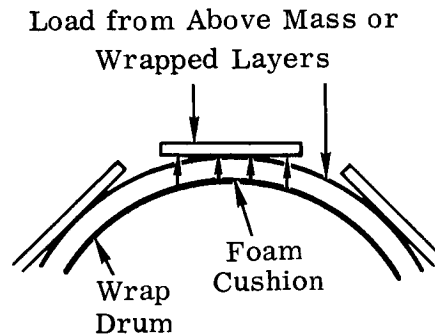


Figure 17. Typical Static Stress-Strain Curve for Flexible Polyurethane Cushion at Room Temperature

Critical loads for analysis are based on dynamic loads on the wrapped layers (1.53×10^{-3} lbs/square inch per wrap layer which gives a static load of 1.83×10^{-2} pound/square inch on inner wrap layer separation medium) assuming all layers above the layer in question act as a rigid body on that wrap layer separation medium. Cylindrical stiffening effects of the wrapped substrate will be considered negligible in this analysis.



Loads on Solar Cell



$$f_b = F_{t(\text{glass})} = \frac{g \cdot M \cdot x \cdot .006}{I} = 5000 \text{ psi}$$

$$M = \frac{wl^2 n}{8} = \frac{1.15 \times 10^{-3} \times .75^2 n}{8} \quad \left| \quad I = \frac{.75(.012)^3}{12} = .108 \times 10^{-6} \text{ in}^4 \right.$$

$$M = .081 \times 10^{-3} n$$

Then,

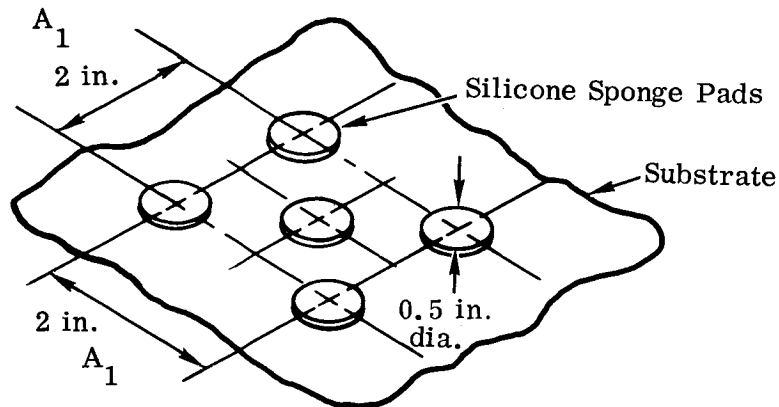
$$g = \frac{5000 \times I}{.006 M} = \frac{5000 \times .108 \times 10^{-6}}{.006 \times .081 \times 10^{-3} n} = \frac{1111}{n} \quad \left| \quad \begin{array}{l} n = \text{wrap layer num-} \\ \text{bering from outside} \\ \text{layer as 1} \end{array} \right.$$

which is probably only slightly conservative for a foil thick Kapton (or fiberglass) substrate. A maximum permissible deflection of the wrap layer in question will be limited to 0.10 inch to prevent edge contact of adjacent solar cells at that respective layer; this is a conservative approach since it is based on a perfect radial breathing mode of vibration which is highly improbable with induced sinusoidal vibration in one axis. This appears to be a more realistic design constraint since, as is shown in the above analysis, the G level required to induce solar cell fracture is large (larger than the optimum design will experience).

Analysis is made for this study by calculating dynamic sinusoidal deflection of a separation medium configuration with a given frequency and then determining its weight based on a thickness equal to its calculated dynamic deflection plus a certain percentage of dynamic deflection which will correspond to the static spring rate, K, used for analysis. This is made possible by limiting spacing between local disc pads, where considered, to three inches maximum to limit wrapped panel deflection between pads to a negligible magnitude. A minimum medium thickness of 0.05 inch is used as a requirement to prevent solar cell damage when wrapping around the drum, extrapolated from wrap tests conducted by Ryan; Reference 15, p. 70.

In selection of the optimum medium configuration, we shall not consider a thickness greater than 0.15 inch. This limit is made to prevent excess build-up of wrapped panel which forces an excessive weight increase of the guide sleeve mounts.

Analysis of a given silicone foam configuration follows for presentation of the approach taken. Consider an inner wrap layer, disc pad configuration as shown, supporting all 12 wrap layers.



The fundamental frequency, F_n , for the above separation medium configuration is calculated by the equation,

$$F_n = \frac{(K/m)^{1/2}}{2\pi} = \frac{(K \cdot g/\text{load})^{1/2}}{2\pi} = \left(\frac{g}{\text{static defl.}} \right)^{1/2}$$

K, from compression-deflection curve for 12 wrapped panel layers in lg field acting on area AA

$$K = \frac{\text{Load}}{\text{Deflection}}$$

Deflection, from Curve,

$$\begin{aligned} \text{For } \frac{\text{Load}}{\text{Pad Area}} &= \frac{4 \times 1.53 \times 10^{-3} \times 12}{2\pi \times .25^2} \\ &= \frac{.073 \text{ lbs}}{.393 \text{ in}^2} = .19 \text{ psi} \end{aligned}$$

$$K = \frac{.073}{.013} = 5.61 \frac{\text{lbs.}}{\text{in.}}$$

$$F_n = \frac{\left(\frac{5.61 \times 386.4}{.073} \right)^{1/2}}{2\pi} = \frac{172}{2\pi} = 27 \text{ cps}$$

Dynamic deflection at F_n of the above configuration is calculated by,

$$\alpha_{\text{dyn.}} = \frac{386.4 \text{ g}_{(\text{response})}}{(2\pi F_n)^2}$$

$$G_{(\text{response})} = 66 \quad \begin{array}{l} \text{From wrapped panel freq. vs.} \\ \text{response accel. curve} \end{array}$$

$$\alpha_{\text{dyn.}} = \frac{386.4 \times 66}{(2\pi \times 27)^2} = .89 \text{ in.}$$

Then,

Static thickness for weight purposes = $\alpha_{\text{dyn.}}$ + A percent of $\alpha_{\text{dyn.}}$
using K based on 1G deflection (K = constant)

The above calculations are only for an example configuration. The resulting deflection, however, shows that the system frequency must be considerably greater, probably above 60 cps (as can be seen from the wrapped panel frequency versus response acceleration curve) in order to reduce the deflection and the resulting effective separation medium weight. The plots in Figures 18 and 19 show the results of similar calculations for various configurations utilizing silicone or polyurethane foam.

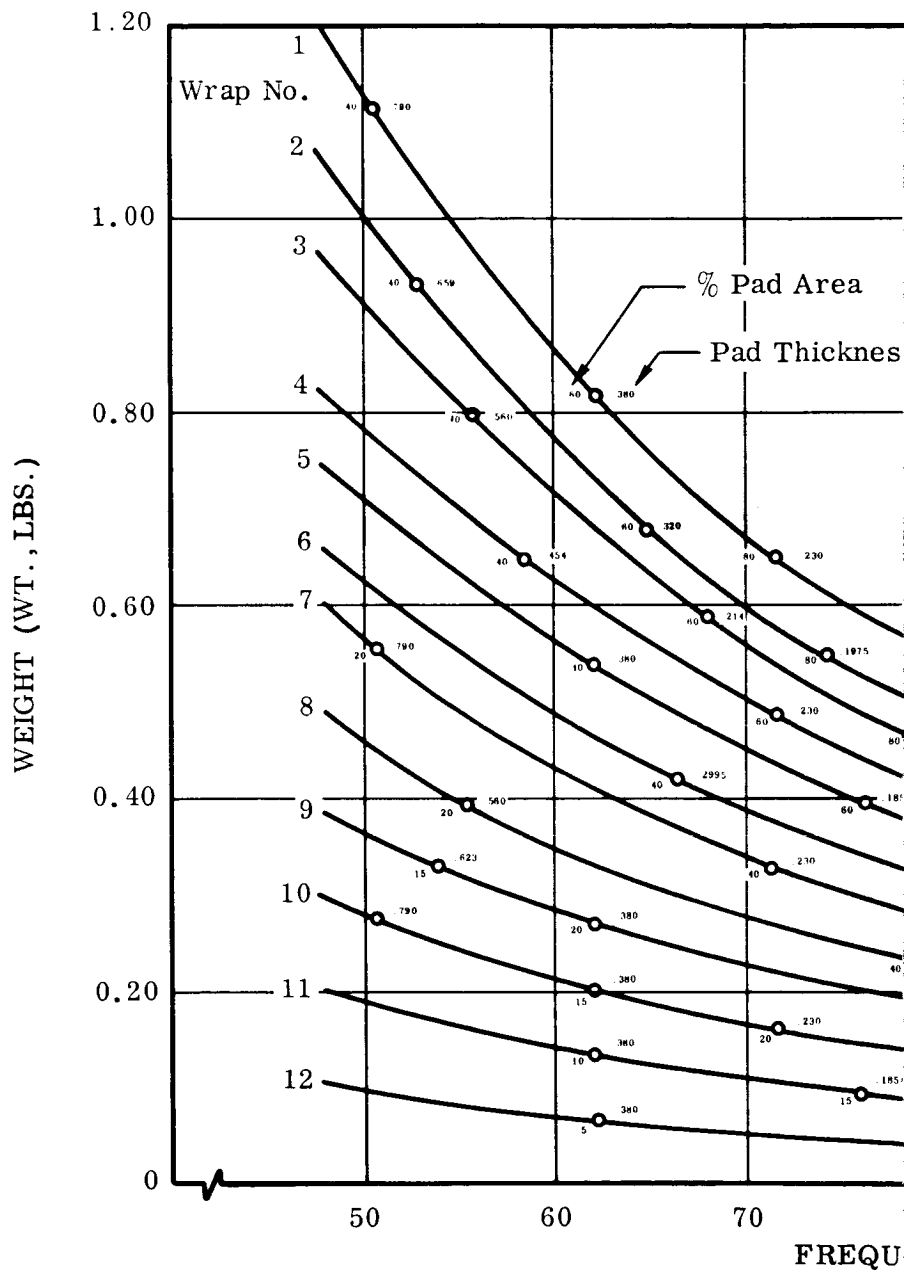
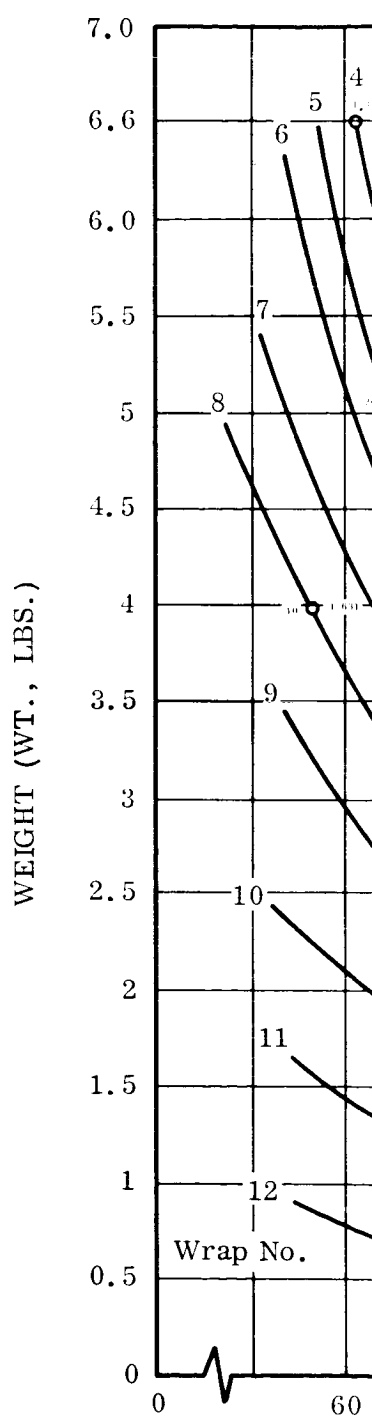
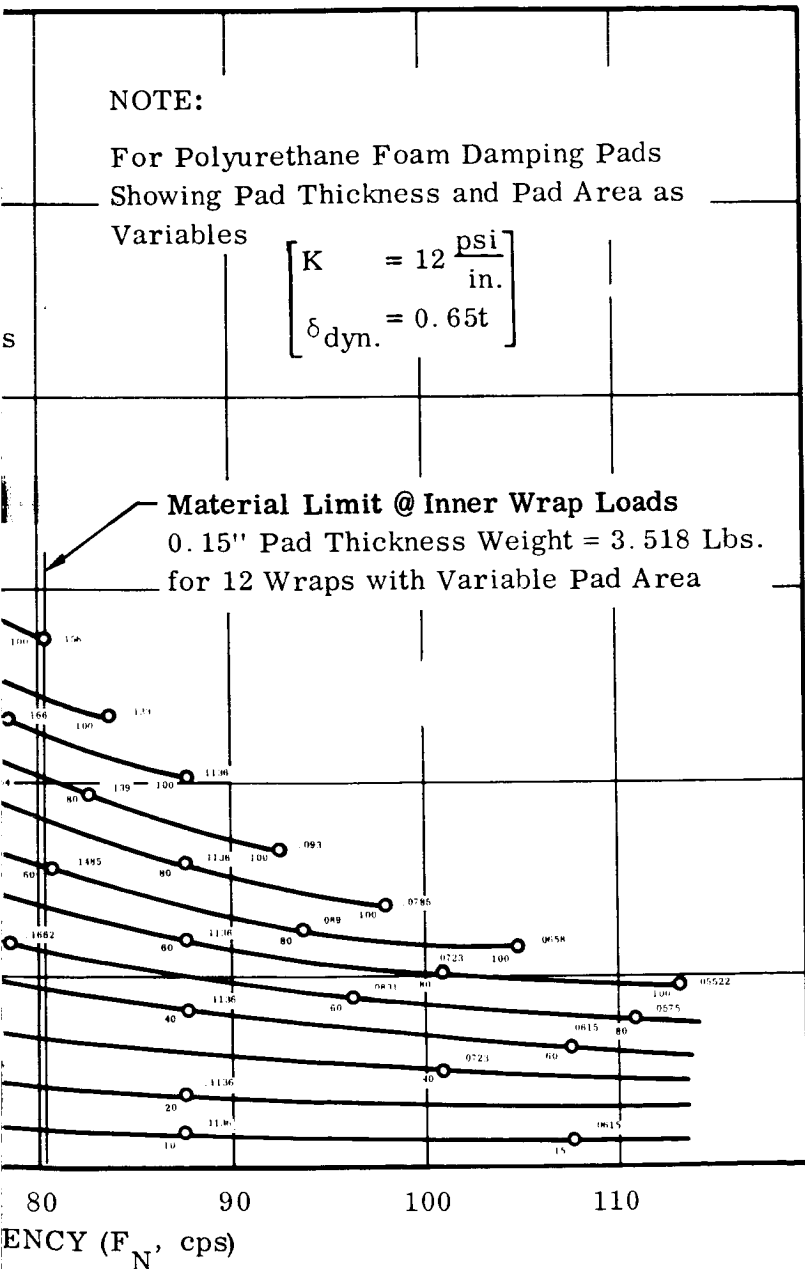


Figure 18. Polyurethane

97-A



ane Weight vs. Frequency

97-B

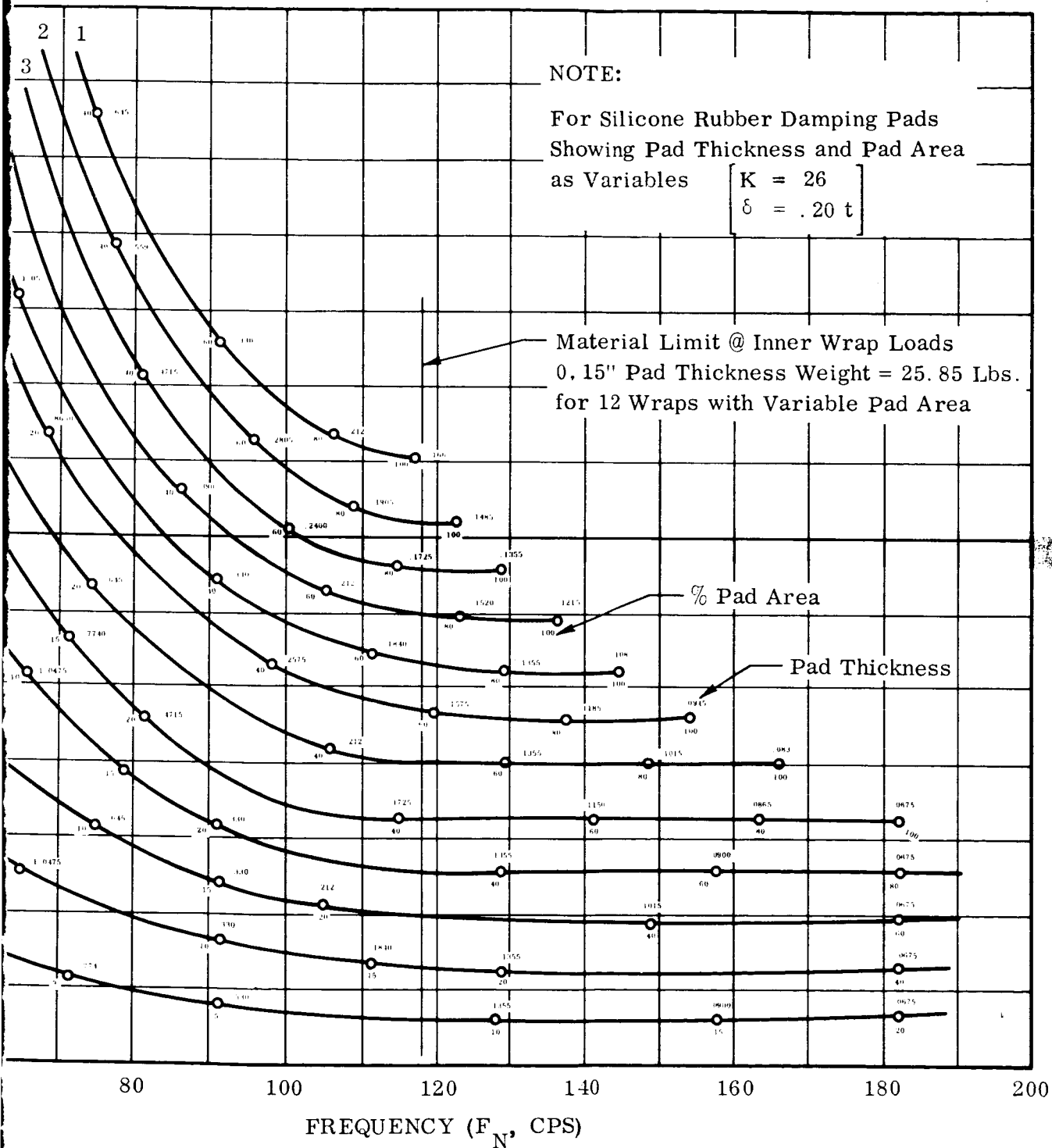


Figure 19. Silicone Weight vs. Frequency

Conclusions:

The analysis presented was made to find the lightest weight separation medium configuration using the constraints set forth:

1. Dynamic deflection under sinusoidal excitation at resonance ≤ 0.10 inch to prevent edge contact of solar cells.
2. Separation medium thickness ≤ 0.15 inch to prevent excessive build-up of wrap thickness, resulting in contact of wrapped substrate and drive torque tube at sinusoidal resonance of same and possible damage to solar cells.
3. A spacing between local disc pads of ≤ 3 inches so that sinusoidal vibration deflection of the wrapped substrate is negligible between pads; an analysis based on separation medium deflection only is thereby made possible.
4. Separation medium thickness ≥ 0.05 inch to prevent damage to solar cells subject to possible loads during wrapping around drum.
5. A constant thickness separation medium to facilitate ease of tuning (coordinating beam and panel wrap rates).

The plots of frequencies of support medium configurations versus weight for each of the panel wraps shows that the lightest weight medium will result using polyurethane foam. A foam of 2 pounds/cubic foot density was considered for the analysis, which is about the minimum obtainable. Utilization of silicone foam of minimum density (13.8 pounds/cubic foot) will result in a total medium weight of approximately 26 pounds as compared to 3.5 pounds for polyurethane. A constant thickness design constraint is satisfied by using the minimum thickness possible for the inner wrap, which is 0.15 inch. A thickness less than this would not correspond with the spring rate, K , for the respective load at that wrap layer. The medium configurations corresponding to the weight versus frequency plots indicate a large area of substrate coverage and may induce thermal problems with the solar cells (too high temperature to give the required 10 watts/ft² at the astronomical unit). The effects of this large area damping medium on solar cell operating temperatures is in work. The thermal analysis will be evaluated along with vibration test results of a small cylindrical panel specimen using polyurethane damping medium requirements as suggested in this study.

3.3.2.9 Thermal Studies

General

A preliminary thermal analysis of the deployed solar array is made to determine the solar cell operating temperature and the thermal gradient across the substrate. Two models are considered in the analysis. One model is representative of the inner panel (adjacent to wrap drum) and one model represents the outboard panel, both considering Kapton and fiberglass substrates. The difference between the two models is the size and the percent of area covered by the foam dampening pads on the back side of the substrate.

For the analysis, a solar radiation environment, representative of that encountered in the vicinity of Venus ($830 \text{ BTU/ft.}^2/\text{hr.}$, 260 mw/cm^2), is used. The resulting temperatures are extrapolated for 1 AU radiation input.

Nodal Breakdown

Outer Solar Cell Area of Panel

Figure 20 shows a small section of the outer solar cell wrap which was used for this model. This small section was reduced into nine smaller sections, which were then divided into isothermal nodes corresponding to layers in Figure 22.

Inner Solar Cell Area of Panel

Figure 21 shows a small section of the inner solar cell wrap used for the model. The difference between this and the outer wrap is in the size of the cushioning pads.

The results of the computer analysis for the inner and outer wrap cases are given at the end of this paragraph. Steady state in both cases was reached in a short time (less than 0.05 hour). The nodal breakdown for section 9 is shown in Figure 22. The breakdown for sections 1 through 8 were similar.

Assumptions and Material Properties

In the case of both the inner and outer wrap models it was assumed that the adhesive bonding in the layers had little effect on the model and, therefore, these layers were neglected (except for the calculation of the

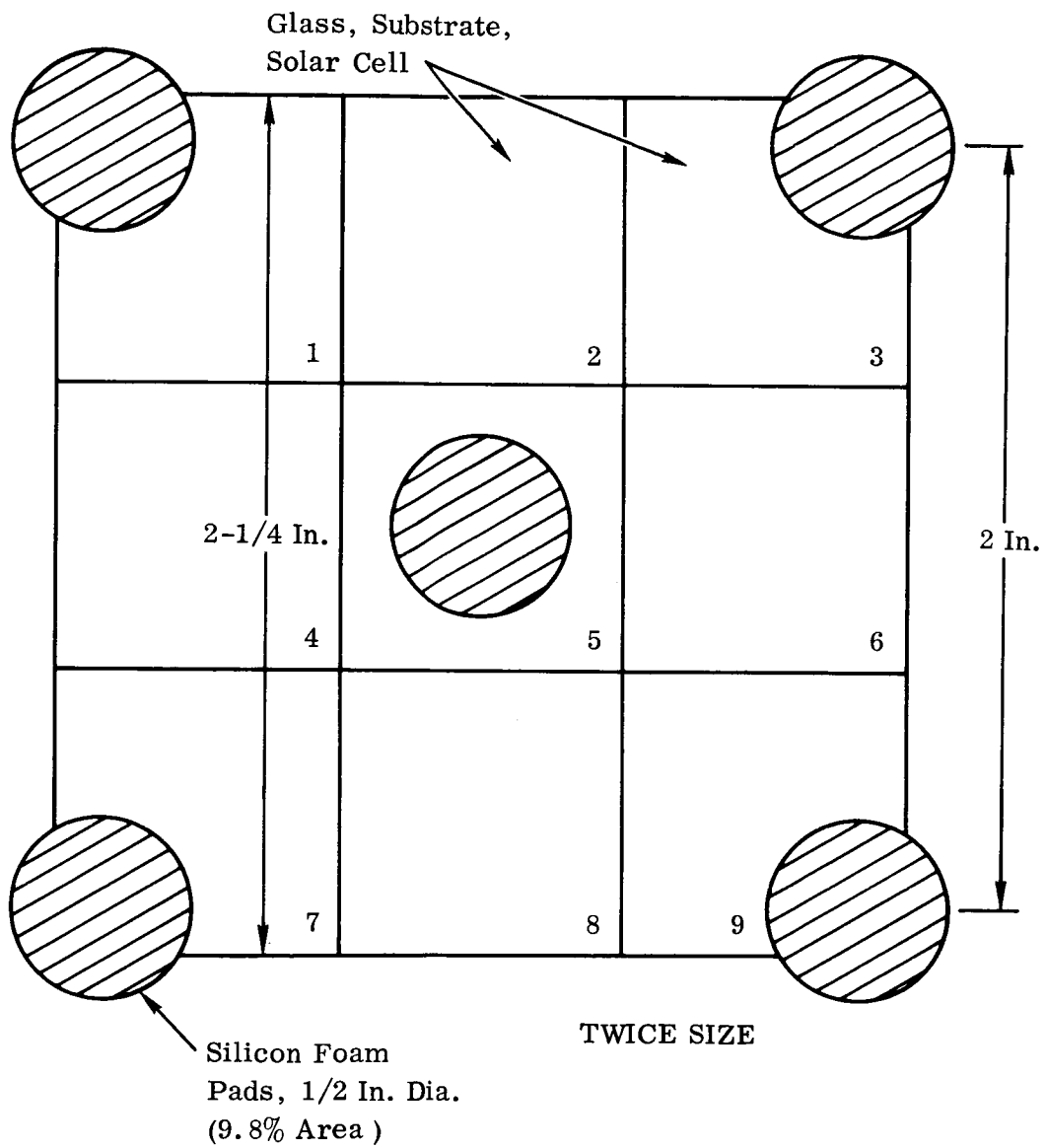


Figure 20. Thermal Model Section - Outer Solar Cell Wrap

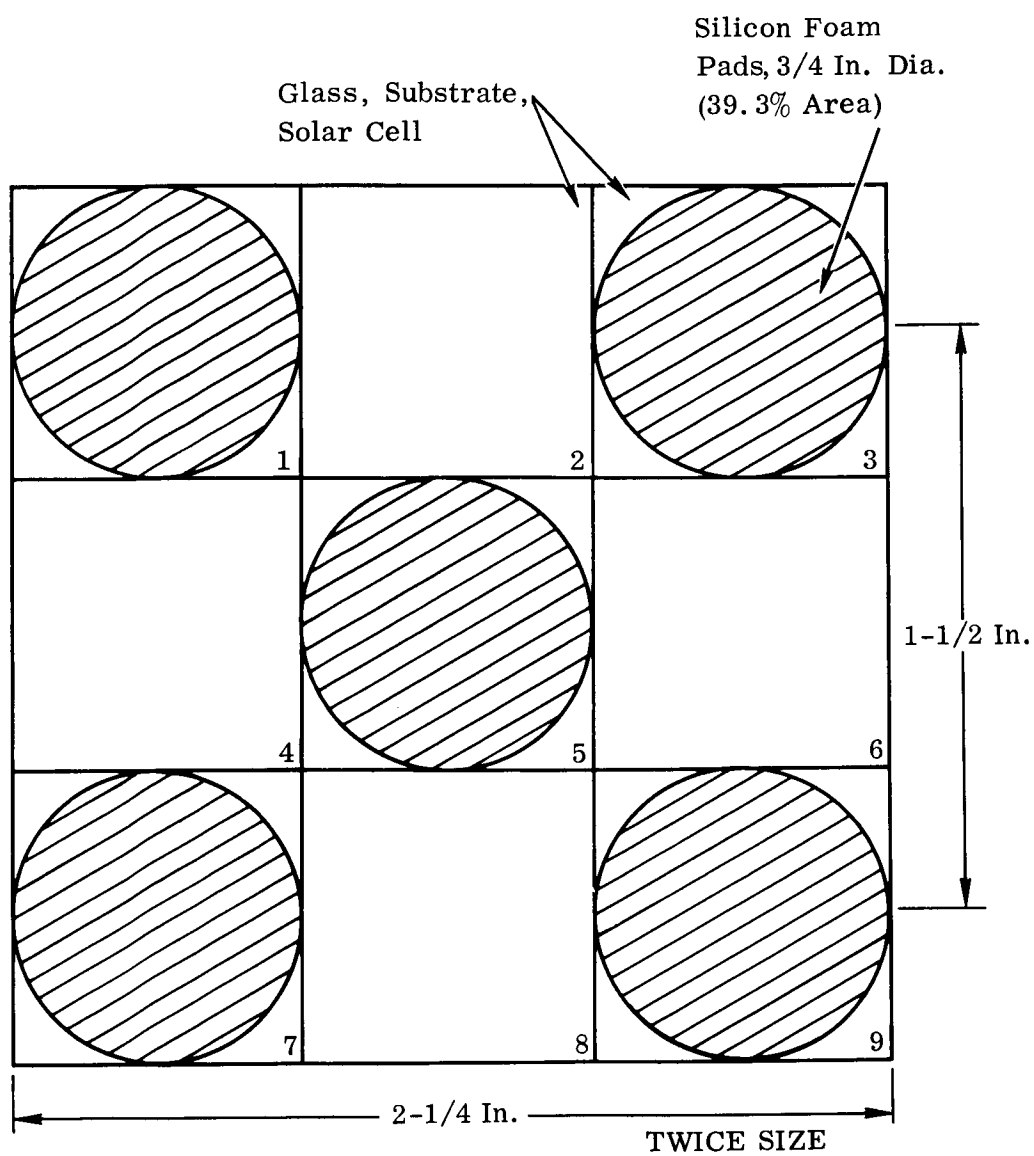


Figure 21. Thermal Model Section - Inner Solar Cell Wrap

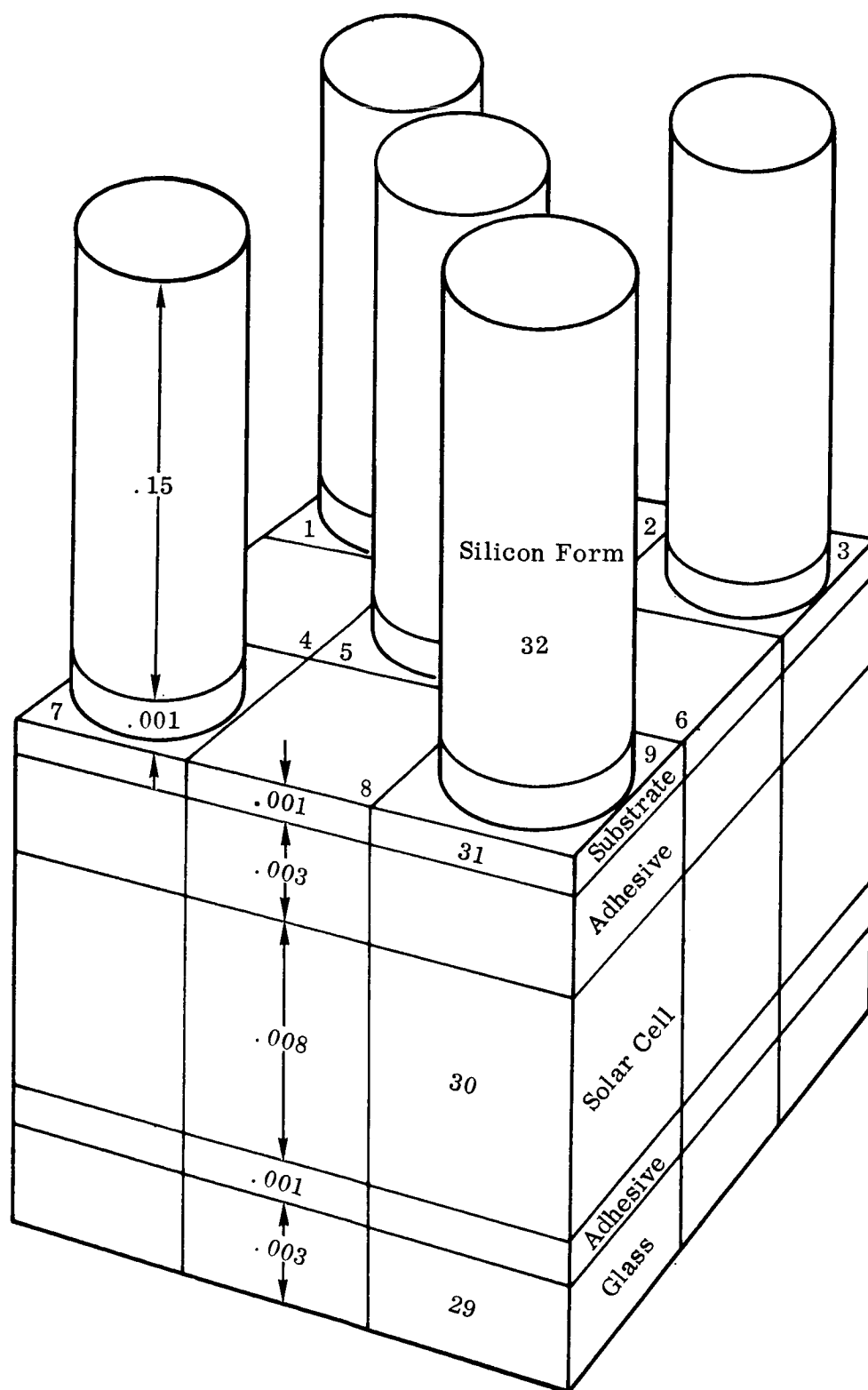


Figure 22. Isothermal Nodes - Outer Cell Wrap

conductivity). It was also assumed that the substrate was the only material which has an effect on the lateral transfer of heat. This is a reasonable assumption since the solar cells are separated on the panel. The materials used in the solar panel and some of their properties are listed in Table 6.

Results Using Fiberglass Substrate

Figures 23 and 24 show the temperature of some of the nodes in the inner and outer wrap analysis. The symmetry in the temperatures was expected from the symmetry of the model. Also, as should be expected, the center nodes are colder than the outer nodes for both cases.

Conclusions

Comparison of solar cell temperatures as affected by the use of Kapton substrate vs. fiberglass can not be made until analysis is completed for Kapton. These results will be included in the next report. However, preliminary study indicates that either will be satisfactory provided the damping medium on the back face of the substrate does not cover too large an area. Extrapolation is made of analytical solar cell temperature results (considering damping medium areas of 9.8% and 39.3% as expressed in this section) from a solar flux of 260 mw/cm^2 to that at 1 A.U. It results in respective temperatures of 109°F and 116°F . These temperatures are within the upper limit of 131°F . which corresponds to a power output of 10 watts/ft.^2 at 1 A.U.

TABLE 6
MATERIALS AND THEIR PROPERTIES
CONSIDERED IN THERMAL ANALYSIS

Node lb.	Material	Specific Heat	$\frac{\text{BTU}}{\text{LB } ^\circ\text{R}}$	α	ϵ
1, 5, 8, 12, 15, 19, 22, 26, 29	Silicon Glass	0.20			
2, 6, 9, 13, 16, 20, 23, 27, 30	Solar Cell	0.15		.84	
3, 7, 10, 14, 17, 21, 24, 28, 31	Fiberglass	0.261			.9
4, 11, 18, 25, 32	Silicon foam	0.20			

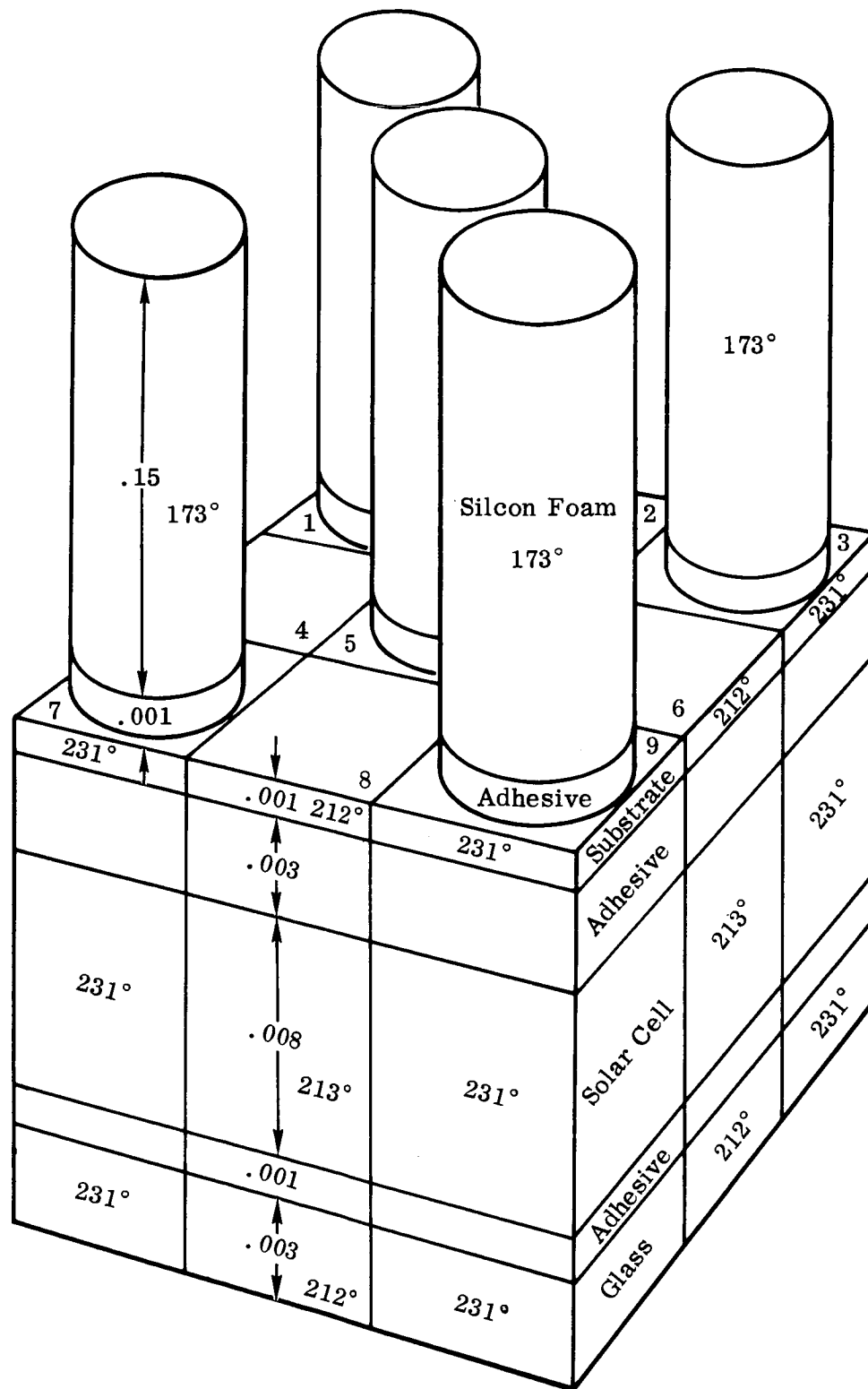
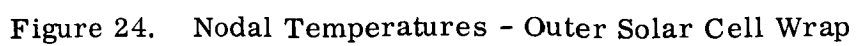


Figure 23. Nodal Temperatures - Inner Solar Cell Wrap

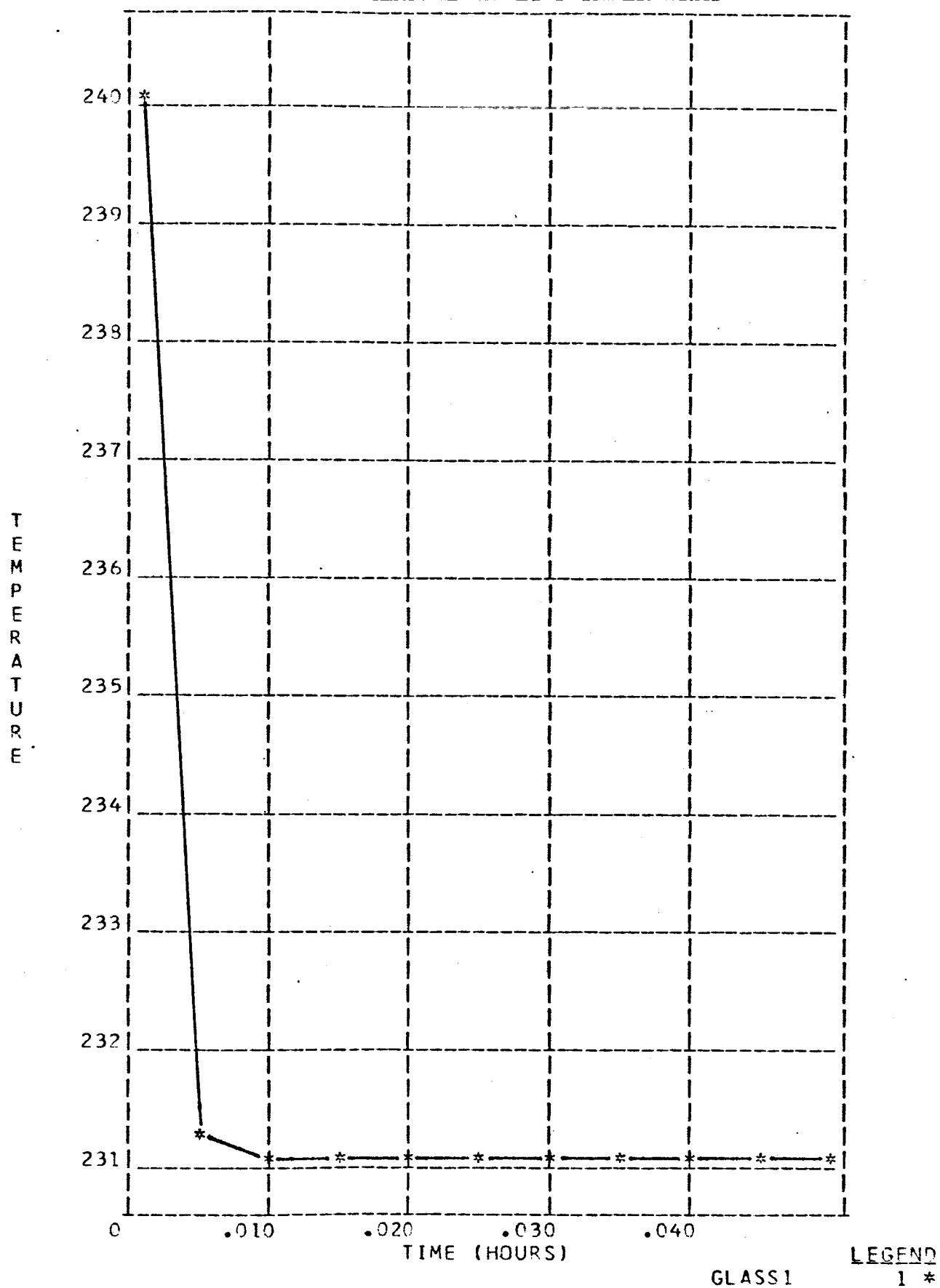


23 OCTOBER 1967

BOB TRAYLOR

EAAB 6193

SOLAR CELL THERMAL ANALYSIS INNER WRAP

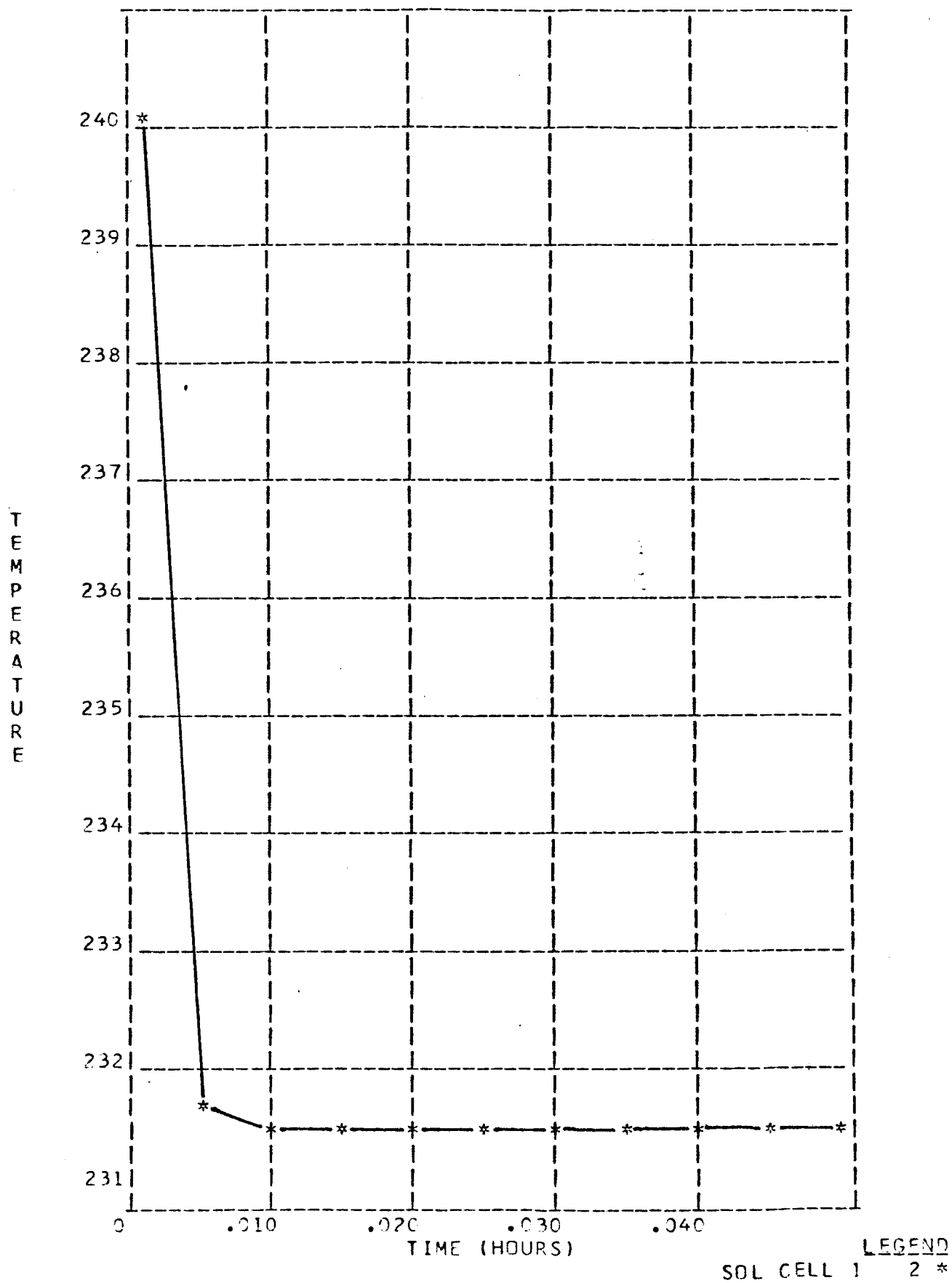


23 OCTOBER 1967

BOB TRAYLOR

EAAB 6193

SOLAR CELL THERMAL ANALYSIS INNER WRAP

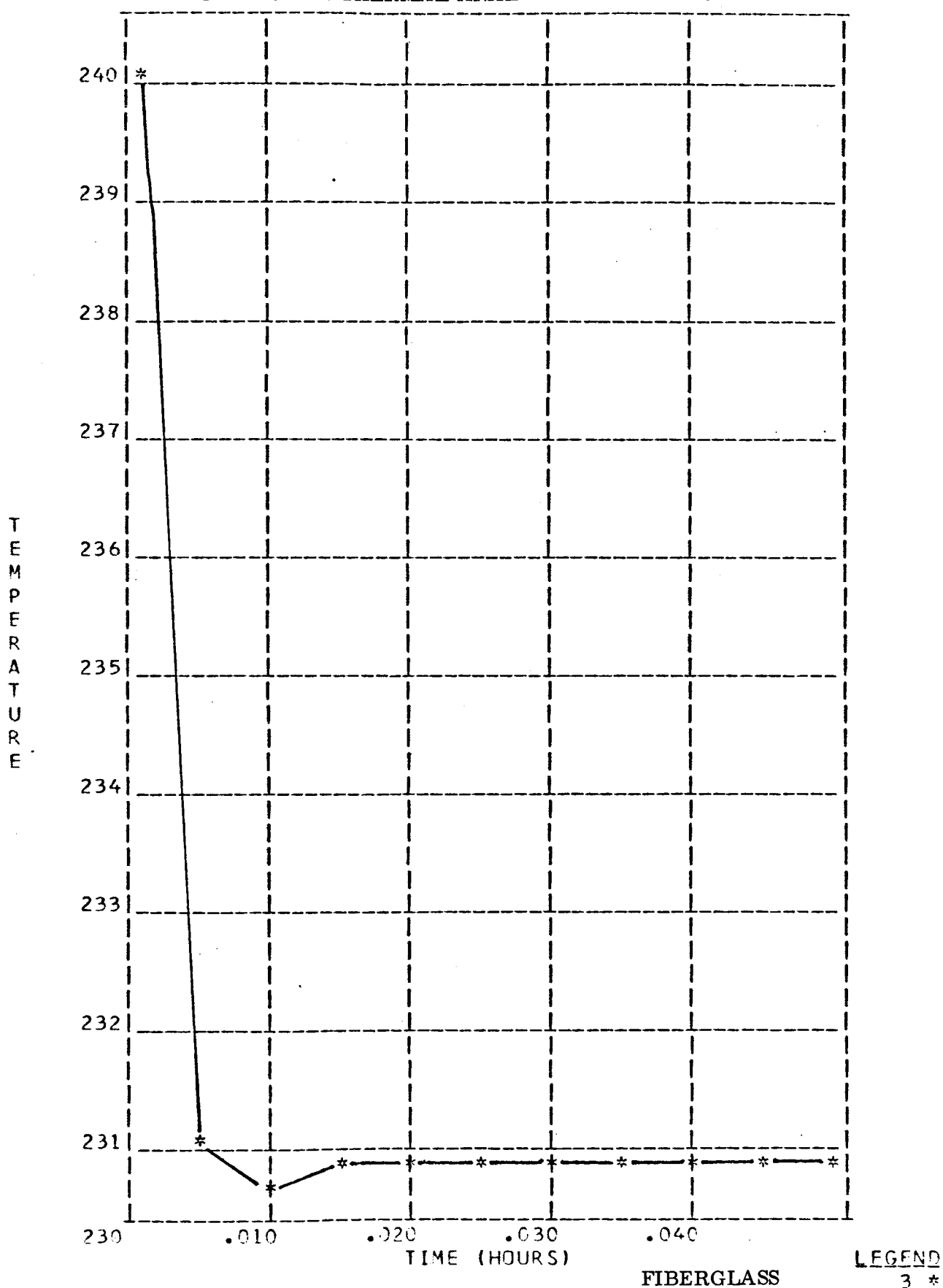


23 OCTOBER 1967

BOB TRAYLOR

EAAB 6193

SOLAR CELL THERMAL ANALYSIS INNER WRAP

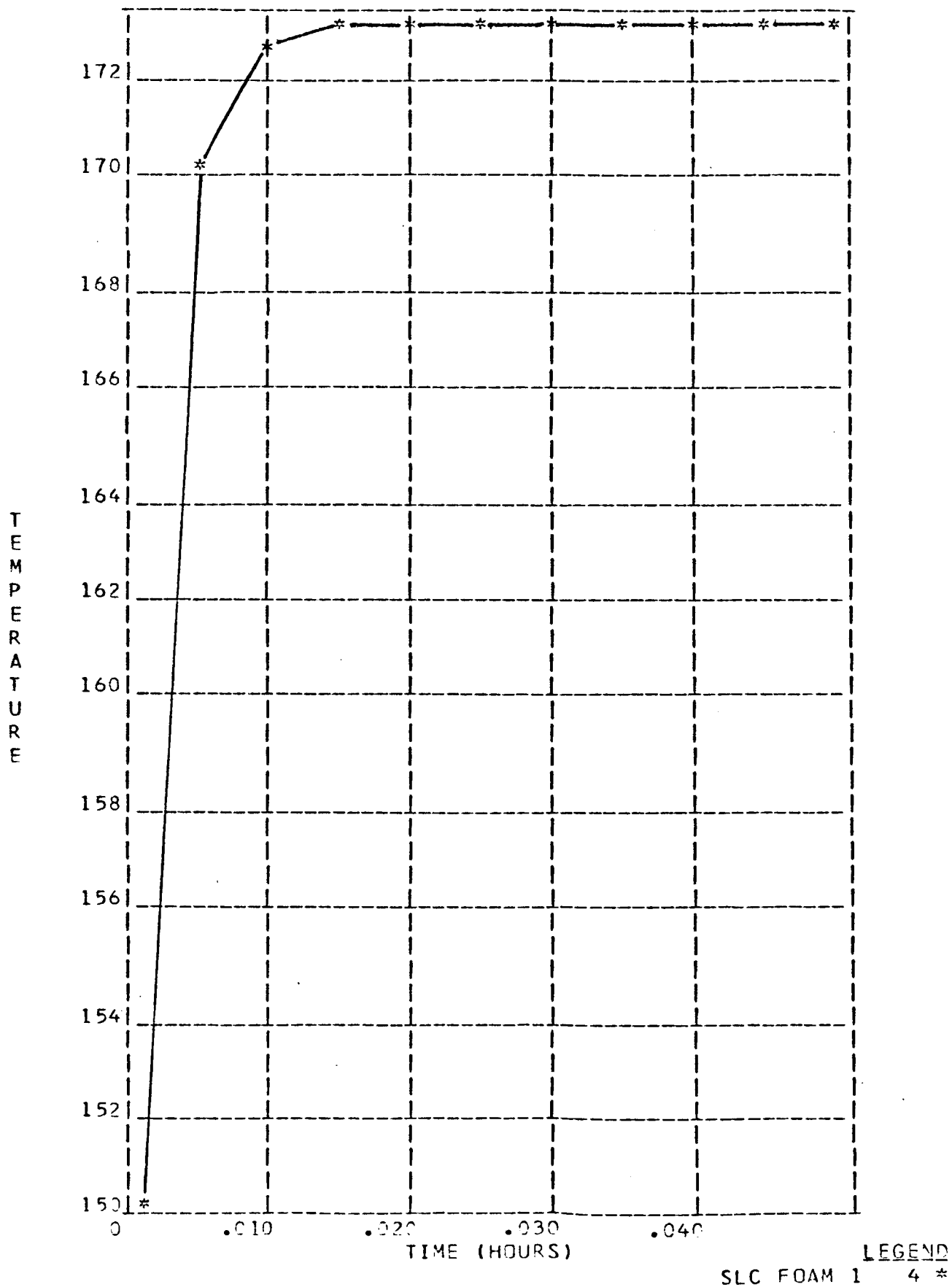


23 OCTOBER 1967

BOB TRAYLOR

EAAB 6193

SOLAR CELL THERMAL ANALYSIS INNER WRAP

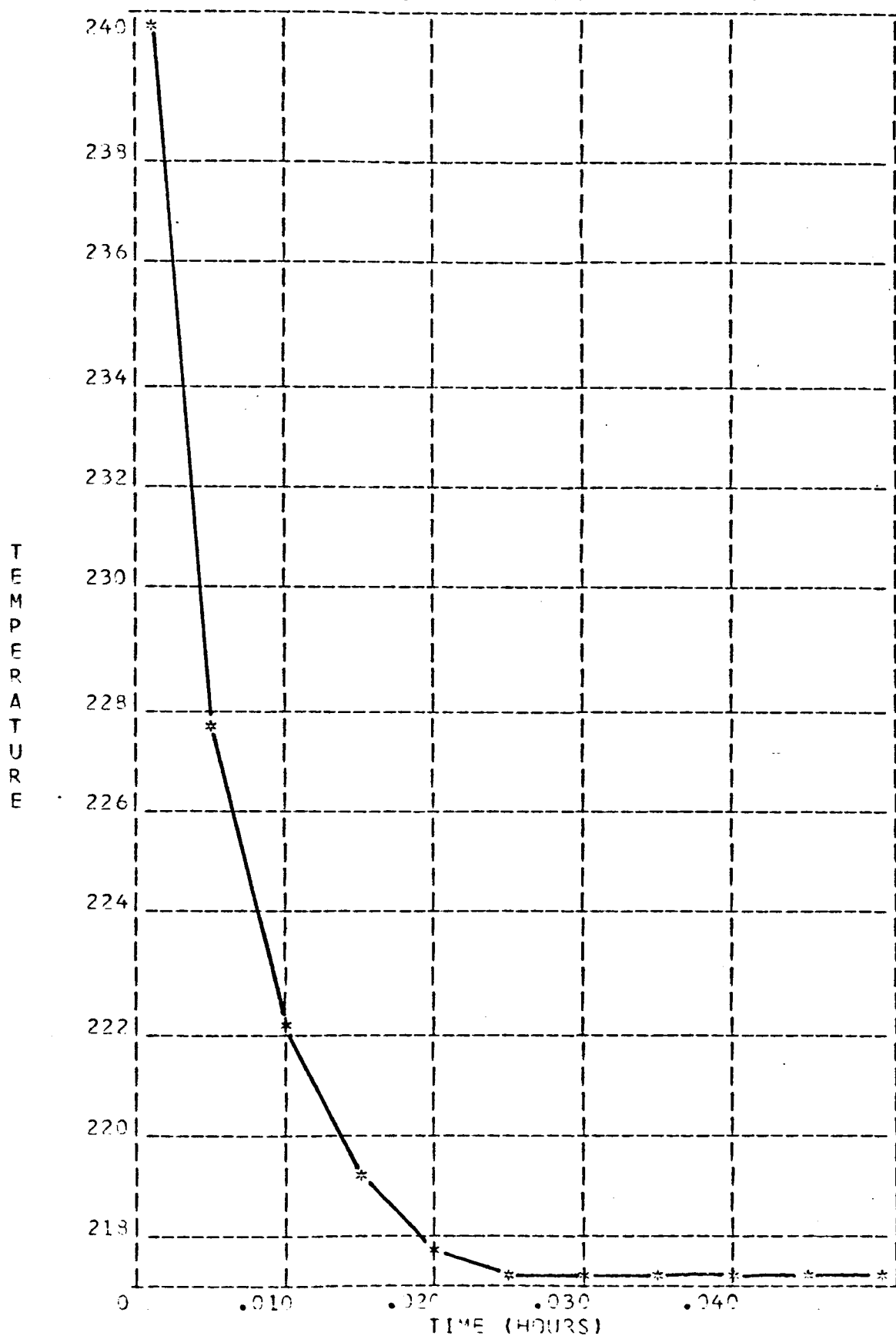


18 OCTOBER 1967

BOB TRAYLOR

EAAB 6193

SOLAR CELL THERMAL ANALYSIS OUTER WRAP



GLASS1

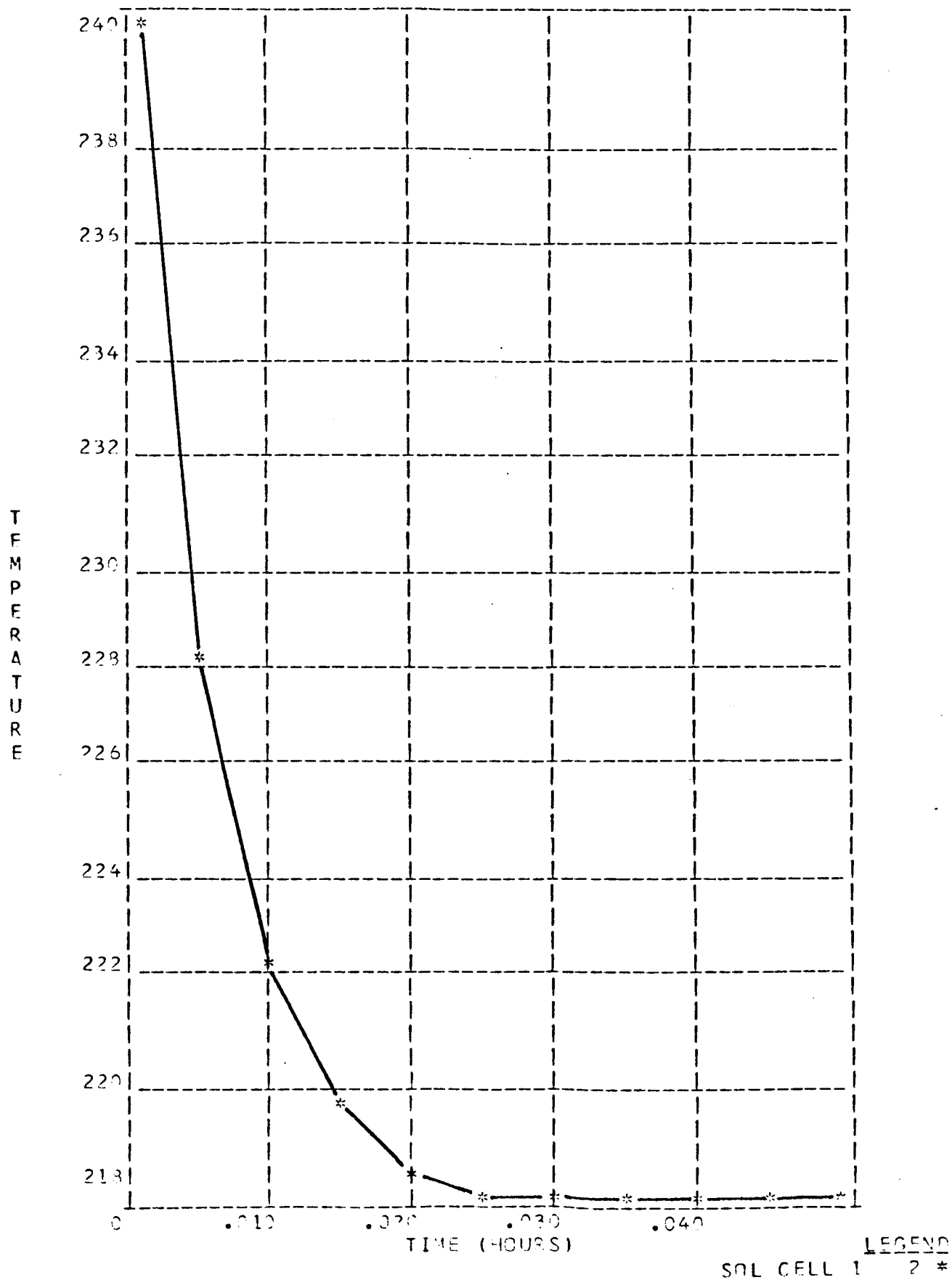
LEGEND
1 *

18 OCTOBER 1967

BOB TRAYLOR

EAAB 6193

SOLAR CELL THERMAL ANALYSIS OUTER WRAP

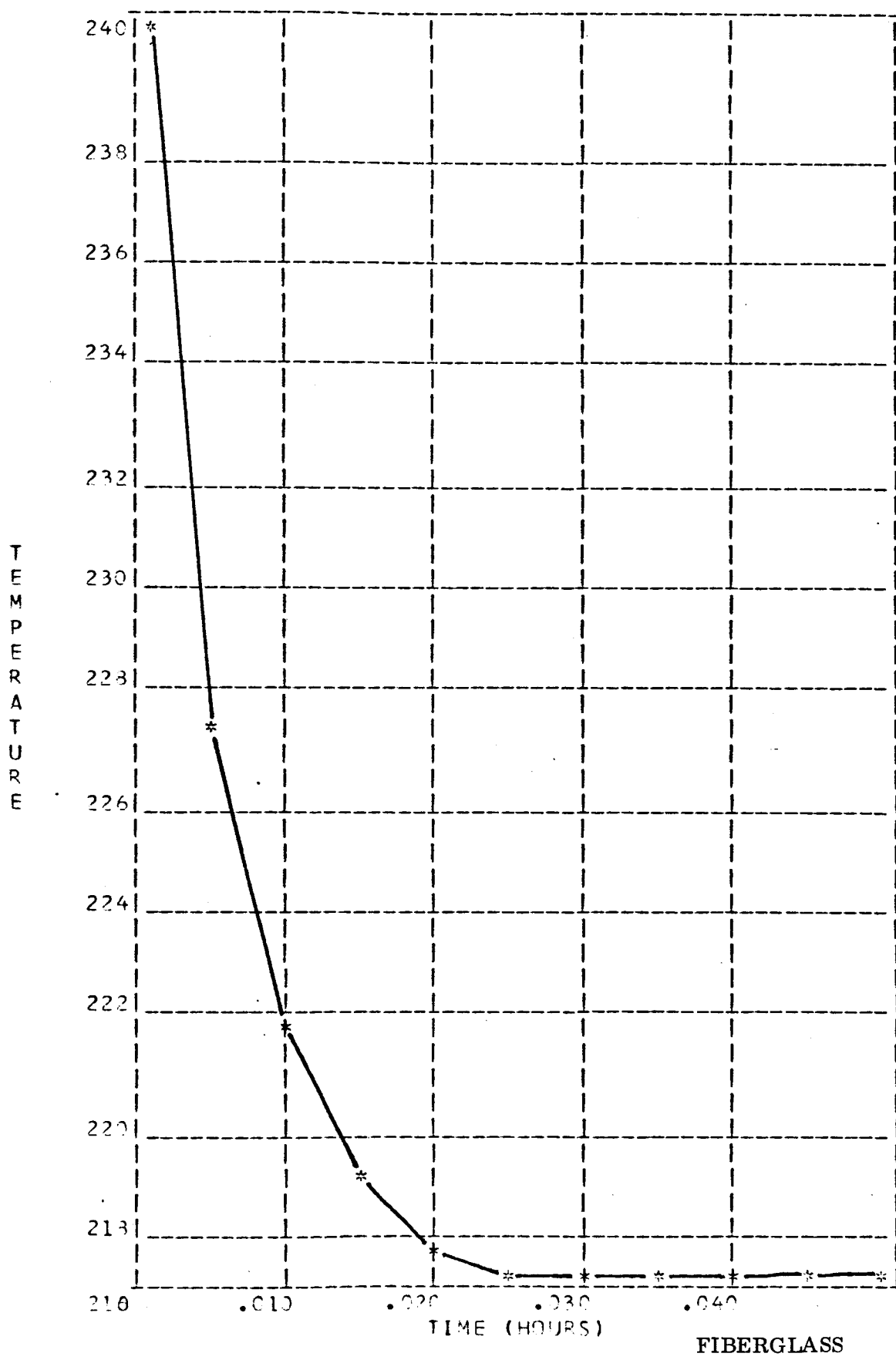


18 OCTOBER 1967

BOB TRAYLOR

EAAB 6193

SOLAR CELL THERMAL ANALYSIS OUTER WRAP

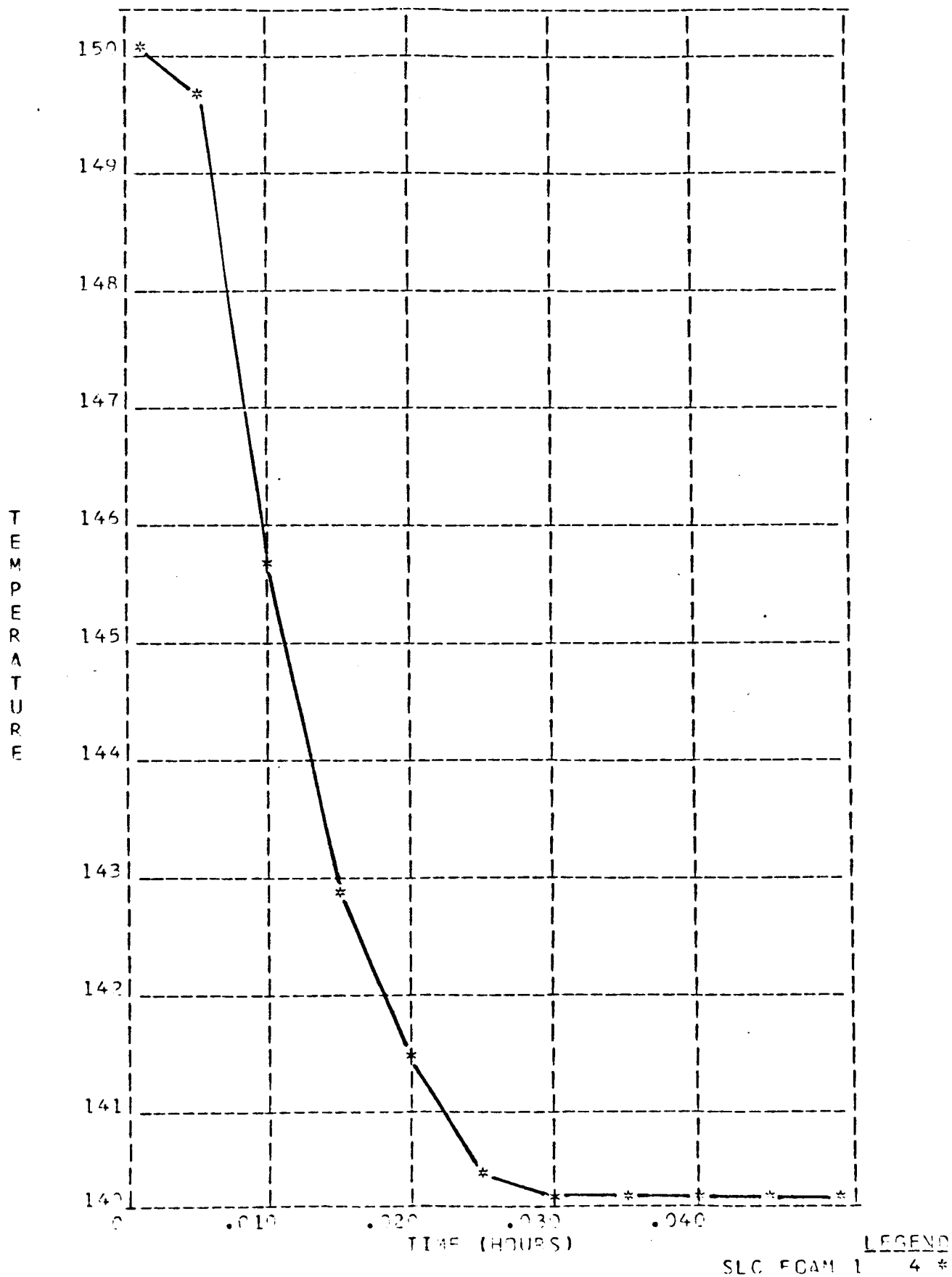


18 OCTOBER 1967

BOB TRAYLOR

EAAB 6193

SOLAR CELL THERMAL ANALYSIS OUTER WRAP



3.3.2.10 Solar Cell Installation Studies

3.3.2.10.1 Circuit Layout Analysis

The solar cell array is the principal power source on present day satellites. The physical, mechanical and electrical restraints which govern the design of a deployable rollup solar cell array will be discussed in the following paragraphs.

Area Utilization

Area utilization is defined as the maximum number of solar cells that can be bonded to a given area of substrate. Percent utilization is a function of solar cell size, spacing between cells, circuit termination design, substrate size and optimized circuit output power considerations.

Solar Cell Size

Area utilization or packing factor will be based on industry standard sizes for solar cells currently being manufactured. For a 2x2 cm cell these dimensions are $.788 \pm .005 \times .788 \pm .005$. For a 2x6 cm cell these dimensions would be $.788 \pm .005 \times 2.394 \pm .005$. The $2.394 \pm .005$ dimension for the 2x6 cm cell utilizes the .005 wasted space between 2x2 cm cells and increases the packing factor by 0.63 percent.

Solar Cell Spacing

Nominal spacing between parallel solar cells is .005 inch. This spacing achieves a parallel cell pitch (distance from one cell edge to the corresponding edge of an adjacent cell) of .798 inch. Nominal spacing of series connected cells is .012 inch. This spacing achieves a cell pitch of .805 inch. Upper size limits on cell size dimensions were selected to avoid the possibility of interference between cells and coverglass and to allow greater flexibility in assembly tooling.

Spacing between adjacent portions of a circuit will be .012 inch. Spacing between complete circuits will be .012 inch.

Circuit Layout

The major parameters to be considered at this time are substrate size, operating voltage, and magnetic field considerations.

The original substrate cell laydown area dimensions were 83.80 x 36.50 inches. These dimensions were subsequently changed to 76.83 x 36.81 inches during a design conference. This dimension change alleviated a problem area which developed during vibration tests and allowed a more desirable solar cell circuit to be designed. The 36.81-inch dimension allows 45 2x2 cm cells to be placed in series. The 76.83 inches allows 96 2x2 cm cells in parallel plus appropriate intercircuit spacing.

If 2 x 2 cm cells are used, each substrate will consist of 4320 individual 2 x 2 cm cells connected in series parallel in eight circuits. Each circuit consists of 3 cells in parallel by 180 in series (4 subcircuits of 45 cells in series). The even number of circuits minimizes the magnetic field associated with the completed solar cell array.

Operating Voltage

A study of current space power conditioning equipment revealed that the optimum operating voltage should be in a range of 50 to 100 volts for maximum power conversion efficiency. The aforementioned configuration utilizing a 2-ohm base resistivity solar cell at a temperature of 55°C will generate approximately 76 volts at the maximum power point. This voltage is within the 50 to 100 volts considered optimum.

A second configuration consisting of 90 solar cells connected in series was considered. The voltage produced by this configuration was 38 volts but the output current was doubled. The higher output current necessitated the installation of substantially heavier wiring. This configuration was consequently rejected.

3.3.2.10.2 Power Analysis and Trade-Offs

The following parameters established the baseline for an analysis of the large area roll-up solar cell array.

- (1) Power output 10 watts per square foot of the solar cell area. This is the area covered by solar cells including intercell spacing.
- (2) Illumination intensity at air mass zero and 1 A.U. equivalent solar intensity.
- (3) Operating solar cell array temperature assumed to be 55°C.
- (4) An over-all power to weight ratio of 30 watts per pound. (.0333 pounds per watt.) This total weight was divided so that 54 percent was allocated to the solar cells and associated wiring and 46 percent was allocated to the deployment mechanism and substrate.

The general approach to the power analysis will be discussed in the sequence in which pertinent steps were performed.

Solar Cell Analysis

Typical I-V curves for 2 ohm and 10 ohm centimeter base resistivity solar cells in various thicknesses were selected from the report entitled "Performance of Very Thin Silicon Solar Cells" included as an appendix to this report. Appropriate extrapolation was performed to extract maximum power voltage and current at the specified operating temperature (55°C).

The I-V curves presented in the aforementioned report were for a 2x2 centimeter solar cell with a corner dart contact configuration.

The maximum power current and voltage were adjusted to reflect losses due to coverglass installation, assembly and mismatch. Based on dimensions discussed in an earlier paragraph of this report it is possible to determine that 224 solar cells measuring 2x2 cm will occupy an area of one square foot.

Three types of solar cell configurations will be considered: the bar contact, large bar contact, and the corner dart contact. The latter offers the distinct advantage of supplying a significantly higher power output for a given gross area of silicon. This additional power is due to the larger solar cell active area. The magnitude of this power gain is approximately 2.3 percent greater than the bar contact configuration solar cell.

Curves have been developed for power output per unit area versus solar cell thickness for both bar contact and corner dart contact cells with silicon base resistivities of 2 ohm and 10 ohm centimeters. These curves are presented in Figures 25 and 26.

Weight Per Unit Area Calculation

The weight per unit area was divided into two areas: weight directly associated with the solar cell, and weight associated with the power collection and transmission system.

Weights associated with a 2x2 cm silicon solar cell area follow:

Solar Cell	23.65 milligrams per mil thickness
Cover Glass	24.28 milligrams per mil thickness
Cover Glass Adhesive	18.00 milligrams per cell

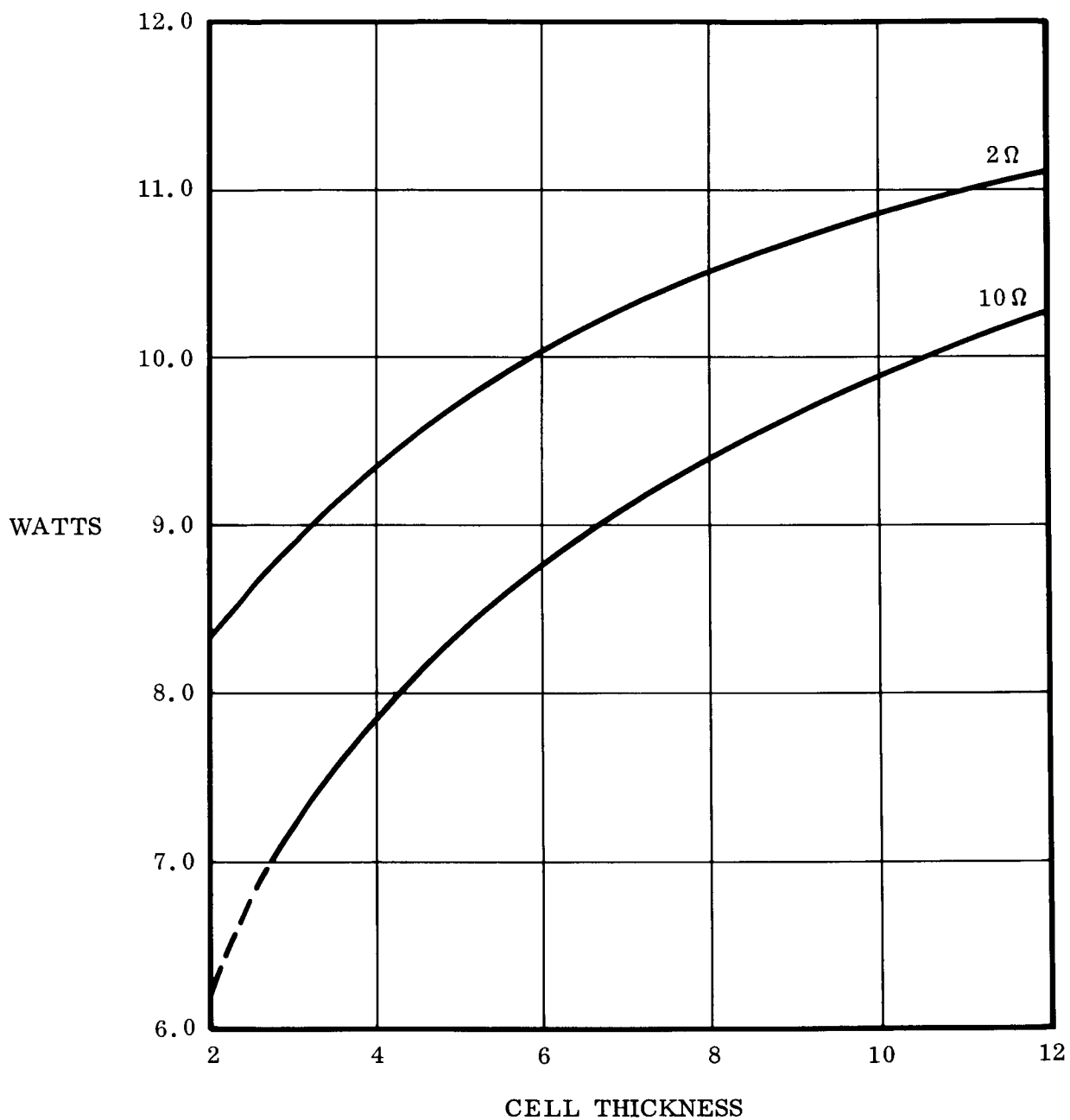


Figure 25. Power Output per Cell Thickness (Watts/Ft. ²)
2 x 2 cm Corner Dart Contact

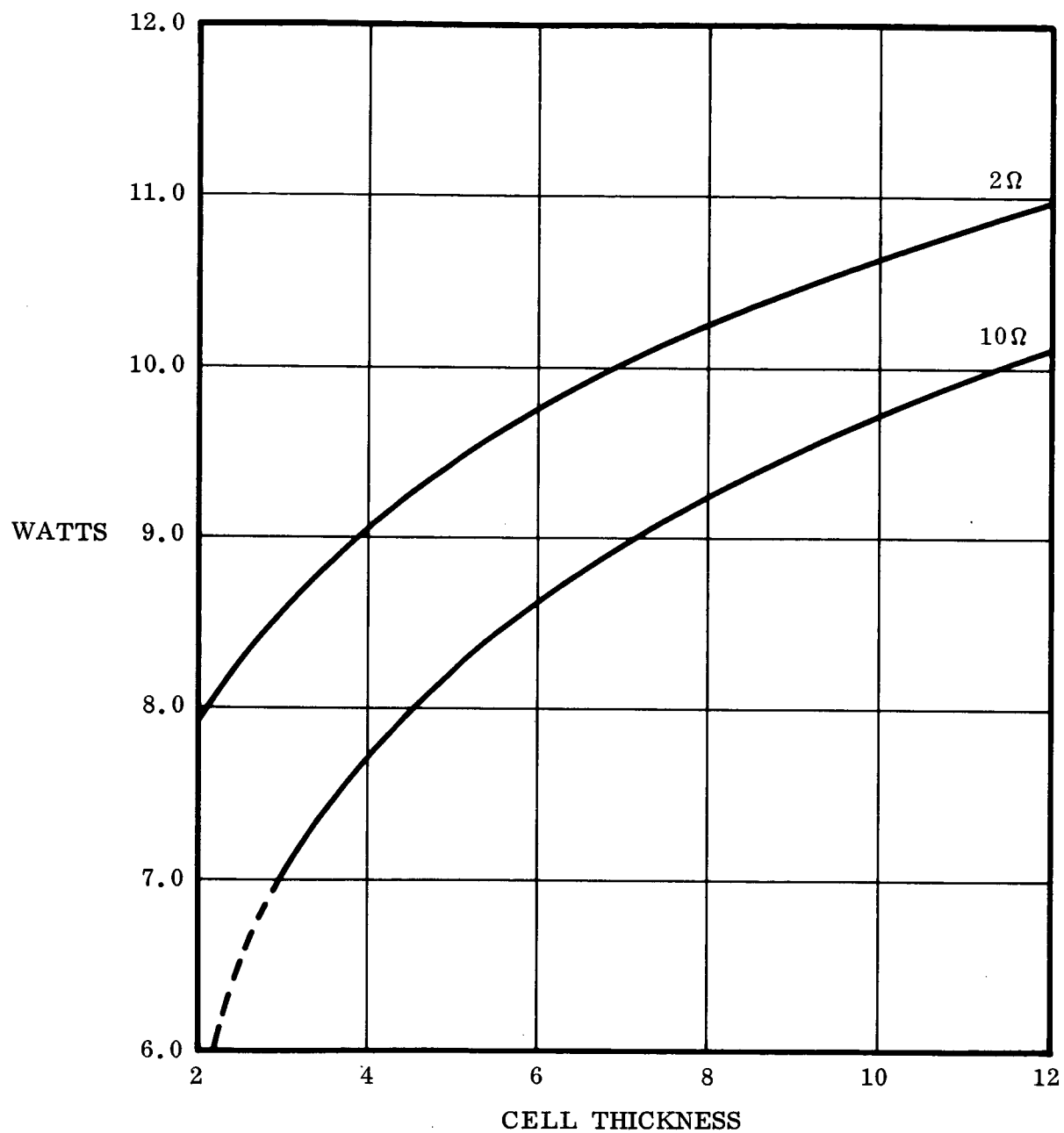


Figure 26. Power Output per Cell Thickness
Watts/Ft.² 2 x 2 cm Bar Contact

Solar Cell Adhesive	14.80 milligrams per cell
Copper Bus Bar	41.60 milligrams per cell
Solder	3.80 milligrams per cell

Based upon 224 2x2 cm solar cells 8 mils thick with a three mil cover glass, the weight is 0.1678 pounds per square foot.

Prior to calculating the weight of the power collection and transmission system it was necessary to establish the allowable power loss per square foot that could be tolerated. Figures 25 and 26 indicate that 0.10 watts per square foot would be a reasonable baseline figure. The power loss for one module (4320 cells) would therefore be 1.93 watts. This represents a power loss due to a module current of 2.72 amperes.

Utilizing ohms law $P = I^2R$ and solving for R, $R = 0.0260$ ohms.

This resistance is used to determine module cross-sectional area. Individual conductors are integrated to form longitudinal buses.

Major weight contributing elements are listed below.

<u>Item</u>	<u>Material</u>	<u>Weight</u>
Bus bars	Aluminum	1.152
	Copper	2.315
Transverse collector	Copper	.257
Feedthrough	Copper	.053
Solder		.009
Adhesive		.782
Insulation		.185
Total Weight Aluminum Bus		2.438 lbs.
Total Weight W/Copper Bus		3.601 lbs.

Total solar cell area for thirteen modules is 250.714 square feet; edge-to-edge, no allowances for turn around and terminating buses.

Power transmission system weights based on a square foot basic are:

- (1) .00972 pounds/ft² if aluminum foil is used
- (2) .01436 pounds/ft² if copper foil is used

The choice of the conductors is discussed in a later section of this report.

Curves of the weight per unit area are presented in Figure 27. These curves indicate the effect of using cover glass of different thicknesses. These curves have been plotted for only one type of solar cell due to the fact that the weights of bar contact and corner dart cells of a given thickness are almost identical. Two sets of curves are presented in Figure 27. One set indicates the weight of the solar cell array exclusive of the substrates, and the second set of curves indicates the overall proposed array weight. This was achieved by adding .150 pounds per square foot to the basic solar cell array weight.

The adjusted weight per unit area values for various cell thicknesses were used to calculate a new family of curves which indicate the power-to-weight ratio for the complete solar cell array. These curves are presented in Figures 28 and 29.

A third solar cell configuration should be considered at this time. This is the large area solar cell. For this particular application the 2x6 cm cell is ideal and presents several advantages over the present industry standard sizes. One advantage is the increased power output. This is achieved by more efficient area utilization and a flatter cell surface. This power gain is approximately 2 percent to 3 percent greater for a given area occupied by three individual 2x2 cm solar cells. A curve of weight per unit area is presented in Figure 30.

A further consideration to be evaluated is the significant cost saving that can be realized in the use of the larger solar cell. A discussion of cost is beyond the scope of this report but will be taken up at a later time. It will be sufficient to state that the cost saving is due to smaller number of units which must be handled.

3.3.2.10.3 Magnetic Moment Determination

The Roll-up Solar Panel has been designed in a manner to render the magnetic moment (M) and generated external magnetic field (B) minimum in values. This has been accomplished by alternating the direction of current flow in adjacent circuits for which the geometry is equivalent. Following is an analysis performed to determine the order of magnitude of the residual magnetic moment and external magnetic field.

Cross Configuration

Each individual solar cell circuit consists of 180 2x6 cm N/P solar cells laid out in a configuration as shown on page 126:

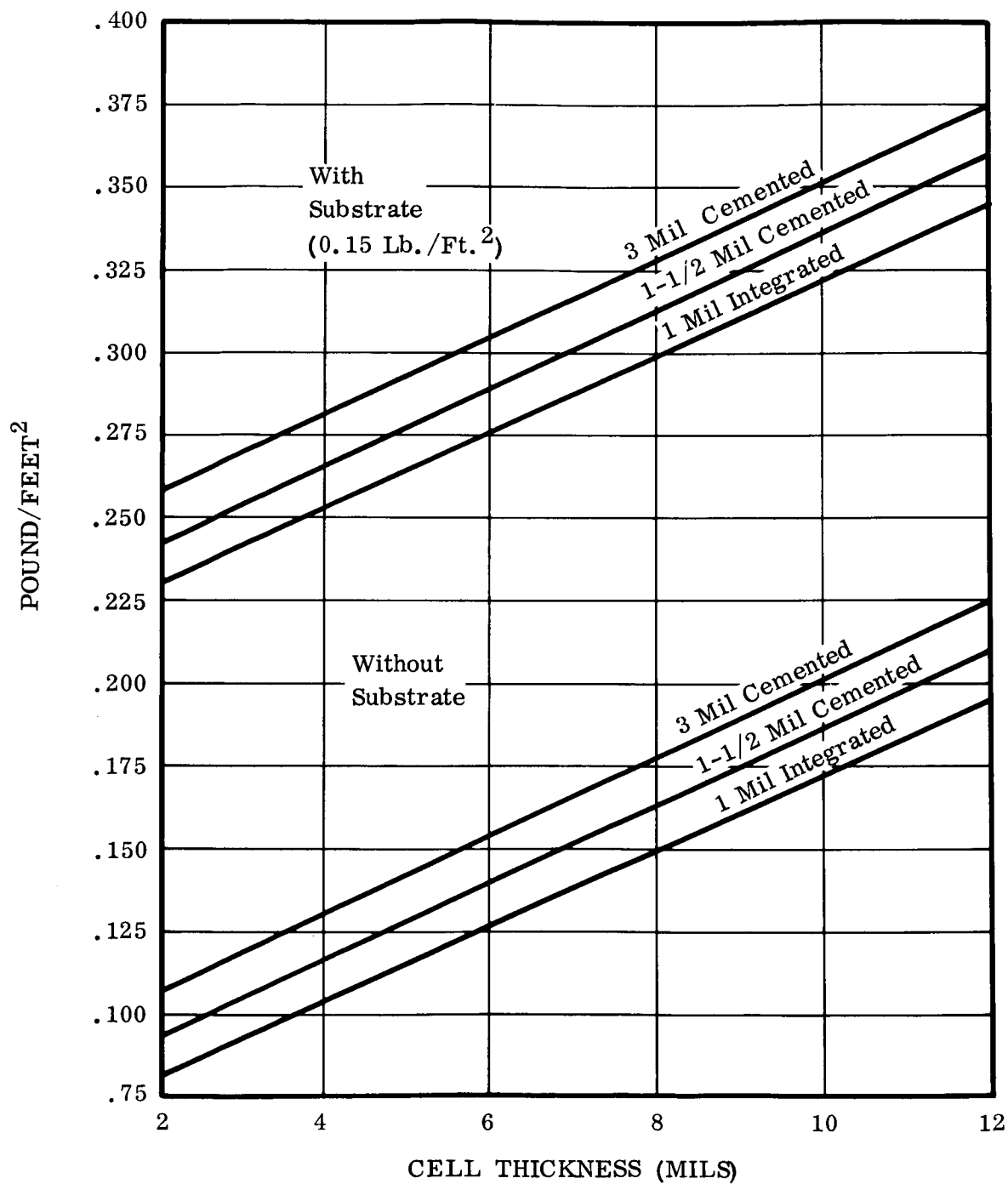


Figure 27. Weight/Area vs. Cell Thickness, 2 x 2 cm, Corner Dart Contact, Various Coverglass Thicknesses and Systems

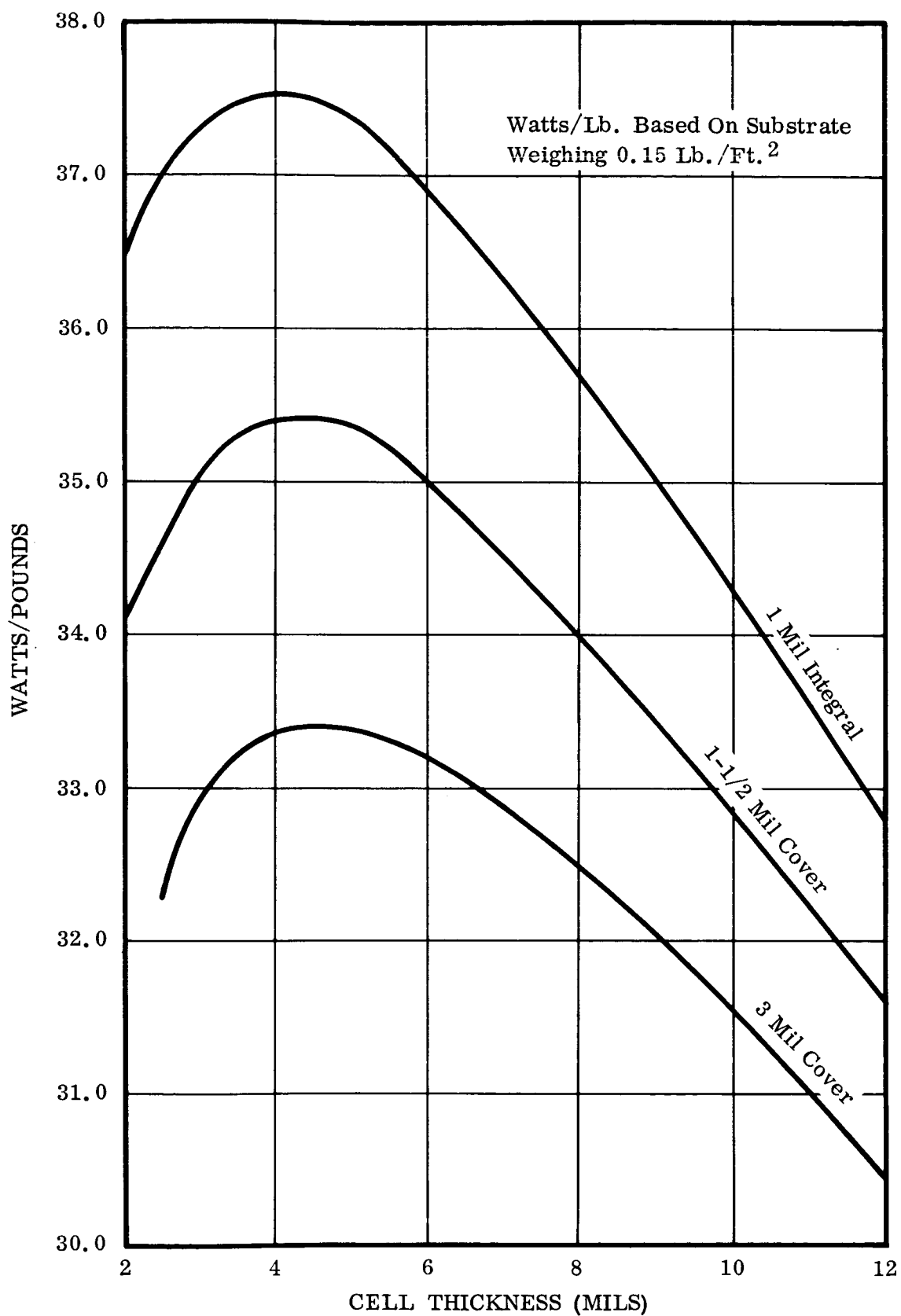


Figure 28. Specific Power Output per Cell Thickness, 2 ohm cm, Dart Contact Cell

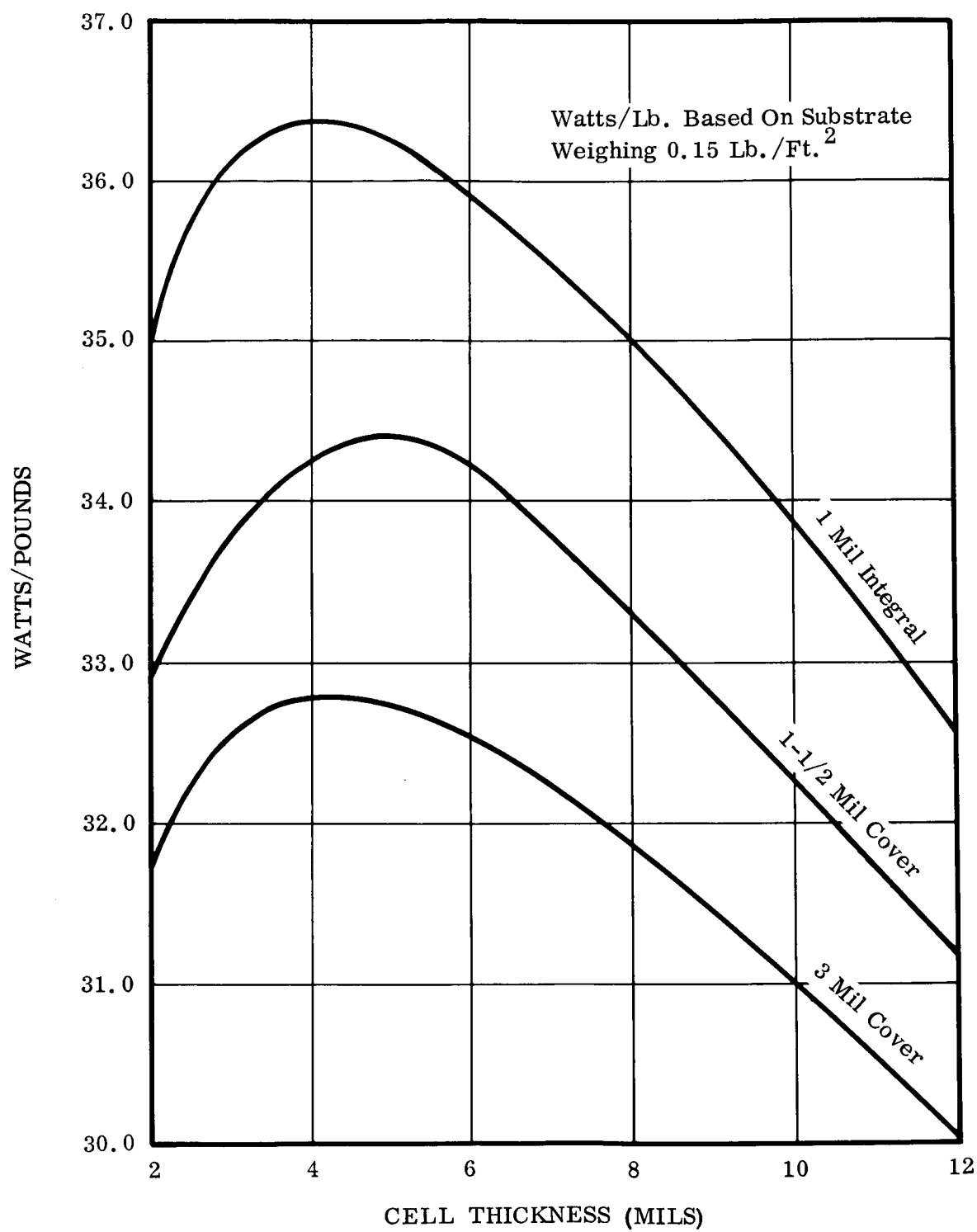


Figure 29. Specific Power Output per Cell Thickness,
2 ohm cm, Bar Contact Cell

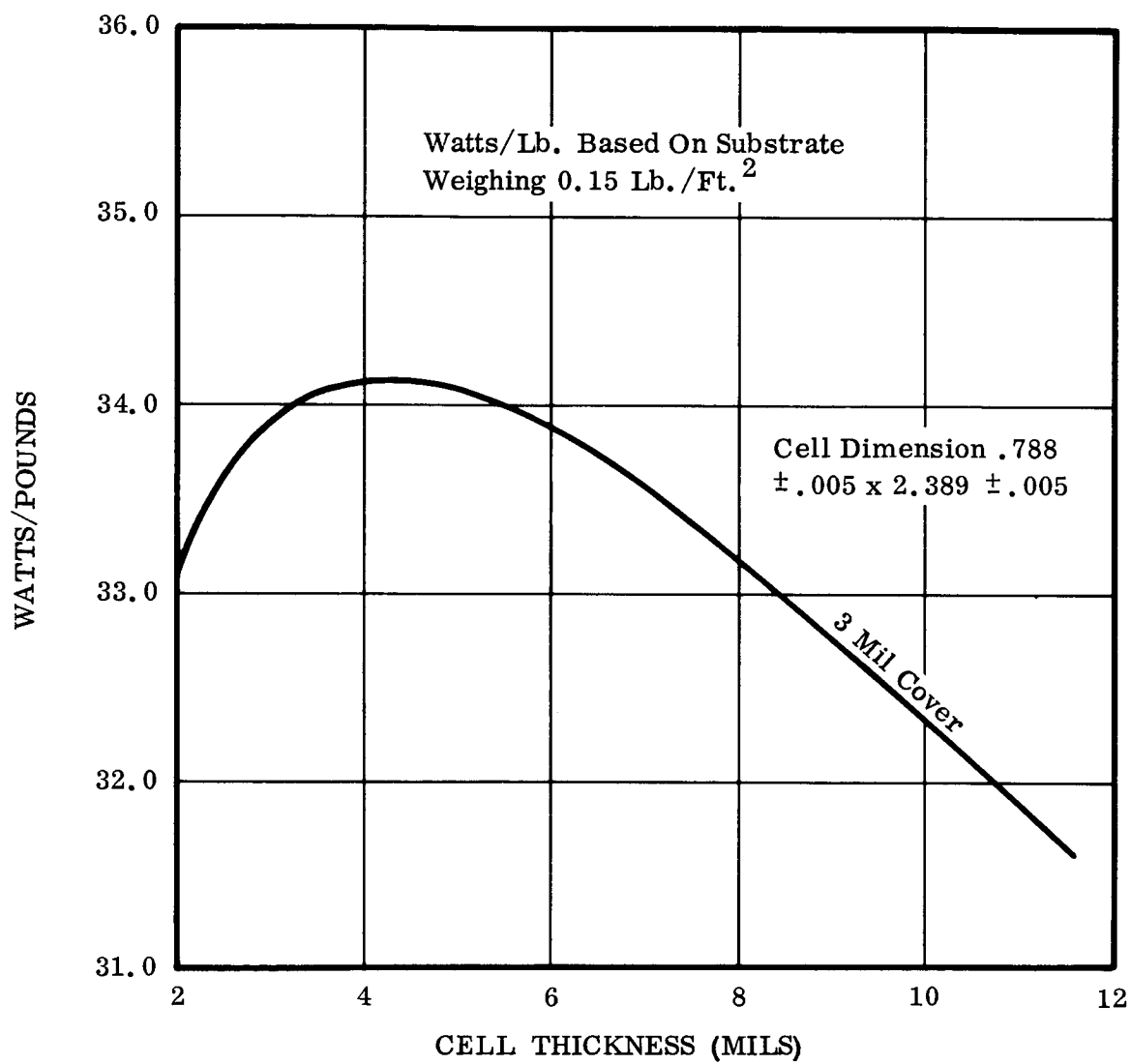
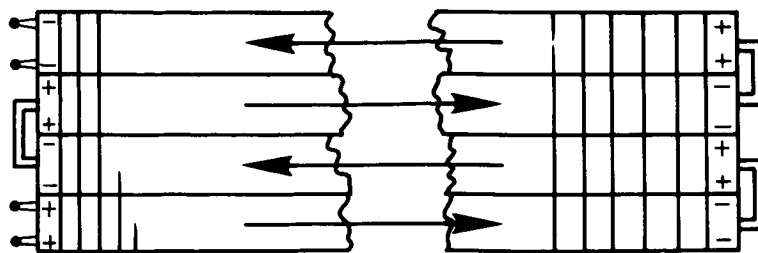


Figure 30. Specific Power Output per Cell Thickness,
2 ohm cm, Bar Contact, 2 x 6 cm Cell



-----45 series solar cells in each circuit leg -----

The direction of the electron flow is indicated by the arrows. Eight such circuits are connected electrically in parallel with polarity of adjacent circuits being geometrically reversed. (See Spectrolab Drawing SK-0007, Figure 31). Parallel connection is accomplished by two strip bus bars of .001 inch thickness which are separated by .0005-inch thick insulation. These bus bars run transverse to the direction of the paddle and are connected to a redundant set of panel bus bars of the same cross-section and separation which run in a longitudinal direction. A total of 13 sets of 8 circuits are connected in this manner to the panel bus bars for a total of 104 circuits for the entire panel.

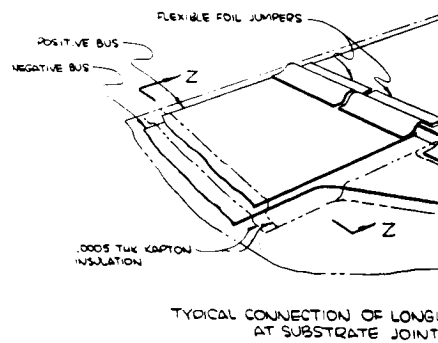
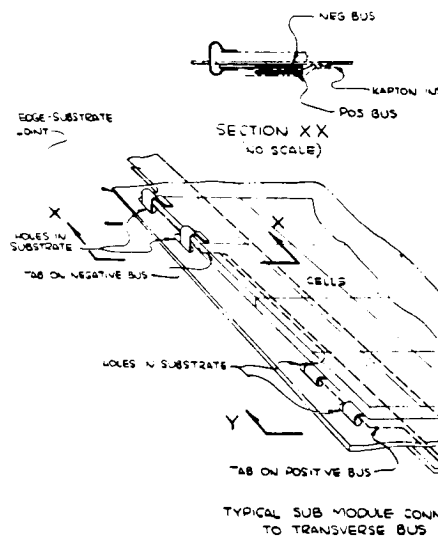
Magnetic Moment

The magnetic moment (M) is defined by the expression
$$M = \sum_{n=1}^3 i a_n X_{on}$$
 where i is the current, measured in amperes and a_n is the projection of the circuit area in a plane for which X_{on} is the normal unit vector, and for which the three unit vectors are orthogonal.

In the case of the roll-out panel, it is convenient to define the orthogonal set of unit vectors as being normal, transverse, and longitudinal to the panel substrate in the extended position. Each component of the magnetic moment shall be considered in turn.

Normal Component of Magnetic Moment

The normal component of the magnetic moment for each individual circuit will be equal to the circuit current of 0.341 ampere times an effective area of $18 \times 90 \text{ cm}^2 = 0.162 \text{ m}^2$, which equals $5.52 \times 10^{-2} \text{ amp-meter}^2$. Since adjacent solar cell circuits have reversed direction of the electric current, the contributions to the normal component of the magnetic moment from all the circuits on the panel will cancel in pairs. Thus, the normal component of magnetic moment will vanish.



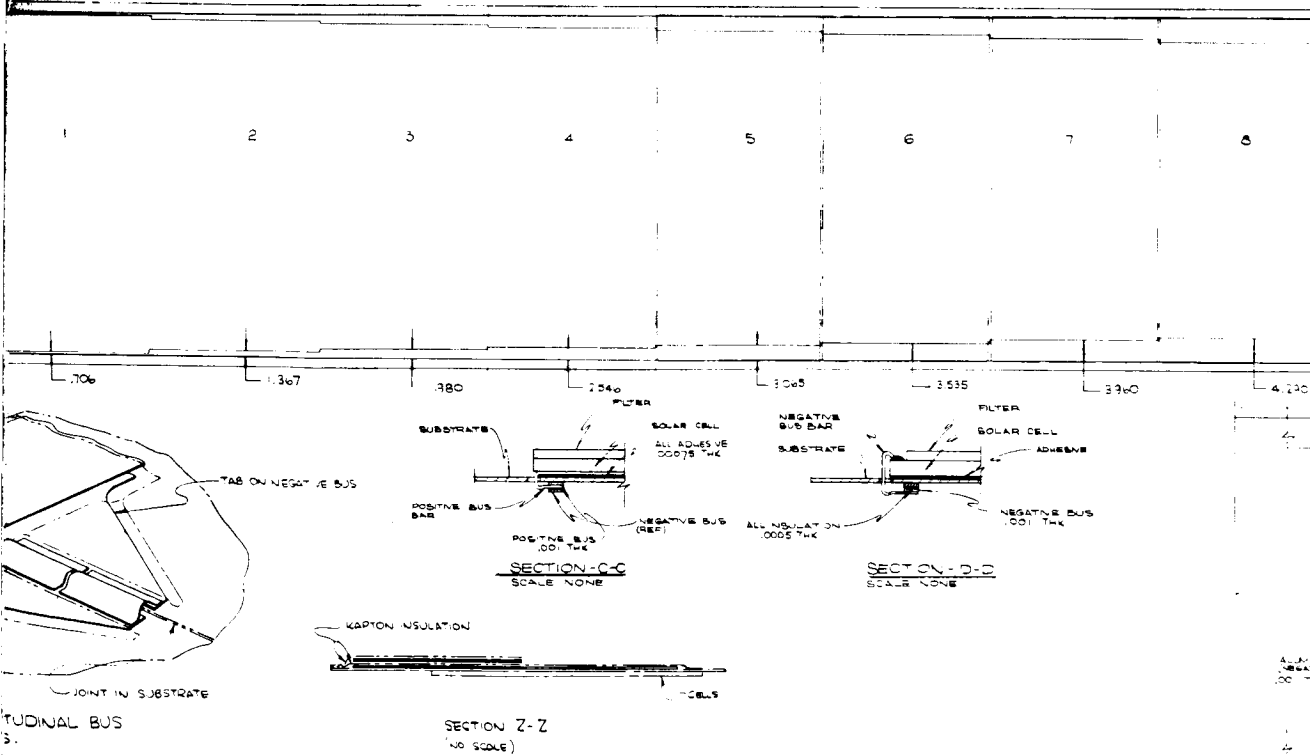
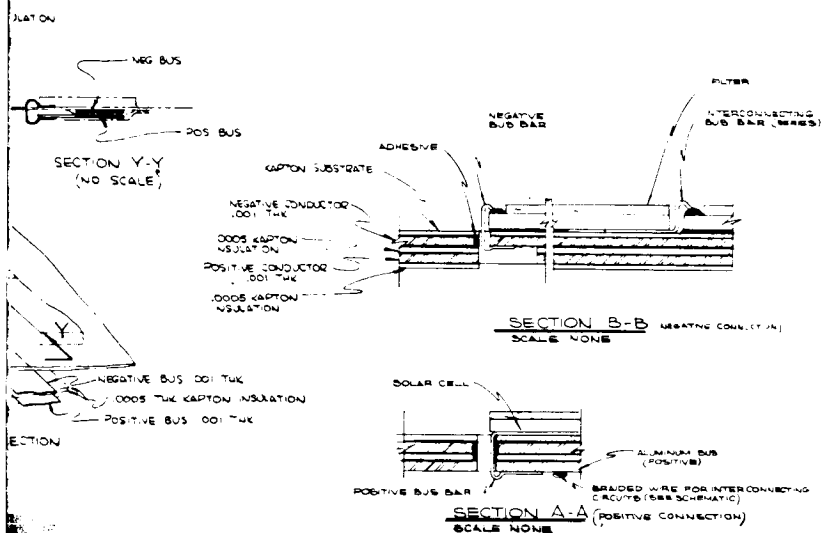


Fig 31

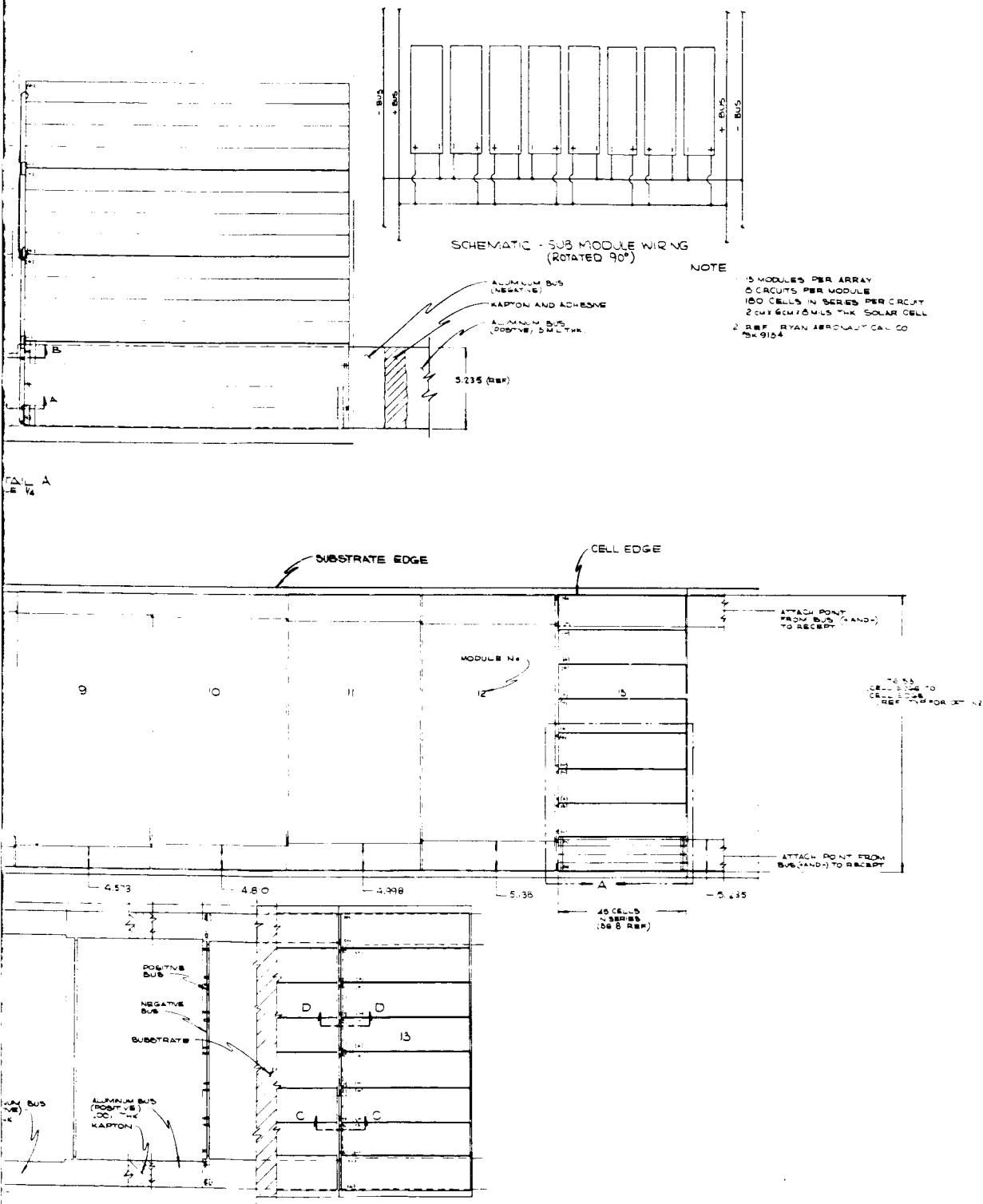


Figure 31. Spectrolab Drawing SK-0007

Longitudinal Component of Magnetic Field

As a result of the collection of the current from each section of eight circuits by the transverse circuit bus bars for distribution to the longitudinal panel bus bars, a component of the magnetic moment in the longitudinal direction will exist.

A net effective current equal to 8×0.341 amperes = 1.36 amperes will traverse a loop bounded by the width of the panel, 1.95 meters and the mean separation of the bus bars which is $0.0015 \text{ inch} = 3.75 \times 10^{-5}$ meters. The area of this loop is then $7.31 \times 10^{-5} \text{ m}^2$ and the magnetic moment contribution is $9.96 \times 10^{-5} \text{ amp-meter}^2$. Since there are a total of 13 such bus bar loops the total value of the longitudinal component of magnetic moment for the entire panel will be $1.3 \times 10^3 \text{ amp-m}^2$.

Transverse Component of Magnetic Moment

The panel bus bars extend a distance of 12.15 meters along the length of the extended panel. The mean separation of these bus bars will be the same as in the previous case so that the total area of the current loops will be $4.56 \times 10^{-4} \text{ m}^2$. The effective current passing through this loop will be one-half of that at the termination which is $\frac{8 \times 13 \times .341}{2} = 17.70$ amperes.

The effective transverse component of magnetic moment for the panel is then computed to be $8.1 \times 10^{-3} \text{ amp-m}^2$.

Reduction of Magnetic Moment

The components of magnetic moment in the transverse and longitudinal can only be reduced as a result of reducing the effective thickness between the bus bars. This may be accomplished only as a result of reducing the thickness of the bus bars and insulation. For mechanical stress considerations, this does not appear to be prudent.

Consideration of Magnetic Field Strength

It has not been stipulated at what position relative to the panel the magnetic field strength was to be evaluated, and if it were so stipulated it would be virtually impossible starting from basic definitions to perform such an evaluation (i.e., uses of law of Biot and Savart). Certain generalizations, though, can be made, which would be of qualitative nature:

- As a result of the reversal of current direction in each of the individual circuits relative to its neighboring circuits, the component of the magnetic field normal to the plane of the panel will tend to average to zero at a given point in space. This approximation will be more accurate at greater distances from the panel.
- The magnetic fields resulting from the transverse and longitudinal bus bars will cancel for each pair of positive and negative bus bars except in regions very close to the bus bars and that region between the two bus bars. As a result of the additive effect, the magnetic intensity will be of the extreme values in the region between the bus bars. Since no ferromagnetic materials will be placed in this region, this field should not affect the operation of the solar panel or adjacent equipment.

3.3.2.10.4 Conductor Selections

Conductor selection was governed by three basic considerations. These were minimum weight, optimum power loss per square foot of panel area, and a minimum thickness buildup during retraction.

The following conductors were evaluated:

- (1) Teflon insulated stranded wire
- (2) Teflon insulated ribbon conductors
- (3) Kapton insulated ribbon conductors
- (4) Copper foil conductor
- (5) Aluminum foil conductor
- (6) Copper clad aluminum foil conductor

The first three items were eliminated due to excess weight.

Copper and aluminum foils were compared. The weight saving realized by using a 0.001-inch aluminum foil was 1.163 pounds. Problems associated with joining aluminum will be alleviated by silver plating the aluminum in the areas to be soldered.

The copper clad aluminum foil would be an excellent material for this application but it is not available at this time. One manufacturer stated it would be approximately six months before samples would be available. This foil would consist of a layer of aluminum between two layers of copper; layer thickness would be of a 20:60:20 proportion. Handling and fabrication would be greatly simplified by the use of this material.

The aforementioned discussion was concerned with longitudinal bus bars which transmit power from the thirteen modules to the inboard end of the solar cell array.

The transverse collector strips which carry current from the positive and negative circuit terminations to the longitudinal bus will be either a braided wire or 0.002-inch thick x 0.200-inch wide silver-plated copper. No decision has been made pending a more rigorous investigation.

Feedthrough from the solar cell circuit terminations will be accomplished through the use of 0.002 by 0.100-inch silver-plated copper strips. Two strips will be used for each circuit termination to increase redundancy.

3.3.2.10.5 Blocking Diodes

Paragraph 3.7.1.2 of JPL document No. 501407 states that the possibility of shadowing is to be considered. This shadowing was not due to any appendages on the spacecraft but would be more total in nature such as complete shadowing of the entire spacecraft. Because of this possibility, the use of circuit-blocking diodes is not being considered. The only question which applies here is whether or not the vehicle will enter into such a situation that diodes would be needed, since any increase in panel components will only lower over-all reliability. For the illuminated situation, only the shorting of a cell to the substrate would produce a catastrophic failure. Because of the relatively conservative design the nonconducting substrate material employed, such a failure has a negligible probability. Thus, any cell failure would be either an open failure or a partial degradation in cell power output. In neither case would a circuit-blocking diode be necessary or beneficial. Since the array is to be oriented, any shadowing would be due to occultation of the sun by the earth, moon, or other large body. In such an occurrence, the whole array would be in shadow (except for the initial and final periods of occultation) and consequently other power sources would be in use.

A significant power saving would also be realized if the diodes are eliminated. This saving would amount to approximately 0.12 watts per square foot. A weight saving of 0.11 lbs. would also be realized.

After weighing all of the pertinent information it is recommended that the isolation diodes should be eliminated.

3.3.2.11 Weight Analysis

This section presents calculated weights of sub-elements of the solar array (based on nominal sheet thickness and engineering tolerances) for various configurations investigated to date. (The trade-off study phase of the program.) These calculations are compared with initial estimated weights which served as target weights for design control purposes. Data is summarized in Table 13. Tables 7 through 12 present weight calculations for sub-elements of the array.

The power to weight capabilities of the solar array is calculated considering various solar cell power output levels, combined with nominal and maximum expected solar array weights. These values establish a reasonable envelope of obtainable performance and indicate that the objective of the contract can be achieved. The equation used for these calculations is:

$$\text{Watts/Pound} = \frac{(\text{cell output})(\text{gross cell area})}{(\text{nominal array wt.})(K)}$$

Where:

$$\text{Gross cell area} = 250.71 \text{ Sq. Ft.}$$

$$K = (\text{growth allowance})(\text{tolerance allow.})(1.05)(1.04)$$

Figure 32 is a power to weight curve that illustrates changes which incurred during trade study activity and considers:

- (a) An electrical installation weight (cells, wiring, interconnections and adhesives) of, 0.19 lb/ft^2 of gross cell area; utilizing $2 \times 2 \text{ cm} \times 0.008 \text{ mil}$ cells with 0.003 mil cover glass. This solar cell installation concept will provide $10.0 \text{ watts per square foot}$ power at 1 A. U.
- (b) Structural/mechanical weight at 4% above nominal to account for material and fabrication tolerances.

TABLE 7

DRUM SUPPORT AND GUIDE SLEEVE MOUNT ASSEMBLY


Item	Trade Study Cal. Wt.		Target Wt.
	Built-up Structure	Machined Structure	
1. Support Channels	0.510	0.375	0.456
2. Slide Guide	0.177		0.200
3. Slide	0.165	0.102	0.171
4. Slide Guide Fitting		0.839	
5. Slide Retaining Angles		0.052	--
6. Bulkhead and Adjustment Screws	0.146		0.108
7. Springs	0.140	0.140	0.140
8. Spring Fittings	0.027	0.014	0.027
9. Mount Lugs	0.074		0.074
10. Shims	0.030		
11. Mount Bolts		0.046	
12. Helicoil Inserts		0.024	
13. Retaining Screws		0.026	
14. Stop Mechanism	0.303	0.303	
TOTAL WEIGHT	1.572	1.921	1.176
SELECTED CONFIGURATION 			

TABLE 8

BEAM GUIDE SLEEVES

Item	Trade Study Cal. Wt.	Target Wt.
1. Side Plates O/B	.3203	} .3130
2. Side Plate I/B	.2014	
3. Top Plates	.1764	} .2660
4. Bottom Plates	.0559	
5. End Plates I/B	.1457	} .054
6. End Plate O/B	.0148	
7. Internal Bulkheads	.1184	.131
8. Attach Angles	.0380	
9. Frame Angle	.0409	
10. Closing Angle	.0096	
11. Guide Inserts	.0842	} .429
12. Top Plate (Support)	.0432	
13. Support (Guide insert)	.2284	
14. Angles (Clutch end)	.0075	
TOTAL WEIGHT	1.4847	1.193
<div> SELECTED CONFIGURATION <div> </div> </div>		

TABLE 9

WRAP DRUM ASSEMBLY

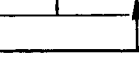
Item	Trade Study Cal. Wt.		Target Wt.
	Coiled Harness	Slip Ring	
1. Skin (Mag.)	4.794	4.794	5.696
2. Intermediate Rings	.111	.111	.115
3. Harness Retaining Ring	.102	.102	.106
4. End Plate Rings	.300	.300	.113
5. End Plates	2.172	2.172	1.786
6. Harness Spool	.101	-	.101
7. Roller Brgs	.160	.160	-
8. Electrical Harness	1.600	-	1.600
9. Electrical Wiring	.500	.600	-
10. Bushing Supports	-	-	.167
11. Spindle	.167	.167	-
12. Snap Rings	.009	.009	-
13. Sleeve Holder	-	.076	-
14. End Caps	-	.065	-
15. Sleeves	-	.246	-
16. Sleeve Flanges	-	.056	-
17. Contact Rings	-	.098	-
18. Ring Holders	-	.164	-
19. Insulator	-	.005	-
20. Contacts	-	-	-
21. Screws	-	.010	-
TOTAL WEIGHT	10.016	9.135	9.684
SELECTED CONFIGURATION 			

TABLE 10

SPACECRAFT MOUNT ASSEMBLY

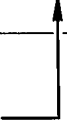
Item		Trade Study Cal. Wt.		Target Weight
		Titanium Support Structure	Alumin. Support Structure	
1. Top and Bottom Plates	(.025)	1.6752	1.0470	.466
2. Side Plates	(.028)	1.1146	.6966	.368
3. Internal Bulkheads	(.020)	.5596	.3498	.074
4. Closure Angles		.4154	.2596	.093
5. Spacecraft Mount Fttg's	(2)	.0669	.0669	.033
6. Drum Mount Fttg's	(4)	.0374	.0374	.039
7. Center Attach Fttg's	(2)	.0366	.0366	.098
8. Truss Tubes	(4)	.2491	.2491	1.787
9. Center Truss Tubes	(2)	.0827	.0827	.029
10. Truss Pins	(12)	.1176	.1176	.132
11. Fasteners Attach Fttg's (#6 alum. huckbolts)	(24)	.0960	.0960	
12. Corner Bracket	(2)	.0406	.0406	
TOTAL WEIGHT		4.4917	3.0799	3.119
<div>SELECTED CONFIGURATION</div> <div>  </div>				

TABLE 11

SUBSTRATE INSTALLATION WEIGHT


Item	Trade Study Cal. Wt.		Target Weight
	Fiberglass Substrate	Kapton Substrate	
1. Substrate (.001 Kapton)	-	2.016	3.233
2. Substrate (.001 Fiberglass)	3.024	-	
3. Substrate - Beam Attach Clips (.280)	.043	.043	} .050
4. Substrate Clips (240)	.058	.058	
5. Beam Tabs (260)	.063	.063	.045
6. Side Beams (Basic)	3.029	3.029	3.272
7. Tip Intercostal	.263	.263	} .502
8. Stop Damper Pad	.012	.012	
9. Substate Doublers (240)	.061	.061	.082
10. Drive Strips (1/2" Wire)	.536	.536	.599
11. Damper Pads	3.454	3.454	2.527
12. Adhesive (Item 10)	1.382	1.382	-
13. Outer Wrap Blanket	-	-	.158
TOTAL WEIGHT	11.925	10.919	10.469
SELECTED CONFIGURATION 			

TABLE 12
DEPLOYMENT/RETRACTION SYSTEM

Item	Trade Study Cal. Wt.		Target Weight
	Redundant System	Non- Redundant System	
<u>Extension System</u>			
1. Drive Motor and Pinion	2.000	.756	.756
2. Motor Brace	.021	-	.017
3. Motor Mount	.017	.017	.023
4. Idlers	.240	.240	.240
5. Torque Tube Shaft	.234	.234	.090
6. Drive Sprockets	.208	.208	.230
7. Torque Tube End Caps	.106	.106	.111
8. Torque Tube	1.481	1.481	1.607
9. Torque Tube Support	.234	.234	-
10. Bushings and Retainers	.033	.033	.071
11. Roll Pins	.013	.013	
12. Attach Bolts (Shaft)	.060	.060	
13. Attach Bolts (Motor)	.040	.040	
14. Limit Switch and Drive	.200	.200	.100
15. Electrical Wiring	.200	.200	
<u>Retraction System</u>			
16. Drive Shaft-Pulley	.107	.107	
17. Drum Pulley and Clutch	.206	.206	
18. Spring Belt	.150	.150	
19. Belt Retainer	.021	.021	
20. Fasteners	.035	.035	
TOTAL WEIGHT	5.606	4.341	3.245
SELECTED CONFIGURATION			

TABLE 13
WEIGHT SUMMARY

Array Subassembly Item	Calculated Weight Selected Configuration	Target Weight	Calculated Weight, as percent of total
Drum Support and Guide Sleeve Mount Assembly	1.921	1.176	2.5
Beam Guide Sleeves	1.485	1.193	1.9
Wrap Drum Assembly	9.135	9.684	11.9
Spacecraft Mount Assembly	3.080	3.119	4.0
Panel Assembly	10.919	10.469	14.2
Deployment/Retraction System	5.606	3.245	7.3
TOTAL STRUCTURAL WT.	32.146	28.886	41.8
Solar Cell and Electrical Installation Wt. (2 x 2 x .008 with .003 CG. - 250.714' @ .178 lb/ft ²)	44.627	47.636	58.2
TOTAL ARRAY WT.	76.773	76.522	100.0

Power/Weight Summary

The watts/pound capability of the selected solar array configuration (the result of the trade-off studies), as influenced by the various considerations discussed in this section, is determined as follows:

1. Nominal solar array weight with 10.0 watts per square foot solar cell power output.

$$\text{Watts/Pound} = \frac{(10) (250.714)}{76.773} = \underline{\underline{32.66}}$$

2. Maximum solar array weight which allows for a 5% growth of the array during detail design and a 4% tolerance for material and fabrication tolerances with power at 10 watts/square ft.

$$\text{Watts/Pound} = \frac{(10)(250.714)}{(76.773)(1.04)(1.05)} = \underline{\underline{29.91}}$$

3. Solar Array with

a. Nominal wt. = 76.773 pounds

b. 2 x 2 - .008 cells, .003 cover glass with power of 10.25 watts/ft² as calculated for proposed design - Ref: Section 3.3.2.10.2

$$\text{Watts/Pound} = \frac{(10.25)(250.714)}{76.773} = \underline{\underline{33.47}}$$

4. Maximum solar array weight as defined in 2.0 above with a power output of 10.25 watts/ft².

$$\text{Watts/Pound} = \frac{(10.25)(250.714)}{(76.773)(1.04)(1.05)} = \underline{\underline{30.65}}$$

Ryan Selected Configuration

5. Solar array with

a. Nominal weight = 76.773 pounds

b. 2 x 6 - .008 cells, .003 cover glass with power output of 10.50 watts/ft² - Ref: Section 3.3.2.10.2.

$$\text{Watts/Pound} = \frac{(10.50)(250.714)}{76.773} = \underline{\underline{34.27}}$$

6. Maximum solar array weight as defined in 2.0 above with power output of 10.50 watts/ft².

$$\text{Watts/Pound} = \frac{(10.50)(250.714)}{(76.773)(1.04)(1.05)} = \underline{\underline{31.31}}$$

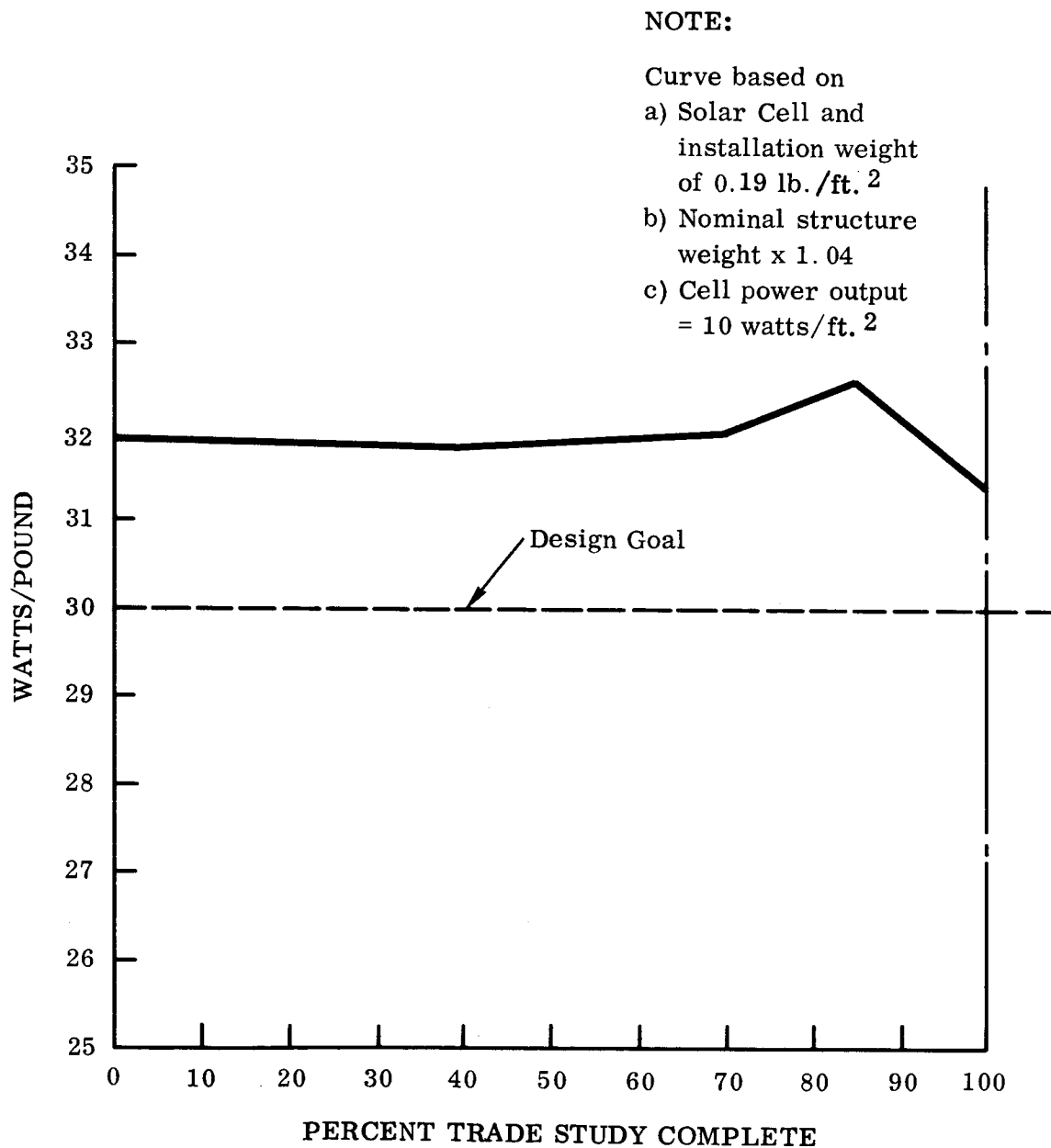


Figure 32. Power/Weight Monitor

3.3.2.12 Reliability Considerations

3.3.2.12.1 Array Structures and Mechanisms

A review of the reliability requirements for the 30 watt per pound roll-up solar panel was performed. The structural reliability goal appears reasonable but methods for predicting statistical structural reliability with confidence, without benefit of substantiating tests involving exorbitant costs, have yet to be developed.

Testing accomplished by Ryan on a similar structure (a 50-square-foot roll-up solar array, Ref. 1) has developed confidence that the reliability objectives for the 250 square foot solar array can be achieved. The 50-square-foot array has been deployed and retracted approximately one hundred times without a critical structural failure occurring. A collapsible titanium beam, very similar to the beam design to be used on the 250-square-foot array, was deployed from a drum and retracted 2,000 times without a failure of catastrophic nature. Some local buckling and cracks were evident but did not detract from functional capability. This simile is considered to be a valid comparison to the subject design, even though conducted at room ambient temperatures and sea level pressures, as titanium is unaffected by space environment except for temperature, (in this case, -150 to + 300 °F). A range that would have negligible effect on the properties of titanium. Extensive tests have also been conducted on the clips and plastic materials to be used to attach the substrate panels to the extendible beams. The tests demonstrated the feasibility of the attachment design and provided some statistical evidence of the suitability of the clip material. Engineering confidence tests such as this detect potential failure modes and provide the opportunity to institute corrective measures in the conceptual design phase.

Reliability studies of the drive motor arrangement used to deploy the array indicated that a proposed motor redundancy would not necessarily assure reliability. Partial redundancy is expected by utilizing two motors coupled through a differential to drive the roll-up drum. Even though the motor failure rates are relatively high (77.0 failures per 10^6 hours) the actual deployment or mission time is so small that the probability of success for one mission is very high

Motor failure rate	15.4/ 10^6 hours
Missile K factor	5.
Mission time	.1 hour

$$R = e^{-t} \text{ or for case}$$

$$\text{Where } (\lambda t) \text{ is } < .01, R = 1 - \lambda t,$$

$$R = 1 - .1 \times 77.0 \times 10^{-6}, R = 1 - 0.000007, R = .999993$$

For completely redundant devices with identical reliabilities the total reliability is approximately equal to one (1) minus the n^{th} power of the unreliability of a single device. The relationship is shown mathematically as:

$$R_{\text{red.}} = 1 - (1 - R_i)^n$$

or

$$R_{\text{red.}} = 1 - Q^n$$

where

Q = the device unreliability

and

n = the number of devices in parallel.

Several methods were studied for ways of transmitting collected array power to busses on the spacecraft via the rotating wrap drum. The major obstacle is the problem of maintaining electrical contact during movement of the drum. A system of making contact after completion of deployment was considered but was discarded because partial deployment would have resulted in a complete failure to connect (complete contact) the array. Another consideration was to utilize a conductor that would roll and unroll around the drum mandrel and permit permanent contact to terminals beyond the drum. This method is very reliable but was rejected because of the high weight of the required conductor material as well as possible flexure and position problems with the conductor. The selected method affords high reliable and lowest weight. This method uses brushes and slip rings to provide for rotational termination. Complete electrical transmission redundancy is provided from the substrate termination through the slip ring to the spacecraft terminal.

A re-evaluation of the potential failure modes discussed in the pre-contract proposal resulted in tradeoffs during the design study phase to

reduce the probability of occurrence or to change the effects of such failures. Modes that were discussed and action that has been taken are:

<u>FAILURE MODE</u>	<u>ACTION</u>
1. Boom - local buckling with permanent set wrinkles.	Analysis has determined that in-flight loads are insignificant. The beam has been designed for ground handling conditions which are more critical. Consequently, the assembly can be inspected for any suspect conditions and the probability of any in-flight failure occurring is very remote.
2. Beam to substrate attachment separation.	Multiple, redundant attachments have been incorporated. Quantitative testing has been performed to evaluate the design.
3. Differential boom deployment rates.	Design incorporates positive drive arrangement to prevent this occurrence. A single torque tube with rigidly mounted, gear-toothed sprocket wheels on both ends will drive integral racks on the beams.
4. Proposed damping pads between panel wraps on support drum do not provide adequate cell protection under specified environmental conditions.	Extensive dynamic analysis performed to establish dynamics of wrapped drum. Testing of 50-square-foot array is currently in progress and is being carefully monitored for applicability of characteristics to 250-square-foot array design. Dynamics and stress analysis on larger array being updated as necessary. Vibration model of the wrap drum and installed substrate to be built and tested.

An additional failure mode was revealed during re-evaluation. It concerns the possibility of drum buckling during launch vibrations. Such a failure would be catastrophic, resulting in complete failure of an array with possible serious consequence in the performance of the prime vehicle. Several corrective methods were analyzed but the method selected which

corrected the problem was a redesign of the drum mounts to provide more positive drum support. The safety margin associated with the new approach provides qualitative assurance that the failure probability of this mode of failure is remote.

3.3.2.12.2 Solar Cell Power Supply

Reported herein are the results of the Reliability Analysis performed on the proposed design of a solar cell power supply for a roll-up array.

Included is a failure effect analysis and reliability model with appropriate calculations of system reliability and maximum anticipated power degradation. In view of the unusual characteristics of a roll-up array, descriptions and results of the experimental and analytical aspects of the array development will also be included.

The Array Configuration

Two array configurations are being considered. Both consist of 13 modules. Each module will contain 8 circuits. For Configuration A, the circuits will consist of 540 2x2 cm solar cells, 3 in parallel by 180 in series. For Configuration B, the circuits will have 180 2x6 cm solar cells in series. All wiring and connections will be redundant. An array lifetime of two years will be used for reliability calculations.

Diodes

Diodes will not be employed in either proposed array. A further discussion is contained in Appendix Section, 8.6.

SOLAR CELL FAILURE ANALYSIS

Failures Resulting in Complete Loss of Solar Cell Power

Short Circuit Failures

A short circuit of a solar cell results when a conducting path exists between the upper and lower surface of a cell. The most probable cause for this type of failure is a contact between the lower surface of the cell and the lead from the submodule bus bar which is connected to the top surface of the same cell. This will result in a short circuit of the affected cell. There will be a slight variation in the operating voltage and current for the other cells in that string resulting in a correspondingly small power degradation. This power degradation will be of the order of

one-half percent for the affected string when operating at no failure maximum power voltage. A total power degradation of the order of 1/10 percent per failure will result for the entire module. Quality control inspection of the intercell connections substantially eliminates the possibility of occurrence of such a failure. The probability of occurrence of this failure is therefore assumed to be zero. The configuration of 2x6 cm cells will have a slightly greater circuit reliability than the comparable configuration of 2x2 cm cells due to the reduction in cell interconnections.

A second source of shorting is caused when the negative bus contacts the positive bus causing complete loss of power for the whole array. The design as proposed will use Kapton H film insulator between both busses thick enough to prohibit any possible arcing. Quality control inspection of the assembly with bus bars and insulation will eliminate any human induced failures introduced during fabrication. The probability of such a failure occurring will again be zero.

Open Circuit Failures

Each solar cell is soldered at five points on its lower surface to a submodule bus bar. The series connection to the next submodule bus bar is completed by four solder joints on the top surface of each cell. For soldering performed with a high degree of workmanship, the solder joint reliability is 1.0×10^{-7} failures per 1000 hours and the probability of failure of a solder joint is 1.75×10^{-6} for two years. Since the four solder connections on the upper surface represent threefold redundancy, the probability that the cell will open circuit as a result of failure of all solder joints at the upper surface will be of the order of 10^{-27} for two years. The probability that a cell will open circuit as a result of a solder joint failure on the lower surface will be of the order of 10^{-33} for two years.

For a 2x2 cm cell with the Solaflex connections, there are three solder points on the lower surface and two (or four) on the upper surface which gives a probability of open failure of the order of 10^{-16} and 10^{-12} for the lower and upper surface respectively.

An open-circuit cell failure may result from the fracture of a cell. The probability is extremely small for such a failure not being detected during preliminary inspections or occurring during normal operating conditions. An open-circuit failure caused by the separation of the electrode grid from the upper surface of a cell may result from thermal cycling of the cell and/or vibration of the cell. If all possibilities of open-circuit

failure for normal operation are considered, the probability of an open-circuit failure of an individual solar cell is no greater than 3.2×10^{-5} per 1000 hours.

Investigations of cell fracturing have shown that due to the use of extended Solaflex® solder tabs, open failures will result in only a very small part of all cell fractures. A comparison of fracturing of the 2x6 cm cell and the 2x2 cm cell is contained in Appendix Section, 8.7.

Cell Failure Probabilities

In this section reliabilities will be calculated for the cells in configurations A and B. The 2x2 cm cell configuration will be examined first. The probability of "n" failures, out of a total of N cells, can be written as

$${}_N P_n = \frac{N!}{(N-n)! n!} P^n (1-P)^{N-n}$$

where P is the probability of failure for one cell during a two year period. For the 2x2 cm cell P equals 7.7×10^{-5} . Thus the probability of losing "n" 2x2 cm cells in the proposed array A (56,160 cells), will be

$${}_{56160} P_n = \frac{56160!}{(56160-n)! n!} P^n (1-P)^{56160-n}$$

The values of ${}_{56160} P_n$ for $n = 0, 1, 2, 3, 4, 5$, are

$n = 0$	0.007259
$n = 1$	0.035754
$n = 2$	0.088056
$n = 3$	0.144574
$n = 4$	0.178022
$n = 5$	0.175365

The sum of the ${}_N P_n$ from $n = 0$ to $n = K$ will be the probability that no more than K of the N cells will fracture. This can be called the reliability of no more than K failures, or R_K .

$$\left(R_K = \sum_{n=0}^K {}_N P_n \right)$$

For proposal A, 16 cell failures will give an R_K of 0.999918, i.e., there is a probability of 0.999918 that during a two year mission no more than 16 cells will fracture. Employing this figure in the total array reliability (including wiring, insulation, etc.) a total reliability of 0.9999 can be achieved. This calculation will be shown later.

The 16 cell failures will distribute themselves among the 13 modules. The probability of n failures within a single module will be $n p_{4320}$. Values for $n=1, 2$, and $3, 4$ are

$n = 1$	0.259
$n = 2$	0.049
$n = 3$	0.006
$n = 4$	0.00004

This indicates that the probability of 3 cells failing in the same module will be approximately $1/40$ the probability that one will fail. Since only 16 failures are considered this would imply that in the worst case the failures will distribute themselves such that 10 modules have one cell failure each and 3 modules have 2 cell failures each. By examining $n p_{540}$ the distribution of failures among the 8 circuits (each with 540 cells) can be found.

We get for $n = 1, 2, 3$

$n = 1$	0.045
$n = 2$	0.001
$n = 3$	0.00002

Thus the probability of two failures occurring in one circuit is $1/45$ the probability that one failure will occur. Since in the worst case, a module will have at most two failures, the most probable distribution among the circuits would be for two circuits to have one failure each, and 6 circuits to have no failures.

For Configuration A then, a total array probability of 0.99975 can be achieved with 16 failures distributing themselves in the worst case among the 13 modules, each with 8 circuits, as described above. This would represent a power loss for the array of approximately 0.05%, based on cell fracture power losses as described in Appendix 8.7.

For Configuration B (2x6 cm cells) a similar analysis can be conducted. In this case a two year failure probability of 19.3×10^{-5} is assigned to the 2x6 cm cell. In this configuration the array consists of 18,720 cells,

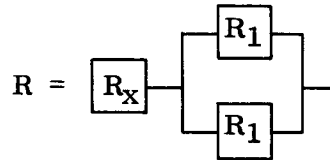
each module has 1440 cells, and each circuit has 180 cells. To achieve a total array reliability of 0.99975, 14 cell fractures will be necessary. These will, in the worst case, distribute themselves such that 11 modules will have one failure, 2 modules will have two failures, and one module will have no failures ($1P_{1440} = 0.230$, $2P_{1440} = 0.036$, and $3P_{1440} = 0.004$). No circuit in the worst probable case will have more than one cell failure ($1P_{180} = 0.0380$, and $2P_{180} = 0.0007$). Thus, an array power loss of approximately 0.05% will occur based on cell fracture losses as described in Appendix 8.7.

As shown in Appendix 8.7, roughly the same module power loss will occur for each fracture of a 2x6 cm cell as for a 2x2 cm cell. In view of this, the 2x6 cm configuration would exhibit a slight power advantage since 2 less cell fractures would be expected for a 0.99975 total array reliability.

WIRING RELIABILITY AND FAILURE ANALYSIS

Total Roll-out Array Reliability

The total array reliability, R , will depend upon the total reliability of the solar cells, R_x , and the panel wiring reliability, R_1 .

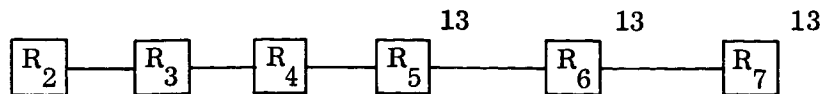


$$R = R_x \left[1 - (1 - R_1)^2 \right]$$

Panel Wiring Reliability

The panel wiring reliability will depend on the positive longitudinal bus reliability, R_2 , the inter bus insulation, R_3 , the negative longitudinal bus reliability, R_4 , the positive longitudinal bus to transverse bus solder connection reliability, R_5 , the negative longitudinal bus to transverse bus solder connection, R_6 , and the module wiring reliability, (R_7).

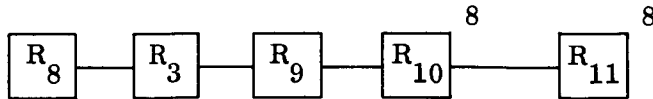
$$R_1 = R_2 \cdot R_3 \cdot R_4 \left[R_5 \cdot R_6 \cdot R_7 \right]^{13}$$



Module Wiring Reliability

The module wiring reliability, R_7 , depends on the positive transverse bus reliability, R_8 , the negative transverse bus reliability, R_9 , the positive circuit to transverse bus connection reliability, R_{10} , the negative circuit to transverse bus connection reliability, R_{11} and the reliability of the inter-bus insulator, R_{13} .

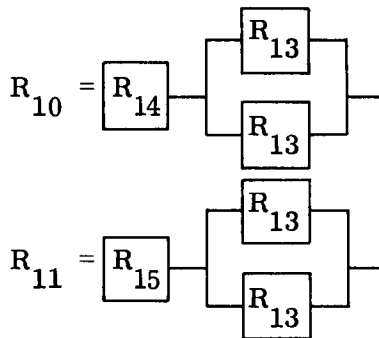
$$R_7 = R_8 \cdot R_3 \cdot R_9 \left[R_{10} \cdot R_{11} \right]^8$$



R_{10} (and R_{11}) will depend on the circuit bus bar to transverse module solder connection reliability, R_{13} , and the positive (negative) circuit bus bar reliability, R_{14} , (R_{15}).

$$R_{10} = R_{14} \left[1 - (1 - R_{13})^2 \right]$$

$$R_{11} = R_{15} \left[1 - (1 - R_{13})^2 \right]$$



Experienced Failure Rates

	<u>Component Failures/ Hr.</u>	<u>Reliability For (2) Years</u>
R		0.9999
R ₁		0.999999
R ₂	1.0×10^{-11}	0.9999998
R ₃	1.0×10^{-11}	0.9999998
R ₄	1.0×10^{-11}	0.9999998
R ₅	1.0×10^{-11}	0.9999998
R ₆	1.0×10^{-11}	0.9999998
R ₇		0.9999998
R ₈	No failures have occurred to present time.	1.0
R ₉	No failures have occurred to present time.	1.0
R ₁₀		0.999999999999
R ₁₁		0.999999999999
R ₁₃	1.0×10^{-11}	0.9999998
R ₁₄	No failures have occurred to present time.	1.0
R ₁₅	No failures have occurred to present time.	1.0

3.3.2.13 Handling Provisions & Ground Support Equipment

Design studies to date have not included a concentrated effort to identify a complement of special handling and test equipment. Trade-off studies have considered the handling and testing tasks as important requisites in evaluating design concepts but not to the extent of conceiving preliminary designs at this time. It is planned that development of special support equipment requirements and configurations will be accomplished concurrently with the detail design of the array. Since designs for subelements of the array must be compatible with fabrication capabilities, a concept of the general manufacturing plan will evolve with preparation of detail designs. This effort will expose and define basic parameters for handling aids and factory support equipment. It is quite reasonable to anticipate that these same fixtures and test equipment can be developed, and given consideration in design to weatherproofing and related environmental constraints for service as principal Ground Support Equipment (GSE) for use at an integration contractor's site and at the launch site.

Minimum equipments and their use are expected to include:

- Solar cell subpanel support frame. This fixture would be used to position, support, and restrain the flexible substrate. It would be used during cell installation and test and for transporting and storage of the solar cell subpanel until assembled into the complete array. The support frame would consist of a rectangular panel with index and retaining tabs around the outer edge. These tabs would match the edge slots in the substrate. Suitable covers would be provided for transportation and storage.
- Solar array support platform. This equipment would consist of a rectangular table with provision to support the wrap drum assembly and drive mechanism. It would also provide a roller system for continuous support of the beams and substrate installation when an array deployed or retracted. A protective cover would be provided to permit temporary storage of the array in a deployed mode.
- Shipping containers for interplant transportation of solar cell subpanels. The container arrangement would be capable of accommodating from one to four subpanels mounted in support frames.

- Shipping container for a complete roll-up solar array. The array assembly would be mounted to the container by means of the spacecraft attachment provisions and would be isolated from the basic container to inhibit ground handling damage. Adequate covers would be provided to augment container provisions for transportation and storage.

No other peculiar equipment requirements have developed in solar cell investigations except for the possibility of a need for air-conditioned, protective enclosures for electrical testing large modules in an outdoors environment, (e.g. Table Mountain site).

3.3.3 Test Data

Data presented in this section consists of test descriptions and results, performed to obtain data to support or substantiate analyses. The information presented in the same format as generated so that publication does not detract or depart from test data that is unique to the test materials and procedures utilized.

3.3.3.1 Adhesive Evaluations — Environmental

An evaluation of various adhesive systems currently in use on solar cell arrays was performed to ensure compliance of these systems with paragraph 3.3.1c of the JPL specification, SS501407A. This test was conducted to determine material selection only. The purpose of the test was to establish whether (1) adhesive properties suffered any appreciable degradation when thermal cycled in a high vacuum and (2) the adhesives showed any appreciable weight loss after being subjected to high and low temperature extremes in a high vacuum.

Tests were conducted on the following adhesives:

Coverglass	Solar Cell Bonding	Kapton Bonding
(1) LTV 602	RTV 41	Silastic 140
(2) Sylgard 182	RTV 511	Schjeldahl GT-100
(3)	RTV 577	

The sample preparation and testing was performed in the following manner:

Three adhesive specimens for each adhesive system were tested.

Cell to Substrate Adhesives RTV 577, RTV 511, RTV 41 and Silastic 140

- (1) Each specimen was fabricated using two standard 3/8 inch by 1 inch long hex head aluminum bolts with test adhesive. The head of each bolt was machined .215 inch thick and .564 inch in diameter. This would give a contact area between faces of 1/4 square inch. The bolt specimens were then paired up and mounted in vee blocks to line up the transverse axis and parallel the faces. The faces were lined up at a distance of 250 mils or 100 mils apart (100 mils for Silastic 140). The heads were then wrapped together circumferentially leaving a cylindrical shaped space between the

faces. Into this space was then injected the desired adhesive using a compressed air syringe. Each adhesive was mixed and cured in accordance with manufacturer's instructions. These specimens are for testing cell to substrate adhesives.

(2) Cover Slide Adhesives — LTV 602 and Sylgard

For these test specimens a solar cell was laminated to one bolt and a matching cover glass of the matching bolt. The two sections were then lined up in the V blocks, keeping the cell flush to the cover glass, and then cemented with test adhesive. Mixture procedures and curing were conducted according to manufacturer's instructions.

(3) Kapton Repair Adhesive — Schjeldahl GT-100

Two small squares were cut from a sheet of GT-100 (each 1 mil thick). They were then placed together and clamped between two paired bolts in the same manner as the other samples to give a desired 2-mil-thickness of adhesive.

The assembly of clamp and specimens were then placed in the curing oven (approximately 300°F for 15 minutes). The specimen was then removed from the oven to harden.

Test Procedure

Each sample was weighed and numbered before test and the weight recorded from an analytic balance. One control sample was then selected from each group of three adhesive samples. A pull test was performed to check the strength before subjection to thermal vacuum. The remaining samples were then placed in the thermal vacuum chamber. They were subjected to ten (10) cycles between -319°F and +284°F at a vacuum of 10^{-7} Torr and a temperature gradient of 6.7°F/minute. (90 minute cycle). Specimens were given a dwell time for stabilization at each temperature.

When thermal vacuum testing was complete, samples were reweighed to check for any outgassing during test. A tensile test was then conducted on the samples to check any degradation in adhesive strength.

Test Results

The adhesive samples were identified by the following numbers. The weight of each sample is included at this time so that an evaluation of outgassing can be performed.

SAMPLE NO.	MATERIAL	WT. BEFORE TEST (GRAMS)	WT. AFTER TEST (GRAMS)	CHANGE (GRAMS)
1 Control	LTV 602	13.455	13.456	—
2	LTV 602	13.491	13.479	.012
3	LTV 602	13.468	13.465	.003
4 Control	Sylgard 182	13.442	13.442	—
5	Sylgard 182	13.454	13.443	.011
6	Sylgard 182	13.533	13.522	.011
7 Control	Schjeldahl	12.326	12.327	—
8	GT-100	12.181	12.182	—
9	GT-100	12.195	12.197	—
10 Control	RTV 577	13.614	13.616	—
11		13.543	13.525	.018
12		13.428	13.409	.019
13 Control	RTV 511	13.487	13.489	—
14		13.443	13.436	.007
15		13.502	13.494	.008
16 Control	RTV 41	13.535	13.536	—
17		13.486	13.484	.002
18		13.455	13.450	.005
19 Control	Silastic 140	12.629	12.630	—
20		12.481	12.480	—
21		12.571	12.570	—

The average adhesive weight of RTV 577, RTV 511 and RTV 41 was approximately 1.480 grams, consequently the weight loss of the thermal vacuum samples represent a loss of about 1%, which will not degrade any of the spacecraft systems.

Stress strain curves were plotted for each of the test samples after the thermal vacuum tests. The curves of similar samples were compared for any gross deviations (± 10 percent) from the control samples. Any deviation in excess of 10 percent would indicate a severe degradation in the adhesive.

None of the samples, with exception of the Schjeldahl GT-100, showed any appreciable degradation due to thermal cycling in a vacuum.

It should be mentioned that the highest vacuum achieved during test was 1×10^{-6} Torr. This is a slight deviation from the specification pressure of 1×10^{-7} Torr. but this difference is of minor importance.

A copy of the thermal cycle test log is included in the Paragraph 8.8.

3.3.3.2 Peel Strength of Cell Bonding Adhesives

Objective

Ascertain an acceptable peel strength of cell bonding adhesives.

Materials Tested

- (1) Micaply, 2 to 3 mil (standard insulating material)
- (2) Kapton H
- (3) RTV 41 and RTV 511
- (4) 1 1/2 mil fiberglass

Method

Solar cells 2 x 2 cm were bonded face down on a heavy sheet of aluminum. Cell surface and material to be bonded to cell were coated with suitable primer and allowed to set for a period of 30 minutes. Adhesive was mixed and a metered amount was applied to the cell and squeegeed out to a uniform thickness of about 0.001 to 0.0015 inches. The adhesive was allowed to cure and was subjected to a 90° pull test. The pull rate was 4.4 millimeters per second.

Note: The Kapton H was subject to a chromic acid etch for 5 minutes and rinsed prior to priming.

Results

Material	Adhesive	Peel Strength (pounds)	Peel Strength (pounds/inch)
Micaply	RTV 41	$(2.2-2.5) \pm .3$	2.7 - 3.0
	RTV 511	$(1.6-2.0) \pm .1$	2.1 - 2.7
Kapton H	RTV 41	$2.0 \pm .1$	2.7
	RTV 511	$1.1 \pm .1$	1.4
1 1/2 mil Fiberglass	RTV 41	Fiberglass tore	—
	RTV 511	Fiberglass tore	—

3.3.3.3 Screening Tests on Kapton Bonding

Summary

This study was made to evaluate the adequacy of Kapton bonding for solar panel substrate. The Kapton film developed acceptable bond strengths with several adhesive systems.

The test results indicate that Kapton and four adhesive systems should be subjected to additional tests to determine their ability to meet all design requirements. The adhesives that warrant further testing are RTV3145, Dow Corning 92-024, FM1044R and TR150-25.

Materials

Materials used in the test were as follows:

- a. Kapton film, Type 100H
- b. Kapton film, Type 500H
- c. Adhesive systems (see Tables 14 and 15)

Test Methods

Kapton bonding studies were divided into two categories, solar cell bonding and Kapton splicing. Solar cell bonding was evaluated by performing peel tests. Kapton splicing was evaluated by performing lap

TABLE 14
SPLICING ADHESIVES

Adhesive	Temperature Curing (Deg. F)	Heat Up Time (Minutes)	Cure Time (Minutes)
TR-150-25	350	30	60
FM-1044R	350	30	60
Narmco-225	225	30	60
FM-96U	350	30	60
Narmco-329	350	30	60
Mystic Tape 7366	---	--	--
Mystic Tape 7361	---	--	--

TABLE 15
CELL BONDING ADHESIVES

Adhesive	Primer	Primer Drying Time (Minutes)	Cure Time (Hours)
RTV-102	---	--	168
RTV-3145	1200 Primer	30	168
RTV-108	SS-4155	60	168
RTV-60/Thermolite 12	SS-4155	60	168
92-024	---	--	168

shear and peel tests. Test specimens were prepared by the following methods:

Solar Cell Bonding Specimens

- Method 1 - Peel Test, Kapton bonded to aluminum.
- Method 2 - Peel Test, Kapton bonded to solar cells.

Kapton Splicing Specimens

- Method 3 - Lap Shear, Kapton bonded to Kapton.
- Method 4 - Peel Test, Kapton bonded to Kapton.

Peel specimens, prepared per Method 1 and 4, were cut into one-inch strips and peeled at a 90° angle on a Universal testing machine. The rate of peel was 2 inches per minute.

Peel specimens, prepared per Method 2, were cut into 0.5-inch strips and peeled at a 90° angle on a Universal testing machine. The rate of peel was 2 inches per minute.

Lap shear specimens prepared per Method 3 were cut into one-inch strips and loaded to failure in a Universal testing machine. The test specimens were loaded at a rate of 25 pounds per minute per 0.25 square inch of bond area.

Results

The peel data on the cell bonding adhesives is presented in Tables 16 and 17.

RTV-3145 and Dow Corning 92-024 developed the highest peel strengths. The other adhesives showed negligible peel strength.

Physical test data on the splicing adhesives is presented in Tables 18, 19, and 20.

For the 0.001 inch Kapton, the lap shear strength of the bond exceeded the tensile strength of the Kapton for all adhesive systems tested. Lap shear tests on 0.005 inch Kapton were performed to compare pressure sensitive tapes with the splicing adhesives. The tests showed the splicing adhesives to have 5 to 10 times the strength of the pressure sensitive tapes.

Peel strength of the splicing adhesives was only partially obtained. Peel samples prepared with FM-96U and TR-150-25 adhesives systems were not tested as the Kapton failed before a peel could be started. Of the other three adhesive systems, only FM-1044R showed acceptable peel strength.

TABLE 16
PEEL TEST DATA -- 0.001 INCH KAPTON TO ALUMINUM

Adhesive System	Average Peel Strength (lbs/in)	Failure Description
RTV-3145	9.5	Failed cohesively
RTV-102	< 0.2	Adhesion to Kapton
RTV-60/Thermolite 12/SS-4155	< 0.1	Adhesion to Kapton
92-024	2.0	Adhesion to Kapton
RTV-108/SS-4155	< 0.1	Adhesion to Kapton

TABLE 17
PEEL TEST DATA -- 0.001 INCH KAPTON TO SOLAR CELLS

Adhesive System	Average Peel Strength (lbs/in)	Failure Description
RTV-3145/1200 Primer	0.3	Adhesion to Kapton
92-024	2.5	Adhesion to Kapton
RTV-102	< 0.1	Adhesion to Kapton

TABLE 18
LAP SHEAR TEST DATA
KAPTON TO KAPTON -- 0.001 INCH THICK

Adhesive System	Average Shear Stress At Failure (PSI)	Failure Description
Narmco-225/2366 Primer	88.8	Kapton failed at edge of lap joint
Narmco-329/Narmco-329, Type II	92.0	Kapton failed at edge of lap joint
FM-1044R	108.8	Kapton failed in tension
FM-9611	88.8	Kapton failed at edge of lap
TR-150-25 "B" Staged	103.5	Kapton failed at edge of lap

TABLE 19
LAP SHEAR TEST DATA
KAPTON TO KAPTON -- 0.005 INCH THICK

Adhesive System	Average Shear Stress At Failure (PSI)	Failure Description
TR-150-25	240	At edge of lap-Kapton failure
TR-150-25 "B" Staged	141	Cohesive
Mystic Tape 7366	30	Adhesive failure
Mystic Tape 7361	47	Adhesive failure

TABLE 20
PEEL DATA -- 0.001 INCH KAPTON TO 0.005 INCH KAPTON

Adhesive System	Average Peel Strength (lbs/in)	Failure Description
FM-960	----	Unable to start the peel on 0.001 Kapton
TR-150-25	----	Unable to start the peel on 0.001 Kapton
FM-1044R	2.31	Failed adhesively
Narmco-329	0.22	Failed adhesively
Narmco-325	0.75	Failed adhesively

Discussion of Results

RTV-3145 peel tests gave conflicting values of peel strength. For the Kapton to aluminum bond, the peel value was 9.5 pounds per inch width and the failure was cohesive. For the Kapton to solar cell bond, the peel value was 0.3 pound per inch width and the failure was adhesive, occurring at the Kapton-RTV-3145 interface. The solar cell peel test used 1200 Primer which may have caused the lower value. This assumption is based upon the results of the aluminum-Kapton peel test which showed the Kapton to adhesive bond was stronger in peel than the adhesive to adhesive bond.

Some difficulties were experienced in application of the 92-024 adhesive due to its higher viscosity.

The peel strength of the three remaining adhesive systems were too low for further consideration. RTV-3145 and Dow Corning 92-024 remain as the candidate adhesives for solar cell bonding.

The selection of candidate adhesives was based on lap shear values and adhesive film weights. The thinner adhesives, FM-1044R and TR-150-25 developed the highest lap shear values. In addition these two adhesive systems possessed the lower film weights. Listed below are the uncured film weights of the splicing adhesives:

Metlbond-225	--	60 lbs per 1,000 ft ²
Metlbond-329	--	95 lbs per 1,000 ft ²
FM-96U	--	65 lbs per 1,000 ft ²
FM-1044R	--	13 lbs per 1,000 ft ²
TR-150-25	--	12 lbs per 1,000 ft ²

On the basis of lap shear strength and weight, FM-1044R and TR-150-25 were selected as candidate adhesives for Kapton splicing.

3.3.3.4 Substrate Attachment Pull Test

3.3.3.4.1 Ultimate Load Tests

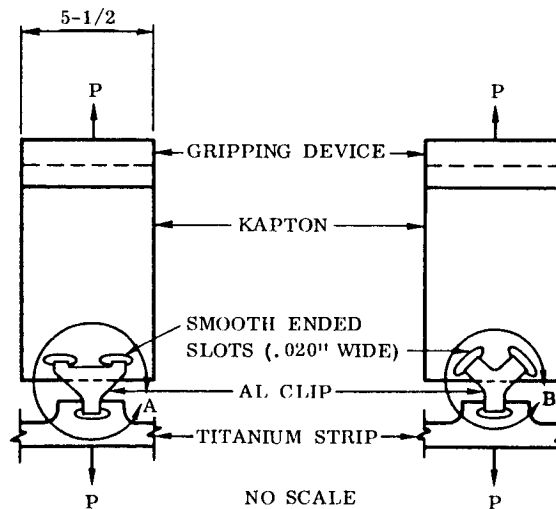
Objective

To determine the bearing and tear out strength at attachment of substrate to deployable beams using suitable substrate materials, namely fiber-glass, Kapton and Mylar. Thin sheets are investigated for weightsaving reasons. A desing load capability of 16 ounces ultimate per clip is required to satisfy the edge support arrangement and resulting design loads as established in Paragraph 3.3.2.2.

Procedure

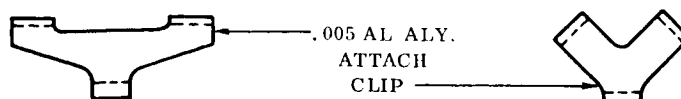
Five sheet thicknesses of film 0.001, 0.002, 0.003, 0.004, and 0.005 inch thickness are tested. The load is applied by a spring scale.

The typical test specimens are sketched below . The clips are attached to the Kapton film by bending the clips through slots cut in the Kapton. The other end is clipped into a titanium strip.



DETAIL "A" SCALE 1:1

DETAIL "B" SCALE 1:1



TYPICAL SUBSTRATE TEST SPECIMENS AND
ATTACHMENT CLIP CONFIGURATIONS

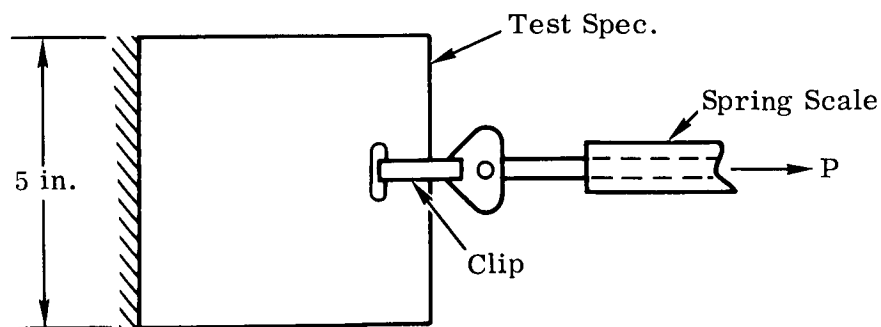
The loads are applied at a slow rate in 0.25 pound increments. The tests are run at room temperature.

Results of the tests are summarized to provide bearing and tear-out allowables for future analysis.

Preliminary Substrate Attachment Bearing and Tearout Test:

The preliminary test consisted of test specimens which are approximately five inches square with slots punched in them to facilitate clip ties. One end of the specimen was held uniformly along its entire length and the other end was loaded through the clip by means of a spring scale. The scale was calibrated in ounces with a maximum scale reading of 64 ounces, or four pounds. An additional clip configuration was also tested as illustrated below. Five Kapton test specimens were tested, ranging in thickness from 0.001 inch to 0.005 inch. One Mylar specimen 0.005 - inch thick was also tested. Each specimen was pulled, using each configuration of clip as the loading member.

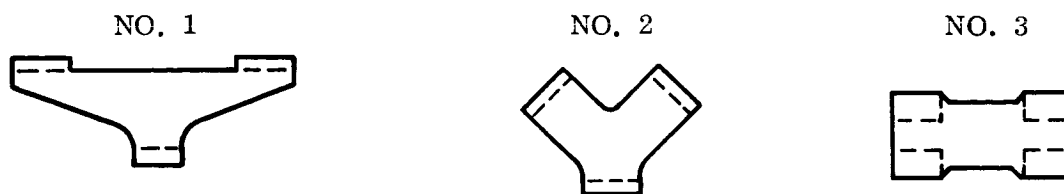
These tests served as a guide for the subsequent larger tests in predicting what clip configuration is more efficient and what gage sheet should be tested to achieve the desired loading.



TYPICAL TEST SETUP

Preliminary Substrate Attachment Bearing and Tearout Test Clip Configurations:

SCALE 1/1



(Inch) Thickness	Material	Clip Configuration		
		Load Oz. #1	Load Oz. #2	Load Oz. #3
.005	Mylar	64+	64+	64+
.001	Kapton Type "H"	26	23	24
.002	Kapton Type "H"	42	64+	64+
.003	Kapton Type "H"	48	64+	64+
.004	Kapton Type "H"	Not Tested	Not Tested	Not Tested
.005	Kapton Type "H"	64+	Not Tested	64+

Figure 33. Test Results of Substrate Attachment

Mode of Failure

The substrate would fail when it distorted enough to allow the clip edges to cut through the material and complete pull-out failure immediately followed. All specimens, including the 0.001-inch sheet carried loads at failure sufficient for the intended use. There was insignificant difference in test results when using clip configurations 2 and 3, which in most cases carried the higher loads. Clip configuration 3 is available and will therefore be used for further testing.

3.3.3.4.2 Substrate Deformation Tests

Objective

To determine the deformation under loading of thin gage Kapton (Type H), Mylar and epoxy impregnated glass cloth.

Procedure

Materials to be tested:

0.001 Mylar (0.0008 actual)
0.002 Mylar (0.0019-0.0022 actual)
0.0015 Kapton (0.0013-0.0015 actual)
0.001 Epoxy impregnated glass cloth (0.0013 actual)

Epoxy Resin - Epon 828
Catalyst - Dion RP7A
Glass Cloth - Style 104, 0.001 thickness
47 percent resin content by weight

Adhesive (to bond doublers)

Epon 828	}	1 to 1 mixture
Versimade		

Method of Testing

The free end of the specimen is securely fastened to a table top. The slotted end is loaded using a spring scale. The specimen is to be inspected at two-ounce intervals for deformation or failure. Photographs to be taken when deformation is noticeable. This point will be considered the capacity of the specimen since loads would be induced into the fragile solar cells at greater deformation, possibly damaging the cells.

The specimen configurations to be tested are:

Mylar:

Specimen M1	-	0.002 with 0.50-inch holes at 0.77-inch centers
Specimen M2	-	0.001 with 0.50-inch holes at 0.77-inch centers and one 0.001-inch mylar doubler at each load area

Specimen M3 - 0.001 plain sheet
 Specimen M4 - 0.001 with doublers

Kapton:

Specimen K1 - 0.0015 with 0.50-inch holes at 77-inch centers and one 0.0015-inch Kapton doubler at each load area.
 Specimen K2 - 0.0015 with one 0.0015 Kapton doubler at each load area
 Specimen K3 - 0.0015 plain sheet

Glass Cloth Impregnated with Epoxy Resin:

Specimen G1 - 0.001-inch cloth composite with 0.50-inch holes at 0.77-inch centers and one 0.001-inch cloth composite doubler at each load area.
 Specimen G2 - 0.001 with one doubler at each load area.
 Specimen G3 - 0.001 plain sheet

Test Results:

Spec. No.	Load/Clip (oz.)	Comments
M1	- Mylar Specimens - 15	Noticeable distortion in solar cell area of substrate
	32	Little change in distortion
M2	4	Noticeable distortion in solar cell area of substrate
	32	Increased distortion
M3	3	Noticeable distortion in solar cell area of substrate
	13	Substrate tear-out failure at clips.
M4	16	Noticeable distortion in solar cell area of substrate
	32	Increased distortion.

Test Results (cont.)

Spec. No.	Load/Clip (oz.)	Comments
K1	- Kapton Specimens - 6	Noticeable distortion in solar cell area of substrate
	32	Increased distortion
K2	16	Noticeable distortion in solar cell area of substrate
	24	Increased distortion
K3	13	Noticeable distortion in solar cell area of substrate
	23	Substrate tear-out failure at clips.
G1	- Fiberglass Specimens - 4	Noticeable distortion in solar cell area of substrate
	16	Increased distortion.
G2	10	Noticeable distortion in solar cell area of substrate
	32	Little change in distortion.
G3	4	Noticeable distortion
	18	Substrate tear-out failure at clips.

Conclusions:

The required ultimate pull load at each clip as given at the outset of this section as 16 ounces. This is now defined as a load at which distortion becomes noticeable. If the load is limited at the attach clip to this condition, (1) a load level is obtained for comparing relative performance of each substrate tested, and (2) some degree of confidence is realized, in lieu of testing, that the solar cell installation will not be damaged. The following specimens are considered as candidates for possible use as a result of the testing:

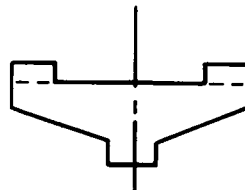
Mylar Specimen M4
Kapton Specimen K2
Fiberglass Specimen G2

All specimens which included lightening holes or were of plain sheet exhibited excessive distortion and, therefore, these configurations will not be used. Of the three possible configuration candidates, the Mylar specimen M4 is the most desirable from a weight standpoint; but an equal thickness sheet of Kapton (0.001 inch nominal) could be substituted with a negligible weight penalty (0.0001 pound/square foot, 0.025 pound/rollup), resulting in an improvement in the following desired properties:

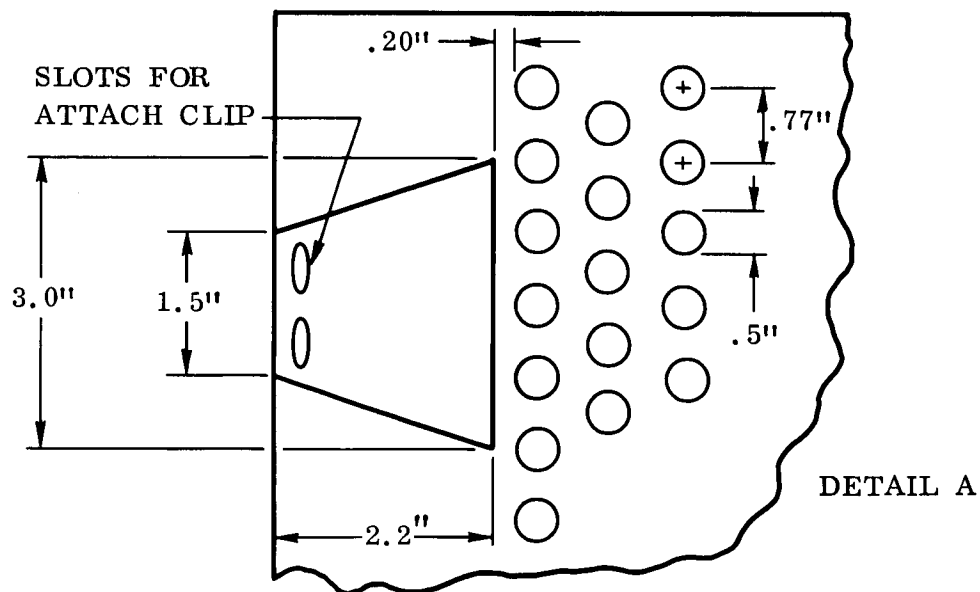
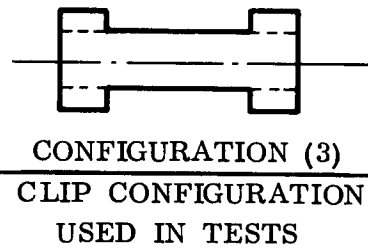
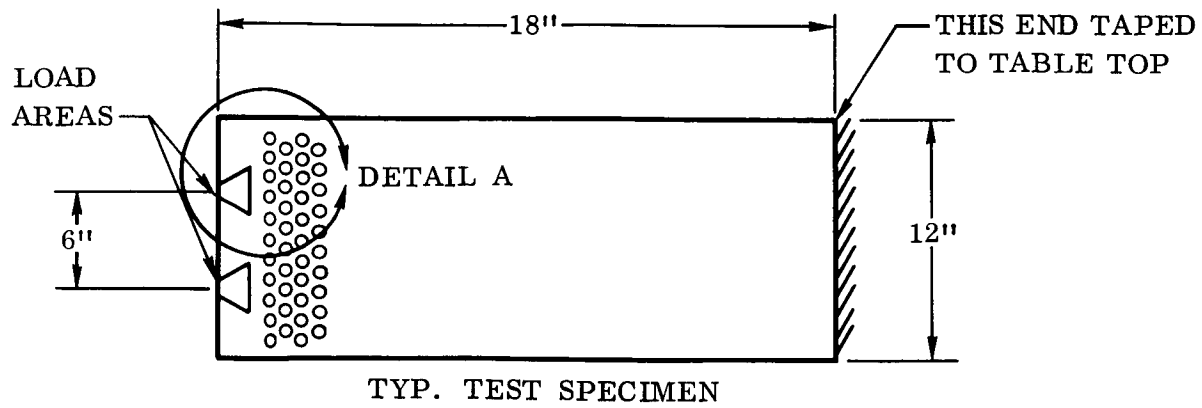
- Reduction in elongation
- Increase in resistance to gamma particles
- Nonflammable
- Nonmelting (mylar melts at 250°C)
- Increased cut through temperature (435°C)

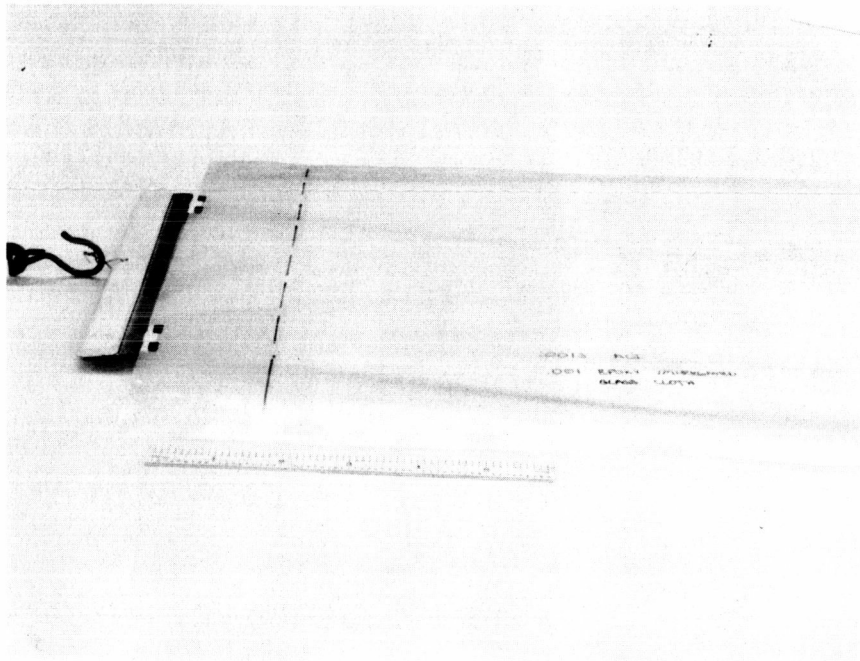
The electrical properties of Mylar and Kapton are essentially the same. The questionable characteristics at this time with Kapton are (1) the ability to bond solar cells to it satisfactorily (more quantitative testing is needed) to withstand the thermal shock environment and (2) the repairability. These aspects are being investigated. The least desirable substrate candidate from a weight standpoint is fiberglass, which would weight 0.00197 pound/square foot (0.493 pound/rollup) more than Kapton, both of 0.001-inch thickness.

Based on substrate deformation as a limiting factor, any of the three clip configurations which were considered are satisfactory. In summation, the recommended clip design will be changed from configuration (3) to configuration (1) for weight savings reasons, and will be made of 0.003 aluminum rather than 0.005. The clip spacing will be reduced to four inches as suggested in the substrate attachment study. It is doubtful as a result of testing in this section that the load level at which substrate deformation becomes noticeable would be any different for a four-inch clip spacing or the six-inch clip spacing used here.

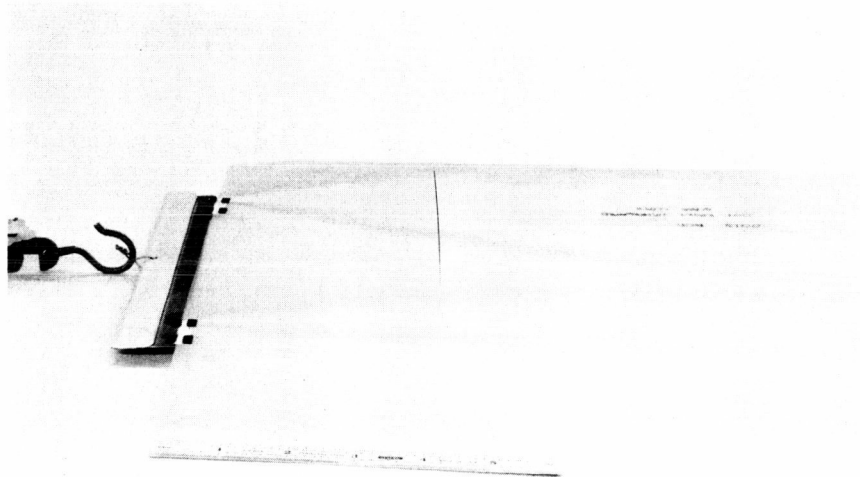


CONFIGURATION (1)

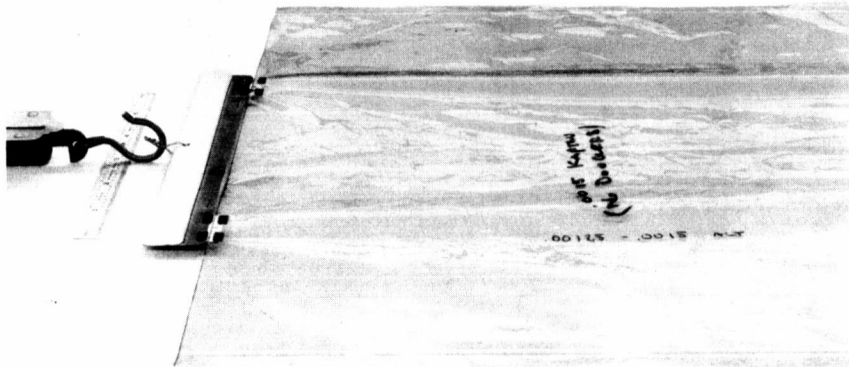




Spec. #G2 - Noticeable Distortion at 10 oz. Tension/Clip



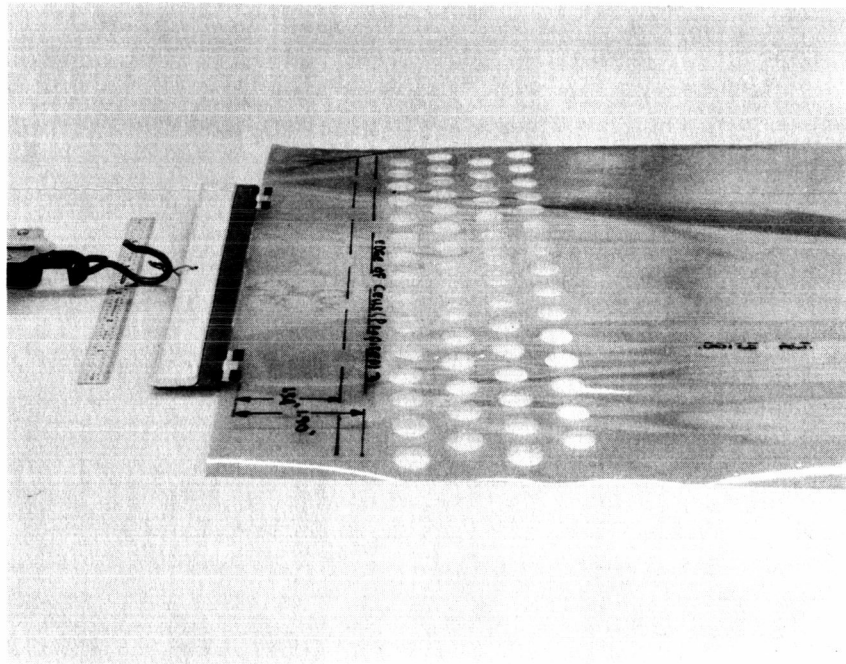
Spec. #G3 - Noticeable Distortion at 4 oz. Tension/Clip



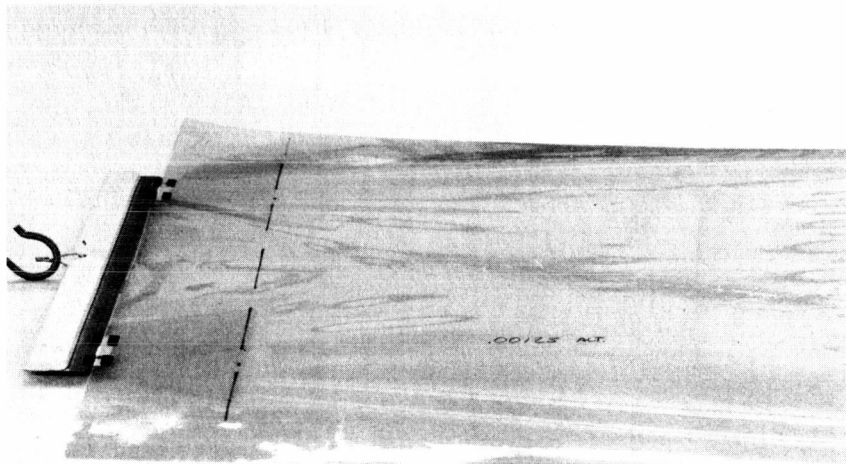
Spec. #K3 - Noticeable Distortion at 4 oz. Tension/Clip



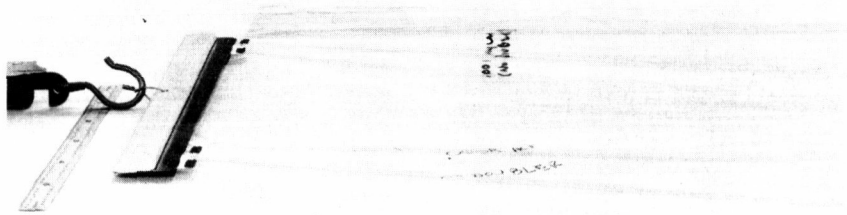
Spec. #G1 - Noticeable Distortion at 4 oz. Tension/Clip
(1 Clip Specimen)



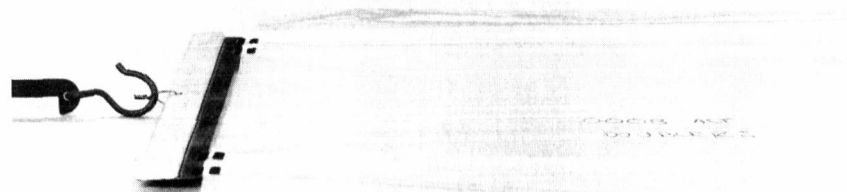
Spec. #K1 - Noticeable Distortion at 6 oz. Tension/Clip



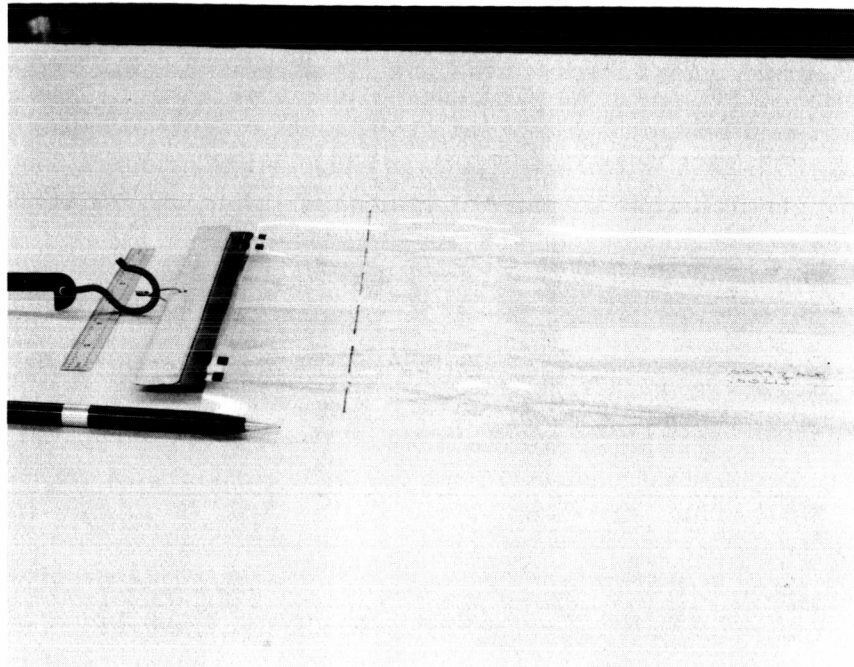
Spec. #K2 - Noticeable Distortion at 16 oz. Tension/Clip



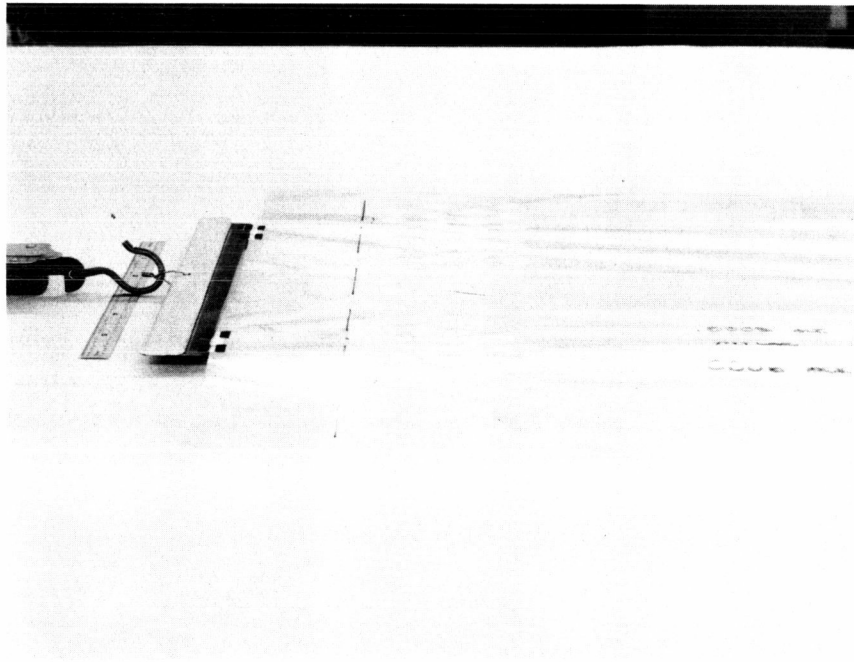
Spec. #M3 - Noticeable Distortion in Solar
Cell Area of Substrate at 3 oz. Tension/Clip



Spec. #M4 - Noticeable Distortion in Solar
Cell Area of Substrate at 16 oz. Tension/Clip.



Spec. #M1 - Noticeable Distortion Begins in Solar Cell Area of Substrate at 15 oz. Tension/Clip.



Spec. #M2 - Noticeable Distortion at 4 oz. Tension/Clip.

3.3.3.5 Solar Cell Interconnection Test

Abstract

The scope of this test involves the effect of thermocycling one hundred (100) times from -148°F to $+168^{\circ}\text{F}$ with a temperature gradient of $54^{\circ}\text{F}/\text{min}$. The following are bus bar materials:

- 1) Aluminum with copper flash and silver plate
- 2) Aluminum with nickel flash and silver plate
- 3) Copper with silver plate
- 4) Molybdenum (silver clad)

The specimen with the least degradation was the copper with silver plate. For interest of weight saving and over-all durability, however, it was hypothesized to be molybdenum with a nickel flash and silver plating or a gold flash and silver plating.

Apparatus

The apparatus used for thermocycling was as follows:

- 1) Bemco Thermo Chamber #LNF-275/350-3, Serial F 2022
- 2) Honeywell 24 point Recorder #08001

Purpose

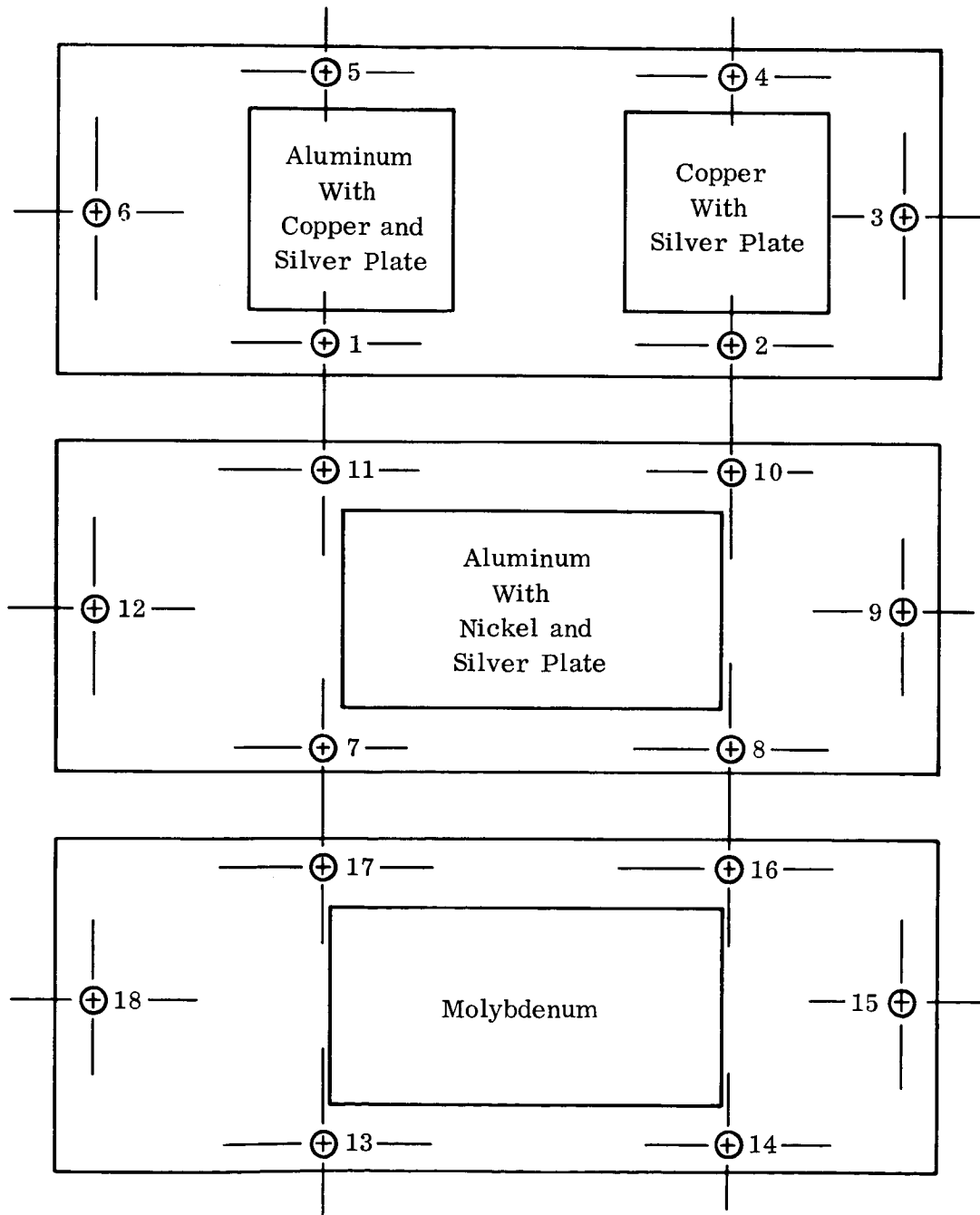
The purpose of the test was to investigate any physical changes from thermocycling in various bus bar materials. Physical investigation included discoloration, fatiguing, and separation of solder joints from the solar cell as the main points. Four bus bar materials were used:

- 1) Aluminum with copper flash and silver plate
- 2) Aluminum with nickel flash and silver plate
- 3) Copper with silver plate
- 4) Silver plated molybdenum

Procedure

The four modules were placed on three shelves with Kapton tape in the test chamber. The bus bar side was placed on the shelves to contact the same temperatures as the thermocouples and to eliminate heat transfer through the cells.

Eighteen (18) thermocouples in all were used on the four modules, six thermocouples per shelf (See illustration below.).



All cells used were bar contact 2x6 cm. Molybdenum and aluminum with copper and silver plating modules used six cells. The copper with silver plate modules used four cells. The aluminum with nickel and silver plating used eight cells.

Three modules were placed in the chamber; molybdenum was added at the 50th cycle. One hundred cycles were run from $+168^{\circ}\text{F}$ to -148°F with a minimum temperature gradient of 54°F per minute between hot and cold stabilization. Once stability of the chamber occurred, thermocouples were given a five-minute stabilization time. When stabilization was completed temperature was held for an additional one minute for the timed soak period. All modules, upon the completion of each ten cycles, were removed from the chamber and inspected for any discrepancies, as described before. This procedure was carried out for one hundred (100) cycles (fifty for molybdenum) at which time the test was complete.

Cooling was accomplished by means of liquid nitrogen distributed uniformly throughout the chamber. Heating was attained through built-in heaters drawing one kilowatt. These were used during stabilization. To attain the 54°F per minute temperature gradient an additional six heating coils were added supplying an additional three kilowatts. These additional units were shut off, once stabilization was attained, to avoid overheating. The radiation and convection characteristics of the chamber were such as to heat as evenly as possible. To insure uniform temperature during all phases of cycling a centrifugal blower mounted in the chamber was kept running continuously.

Inspection was conducted in two major areas. The bus bar assemblies were inspected under a thirty (30) power stereomicroscope for discoloration, buckling and various other visible problems mentioned earlier.

The second area of consideration was that of solder joints. Each solder connection between cell and bus bar was pried, under magnification, to observe any sign of brittling or separation. When inspection was complete the modules were replaced in the chamber.

Results

Of the four modules tested degradation was evident in three. The two aluminum bus bar samples; i.e., with nickel and silver plate, and copper and silver plate, showed a tendency to stretch and wrinkle slightly over one hundred cycles. The molybdenum showed signs of severe discoloration on two of the six bus bars, after forty cycles. Further investigation, however, revealed this to be an oxidation of the silver plating. The copper with silver plate bus bar showed virtually no sign of any degradation.

Several broken tabs and a few cracks were noted at the cell junction. This, however, can be attributed to fatigue from handling, as it was practically impossible to remove and replace without bending slightly. No solder failures were noted.

Conclusions

From the results of this test it would appear that the copper with silver plate is the best combination. For interest in weight saving, however, the choice would have been aluminum providing the problem of wrinkling and embrittlement can be resolved and eliminated.

A previous test program indicated that the silver-clad molybdenum was capable of withstanding temperature gradients far in excess of the 54° F per minute. The principal problem associated with molybdenum is the difficulty of obtaining vendors capable of plating molybdenum. This problem could have a profound influence on any large program with an accelerated delivery schedule.

3.3.3.6 Test Procedures — Solar Cell Installation

Testing should proceed in a well organized and meaningful sequence to ensure that the finished product will conform to minimum design standards. Two of the most critical factors governing accurate solar cell arrays are (1) an acceptable illumination-intensity-measuring device, and (2) an accurate means of measuring temperature of the solar cell.

The most satisfactory method of determining illumination intensity is through the use of solar cells selected from the same production run as cells used on the array. At least four of these cells covered with the same coverslide should be calibrated, utilizing the high altitude aircraft technique. These standard cells should be mounted to a water cooled fixture with a low thermal inertia.

The test procedure would begin with AMO tests conducted on individual parallel cell submodules prior to assembly into circuits. This would be performed if the submodules consisted of one large or three small cells. The next test would be performed when all eight completed circuits were bonded to the substrate. It would be advisable to perform this electrical performance test under an AMO solar simulator. Spectrolab has a solar simulator currently in operation which will illuminate an area 29 by 29 inches. With modifications this simulator would illuminate an area 10 by 38 inches which would be adequate to illuminate one complete circuit to AMO with a uniformity of approximately ± 2.0 percent.

An alternate method of illumination would be Table Mountain. This would be feasible if a covered test chamber with suitable air conditioning were designed and fabricated. This alternate could cause serious schedule delays due to unpredictable test conditions.

A final electrical functional test should be conducted on the complete solar array. This test would be restricted to a natural sunlight test and could prove to be hazardous if suitable provisions for wind loading are not included in the test facility.

Temperature measurement can be accomplished by two basic methods; by use of some type of sensor, or by a careful calibration and monitoring of the open circuit voltage of the solar cell circuits or module.

In the case of sensors, it is suggested tha 30-guage copper constantan thermocouples be secured to the rear surface of the Kapton by the use of tape or adhesive. Temperature gradients between front and rear surfaces would occur and would require compensation.

The use of the open-circuit voltage technique would require the use of a water cooled vacuum hold-down fixture in order to achieve satisfactory temperature uniformity for calibration. Once a calibration voltage was established the average temperature of any circuit could be readily calculated. This method is susceptible to error if a reasonable amount of caution is not exercised.

The optimum test fixture would include the use of thermocouples with a suitable fixture. Open-circuit voltage would be measured as a verification of temperature.

3.3.3.7 Design Development Tests

These tests will be conducted to determine effects of variables too complex to assure reasonable conclusions by analytical procedure. Information obtained by these tests will be used for (1) support of component concept selection, (2) reliability predictions and (3) for use in the detail design phase.

Small Sample Vibration Test

The intent of this test is to determine the amount of structural vibration damping that is provided by a selected configuration of substrate wrap layer separation medium. The installation of separation medium on the substrate is selected to limit temperature to no more than 55° centigrade at the solar cells when exposed to solar flux at 1 A.U. The medium will be polyurethane pads 0.75 inch diameter x 0.15 inch thick, arranged on the panel substrate to cover approximately 35% of the area. The opposite side of the substrate will have one 4 x 14 wired solar cell matrix utilizing 2 x 2 cm x 0.008 solar cells and 0.003 cover glasses. The substrate will be of 0.003 fiberglass, rather than 0.001 inch Kapton but this is not expected to yield errors in testing since the major damping effect will be from the polyurethane pads which support the weight of the specimen.

The specimen will be draped over a six-inch radius aluminum, cylindrical half section fixture and clamped to it at its two ends. The fixture will be mounted to a sine wave vibration exciter and the specimen natural frequency and response acceleration monitored at increments between 1g (0-peak) and the maximum capacity of the exciter. The solar cells will be visually inspected for cracks before increasing the input excitation levels between increments. The transmissibility obtained will be used to determine which of the 12 wrap layers on the test configuration corresponds with the design.

Solar Cell Adhesive Evaluation Test

This test will be conducted to determine the compatibility of the solar cell - substrate bond under flexing conditions simulating cold deployment at -150°F. Solar cells, in a 4 x 7, non-wired matrix will be used. The specimen will be draped over a six-inch radius of curvature aluminum fixture and mounted in a vacuum chamber equipped with a liquid nitrogen cold wall shroud. When stabilized at -150°F, on the solar cells, the specimen will be drawn by motor into the horizontal position. The specimen will be inspected for loosened solar cells after the test.

Stowed Panel Vibration Test (See Figure 34)

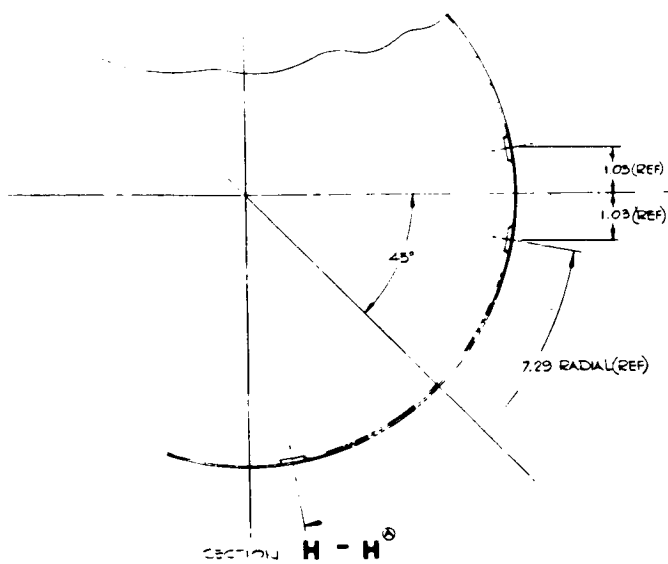
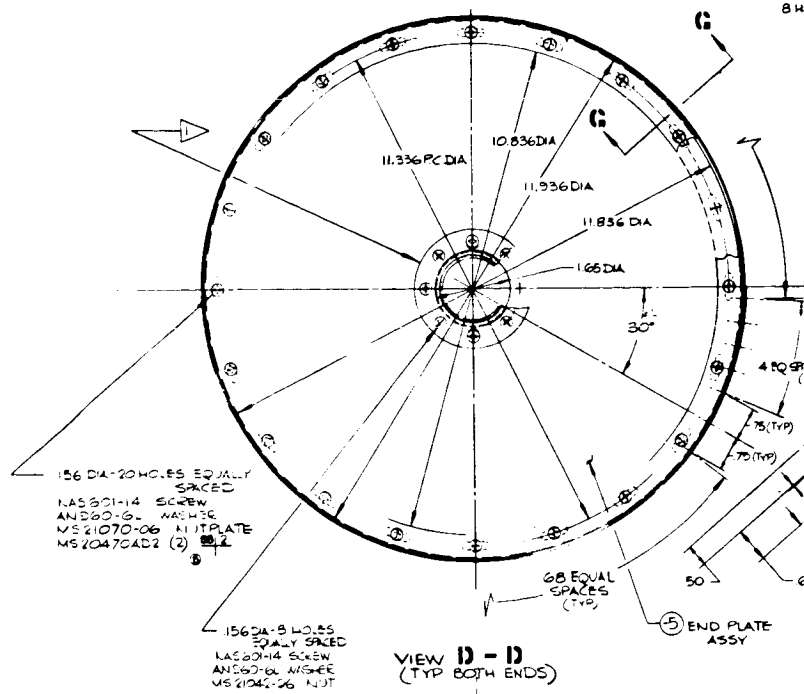
This test will be conducted to determine the following characteristics. The wrap drum configuration selected in the trade-off studies will be used plus approximately 50% of the total substrate area; 100% of the wrapped panel mass is simulated:

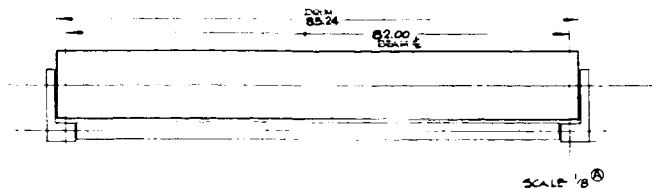
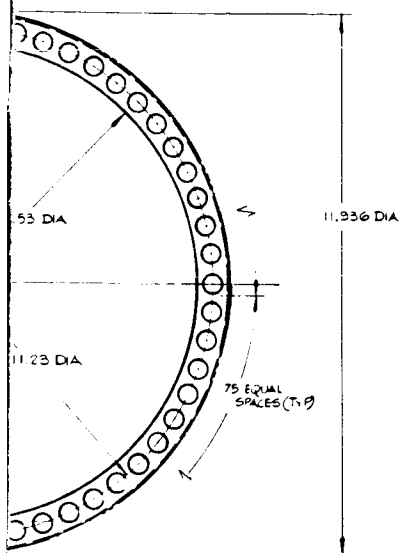
- dynamic transmissibility through drum mount bearings,
- damping effect of each wrapped panel layer or drum at its natural frequency, and
- damping of each wrap layer at its respective natural frequency and respective mode shapes.

The desired information will be obtained by monitoring output sine wave response on the drum and each wrap that is used. The substrate wraps are added at their respective resonances until 50% of the total substrate area has been wrapped onto the drum. Dummy chips, 2 x 2 inch size of 0.02 inch thick magnesium simulating a mass of 0.19 pound/square foot, will be used to simulate solar cells; two wraps will have copper chips 2 x 2 cm in size, 0.0165 inch thick, to represent the remaining 50% of mass.

Each panel wrap will have a non-wired matrix of 2 x 2 cm x 0.008 inch solar cells with 0.003 inch covers and a non-wired matrix of 2 x 6 cm x 0.008 solar cells with 0.003 inch covers in order to evaluate the effects of vibration on these two possible solar cell sizes. The excitation levels will be increased in increments until the design specification level of 4g (0-peak) is reached. Solar cells will be visually inspected periodically during the test.

The test substrate will be wrapped to simulate a desired condition of compactness by placing the flat panel on a table and rolling the drum over it as it is assembled to the drum; no tangential tension applied.





- ⑤ LIGHTENING HOLE PATTERN SHOULD CLOSELY APPROXIMATE THE SPACING USED ON THE MODEL 208 DRUM - INFORM ENGINEERING DEPT OF DIMENSIONAL CHANGES IF ANY
- ⑥ RAFNIR BEARING CO LOS ANGELES, CALIF
- ⑦ ALL PROCESSES TO BE IN ACCORD WITH RYAN SPEC 208-5-002
- ⑧ SHEET STOCK TO LIMITS $\pm .010$ SHT TOL
- ⑨ COAT WITH DOW 19 AND CAT-A-LAC 473-1-500 (0005 TO 001)
- ⑩ PRIOR TO SPOTWELDING COORDINATE WORK 12 0000 A OF -11 SKIN WITH -13 AND -5 ASSYS
- ⑪ BOND -19 BULKHD TO -21 SKIN WITH EC1300
- ⑫ ALL PROCESSES TO BE IN ACCORD WITH RYAN SPEC 208-5-002
- ⑬ ENIL WITH EPM 234

NOTES

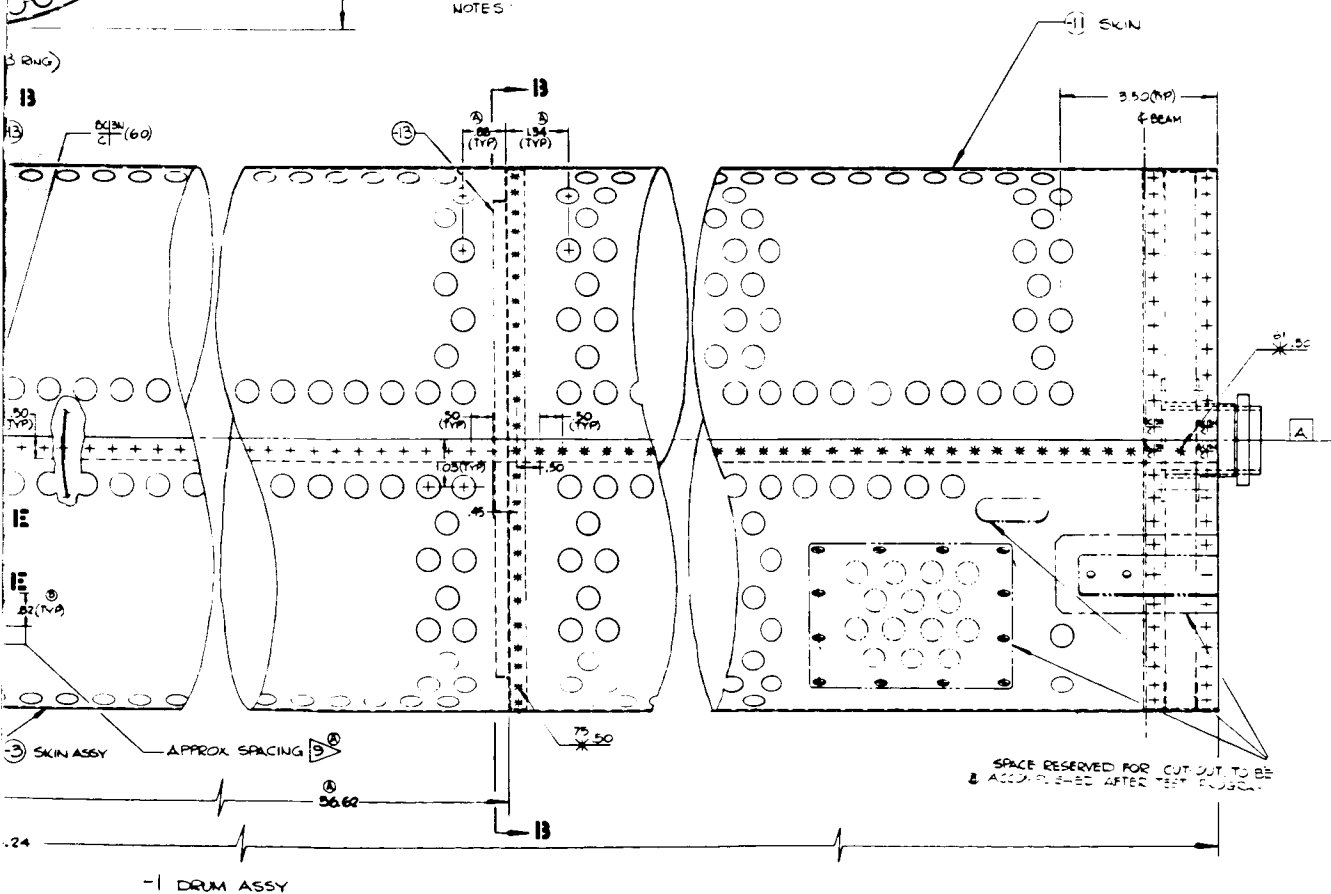


Figure 34. Drum Assembly - Vibration Test, Model 400

184 - B

4.0 CONCLUSIONS

Conclusions regarding designs and materials which were investigated for the principal elements of the solar cell array assembly are summarized in Table 21. The numerals shown in the various boxes represent choice, and in some cases, opinion, and should not be construed as representative of any arithmetical rating system.

In some instances, the estimated weight outweighed other considerations. In other selections, manufacturing feasibility (as studied in this first quarter effort) became more important than extreme low weight; case-in-point, a beryllium structure.

Discussion which follows is intended to amplify concept selections which may not be self evident to the reader.

Item	Description	Concept No.	Weight (overall weight effect)	Fabrication Feasibility	Reliability	Relative Cost	Comments	Final Evaluation
1. Drum/Beam Mounting	Fixed Drum and Pivoting Guide	1a	2	2	2	Equal	Design Based on JPL Model 208. Large Retracted Size Caused Excessive Guide Movement.	2
	Floating Drum and Fixed Guides	1b	1	1	1		System Eliminates Less Desirable Features of 208 Model.	1
2. Mounting to Vehicle	Tubular Mounting	2a	3	2	1	1	Dynamically Unfavorable	3
	"X" Form Mounting	2b	2	3	3	3	Dynamically Unfavorable	2
	Box Mounting	2c	1	1	2	2	Dynamically Acceptable	1
	Mounting with Shock Mounts	2d	4	4	4	4	Large Excursion of Shock Mounts (1:3) Makes Design Unfavorable	4
3. Substrate	Fiberglass	3a	2	3	2	3	Brittle and Prone to Handling Damage. Good Bonding Properties. Good Repairability and Tear Resistance.	2
	Mylar	3b	1	2	3	1	Relatively Good Handling Characteristics. Bonding Susceptible to Gamma Radiation Damage. Poor Resistance to Soldering Heat.	3
	Kapton	3c	1	1	1	2	Relatively Good Handling Characteristics. Bonding and Repairability Qualities Need Improving.	1
4. Beam	Titanium	4a	1	1	1	3	Needs Coatings to Reduce Larger Thermal Gradients.	1
	Beryllium Copper	4b	3	2	3	2	Best Thermal Properties	3
	Stainless Steel	4c	2	3	2	1		2
5. Drum Assembly	Chem Milled Magnesium Skin	5a	3	2	2	2		2
	Honeycomb Drum Skin (No Stiffeners)	5b	4	3	3	3		4
	Beryllium Skin With Stiffeners	5c	1	4	2	4	Considerable Fabrication Difficulty Due to Excessive Handling of Toxic Material. May Have Flaws in Sheet.	3
	Magnesium Skin with Lightness Holes and Stiffeners.	5d	2	1	1	1		1
6. Mechanical Drive System	Silicone to Silicone Friction Drive	6a	4	1	4	1		4
	Toothed Rack on Beam (Silicone or Polyurethane)	6b	2	2		2		2
	Toothed Rack on Beam (Formed Titanium Strip)	6c	1	4	1	4	This Shows Considerable Weight Saving on Other Schemes.	1
	Toothed Sprocket Wheel, Matching Holes in Beam	6d	3	3	3	3		3
7. Electrical Lead-Out	Coiled Continuous Harness	7a	3	1	1	1	Excessive Weight Approx. 100% Heavier than Internal Slip Ring.	2
	External Disc Slip Rings	7b	2	3	3	3	Difficulties due to Floating Drum	3
	Internal Sleeve Slip Rings	7c	1	2	2	2	Considerable Weight Saving Over Other Schemes	1
8. Motor Drive	Single Gearmotor Drive	8a	1		2	1	Failure of Single Motor Makes Roll Up Unit Inoperable.	2
	Double Gearmotor (Redundant Drive)	8b	2	Equal	1	2	Roll Up Unit Capable of Operating With One Motor Dead.	1
9. Cell Layout	180 Series	-	1	1	2	1	More Optimum Match to Converter and Conditioning Equipment.	1
	90 Series	-	2	2	1	2	Higher Power Loss Due to Higher Current	2
10. Solar Cell Type	2 x 2 cm Bar Contact	-	-	1	1	3	Conventional Approach. Highest Reliability. Lowest Power.	3
	2 x 2 cm Corner Part Contact	-	-		2	2	Highest Power per Given Area	2
	2 x 6 cm Bar Contact	-	-	2	3	1	Good Area Utilization. Lowest cost Per Unit Area.	1
11. Bussing Material	Copper	Spectrolab DWG SK-0007	3	3	2	2	Lowest Power Loss. Enhances Structure.	3
	Aluminum		1	1	3	1	Moderate Power Loss. Enhances Structure.	2
	Copper Clad Aluminum		2	2	1	3	Low Power Loss. Good Fabrication. Enhances Structure.	1
	Teflon Coated Individual Wire		6		5	5	High Weight. Difficult to Fabricate	6
	Teflon Coated Ribbon		5		4	4	Excess Weight	5
	Kapton Covered Ribbon		4		4	4	Excess Weight	4
12. Solar Cell Interconnections	Molybdenum, Silver Plate	-	4	2	1	3	High Cost. Difficult to Control Processing	2
	Copper, Silver Plate	-	3	1	1	1	Currently Used on Numerous Satellites	1
	Aluminum, Nickel and Silver Plate	-	1	1	2	2	Difficult to Work	3
	Aluminum, Copper and Silver Plate	-	2	3	3	2	Difficult to Work	4

TABLE 21
TRADE STUDY SUMMARY



4.1 Array Structure and Mechanisms

Drum/Beam Mounting

In the design of the 50-square-foot array (Reference 1), the beams are motivated as the result of wrap drum rotation. On deployment, the beams are literally pushed through the beam guides. This design was reviewed for applicability to the subject program but was rejected for such reasons as:

- The beam is flat as it pays off the drum, into the guide, and has a tendency to "hump" because of insufficient support,
- guides must be coupled to wrap drum in rather a complex way such that the guides are pivoted to accommodate a change in radius in the outer wrap of the substrate, and
- variation in physical dimensions influence frictional effects in beam guides; the result being a tendency of the two beams to drift out of linear synchronization.

The selected concept features fixed guides with the beams positively driven by a common torque tube and rack-and-pinion style gearing. The wrap drum adjusts to beam movement, a condition which has proven to be more manageable.

Mounting to Vehicle

Dynamic analysis did not favor either of two types of truss mountings that were studied without excessive size in members. Weight would have materially increased to develop section properties which were adequate from a dynamics standpoint. Preliminary designs were performed of a vibration isolator type mount (using resilient material) at the interface with vehicle structure. Estimates of amplitude indicated excessive excursion in the mounts.

A box-like structure was selected because unit weight and dynamic qualities were adjudged to be superior.

Substrate

A Kapton film-material was selected over Mylar and fiber glass laminate based on substrate attachment analysis and test and

compatibility studies and adhesive tests performed for solar cell installation purposes.

Extendible Beam

Studies of the beam configuration determined that in-flight (array is deployed) thermal effects are the only serious engineering constraint. That a beam, designed for ground handling effects and of a size and thickness considered to be practical for manufacture, would be adequate to withstand the thermal environment and induced effects. Consequently the trade studies were more concerned with manufacturing feasibility and weight.

A titanium beam was selected because of Ryan's experience with the metal in extendible beam structures and its lower density compared with other useful materials such as beryllium-copper and stainless steel alloys.

Wrap Drum Assembly

Four structural arrangements of a wrap drum were studied:

- A drum made from integrally stiffened (chemical-milling) magnesium skin,
- A drum with the shell manufactured from honeycomb-type material,
- A drum designed to have a beryllium skin with supplemental, internal stiffening rings, and
- A monolithic skinned drum of magnesium with flanged lightening holes and internal ring stiffeners.

The latter concept was selected. Analysis that was concerned with launch environment and effects induced by wrapped, solar celled, substrate determined that the supplementary stiffened magnesium drum was adequate and efficient. A beryllium structure would be an improvement if fabrication feasibility could be resolved within the time span parameters prescribed by contract.

Mechanical Drive System

The drive mechanism for deployment and retraction of the array is a mechanical system whose function will be explained in following

discussion, (Section 4.3). Experience with the 50 square foot roll-out array, Ref. (1), indicated that the boom must be driven directly from a geared motor or equivalent power drive system to assure coordinated, positive movement. A tangential, friction drive arrangement (rotating wheel with silicone facing bearing on rubber strip on the beam) was studied but rejected in favor of a mechanical engagement concept.

Of three variations of a rack and pinion arrangement, a concept which incorporates a corrugated titanium strip on the beam driven by a meshing sprocket wheel, has been chosen. Its principal attribute being lowest weight.

Electrical Lead-Out

Three designs were considered for conducting electrical power from the inboard terminus of the solar cell installation, through a rotating wrap drum, to electrical leads to the vehicle:

- A coiled, continuous harness within the drum (undergoing test on 50 square foot array; Ref. 1),
- External disc slip rings, and
- Internal sleeve slip rings.

The latter concept is chosen over the other two, principally because it represents the least weight for the requirement.

Motor Drive

The motor-gearbox arrangement for driving the deploying members of the array system was evaluated on the basis of either a single geared motor or a double gear motor. Redundancy was considered to be more important than weight in this sub-element of the array and consequently the double gear motor drive was chosen.

4.2 Solar Cell Array and Power Transmission System

Based upon data obtained during the power versus area and power to weight tradeoff studies and the various evaluation tests performed by Ryan and Spectrolab, the following systems when integrated should provide a suitable overall system that will comply with the J. P. L. Specification SS501407A.

Solar Cell Coverglass System

Considering the requirements of paragraphs 3.3.3.1 and 3.3.3.2 of J. P. L. SS501407A systems of cell, coverslide and coverslide adhesive have been selected. This selection is based on weight, power and processing feasibility pending the outcome of UV degradation tests being conducted by Spectrolab. Since no specific orbit has been defined it is difficult to present a detailed analysis at this time.

For maximum power capabilities a 2 ohm base resistivity, solderless, solar cell of the nominal 2x6 cm size has been selected. A 0.003 inch coverglass with a MgF antireflective coating bonded with LTV 602 would present the most attractive system.

Initial loss of transmittance, using an average base cell for reference, should be in the order of 1% to 1.8%.

Adhesive transmittance degradation of 2% during quiet sun conditions is difficult to discuss due to lack of definition of orbit and time in orbit. This figure could vary by an order of magnitude under adverse conditions. The aforementioned conclusions are based upon optimized weight, high initial output power, process feasibility and moderate, not minimum, degradation.

Solar Cell Interconnections

The Spectrolab Solaflex [®] system of solar cell interconnection can be used to great advantage in this application due to ability to withstand repeated flexure. The built-in stress relief for series connected circuits minimizes undue stresses on critical solder joints. The extended lower tabs on the bus bars add significantly to overall reliability.

Several materials and surface treatments were evaluated for this design. Materials tested were:

- Silver Plated Molybdenum
- Silver Plated Copper
- Nickel and silver plated Aluminum
- Copper and silver plated Aluminum

Previous experience with silver plated molybdenum tends to bias this decision but after subjecting several samples to a thermal cycle test between -100°C and 75°C with a temperature gradient of 30°C per minute the following conclusion was reached.

Silver plated copper was satisfactory and presented fewer processing and assembly problems.

Solar Cell Bonding Adhesive

Tests conducted by Spectrolab and Ryan indicate that current cell bonding adhesive used on conventional substratic and insulating materials are readily adaptable to use on prepared Kapton H substrate material. Adhesives exhibiting adequate bonding and peel strength are:

- G. E. RTV 41
- G. E. RTV 511
- G. E. RTV 3145

RTV 41 and RTV 511 have been flown on several spacecraft and exhibit no deleterious affect on adjacent spacecraft components because of outgassing.

Power Transmission System

Three materials were considered for this purpose of power transmission:

- 0.001 copper foil
- 0.001 aluminum foil
- 0.0015 copper clad aluminum foil

Each of these materials presented distinct problems. Copper foil presented a problem of high weight. The aluminum foil must be spot plated to facilitate soldering. The copper clad aluminum is not readily available at this time but may be available within six months.

Conclusions at this time indicate the copper clad aluminum is the most desirable from a weight and process standpoint.

A portion of a materials test program was devoted to evaluating the difference in coefficient of expansion of aluminum and Kapton H. A

.001-in. x 1.50 x 12.00 strip of aluminum was bonded between two strips of .0015 x 2.00 x 10.00 of Kapton H using Schjeldahl GT100. This sample was cycled between -100°C and 75°C for 5 cycles. There was no apparent delamination or wrinkling of either the aluminum or Kapton H. Although not completely conclusive this test indicates that the theory of using foil conductors is feasible.

4.3 Array Sequence of Operation

The events and actions which occur as the solar array is deployed or retracted are as follows:

Deployment

- When deployment is commanded; the motor drive mechanism energizes and begins rotating the torque tube.
- The torque tube which is fitted with drive wheels having sprocket-like teeth, turns in a rotational direction that would extend the beams, outward from the spacecraft.
- Both beams, being equipped with matching gear teeth that interface with the torque tube wheels, are driven outward simultaneously.
- The end of the torque tube, opposite to the drive motor, contains an over-run type clutch that is coupled to a pulley and expandable belt arrangement with the wrap drum. This clutch free-wheels during the deployment cycle.
- The wrap drum responds to the pull on the beams and mechanically moves away from a detent which has held the wrap drum in locked position all through the boost phase of the mission.
- The pivoting axes of the wrap drum slide in structure supported tracks. Through tension springs, the drum (and its axes) are pulled down against the drive sprockets and an idler roller. The free turning idler maintains the position of the wrap drum so that the outer radius of the substrate wrap is always tangentially oriented to the "rim" of the drive sprockets.

- The beams (and the solar panel substrate) continue outward until a limit switch signals motor cutoff. The limit switch is attached to structure, below the torque tube, and is driven by pulley and cogbelt from the torque tube. A revolution counter which has been coordinated to the linear measurement of the substrate, will rotate tumblers in the limit switch until the precise number of revolutions have been completed and a microswitch is activated.

Retraction

- A command signal reverses drive motor polarity and the torque tube, through its sprocket wheels, begins reeving the beams back through guides. The guides direct the beams from open section to flat as they and the solar celled substrate are wrapped back onto the drum.
- The over-run clutch on the torque tube, now that direction has been reversed, activates the pulley and belt connected to the pivot axis of the drum. Consider that the angular velocity of the wrap drum wants to keep pace with torque tube speed. The wrap radius of the substrate on the drum is increasing, therefore surface speed of the wrap and the beams is increasing. This means that tension is increasing in the wrapping beams.
- Over-tensioning is prevented by incorporating an adjustable slip clutch in the hub of the drum axis. The clutch is active only when the belt is operating and this occurs only during the retraction cycle.
- The limit switch cuts off motor drive when the same pre-set revolution counter signals retraction has been completed.

PRECEDING PAGE BLANK NOT FILMED.

5.0 RECOMMENDATIONS

It is a recommendation and the intent of the Contractor to proceed with the preliminary design and analysis and the fabrication of a model to demonstrate deployability of the Roll-Out Solar Array, in accordance with the program plan that has been submitted; Ryan Report No. 40075-1, dated 11 August 1967; Reference 18.

PRECEDING PAGE BLANK NOT FILMED.

6.0 NEW TECHNOLOGY

No items of a "New Technology" nature have been identified to date in performance of this contract.

7.0 REFERENCES

1. California Institute of Technology, Jet Propulsion Laboratory, Contract No. 951107 dated 14 May 1965, titled "Development, Design, and Fabrication of a Prototype Deployable Large Area Solar Array Supporting Structure"; Ryan Concept Model No. 208.
2. Goetzel, Rittenhouse, and Singletary, Space Materials Handbook, Lockheed Missiles and Space Co., Addison-Wesley Publishing Co., Palo Alto, Calif., 1965.
3. Preliminary Development Report - Deployable Large Area Solar Array Structure, Report No. 20869-1, Ryan Aeronautical Company, Lindbergh Field, San Diego California 92112, 30 July 1965.
4. Spacecraft Materials Guidebook. Jet Propulsion Laboratory, California Institute of Technology, Pasadena, California.
5. Final Design Report for Deployable Large Area Solar Array Structure. Report No. 20869-2, Ryan Aeronautical Company, Lindbergh Field, San Diego, California 92112, 5 May 1966.
6. Phase I Report, Positive Deployable Solar Array Development Program, Fairchild-Hiller, Rockville, Md.
7. E. F. Bruhn, Analysis and Design of Flight Vehicle Structures, Tri-State Offset Co., Cincinnati, Ohio.
8. B. Sallman, Large Deflection of Cantilever Beams, Lockheed Aircraft Corp., Burbank, Calif., from Design News Magazine.
9. D. J. Peery, Aircraft Structures, McGraw Hill Book Co., New York, 1949.
10. Lockheed Structures Manual, Stress Memo no. 110, May 1954.
11. Roark, R. J., Formulas for Stress and Strain, McGraw-Hill Book Co., Inc., New York, N. Y., 1954.

12. MIL-HDBK-5, Metallic Materials and Elements for Flight Vehicle Structures, Department of Defense, Washington 25, D.C., Aug. 1962.
13. Structures Manual, Report No. G-42-37, Ryan Aeronautical Company, Lindbergh Field, San Diego 12, California, 1 Aug. 1957.
14. MIL-HDBK-17, Plastics for Flight Vehicles, Part I, Reinforced Plastics, Department of Defense, Washington 25, D.C., June 1955.
15. Phase I Report on the Development of Deployable Solar Arrays, Report 64B119, Ryan Aeronautical Co., San Diego, Calif., 15 October 1964.
16. C. R. Freberg and E. N. Kemler, Elements of Mechanical Vibration, John Wiley and Sons, New York, 1949.
17. J. N. MacDuff and J. R. Curreri, Vibration Control, McGraw-Hill Book Co., New York, 1958.
18. Ryan Report 40075-1, Feasibility Study, 30 Watts/Pound Roll-Up Solar Array, Program Plan, 11 August 1967.
19. Oleesky and Mohr, Handbook of Reinforced Plastics, Reinhold Publishing Co., New York, N.Y., 1964.
20. Silastic RTV S-5370 Foam, Bulletin 08-019, Dow Corning Corp., Midland, Michigan.
21. Zerlaut, Harada, and Berman, Development of Space Stable Thermal Control Coatings, Report No. C6014-13, Illinois Institute of Technology Research Institute.
22. Silastic 140 Adhesive, Bulletin 9-407, Dow Corning Corp., Midland, Michigan.
23. Thermal Radiative Properties of Selected Materials, DMIC Report 177, Battelle Memorial Institute, Nov. 1962.
24. Qualification of Dion RP-7A Epoxy Resin Hardener, Report No. WCLT R58-141, WADC, Wright Patterson AFB, Ohio.
25. Space Materials Data Book for Project Surveyor, Hughes Aircraft Co., Culver City, California.

26. Handbook of Adhesives, Bloomingdale Division, American Cyanimid Co., Aberdeen, Maryland.
27. Liquid Epoxy Hardeners Dion RP-7A and RP-22, Dion Data Sheet 302, Diamond Alkali Co., Western Division, Redwood City, California.

8.0 APPENDIX DATA

8.1 Dynamic Considerations of Proposed Spacecraft Mount

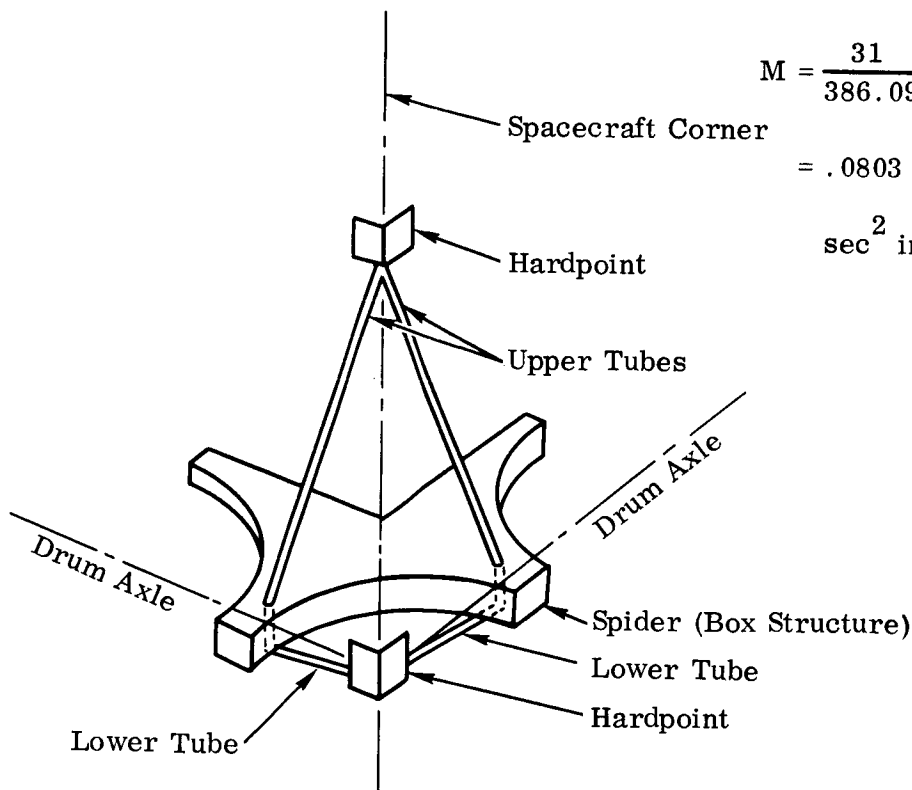
Drum and Wrapped
Panel Weight = 62 lb.

(31 lb. / bearing)

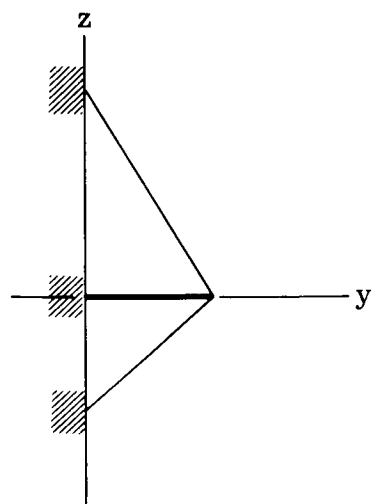
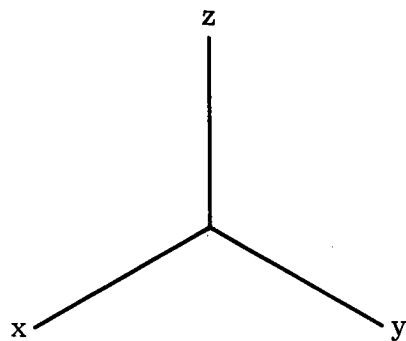
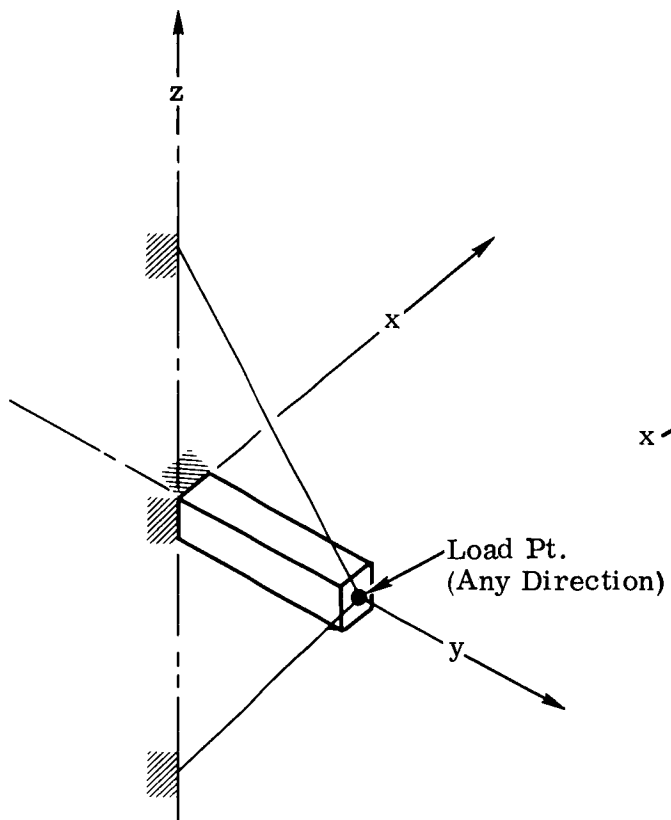
$$M = \frac{31}{386.09}$$

$$= .0803 \text{ lb. (mass)}$$

$$\text{sec}^2 \text{ in.}^{-1}$$



It is assumed that the box structure takes loads in its own plane only; (it is assumed that normal-to-plane loads cannot be reacted by the box). The drum bearing support structure idealization is shown on the next page (one end of drum only is shown). Also, it is assumed the tubes can only be loaded axially.



Stiffness — y Direction

Axial flexibility; tube (1),

$$S = \frac{PL}{AE} \quad \frac{S}{P} = \frac{L}{AE} = \text{Axial flexibility}$$

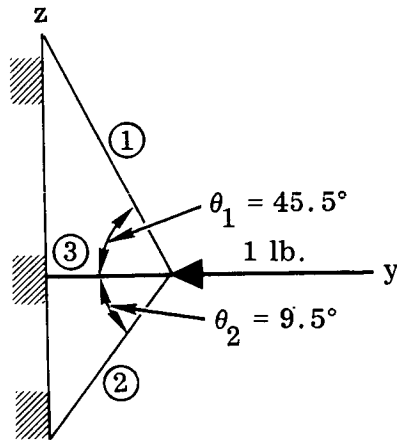
$$L = 11.5 \text{ in.}$$

$$A = .625 \text{ dia} \times .032 = \pi \cdot .593 \cdot .032 = .0596 \text{ in.}^2$$

$$E = \text{MAG} = 6.5 \cdot 10^6 \text{ lb./in.}^2$$

$$\frac{L}{AE} = \frac{11.5}{.0596 \cdot 6.5 \cdot 10^6}$$

$$= 2.9685 \cdot 10^{-5} \text{ in./lb.}$$



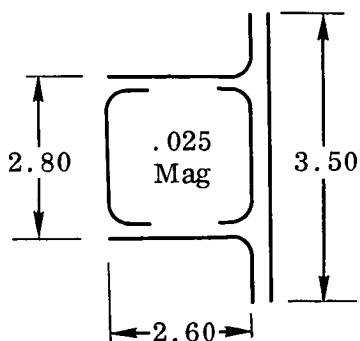
Axial flexibility, tube (2) (same AE), $L = 8.1 \text{ in.}$,

$$\therefore \frac{L}{AE} = \frac{8.1}{3.874 \cdot 10^5} = 2.0909 \cdot 10^{-5} \text{ in./lb.}$$

Axial flexibility, tube (3) (spider)

The spider is a curved box beam but lightening holes in the thick section largely negate axial area.

We take the cross-sectional arrangement shown below and assume it constant.



Developed length,

$$= 2(2.80 - .10) + 6 \cdot 35 + 2(2.60 - .05) + 3.50 = 16.10$$

$$A = 16.10 \cdot .025 = .4025 \text{ in.}^2$$

$$L = 10.0 \text{ in. (}\mathcal{Q}\text{ Drum to spacecraft)}$$

$$\text{Flange length} = \frac{3.50 - 2.80}{2} = .35$$

$$\frac{L}{AE} = \frac{10.0}{.4025 \cdot 6.5 \cdot 10^6} = .3822 \cdot 10^{-5} \text{ in./lb.}$$

Y - Direction Stiffness

Member	Flexibility	Axial Stiffness = $\frac{1}{\text{Axial Flex.}}$	$\cos \Theta$	Y Direction Stiffness = $\frac{\text{Axial Stiff.}}{\cos \Theta}$	
(1)	$2.9685 \cdot 10^{-5}$	33,687	.71325	26,298	} Elements in Parallel
(2)	$2.0909 \cdot 10^{-5}$	47,826	.98629	47,170	
(3)	$.3822 \cdot 10^{-5}$	261,643	1.0	261,643	
				$\frac{261,643}{335,111} \text{ lb./in.}$	

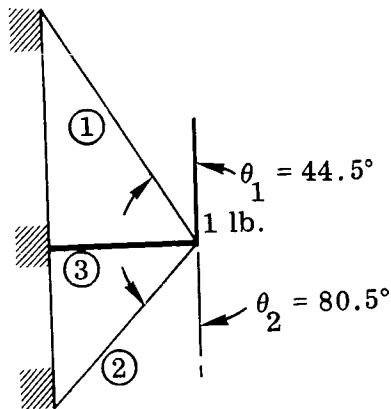
$$K_y = \underline{\underline{335,000 \text{ lb./in.}}} \text{ (in direction of drum axis)}$$

$$W = \sqrt{\frac{K}{M}} = \sqrt{\frac{335,000}{.0803}} = \sqrt{4.172 \cdot 10^6}$$

$$= 2043 \text{ rad/sec A}$$

$$\therefore f = \underline{\underline{325 \text{ cps}}}$$

Stiffness - Z Direction



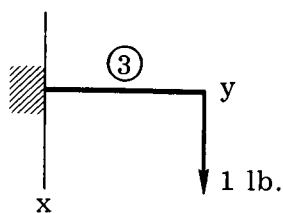
Member (3) is inactive in this system (out of plane load for (3)). Consider (3) as very soft in bending. Also, remember secondary Y direction deflections as out; we're talking about pure Z direction deflections.

<u>Member</u>	<u>Axial Stiffness</u>	<u>cos Θ</u>	<u>Z Direction Stiffness</u>
(1)	33,687	.70091	23,612
(2)	47,826	.16505	<u>7,894</u>
			31,506 lb./in.

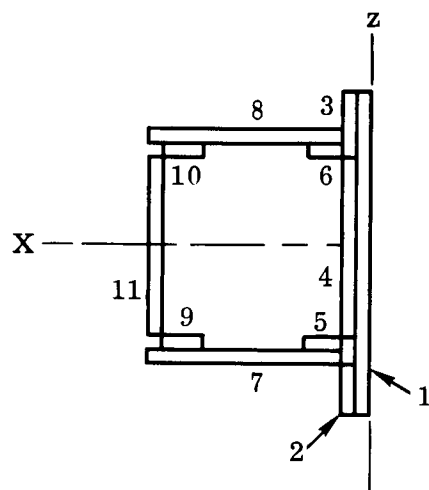
$$K_z = \underline{31,500 \text{ lb./in.}} \quad (\text{in Direction of spacecraft axis})$$

$$f = 325 \sqrt{\frac{31,500}{335,000}} = 325 \cdot .307 = \underline{100 \text{ cps}}$$

Stiffness — X Direction



Here, member (3) is the only active member and it is in bending (in the plane of the spider). Again we assume the structural cross-section shown previously to apply (const. section). We first compute the section I ($I = I_z$),



Ele- ment	A	z	Az	Az^2	I_o
1	.08750	.0125	.00109	.00001	—
2	.00875	.0375	.00033	.00001	—
3	.00875	.0375	.00033	.00001	—
4	.06750	.0375	.02531	.00095	—
5	.00875	.2250	.00197	.00044	.000089
6	.00875	.2250	.00197	.00044	.000089
7	.06375	1.3250	.08447	.11192	.033889
8	.06375	1.3250	.08447	.11192	.033889
9	.00875	2.4000	.02100	.05040	.000089
10	.00875	2.4000	.02100	.05040	.000089
11	.06750	2.5875	.17466	.45193	—
	.4025		.41660	.77843	.00681

$$\bar{z} = \frac{.41660}{.4025} = 1.03503$$

$$A\bar{z}^2 = .41660 \cdot 1.03503$$

$$= .43119$$

$$\begin{array}{r} .77843 \\ - .43119 \\ \hline .34724 \end{array}$$

$$\begin{array}{r} .00681 \\ + .34724 \\ \hline .35405 \end{array}$$

$$\therefore I_z = .35405 \text{ in.}^4$$

$$S = \frac{PL^3}{3EI} \quad (\text{cantilever beam eq.}) \quad L = 10.0$$

$$\frac{S}{P} = \frac{L^3}{3EI} = \frac{10^3}{3 \cdot 6.5 \cdot 10^6 \cdot .35405} = \frac{1}{6.9040 \cdot 10^3} \quad (\text{flexibility}) \text{ in./lb.}$$

$$k_x = \underline{6904} \text{ lb./in.}$$

Desired frequencies are of the order 150 cps. For the Z direction stiffness let's take into account the bending stiffness of the spider (out of plane stiffness). Also truss action of the spider.

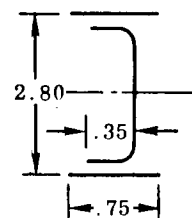
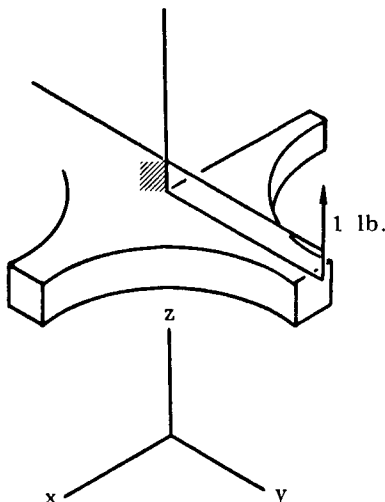
Also, the X direction stiffness is rather crude, and conservative. It should be recalculated on a tapered beam basis which will have a decided effect.

There also is a flexibility that is yet to be accounted for, in the bearing to spider bracketry. This will have a degrading effect.

The Y direction stiffness may require some rework also.

Reanalysis of Z Direction Stiffness

Bending flexibility, spider (member 3)



Beam Section

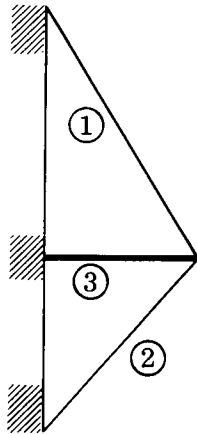
$$30t = 30 \cdot .025 = .750$$

$$I_{xx} = \frac{.025 \cdot 2.70^3}{12} + 2(.025 \cdot 35 \cdot 1.3625^2 + .025 \cdot .75 \cdot 1.3875^2)$$

$$= .14568 \text{ in.}^4$$

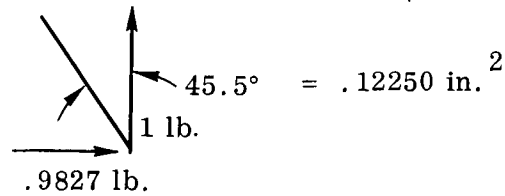
$$\frac{S}{P} = \frac{L^3}{3EI} = \frac{10.0^3}{3 \cdot 6.5 \cdot 10^6 \cdot .14568} = \frac{1}{2841} \text{ in./lb. (Flexibility)}$$

Axial flexibility, Spider (member 3)



If (2) were cut and (3) had no bending rigidity,

$$A = .025(2.70 + 2 \cdot .35 + 2 \cdot .75)$$



$$\frac{S}{P} = \frac{L}{AE} \cdot .98270 = \frac{.98270 \cdot 10.0}{.12250 \cdot 6.5 \cdot 10^6}$$

$$= 1.23416 \cdot 10^{-5} \quad (\text{in } z \text{ direction})$$

$$\text{Stiffness in } z \text{ direction} = \frac{1}{1.23416} \cdot 10^{-5} = 81,027 \text{ lb./in.}$$

The total Z direction stiffness then is:

(1)	23,612
(2)	7,894
(3) Bending	2,841
(4) Axial	81,027
	<hr/>
	115,374 lb./in.

Reanalysis of Y Direction Stiffness

The spider flexibility (member 3) should be on the basis of a better, A; should be

$$\frac{S}{P} = \frac{L}{AE} = \frac{10.0}{.122510 \cdot 6.5 \cdot 10^6} = \frac{1}{79,625}$$

So the total Y direction stiffness, corrected, is,

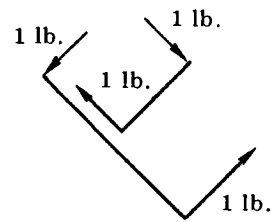
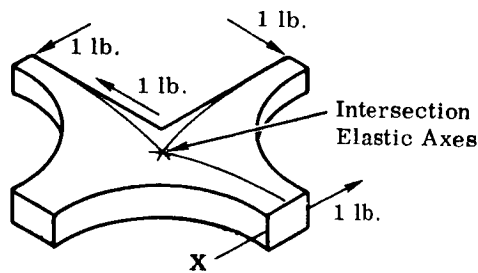
(1) 26,298

(2) 47,170

(3) 79,625

153,093 lb./in. (not critical)

Reanalysis of X direction stiffness



Flexibility

For $W = 2.60$, $I_{zz} = .35405 \text{ in.}^4$

Assume $I_z = Cy^2 = (\text{box beam})$

$$\frac{\Delta W}{\Delta Y} = \frac{4}{9} = \frac{1}{2.25}$$

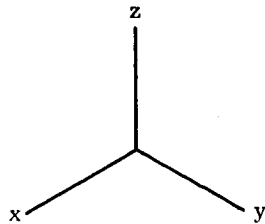
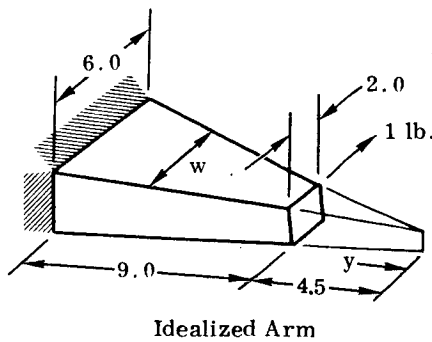
When $W = 2.60$, $Y = 2.60 \cdot 2.25$

$= 5.85$

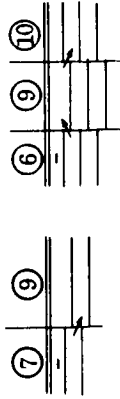
So, $.35405 = C(5.85)^2$

or $C = .0103455$

$\frac{S}{P} = .31269 \cdot 10^{-4}$ (see next page)
Bending



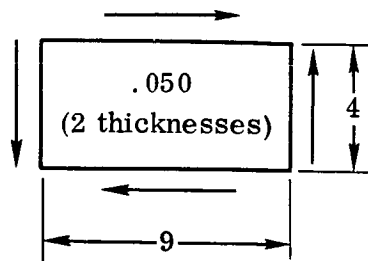
Bending Deflection



$$E = 6.5 \cdot 10^6$$

①	②	③	④	⑤	⑥	⑦	⑧	⑨	⑩	⑪
Station S in.	Bend. Mon. M lb. in.	Mom. of Iner. I in. ⁴	$\frac{M}{EI}$ in. ⁻¹	Average $\frac{M}{EI}$ in. ⁻¹	Strip Width ΔS in.	Strip Area A Rad.	$\frac{\Delta S}{2}$ in.	Slope ΣA Rad.	$(\Sigma A) \Delta S$ in.	Deflection in.
y		$.0103455y^2$	$\frac{2}{(-x(3))}$	$\frac{(4)_{n+1} + (4)_n}{2}$	$(1)_{n+1} - (1)_n$	$(5) \times (6)$	$(7) \times (8)/2$	$\Sigma (7)$	$(9) \times (6)$	$\Sigma (8) + (10)$
0 13.5 9	1.8855	4.7733	4.8612	1	4.8612	2.4306	0	0	0	0
1 12.5 8	1.6165	4.9490	5.0326	1	5.0326	2.5163	4.8612	4.8612	4.8612	2.4306
2 11.5 7	1.3682	5.1162	5.1883	1	5.1883	2.5942	5.0326	9.8938	9.8938	9.8081
3 10.5 6	1.1406	5.2604	5.3077	1	5.3077	2.6539	5.1883	15.0821	15.0821	22.2961
4 9.5 5	.9337	5.3550	5.3531	1	5.3531	2.6766	5.3077	20.3898	20.3898	40.0321
5 8.5 4	.7475	5.3512	5.2533	1	5.2533	2.6267	5.3531	25.7429	25.7429	63.0985
6 7.5 3	.5819	5.1553	4.8655	1	4.8655	2.4328	5.2533	30.9962	30.9962	91.4681
7 6.5 2	.4371	4.5756	3.8853	1	3.8853	1.9427	4.8655	35.8617	35.8617	124.8971
8 5.5 1	.3130	3.1949	1.5975	1	1.5975	.7988	3.8853	39.7470	35.847	162.7015
9 4.5 0	.2095	0	1.5975	1	1.5975	.7988	1.5975	41.3445	39.7470	203.2473

$$\frac{S}{P} = \frac{203.25}{6.5 \cdot 10^6} = .31269 \cdot 10^{-4}$$



Equiv. Shear Panel

$$\gamma = \frac{\tau}{G} \quad \gamma = \text{shearing angle}$$

$$\tau = \text{shear stress}$$

$$G = 2.4 \cdot 10^6 \text{ lb./in.}^2$$

shear modulus)

$$\tau = \frac{1}{2 \cdot .05} = 10 \text{ psi (1 lb. load)}$$

$$\gamma = \frac{10}{G} \quad S = \gamma \ell = 9\gamma$$

$$\frac{S}{P} = \frac{10}{G} \cdot 9 = \frac{90}{2.4 \cdot 10^6} = 37.5 \cdot 10^{-6}$$

$$= .37500 \cdot 10^{-4} \text{ (Shear)}$$

$$\text{Total flexibility} = (.31269 + .37500) \cdot 10^{-4}$$

$$= .68764 \cdot 10^{-4} \text{ in./lb.}$$

and

$$k_x = \frac{1}{.68764 \cdot 10^{-4}} = 11,410 \text{ lb./in. vs } 6904 \text{ lb./in.}$$

Comparisons of stiffness and weight for various materials:

	Mag.	Al.	Titanium	Steel	Beryllum
E	6.5	10.5	16.0	29.0	40.0
ρ	.065	.10	.165	.286	.069

The weight of the support structures is assumed negligible compared to the drum weight. Stiffness is all important in the support structure.

Summary:

Stiffness K, Pounds/Inch

	<u>Direction</u>		
	<u>X</u>	<u>Y</u>	<u>Z</u>
Magnesium	11,410	153,093	115,374
Aluminum	18,431	247,303	186,373
Titanium	28,086	376,845	284,998
Steel	50,906	683,031	514,746
Beryllium	70,215	942,111	709,994

Frequency, F_n, cps

	<u>Direction</u>		
	<u>X</u>	<u>Y</u>	<u>Z</u>
Magnesium	60	220	191
Aluminum	76	279	242
Titanium	94	345	299
Steel	127	469	403
Beryllium	149	545	473

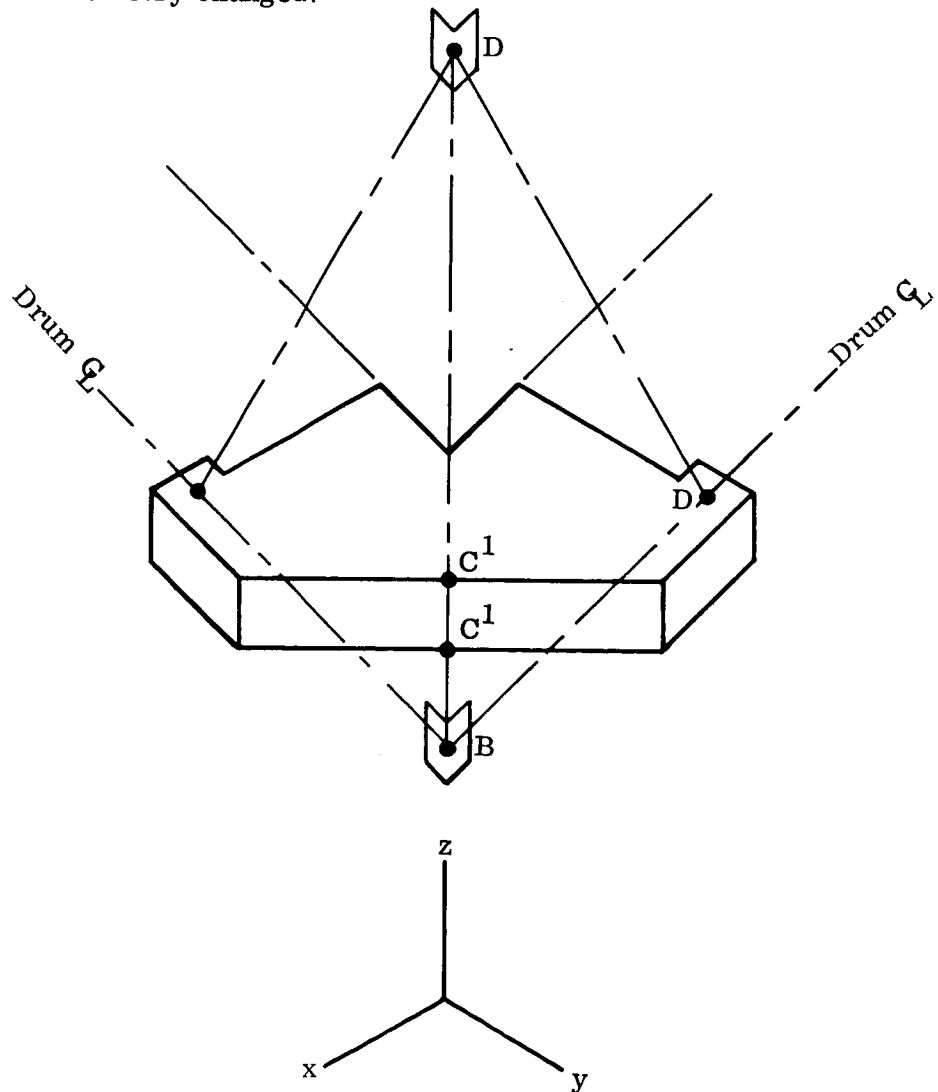
$$f = \frac{1}{2\pi} \sqrt{\frac{k}{m}} \quad m = \frac{31}{386.04} = .08030 \text{ lb. sec}^2 \text{ in.}^{-1}$$

8.2 DYNAMIC CONSIDERATIONS OF REDESIGNED SPACECRAFT MOUNT

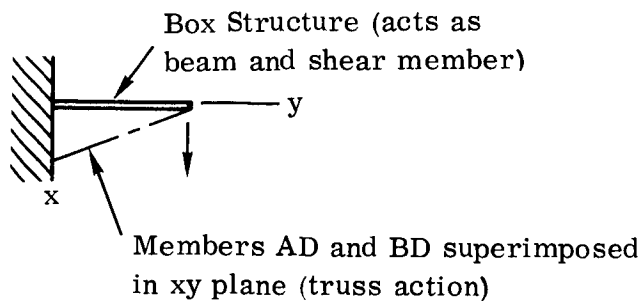
8.2.1 Titanium Box Structure

This analysis considers the use of a titanium box structure and titanium tubes. The changes with respect to the mount analyzed in Section 8.1 are:

1. Box structure beefed up.
2. Tubes beefed up.
3. Tube members AC and BC added.
4. Geometry changed.

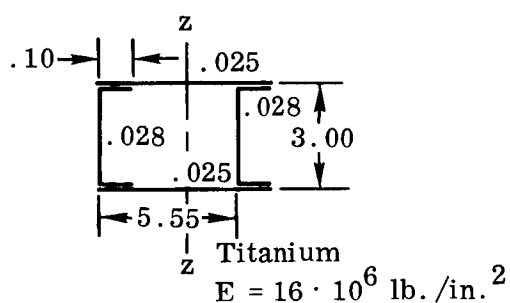


X Direction Stiffness (Along drum axis)

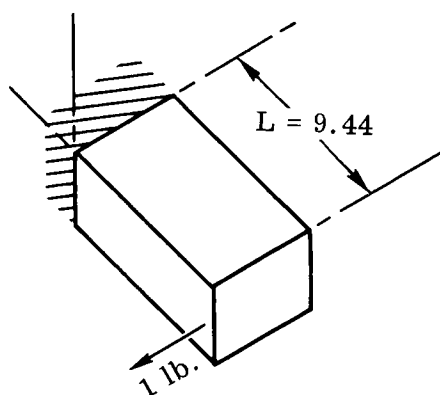


Conservative Approach (Neglects Shear Panels Connecting Idealized Box Beams):

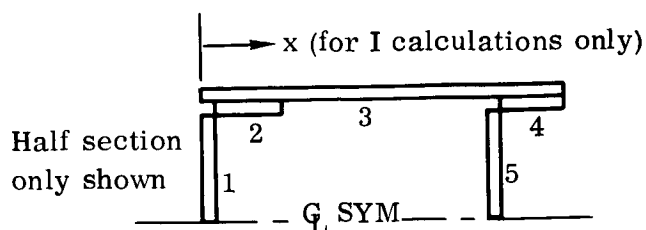
Box beam flexibility, bending (inches/pounds)



Assume no buckling, material width fully effective, i.e., low dynamic stress levels.



Element	Dim.	A	X	AX	AX ²	I _o
1	.028 x 1.447	.04052	.014	.00057	.00001	-
2	.028 x .472	.01322	.264	.00349	.00092	.00025
3	.025 x 6.05	.15125	2.775	.41972	1.16472	.46134
4	.028 x .472	.01322	5.814	.07686	.44686	.00025
5	.028 x 1.447	.04052	5.564	.22545	1.25440	-
		.25873		.72609	2.86691	.46184
					2.86691	
					-2.03767	
					1.29108	



$$\bar{x} = \frac{.72609}{.25873} = 2.80636$$

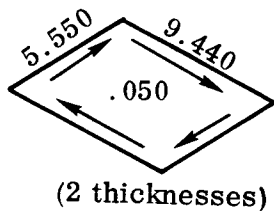
$$A\bar{x}^2 = 2.80636 \cdot .72609 = 2.03767$$

$$I_z = 2 \cdot 1.29108 = \underline{2.5822} \text{ in.}^4$$

$$\frac{S}{P} = \frac{L^3}{3EI} = \frac{9.44^3}{3 \cdot 16 \cdot 10^6 \cdot 2.5822} = 6.7868 \cdot 10^{-6} \text{ in./lb.}$$

(Flexibility)

Box beam flexibility, shear:



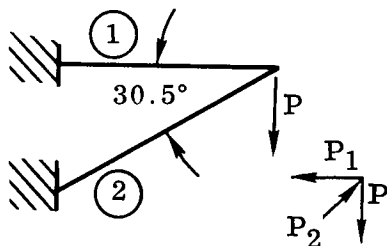
$$\begin{aligned} \frac{S}{P} &= \frac{\ell}{GWt} = \frac{9.440}{6.4 \cdot 10^6 \cdot 5.55 \cdot .050} \\ &= 5.3153 \cdot 10^{-6} \text{ in./lb.} \end{aligned}$$

Bending Shear

$$\text{Box beam flexibility} = 6.7868 \cdot 10^{-6} + 5.3153 \cdot 10^{-6} = 12.1021 \cdot 10^{-6} \text{ in./lb.}$$

$$k = \frac{1}{.121021 \cdot 10^{-4}} = 82.630 \text{ lb./in. (Stiffness, box beam)}$$

Tube Stiffness (truss action):

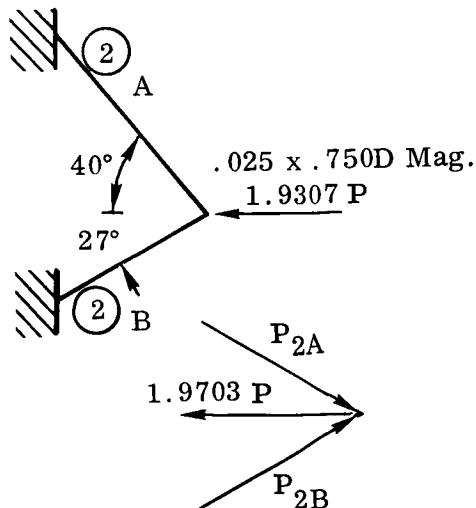


$$\begin{aligned} P_1 &= \frac{P}{\tan 30.5^\circ} = P_{\text{COT } 30.5^\circ} \\ &= 1.6977P \text{ (Tension)} \end{aligned}$$

$$P_2 = \frac{P}{\sin 30.5^\circ} = \frac{P}{.50754}$$

$$= 1.9703P \text{ (Compression)}$$

Looking normal to 2, we have,



$$\begin{cases} P_{2A} \cos 40^\circ + P_{2B} \cos 27^\circ = 1.9703P \\ P_{2A} \sin 40^\circ - P_{2B} \sin 27^\circ = 0 \end{cases}$$

$$P_{2B} = \frac{.64279}{.45399} P_{2A} = 1.4159 P_{2A}$$

$$.76609 P_{2A} + .89101 \times 1.4159 P_{2A} = 1.9703P$$

$$2.0276 P_{2A} = 1.9703P$$

$$P_{2A} = .97174P \text{ (Compression)}$$

$$P_{2B} = 1.4159 \times .97174P = 1.3759P$$

(Compression)

$$U = \frac{P_1^2 \ell_1}{2A_1 E_1} + \frac{P_{2A}^2 \ell_{2A}}{2A_{2A} E_{2A}} + \frac{P_{2B}^2 \ell_{2B}}{2A_{2B} E_{2B}} \text{ (Strain energy of}$$

truss action)

$$A_1 = 2 \cdot .25873 = .51746 \text{ (freq. 2)}$$

$$E_1 = 16 \times 10^6 \text{ (Ti)}$$

$$\ell_1 = 9.440$$

$$A_{2A} = \pi \cdot .725 \cdot .025 = .056941$$

$$E_{2A} = 6.5 \cdot 10^6 \text{ (Mag.)}$$

$$\ell_{2A} = 14.159$$

$$A_{2B} = .056941$$

$$E_{2B} = 6.5 \cdot 10^6$$

$$\ell_{2B} = 10.735$$

$$U = \frac{(1.6977P)^2 \cdot 9.440}{2 \cdot .51746 \cdot 16 \cdot 10^6} + \frac{(-.97174P)^2 \cdot 14.159}{2 \cdot .056941 \cdot 6 \cdot 5 \cdot 10^6} \\ + \frac{(-1.3759P)^2 \cdot 10.735}{2 \cdot .056941 \cdot 6.5 \cdot 10^6}$$

$$= \frac{P^2}{2} (3.286 + 36.123 + 59.907) \cdot 10^{-6}$$

$$= \frac{P^2}{2} \cdot \underbrace{94.316 \cdot 10^{-6}}_{\alpha}$$

$$S = \frac{\delta u}{\delta \rho} = \frac{2\rho}{2} \alpha$$

$$\frac{S}{P} = \alpha = .94316 \cdot 10^{-4} \text{ (Flexibility, truss)}$$

$$k = \frac{1}{\alpha} = 10,603 \text{ lb./in. (Stiffness, truss)}$$

$$k_x = 82,630 + 10,603 = \underline{\underline{93,233 \text{ lb./in.}}} \text{ (Total 'Y' direction}$$

Stiffness)

Fundamental frequency in X direction

$$f = \frac{1}{2\pi} \sqrt{\frac{k}{m}}$$

$$m = \frac{31}{386.04} = .08030 \text{ lb./in.}^{-1} \text{ Sec}^2$$

(31 lb. drum load per end)

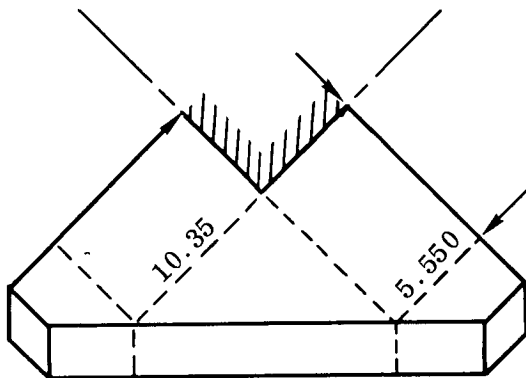
Ref: 62 lb. drum

$$= \frac{1}{2\pi} \sqrt{\frac{93,233}{.08030}} = \frac{1}{2\pi} \sqrt{1.1611 \cdot 10^6} = \frac{1}{2\pi} \cdot 1077.5$$

$$= \underline{171.5 \text{ cps. (mag. tubes)}}$$

More Realistic Approach:

We can't increase the bending effectivity, but we can increase the effective width of the shear panel.



$$W = \frac{10.35}{2} + 5.55$$

$$= 10.725 \text{ vs. } 5.55 \text{ before}$$

$$\frac{S}{P} = 5.3153 \cdot 10^{-6} \cdot \frac{5.55}{10.725}$$

$$= 2.7506 \cdot 10^{-6}$$

$$\text{Box beam flexibility} = 6.7868 \cdot 10^{-6} + 2.7506 \cdot 10^{-6} = 9.5374 \cdot 10^{-6}$$

$$k = \frac{1}{9.5374 \cdot 10^{-6}} = 104,850 \text{ lb./in.}$$

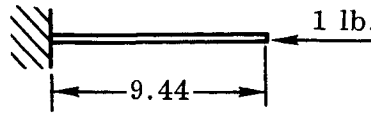
Ti tubes

$$k_x = 109,850 + 24,834 = 129,684 \text{ lb./in}$$

$$F_n = 171.49 \sqrt{\frac{129,684}{93,233}} = 202.3 \text{ cps}$$

Y Direction Stiffners — transverse to spacecraft and drum axis

The tube members account for very little in the total Y direction stiffness (about 99.9% box beam stiffness) when loaded axially.



loaded axially

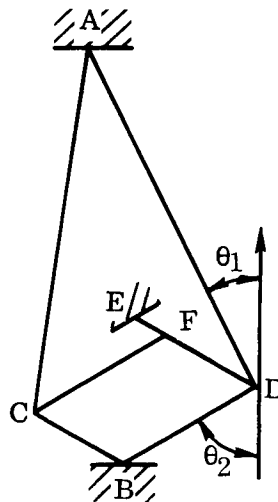
$$\frac{S}{P} = \frac{\ell}{AE} = \frac{9.44}{.51746 \cdot 16 \cdot 10^6} = 1.1402 \cdot 10^{-6}$$

$$k_y = \frac{1}{1.1402 \cdot 10^{-6}} = 877,039 \text{ lb./in.}$$

$$f = \frac{1}{2\pi} \sqrt{\frac{877,039}{.08030}} = 526.0 \text{ cps}$$

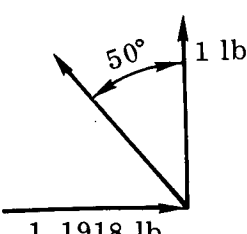
Z Direction Stiffness — Along spacecraft thrust axis

The primary truss system is AD, DE, DB. It is difficult to see how truss AC, CF, CC is loaded much. Truss, ED (the box member) has bending stiffness, but let's leave it out for now. (It was only about 5% of the total stiffness on the analysis in Section 8.1)



axial flexibilities, $\frac{\ell}{\Delta E}$ (Ti tubes and box member)

$$\text{Member AD, } \frac{S}{P} = \frac{14.159}{.056941 \cdot 16 \cdot 10^6} = 15.541 \cdot 10^{-6}$$



$$\text{BD, } \frac{S}{P} = \frac{10.735}{.056941 \cdot 16 \cdot 10^6} = 11.783 \cdot 10^{-6}$$

$$\text{DE, } \frac{S}{P} = 1.1402 \cdot 10^{-6}$$

$$\text{Member AD (} \cos \theta_1 = \cos 50^\circ = .64279$$

$$k = .64279 \cdot \frac{1}{15.591 \cdot 10^{-6}} = 41,361 \text{ lb./in.}$$

$$\text{Member BD (} \cos \theta_2 = \cos 63^\circ = .45399$$

$$k = .45399 \cdot \frac{1}{11.783 \cdot 10^{-6}} = 19,927 \text{ lb./in.}$$

Member DE

If BD were cut and DE has no bending rigidity (conservative)

$$\frac{S}{P} = 1.1918 \cdot 1.1402 \cdot 10^{-6} = 1.3589 \cdot 10^{-6}$$

$$k = \frac{1}{1.3589 \cdot 10^{-6}} = 735,890 \text{ lb./in.}$$

$$k_z = 735,890 + 41,361 + 19,927 = 797,178 \text{ lb./in.}$$

$$f = \frac{1}{2\pi} \sqrt{\frac{797.178}{.08030}} = \underline{\underline{501.5 \text{ cps}}}$$

8.2.2 Aluminum Box Structure

If the box member were made of aluminum alloy instead of Titanium, and the tubes were magnesium (use Section 8.2 for reference); Titanium tubes, Titanium box; all shear material effective in box,

$$F_x = 202.3 \text{ cps}$$

Magnesium tubes, (the rest of the structure the same as above); 7.4% degradation of frequency:

$$F_x = 0.926 \cdot 202.3 = 187.3 \text{ cps}$$

Magnesium tubes, aluminum box (ratio down by equivalent root of E's)

$$F_x = 187.3 \cdot \sqrt{\frac{10.5 \cdot 10^6}{16.0 \cdot 10^6}} = \underline{\underline{151.7 \text{ cps}}}$$

Recheck by component breakdown,

$$\begin{aligned} \text{Box beam flexibility, bending} &= 6.7868 \cdot 10^{-6} \cdot \frac{16.0 \cdot 10^6}{10.5 \cdot 10^6} \\ &= 10.3417 \cdot 10^{-6} \text{ in./lb.} \end{aligned}$$

$$\begin{aligned} \text{Box beam flexibility, shear} &= 2.7506 \cdot 10^{-6} \cdot \frac{6.4 \cdot 10^6}{4.0 \cdot 10^6} \\ \text{(full shear widths)} &= 4.4010 \cdot 10^{-6} \text{ in./lb.} \end{aligned}$$

$$\text{Total flexibility, alum. box beam} = 14.7427 \cdot 10^{-6} \text{ in./lb.}$$

$$\begin{aligned} \text{Stiffness, alum. box beam} &= \frac{1}{14.7427} \cdot 10^{-6} \\ &= 67,830 \text{ lb./in.} \end{aligned}$$

$$\text{Tube stiffness, mag.} = \underline{\underline{10,603 \text{ lb./in.}}}$$

$$\text{Total stiffness, X direc.} \quad 78,433 \text{ lb./in.}$$

$$F_x = \frac{1}{2\pi} \sqrt{\frac{78,433}{.08030}} = \underline{\underline{157.3 \text{ cps}}}$$

Y Direction Frequency

$$f_y = 526.0 \sqrt{\frac{10.5 \cdot 10^6}{16 \cdot 10^6}} = \underline{\underline{426.1 \text{ cps}}}$$

Effect of tubes negligible

Z Direction Frequency

Z direc. stiffness

$$\text{Member AD, } \kappa = 41,361 \cdot \frac{6.5 \cdot 10^6}{16 \cdot 10^6} = 16,803 \text{ lb./in. (mag.)}$$

$$\text{Member BD, } \kappa = 19,927 \cdot 10^{-6} \cdot .40625 = 8095 \text{ lb./in. (mag.)}$$

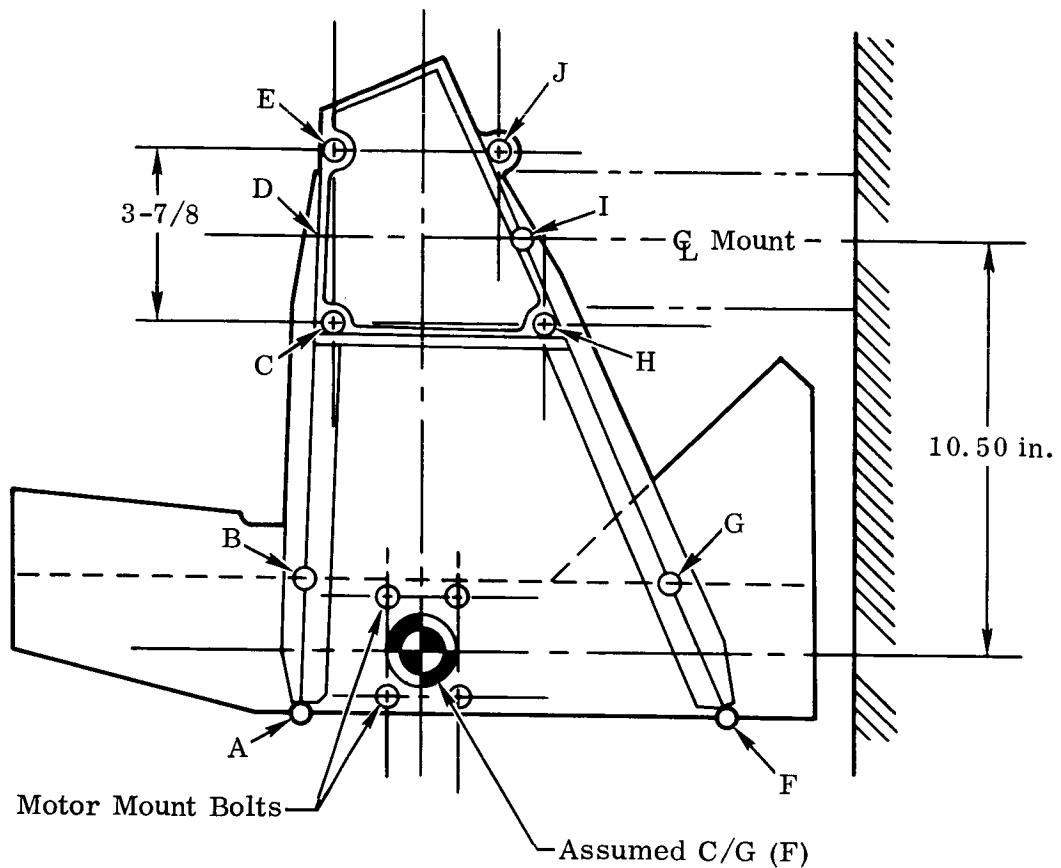
$$\text{Member DE, } \kappa = 735,890 \cdot \frac{10.5 \cdot 10^6}{16 \cdot 10^6} = 482,928 \text{ lb./in. (alum.)}$$

$$507,826 \text{ lb./in.}$$

$$\text{Total, } \kappa_z = 507,826 \text{ lb./in.}$$

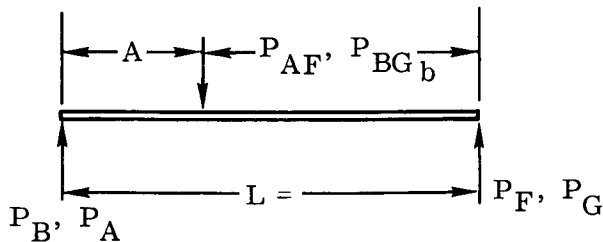
$$F_z = \frac{1}{2\pi} \sqrt{\frac{507,826}{.08030}} = \underline{\underline{400.2 \text{ cps}}}$$

8.3 Dynamic Considerations of Beam Guide Mount



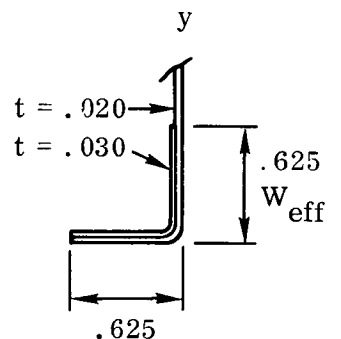
Dynamic loading (F) is applied @ CG thru four motor mount bolts. The motor mount beams the dynamic load without deflection to the motor mount bolts. The load is split and is beamed thru beams "A - F" and "B - G", and then to the spacecraft mounting bolts @ pts. C, E, H, & J.

Beam "A - F" $a = 2.65$ $b = 6.55$ $L = 9.20"$



$$P_{AF} = F(1.20) / 2.2 = .5454 F$$

$$P_F = 2.65 P_{AF} / 9.2 = 2.65(1.2) F / 2.2(9.2) = .1571 F$$



Beam (AF, BG)

$$P_A = (6.55)(1.2) F / 2.2(9.2) = .3883 F$$

$$\rho_{yy} = .323(b - t/z) = .323(.625 - .025) = .1938$$

$$I_{yy} = \Delta \rho_2 = (.625 + .600)(.323)^2 (.60)^2 (.05) = .0023005$$

$$\Delta_{AF} = (Wbx / 6EIL) \left[2L(L - x) - b^2 - (L - x)^2 \right] \quad 0 < x \leq a$$

where $x = a$

$$\Delta_{AF} = (Wab / 6EIL) \left[2L(b) - b^2 - (b)^2 \right]$$

$$\Delta_{AF} = (Wab / 6EIL)(2b)(L - b) = (Wab / 6EIL)(2ab)$$

$$\Delta_{AF} = Wa^2 b^2 / 3EIL$$

$$\Delta_{AF} = (1.2F / 2.2)(2.65)^2 (6.55)^2 / 3(6.5)(10^6)(.0023005)(9.2)$$

$$\Delta_{AF} = 361.5394 F / .907961(10^6)$$

$$\Delta_{AF} = 398.189 F / 10^6$$

Beam B - G $a = 2.10$ $b = 5.35$ $L = 7.45$

$$P_{BG} = 1.0 F / 2.2$$

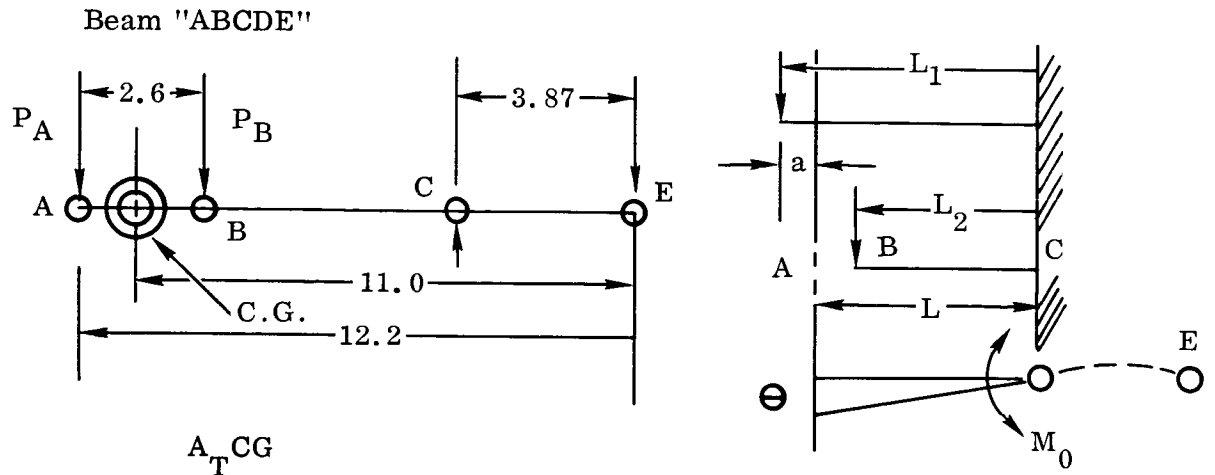
$$P_B = 5.35 P_{AF} / 7.45 = 5.35 F / 2.2(7.45) + .3264 F$$

$$P_G = (2.10) F / 2.2(7.45) = .1281 F$$

$$\Delta_{BG} = (F/2.2)(2.1)^2 (5.35)^2 / 3(6.5)(.0023005)(7.45)$$

$$\Delta_{BG} = 126.225 F / .735251(10^6)$$

$$\Delta_{BG} = 171.676 F / 10^6$$



$$CG = \Delta_A + \Delta_B + L\theta$$

$$\theta = M_0 L_3 / 3EI_3$$

$$M_0 = P_A L_1 + P_B L_2$$

$$\Delta_A = P_A (a^3 - 3L_1^2 a + 2L_1^3) / 6EI$$

$$\Delta_B = P_B (3L_2^2 L - L_2^3) / 6EI$$

$$L_1 = 8.33'' \quad L_2 = 5.63'' \quad L_3 = 3.87'' \quad a = 1.20'', \quad L = 7.13$$

It is assumed that

$$I_1 = I_2 = .056009 \text{ in.}^4$$

$$I_3 = .109342 \text{ in.}^4$$

$$P_A = .3883F \quad P_B = .3264F$$

$$M_0 = (P_A L_1 + P_B L_2) = [.3883(8.33) + .3264(5.63)] F$$

$$M_0 = 5.072171F$$

$$\begin{aligned} \Delta_{AB} &= .3883 F \left[(1.2^3) - 3(8.33)^2(1.2) \right. \\ &\quad \left. + 2(8.33)^3 \right] / 6(6.5) 10^6 (.056009) \\ &\quad + .3264 F \left[(3)(5.63)^2(7.13) - (5.63)^3 \right] / 6(6.5) 10^6 (.056009) \\ &\quad + 5.072171 F(7.13)(3.87) / 3(6.5) 10^6 (.109342) \end{aligned}$$

$$\begin{aligned} \Delta_{AB} &= \left[(.3355 - 48.4987 + 224.4411) / .056009 \right. \\ &\quad \left. + (110.649 - 29.1236) / .056009 + 1279.99 \right] F / 19.5(10^6) \end{aligned}$$

$$\Delta_{AB} = [3147.31 + 1455.58 + 1279.99] F / 19.5 (10^6)$$

$$\Delta_{AB} = 301.686 F / 10^6$$

For beam "FGHIJ"

All dimension are equivalent to beam "ACE" divided by COS 22.5°

$$P_F = .1571 F \quad P_G = .1281 F \quad 1/\cos^3 22.5^\circ = (1.0824)^3$$

$$\begin{aligned} M_0 &= (P_F L_1 + P_G L_2) / \cos 22.5^\circ = F (.1571)8.33 \\ &\quad + .1281(5.63) \cos \end{aligned}$$

$$M_0 = 2.02985 F / \cos 22.5^\circ$$

$$\begin{aligned} \Delta_{FG} &= .1571 F \left[1.2^3 - 3(8.33)^2(1.2) \right. \\ &\quad \left. + 2(8.33)^3 \right] / 6(6.5) 10^6 (.056009) \end{aligned}$$

$$\begin{aligned}
& + .1281 F \left[3(5.63)^2(7.13) - (5.63)^3 \right] / 6(6.5) 10^6 (.056009) \\
& + 2.02985 F 7.13(3.87) / 3(6.5) 10^6 (.109342) (1.0824)^3 \\
\Delta_{FG} & = \left[(.1357 - 19.6218 + 90.8053) / .056009 \right. \\
& + (43.4257 - 11.4299) / .056009 \\
& \left. + 512.245 \right] (1.0824)^3 F / 19.5(10^6) \\
\Delta_{FG} & = (1273.35 + 571.26 + 512.25)(.0650322) F / 10^6 \\
\Delta_{FG} & = 153.272 F / 10^6
\end{aligned}$$

Actual displacement of CG

$$\begin{aligned}
\Delta_1 & = \Delta_{BG} + (\Delta_{AF} - \Delta_{BG})(1.2 / 2.2) \\
& = 171.676 + (398.189 - 171.676)(1.2 / 2.2)(F / 10^6) \\
\Delta_1 & = (171.676 + 118.643) F / 10^6 \\
\Delta_1 & = 290.319 F / 10^6 \\
\Delta_2 & = \Delta_{AB} - (\Delta_{AB} - \Delta_{FG}) \left[\frac{2.10 + (2.65 - 2.10)(1.2 / 2.2)}{7.45 + (9.20 - 7.45)(1.2 / 2.2)} \right] \\
\Delta_2 & = \left\{ 301.686 - (301.686 - 153.272) \left[(2.10 + .30) / 7.45 + \right. \right. \\
& \quad \left. \left. + 95 \right) \right] \right\} F / 10^6 \\
\Delta_2 & = 301.686 - 42.404(F / 10^6) \\
\Delta_2 & = 259.282 F / 10^6
\end{aligned}$$

$$\Delta_{CG} = \Delta_1 + \Delta_2 = (290.319 + 259.282) F / 10^6$$

$$\Delta_{CG} = 549.601 F / 10^6 \quad (\text{Static Deflection})$$

Weight of Structure

(1)	Guide Sleeve Mount Ass'y (30%, 1.9219)	.5766
(2)	Drive System (main)	3.2882
(3)	Tension Drive (50%, .5196)	.2598
(4)	Guide Sleeve (Beam Guide)	<u>1.4847</u>
		5.6093

Per Side $W_s = 5.6093 / 2 = 2.8047 \text{ lb.}$

$$f_N = 3.1268 / \Delta_{ST}^{1/2} = 3.1268 / (549.601 F / 10^6)^{1/2}$$

$$f_N = 3.1268 (10^6) / 23.4436 F^{1/2}$$

For $F = W_s = 2.8047$

$$f_N = 312.68 / 23.4436(2.8047)^{1/2} = 312.68 / 23.4436(1.6748)$$

$$f_N = 79.63 \text{ cps}$$

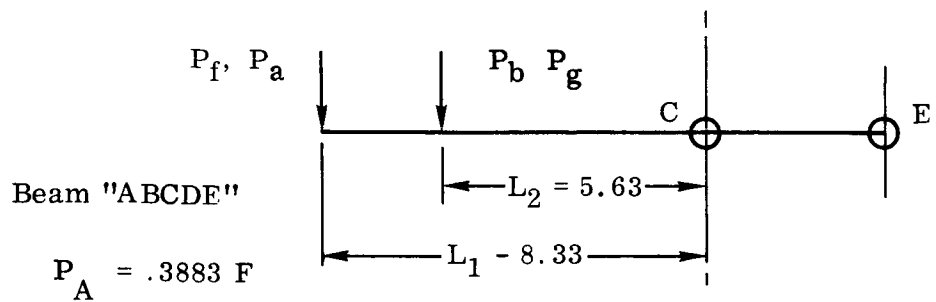
At Resonance and 4G Input, $r / r_2 = .03$

$$\Delta_{Dy} = 4Q\Delta_{ST} = 4(16.667)(549.601)(2.8047) / 10^6$$

$$\Delta_{Dy} = .1028 \text{ in.}$$

$$F_{TR} = F_0 Q = 4W(16.6966) = 4(2.8047)(16.6966)$$

$$F_{TR} = 187.316 \text{ lb (Consider to be limit)}$$



Material = AZ31B Magnesium

$$F_{ty} = 18 \text{ ksi} \quad F_{tu} = 32 \text{ ksi}$$

$$b/t = (.500 - .05) / .05 = 9.0$$

$$F_{CC} = 22,000 \text{ psi}$$

Beam "FGHIJ"

$$P_F = .1571 F \quad P_G = .1281 F$$

$$M_H = (P_F L_1 + P_G L_2) / \cos 22.5^\circ$$

$$= F \left[(.1571)(8.33) + (.1281)(5.73) \right] 1.0824$$

$$M_H = (187.316)(2.04266)(1.0824) = 414.533 \text{ in. /lb.}$$

$$f_b = My / I = 414.533(1.0) / .056009$$

$$f_b = 7401 \text{ psi}$$

Shear at Attach Point C

$$P_C = M_0 / 3.85 = 950.099 / 3.83 = 245.73$$

$$t_C = .050 \text{ Web} \quad 4 \text{ No. 5 Rivets} \quad \text{Ref: 12}$$

$$F_{BR} = 795(50/100) = 398 \text{ lb./Rivet; Adequate BRG.}$$

$$F_{SU} = 566(.981) = 555 \text{ lb./Rivet (Shear) ULT}$$

For $t = .032$

$$F_{BR} = 509(50 / 100) = 254 \text{ lb. ULT}$$

Use 2/3 of the Above Values for Limit

For Channel Section Only

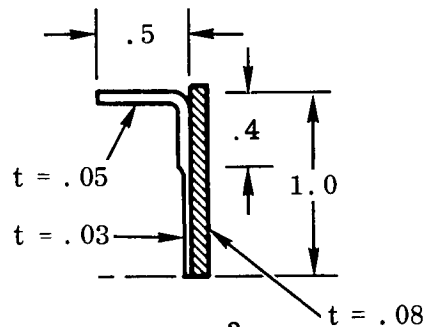
$$I_{NA} = (.45)(.05)(.975)^2$$

$$+ (.40)(.05)(.80)^2$$

$$+ (.6)(.03)(.3)^2 + (.03)(2)^3 / 12 + 2(.02)(.4)^3 / 12$$

$$I_{NA} = .021389 + .0128 + .00162$$

$$+ .020 + .0002 = .056009 \text{ In.}^3 \quad \rfloor$$



Adding the Attach Fitting Value

$$I_{NA} = .056009 + .08(2)^3 / 12$$

$$I_{NA} = .056009 + .05333 = .109342 \text{ In.}^4$$

The following are general equations used in the dynamic response analysis. Also included are derivations and general information.

$$f_N = (1/2\pi) \sqrt{CEIg / WL^3} \quad \text{Beam Weightless with Concentric Load Ref: k p - 128}$$

$$\Delta_{ST} = WL^3 / CEI$$

$$= WL^3 / 48EI \quad C = 48$$

$$f_N = (1/2\pi) \sqrt{g / \Delta_{ST}} = (1/2\pi)(386.1)^{1/2} / \Delta_{ST}^{1/2}$$

$$f_N = 3.1273 / \Delta_{ST}^{1/2}$$

$$\Delta_{ST} = g / (2\pi f_N)^2$$

$$\text{If } \Delta_{ST} = F / K = 4W / K \quad (\text{For 4G Input.})$$

$$\Delta_{Dy} = Q\Delta_{ST} = 4Q\Delta_{ST} = 4gQ / (2\pi f_N)^2$$

$$\text{For Resonance, } v / W_N = 1 \text{ and } r / r_C = .03$$

$$Q = M / F = 1 / \sqrt{\left[1 - (v / W_N)^2\right]^2 + \left[2(r / r_C)(v / W_N)\right]^2}$$

$$Q = 1 / \sqrt{\left[1 - (1)^2\right]^2 + \left[2(.03)(1)\right]^2}$$

$$= 1 / \sqrt{0 + .06^2} = 16.667$$

$$T.R. = \sqrt{1 + \left[2(r/r_C)(v/W_N)\right]^2 / \left[\left[1 - (v/W_N)^2\right]^2 + \left[2(r/r_C)(v/W_N)\right]^2\right]}$$

$$T.R. = \sqrt{1 + \left[2(.03)(1)\right]^2 / \left[\left[1 - 1\right]^2 + \left[2(.03)(1)\right]^2\right]}$$

$$T.R. = (1.0036)^{1/2} / .06 = 16.6966$$

Vibration Ref: 17
For Base Motion (S)

$$S = S_0 \sin wt$$

u = Mass Motion

$$y = u - S$$

$$v = (r' / r'_C) = C / \sqrt{4 kM}$$

$$y_0 = S_0 (M.F.) = (W / W_N)^2 / \left\{ \left[1 - (W / W_N)^2 \right]^2 + (2 v W / W_N)^2 \right\}^{1/2} S_0$$

$$a = D^2 y = -y_0 W^2 \sin(wt - \phi) = -y_0 W^2 \text{ (MAX)}$$

$$\tan \phi = 2v(W / W_N) / \left[1 - (W / W_N)^2 \right]$$

$$a = G's \text{ Applied to Mass (m)} = -y_0 W^2$$

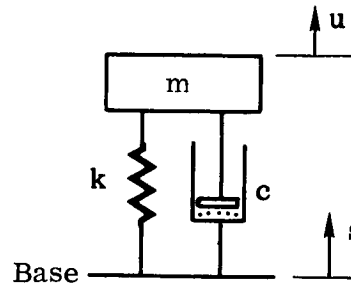
$$u_0 / S_0 = \text{Absolute Motion Response} = Q \text{ (Transmissibility)}$$

$$\frac{F_{TR}}{F_0} = Q \text{ (Transmissibility)} = \frac{\text{Transmitted Force}}{\text{Max. Value of Applied Force}}$$

F_{TR} = Total Force Reaching Base Thru Spring and Thru Dashpot. Transmitted Force

F_0 = Applied Force On Mass

$$F_0 = ma = -y_0 W^2 (m), \text{ or } = m(n - g's)$$



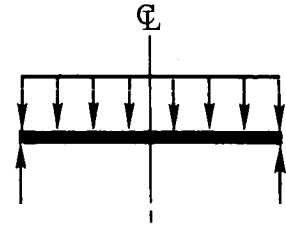
$$Q = \left(\left[1 + (2 v W / W_N)^2 \right] / \left[1 - (W / W_N)^2 \right]^2 + (2 v W / W_N)^2 \right)^{1/2}$$

Same as Case for Force Applied to Mass

Uniformly Distributed Load

$$f_N = (n^2)(\pi/2) \sqrt{gEI / WL^4} \quad (n = 1)$$

$$\Delta_{ST} = \Delta_{MAX} = 5WL^4 / 384 EI @ C_L$$



$$1) \quad \Delta_{DYN} = \frac{\Delta_{ST}(aQ) = (5 WL^4 / 384 EI)(aQ)}{}$$

$$\Delta_{DYN} = g(aQ) / (2 \pi f_n)^2$$

$$\Delta_{DYN} = g(aQ) / (2 \pi)^2 (\pi/2)^2 (gEI / WL^4)$$

$$\Delta_{DYN} = (WL^4 / \pi^4 EI)(aQ) = 5WL^4 / 5 \pi^4 EI(aQ)$$

$$2) \quad \Delta_{DYN} = \frac{g(aQ) / (2 \pi f_n)^2 = (5 WL^4 / 487.05 EI)(aQ)}{}$$

Solving f_N in terms of Δ_{ST}

$$f_N = (\pi/2) \sqrt{g(5)(384EI) / 5WL^4(384)} = (\pi/2) \sqrt{5g / 384 \Delta_{ST}}$$

$$f_N = \pi \left[(5)(386.1 / 384) \right]^{1/2} / 2 \Delta_{ST}^{1/2} = (\pi 2.2422 / 2) / \Delta_{ST}^{1/2}$$

$$f_N = \frac{3.5220}{\Delta_{ST}^{1/2}}$$

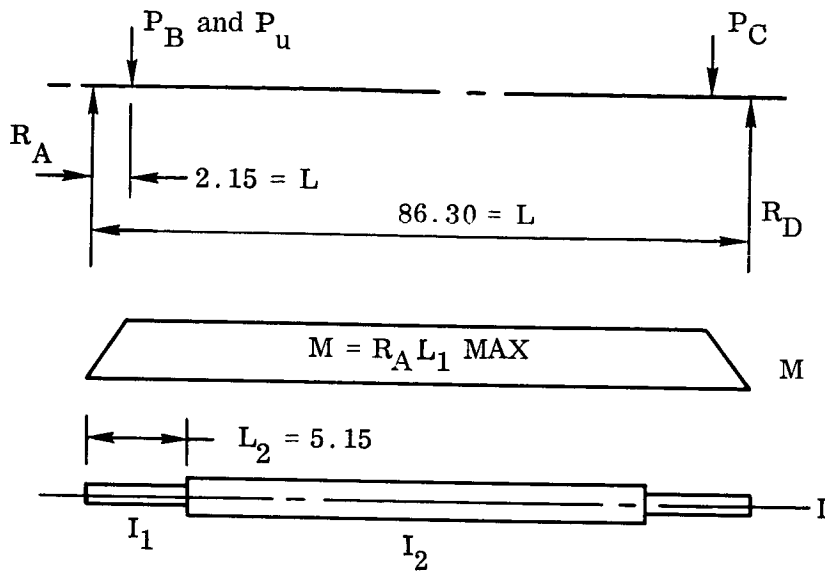
$$2) \quad \Delta_{DYN} = g(aQ) / (2 \pi f_N)^2 = g(aQ) / \left[(2 \pi)^2 (\pi/2)^2 (5g / 384 \Delta_S) \right]$$

$$\Delta_{\text{DYN}} = \left[384 \Delta_{\text{ST}} / (\pi^4)(5) \right] (aQ) = 384(5WL^4 / 384 EI)(aQ) / 5\pi^4$$

$$2) \quad \Delta_{\text{DYN}} = (WL^4 / \pi^4 EI)(aQ) = (5WL^4 / 487.05 EI)(aQ)$$

8.4 CONSIDERATIONS IN USING TORQUE TUBE AS DRUM SUPPORT

8.4.1 No Torque Tube Snubber at Center



$$R_A = (L - L_1)/L$$

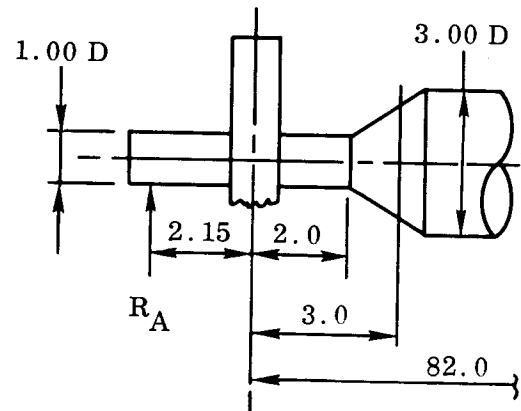
$$M_B = (L - L_1)x/L \quad \text{to B}$$

$$M_D = (L - L_1)x/L - (x - L_1) \quad \text{to D}$$

$$R_A = P_B = P_C = R_D$$

$$\begin{aligned} \Delta_B = \int_0^L M dx / EI &= \int_0^{L_1} M dx / EI_1 + \int_{L_1}^{L_2} M dx / EI_1 \\ &+ \int_{L_2}^{L-L_2} M dx / EI_2 + \int_{L-L_2}^{L-L_1} M dx / EI_1 + \int_{L-L_1}^L M dx / EI_1 \end{aligned}$$

$$I_1 = .3927 t_1 \quad I_2 = 27(.3927) t_2$$



For Actual Loading

$$M_{\text{Max}} = R_A L_1 = 2.15 R_A$$

For Dummy Loading

$$m_B = (L - L_1)(x/L) = (86.3 - 2.15)x/86.3 = .97509x \text{ to } L_1$$

$$m_D = .97509x - (x - 2.15) = 2.15 - .02491x \quad L_1 \text{ to } L$$

$$M_{CD} = [2.15 R_A - (x - 84.15) P_C] = R_A (86.30 - x)$$

$$E\Delta_B = \int_0^{2.15} \frac{(R_A x)(.9751x) dx}{(.3927) t_1} + \int_{2.15}^{5.15} \frac{2.15 R_A (2.15 - .02491x) dx}{(.3927) t_1} + \int_{5.15}^{81.15} \frac{2.15 R_A (2.15 - .02491x) dx}{27 (.3927) t_1} + \int_{81.15}^{84.15} \frac{2.15 R_A (2.15 - .02491x) dx}{(.3927) t_1} + \int_{84.15}^{86.30} \frac{R_A (86.3 - x)(2.15 - .02491x) dx}{(.3927) t_1} = \left\{ \begin{aligned} &\frac{R_A}{.3927} \int_0^{2.15} .9751 x^2 dx/t_1 \\ &\frac{R_A}{(.3927)} \int_{2.15}^{5.15} (2.15^2 - .05356x) dx/t_1 \\ &\frac{R_A}{.3927} \int_{5.15}^{81.15} (2.15^2 - .05356x) dx/27t_2 \\ &+ \frac{R_A}{(.3427)} \int_{81.15}^{84.15} (2.15^2 - .05356x) dx/t_1 \\ &\frac{R_A}{(.3927)} \int_{84.15}^{86.30} (185.545 - 4.30x + .02491x^2) \frac{dx}{t_1} \end{aligned} \right.$$

$$\begin{aligned} \frac{.3927 E\Delta_B}{R_A} &= \left[\frac{.97509 x^3/3}{t_1} \right]_0^{2.15} + \left[\frac{2.15^2 x}{t_1} - \frac{.05356 x^2/2}{t_1} \right]_{2.15}^{5.15} \\ &+ \left[\frac{2.15^2 x - .05356 x^2/2}{t_1} \right]_{5.15}^{81.15} / 27t_2 \\ &+ \left[\frac{2.15^2 x - .05356 x^2/2}{t_1} \right]_{81.15}^{84.15} / t_1 \\ &+ \left[\frac{185.545 x - 4.3 x^2/2 + .02491 x^3/3}{t_1} \right]_{84.15}^{86.30} \end{aligned}$$

$$\begin{aligned}
\frac{.3927 E \Delta_B}{R_A} &= \frac{3.230}{t_1} + 2.15^2 \frac{515}{t_1} - 2.15 - .02678 \frac{5.15^2}{t_1} - 2.15^2 \\
&\quad + 2.15^2 (81.15 - 5.15)/27t_2 - .02678 (81.15^2 - 5.15^2)/27t_2 \\
&\quad + 2.15^2 (84.15 - 81.15)/t_1 - .02678(84.15^2 - 81.15^2)/t_1 \\
&\quad + (185.545)(86.3 - 84.15)/t_1 - 2.15 (86.3^2 - 84.15^2)/t_1 \\
&\quad + .008303 (86.3^3 - 84.15^3)/t_1
\end{aligned}$$

$$\begin{aligned}
.3927 E \Delta_B / R_A &= 3.230/t_1 + 13.868/t_1 - .586/t_1 + 13.011/t_2 \\
&\quad - 6.505/t_2 + 13.868/t_1 - 13.280/t_1 \\
&\quad + 398.922/t_1 - 787.905/t_1 + 389.002/t_1
\end{aligned}$$

$$.3927 E \Delta_B / R_A = 17.119/t_1 + 6.506/t_2$$

$$R_A = P_B, \quad E = 6.5 (10^6) \text{ MAG}$$

$$\Delta_B = (P_B / 10^6) \left[17.119/((.3927) 6.5t_1 + 6.506/((.3927)(6.5) t_2) \right]$$

$$\Delta_B = (6.707/t_1 + 2.549/t_2)(P_B / 10^6)$$

		Δ_1	Δ_2	$(\Delta_1 + \Delta_2)(P_B / 10^6)$
t_1	t_2	$6.707/t_1$	$2.549/t_2$	Δ_B

.060	.030	111.78	84.961	$196.74 (P_B / 10^6)$
------	------	--------	--------	-----------------------

Check Case

$$\Theta_A = M_O L / 2 E I_2$$

$$\begin{array}{c} I_2 = \text{Const.} \\ \hline L = 86.3 \end{array} \quad D$$

$$M_O = 2.15 R_A = 2.15 P_B$$

$$\Theta_A = (2.15 P_B)(86.3) / 2(6.5)(10^6)(27)(.3927)t_2$$

$$\Theta_A = 185.545 (P_B / 10^6) / 137.8377(.03)$$

$$\Theta_A = 44.87 (P_B / 10^6)$$

$$\Delta_B = \Theta_A (2.15) = 2.15 (44.87)(P_B / 10^6) = 96.47 (P_B / 10^6)$$

For Original Shaft For $I = I_2 = \text{Const.}$

$$\Delta_B = (P_B / 10^6) [111.78 (I_1 / I_2) + 84.961] = (P_B / 10^6)$$

$$\Delta_B = (P_B / 10^6) [111.78/27 + 84.961] = 89.106 (P_B / 10^6)$$

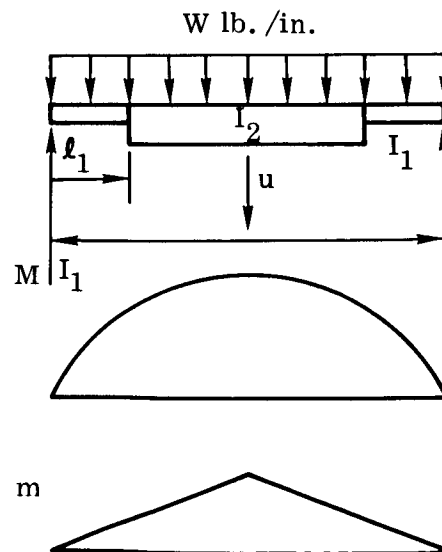
The difference is attributable to M_O is not constant full length of beam

Deflection @ ζ

$$\Delta = \int_0^L M m dx / EI$$

$$\Delta = 2 \int_0^{\ell_1} M m dx / EI_1$$

$$+ 2 \int_{-\ell_1}^{\ell_2} M m dx / EI_2$$



$$M = wlx/2 - wx^2/2$$

$$m = x/2 \quad 0 < x \leq l/2$$

$$I_1 = \pi R_1^3 t_1 = \pi (1/2)^3 t_1 = .3927 t_1$$

$$I_2 = \pi R_2^3 t_2 = \pi (3/2)^3 t_2 = 27(.3927) t_2$$

$$\Delta_1 = 2/EI_1 \int_0^{l_1} (wlx/2 - wx^2/2)(x/2) dx$$

$$= w/2EI_1 \int_0^{l_1} (\ell x^2 - x^3) dx = (w/2EI_1) \left[\ell x^3/3 - x^4/4 \right]_0^{l_1}$$

$$\Delta_1 = (w/2EI_1)(\ell l_1^3/3 - l_1^4/4)$$

$$\Delta_2 = (2/EI_2) \int_{l_1}^{l/2} (wlx/2 - wx^2/2)(x/2) dx$$

$$\Delta_2 = w/2EI_2 \int_{l_1}^{l/2} (\ell x^2 - x^3) dx = (w/2EI_2) \left[\ell x^3/3 - x^4/4 \right]_{l_1}^{l/2}$$

$$= (w/2EI_2)(\ell^4/24 - \ell^4/64 - \ell l_1^3/3 + l_1^4/4)$$

$$\Delta = \Delta_1 + \Delta_2$$

$$= (w/2E)(\ell l_1^3/3I_1 - l_1^4/4I_1 + \ell^4/24I_2 - \ell^4/64I_2 - \ell l_1^3/3I_2 + l_1^4/4I_2)$$

$$L_1 = 5.15 \quad L = 86.3''$$

$$\Delta = (w/E) \left[(86.3)(5.15)^3/6I_1 - 5.15^4/8I_1 + 86.3^4/48I_2 - 86.3^4/128I_2 \right. \\ \left. - 86.3(5.15)^3/6I_2 + 5.15^4/8I_2 \right]$$

$$\Delta = (w/E) \left[(1964.7 - 87.9)/I_1 + (1, 155, 585 - 433, 344 - 1965 + 88)/I_2 \right]$$

$$E = 6.5 (10^6) \quad I_1 = .3927 \quad I_2 = (27)(3927) t_2$$

$$\Delta = (w/10^6) \left[2034.6/6.5 (.3927)t_1 + 720,364/6.5(27)(.3927) t_2 \right]$$

$$\Delta = \Delta_1 + \Delta_2 = (w/10^6) \left[2034.6/2.55255t_1 + 720,364/68.9189t_2 \right]$$

$$\Delta_{\mathcal{L}} = \Delta_1 + \Delta_2 = (w/10^6)(797.09/t_1 + 10,452.3/t_2)$$

A) For Distributed Load

$$\Delta_{\mathcal{L}} \left\{ \begin{array}{ccccc} & & \Delta_1 & \Delta_2 & (\Delta_1 + \Delta_2)w/10^6 \\ t_1 & t_2 & 797.09/t_1 & 10,452.3/t_2 & \Delta_{\mathcal{L}} \\ .060 & .030 & 13,285 & 348,410 & .361,695(w) \end{array} \right.$$

$$\text{For Constant } I_2 \text{ Beam} \quad \left[.349,436(w) \right]^*$$

B) For Concentrated Load @ \mathcal{L}

$$\Delta_{\mathcal{L}} \left\{ \begin{array}{ccccc} & & \Delta_1 & \Delta_2 & (\Delta_1 + \Delta_2)(P/10^6) \\ t_1 & t_2 & 8.919/t_1 & 193.962/t_2 & \Delta \\ .060 & .030 & 148.65 & 6,465.40 & 6,614.05 (P/10^6) \end{array} \right.$$

Check for Constant $I = I_2$

$$* \quad \Delta_{\mathcal{L}} = 5wL^4/384EI = 5w(86.3)^4/384(6.5)10^6(27)(.3927)t_2$$

$$\Delta_{\mathcal{L}} = (w/10^6)(277.345)10^6/26.465(10^3)t_2$$

$$\Delta_{\mathcal{L}} = .010480(w)/t_2 = .349436(w)$$

For Constant I_2 Beam

$$6,476.4 (P/10^6)^*$$

From Diagrams Right

$$m = x/2 \quad 0 < x < L/2$$

$$M = P(x/2) \quad 0 < x < L/2$$

$$\Delta_{\mathcal{L}} = 2 \int_0^{L/2} M m dx / EI$$

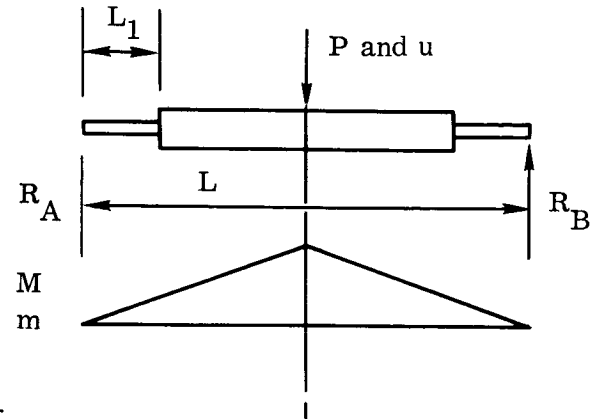
$$\Delta_{\mathcal{L}} = 2 \int_0^{L_1} P(x/2)(x/2) dx / EI_1$$

$$+ 2 \int_{L_1}^{L/2} P(x/2)(x/2) dx / EI_2$$

$$\Delta_{\mathcal{L}} = (2P/E) \left\{ \left[x^3 / 12I_1 \right]_0^{L_1} + \left[x^3 / 12I_2 \right]_{L_1}^{L/2} \right\}$$

$$\Delta_{\mathcal{L}} = P/6E \left[L_1^3 / I_1 + L^3 / 8I_2 - L_1^3 / I_2 \right]$$

$$E = 6.5 (10^6) \text{ MAG}, \quad L_1 = 5.15, \quad L = 86.3$$



Check for Constant $I = I_2$

$$B) * \quad \mathcal{L} = PL^3 / 48EI = P(86.3)^3 / 48(6.5) 10^6 (27)(.3927) t_2$$

$$\Delta_{\mathcal{L}} = P(86.3)^3 / 3308.105 (10^6) t_2 = (P/10^6)(194.291)/t_2$$

$$\Delta_{\mathcal{L}} = 6,476.4 (P/10^6)$$

$$I_1 = .3927 t_1^3, \quad I_2 = 27 (.3927) t_2^3$$

$$\Delta_{\mathcal{L}} = (P/10^6) \left[(5.15)^3 / (6)(6.5)(.3927) t_1 + 86.3^3 / (8)(6)(6.5) 27 (.3927) t_2 - 5.15^3 / (6)(6.5) 27 (.3927) t_2 \right]$$

$$\Delta_{\mathcal{L}} = (P/10^6) \left[5.15^3 / 15.3153 t_1 + 86.3^3 / 3308.1048 t_2 - 5.15^3 / 413.5131 t_2 \right]$$

$$\Delta_{\mathcal{L}} = (P/10^6) (8.919/t_1 + 194.292/t_2 - .330/t_2)$$

$$\Delta_{\mathcal{L}} = (P/10^6) (8.919/t_1 + 193.962/t_2) = \Delta_1 + \Delta_2$$

Torsion

$$f_s = TC/J = TR/2\pi R^3 t = T/2\pi R^2 t$$

$$\text{for } R_1 = 1/2 \text{ in.}$$

$$f_{s1} = T/2\pi(1/2)^2 t_1 = 2T/\pi t_1 = .6366 T/t_1$$

$$\text{for } R_2 = 3.0/2$$

$$f_{s2} = f_{s1}/9 = .6366 T/9t_2$$

Shaft Deflection (Rotational, θ)

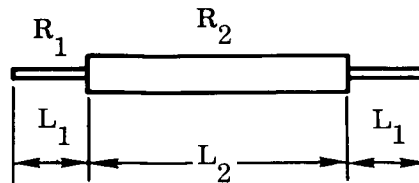
$$\theta = E(TL/2\pi R^3 t G)$$

$$G_1 = 2.4 (10^6) \text{ MAG}$$

$$L_1 = 5.15 \text{ in.}$$

$$L_2 = 86.3 - 2(5.15) = 76.0 \text{ in.}$$

$$\theta = (T) \left[2(5.15)/2\pi(1/2)^3 t_1 (2.4)(10^6) + 76.0/2\pi(3/2)^3 t_2 (2.4) 10^6 \right]$$



$$\Theta = \Theta_1 + \Theta_2 = T \left[(2)^3 (5.15)/\pi 2.4(10^6) t_1 + (2)^3 (76.0)/2\pi(27) 2.4 (10^6) t_2 \right]$$

$$\Theta = T \left[41.2(10^{-6})/(7.53984 t_1) + 608(10^{-6})/407.1514 t_2 \right]$$

$$\Theta = T \left[5.464(10^{-6})/t_1 + 1.4933(10^{-6})/t_2 \right] \text{ RAD}$$

$$\Theta^\circ = \Theta_{\text{RAD}} (180/\pi) = (T/10^6) \left[3.13.081/t_1 + 85.56/t_2 \right]$$

		Θ		Θ°
t_1	t_2	$313.081/t_1$	$85.56/t_2$	
		Θ_1	Θ_2	$(\Theta_1 + \Theta_2)(T/10^6)$
.060	.030	5,218	2,852	8070(T/10 ⁶)

8.4.2 With Center Snubber

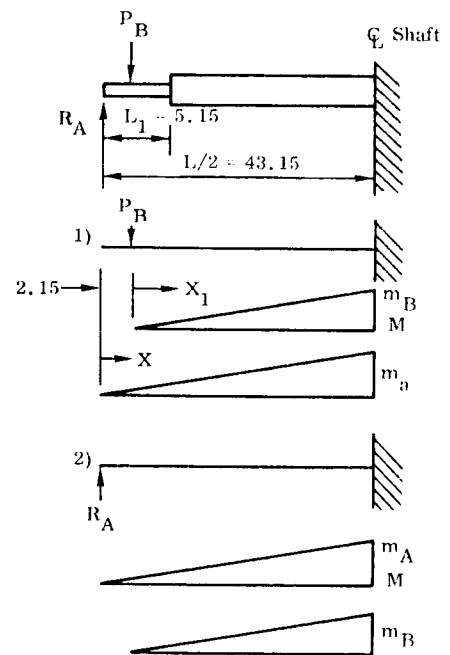
Adding snubber @ \mathcal{C}_L of shaft:

Has effect of cantilever at \mathcal{C}_L of shaft for symmetrical load case

1) P_B only (R_A removed)

$$\begin{aligned} \Delta_{B1} &= \int_0^{41.00} M_B m_B dx_1 / EI(x_1) \\ &= \int_0^{3.00} (P_B x_1)(x_1) dx / EI_1 \\ &\quad + \int_{3.0}^{41.0} (P_B x_1)(x_1) dx / EI_2 \end{aligned}$$

$$\Delta_{B1} = (P_B/E) \left[x_1^3 / 3I_1 \right]_0^{3.0}$$



$$+ P_B/E \left[x_1^3 / 3I_2 \right]_{3.0}^{41.0}$$

$$\Delta_{B1} = (P_B/10^6) \left\{ 3^3/3(.3927) t_1 (6.5) \right.$$

$$\left. + (41.0^3 - 3^3)/3 (27)(.3927 t_2)(6.5) \right\}$$

$$\Delta_{B1} = \frac{(P_B/10^6)(3.526/t_1 + 3.33.344/t_2}{}$$

$$\Delta_{A1} = \int_{2.15}^{43.15} M m a \, dx_1 / EI, \quad \text{Integral } 0 \rightarrow 2.15 = 0$$

$$\Delta_{A1} = \int_{2.15}^{5.15} P_B (x - 2.15)(x) \, dx / EI_1 + \int_{5.15}^{43.15} P_B (x - 2.15) x \, dx / EI_2$$

$$\Delta_{A1} = (P_B/E) \left\{ \left[(x^3/3 - 2.15 x^2/2) / I_1 \right]_{2.15}^{5.15} + \left[(x^3/3 - 2.15 x^2/2) / I_2 \right]_{5.15}^{43.15} \right\}$$

$$\Delta_{A1} = P_B/E \left[(42.2175 - 23.5425)/t_1 + (26,735.12 - 1,973.06)/I_2 \right]$$

$$\Delta_{A1} = (P_B/10^6) \left[18.675/6.5(.3927)t_1 + 24,762.06/27(6.5)(.3927)t_2 \right]$$

$$\Delta_{A1} = (P_B/10^6)(7.316/t_1 + 359.293/t_2)$$

2) R_A Only

$$B2 = \int_{2.15}^{43.15} M m_B \, dx / EI \quad \text{Integral } 0 \rightarrow 2.15 = 0$$

$$\Delta_{B2} = \int_{2.15}^{5.15} R_A (x)(x - 2.15) dx/EI_1 + \int_{5.15}^{43.15} R_A (x)(x - 2.15) dx/EI_2$$

Note

$$\Delta_{B2} = \Delta_{A1}(R_A/P_B) = \frac{(R_A/10)(7.316/t_1 + 359.293/t_2)}{}$$

$$\Delta_{A2} = \int_0^{5.15} (R_A x) x dx/EI_1 + \int_{5.15}^{43.15} (R_A x)(x) dx/EI_2$$

$$\Delta_{A2} = (R_A/E) \left\{ \left[x^3/3I_1 \right]_0^{5.15} + \left[x^3/3I_2 \right]_{5.15}^{43.15} \right\}$$

$$\Delta_{A2} = (R_A/10^6) \left[(5.15^3)/3(6.5) .3927t_1 + (43.15^2 - 5.15^3)/3(6.5)(27)(.3927) t_2 \right]$$

$$\Delta_{A2} = (R_A/10^6) \left[(5.15)^3/7.65765 + (43.15^2 - 5.15^2)/206.75655 \right]$$

$$\Delta_{A2} = \frac{(R_A/10^6)(17.837/t_1 + 387.922/t_2)}{}$$

To solve redundant R_A let

$$\Delta_{A1} + \Delta_{A2} = 0 = (P_B/10^6)(A1) + (R_A/10^6)(A2)$$

$$R_A = -P_B \left[(A1)/(A2) \right] \quad (1)$$

To find Δ_B

$$\Delta_B = \Delta_{B1} + \Delta_{B2} = (P_B/10^6)(B1) + (R_A/10^6)(B2) \quad (2)$$

Substituting Eq (1) into Eq (2)

$$\Delta_B = (P_B/10^6) \left\{ (B1) - (B2) \left[(A1)/(A2) \right] \right\} \quad (3)$$

Note (B2) = (A1) and substituting in Eq (3)

$$\Delta_B = (P_B/10^6) \left[(B1) - (A1)^2/(A2) \right]$$

For $t_1 = .06$ and $t_2 = .03$

$$A1 = 7.316/.06 + 359.293/.03 = 121.93 + 11,976.43 = 12,098.36$$

$$A2 = 17.837/.06 + 387.922/.03 = 297.28 + 12,930.73 = 13,228.01$$

$$B1 = 3.526/.06 + 333.344/.03 = 58.77 + 11,111.47 = 11,170.24$$

$$\Delta_B = (P_B/10^6) \left[(B1) - (A1)^2/(A2) \right]$$

$$\Delta_B = (P_B/10^6) \left[11,170.24 - (12,098.36)^2/(13,228.01) \right]$$

$$\Delta_B = (11,170.24 - 11,090.34)(P_B/10^6)$$

$$\Delta_B = \underline{79.90 (P_B/10^6)} \quad \text{Supported @ } \mathbb{C}_L \text{ shaft}$$

$$\Delta_B = \underline{196.73 (P_B/10^6)} \quad \text{Unsupported @ } \mathbb{C}_L \text{ shaft}$$

8.4.3 Conclusions:

For a dynamic loading of 600#

$$\Delta_B = 79.90 (600)/10^6 = .0479'' \quad \text{Supported @ } \mathbb{C}_L$$

$$\Delta_B = 196.73(600)/10^6 = .1180'' \quad \text{Unsupported @ } \mathbb{C}_L$$

The above deflections are excessive and would create a magnification of dynamic excitations into the wrap drum well in excess of its design limits. Therefore, a shear clip will be used at the bearing support to react drum dynamic loads so that these loads are not transferred to the torque tube.

8.5 DRUM END-ON SOLAR FLUX CONSIDERATIONS

General

A thermal analysis study of the wrap drum was needed to determine temperature gradients present on the drum before extension of the beams and substrate. This is an extreme case condition occurring only if the array is not sun-oriented at time of deployment. The condition is being considered to determine if thermal distortion of the solar panel (the substrate assembly) might occur and what is the effect on panel deployment.

In this analysis, the highest possible temperature conditions were assumed to be in effect. For this analysis it is assumed that all the radiant energy from the sun ($450 \text{ BTU/ft}^2 \text{ hr.}$) is incident on the drum, normal to one end of the drum, with the other end exposed to space. This condition would cause the most drum deformation due to the large temperature gradients.

Nodal Breakdown

The drum, with substrate, was assumed to be in the wrapped configuration. It was divided into nodes where were assumed to be isothermal. Figures A-1, A-2, A-3, and A-4 show the breakdown of the drum ends into the isothermal nodes.

The wrapped area of the drum was divided into ten isothermal nodes, each 8.5 inches long. This was done for both the cylindrical shell of the magnesium drum and the fiberglass substrate wrapping.

The results of the heat flux on the drum reaching a steady state are presented in computer run form, (refer to data which follows nodal location figures). Steady state was reached after a mission time of six hours.

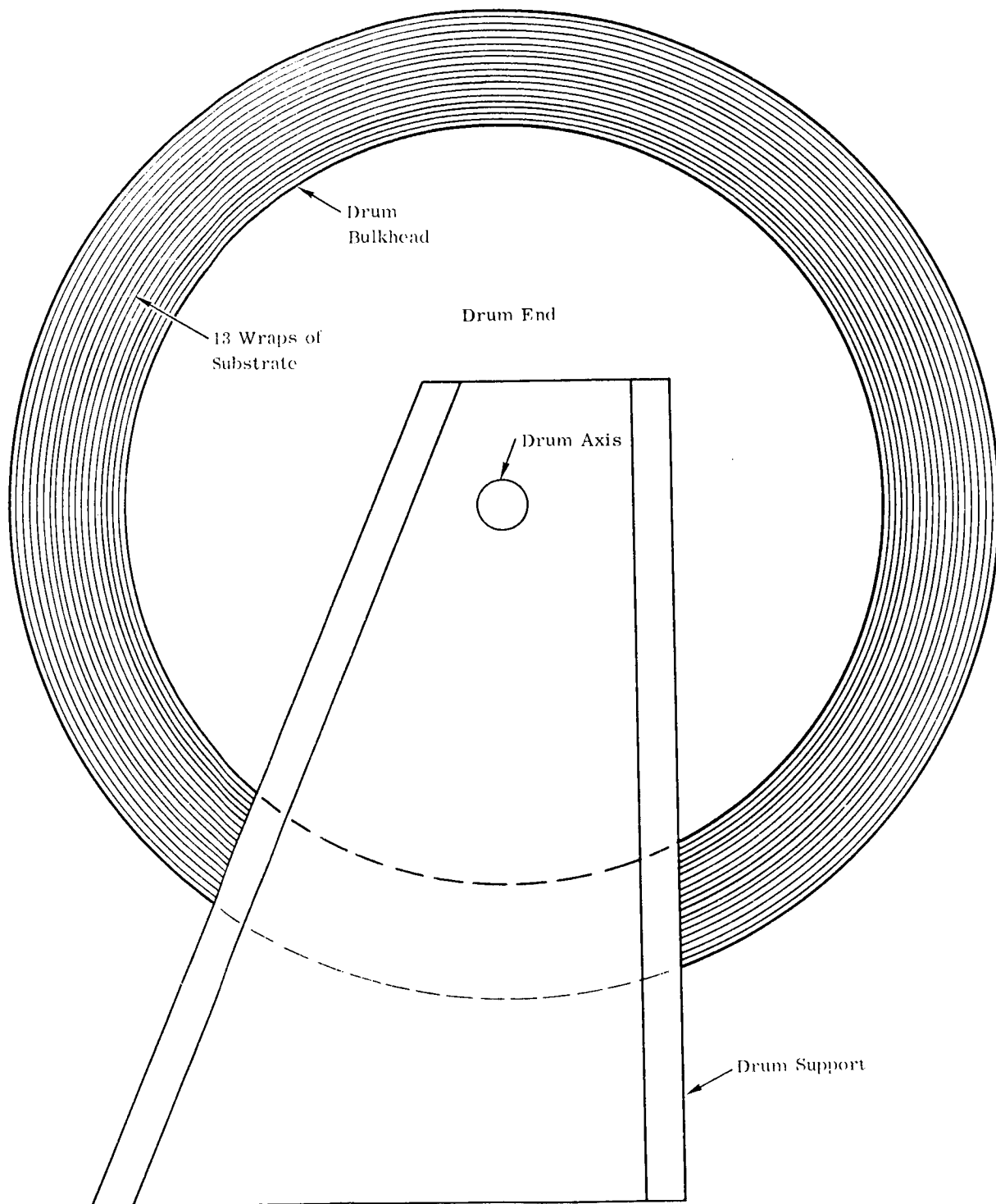


Figure A-1. End-On Solar Flux Consideration, Hot End Nodal Points

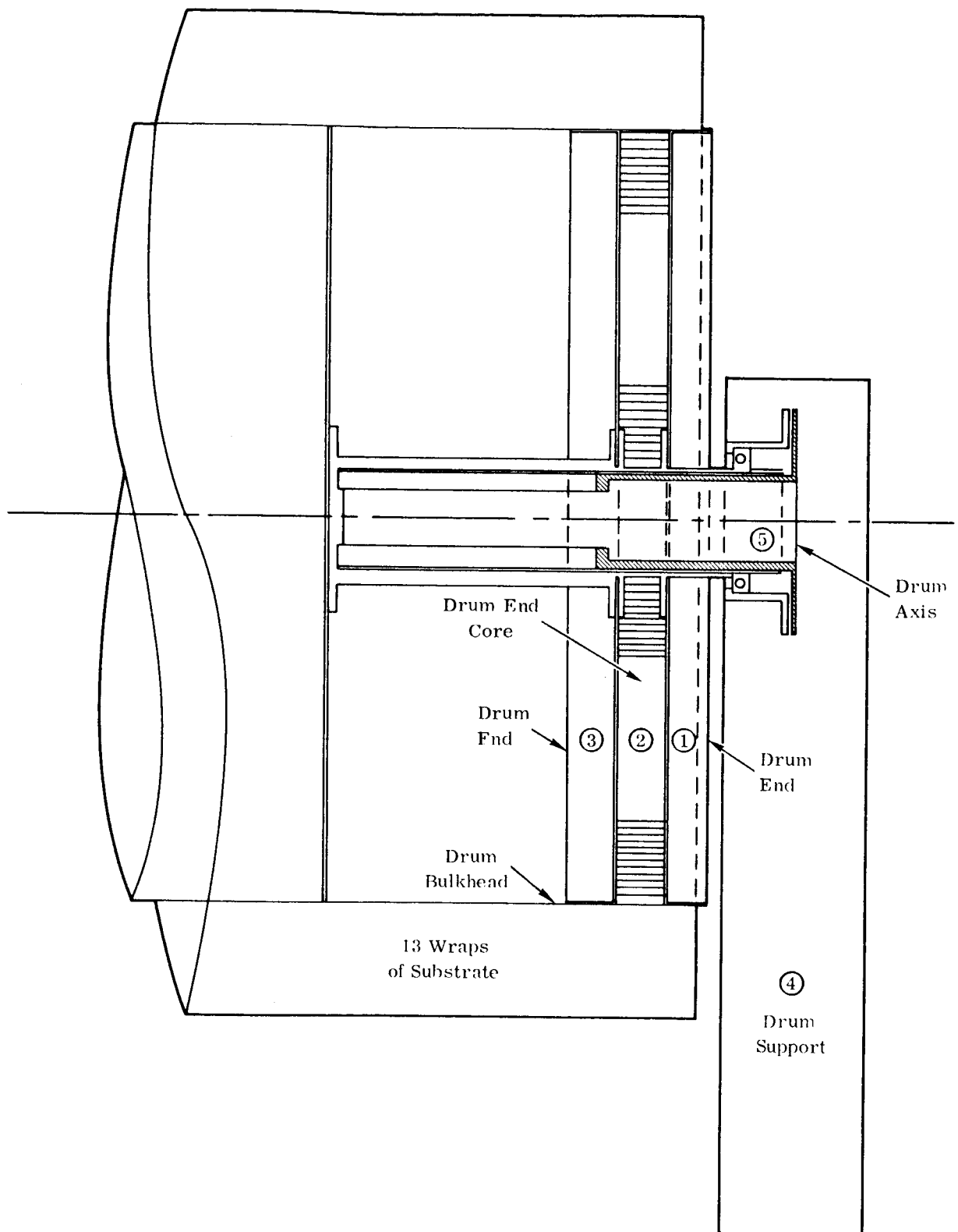


Figure A-2. End-On Solar Flux Considerations, Hot End of Drum and Support, Nodal Points

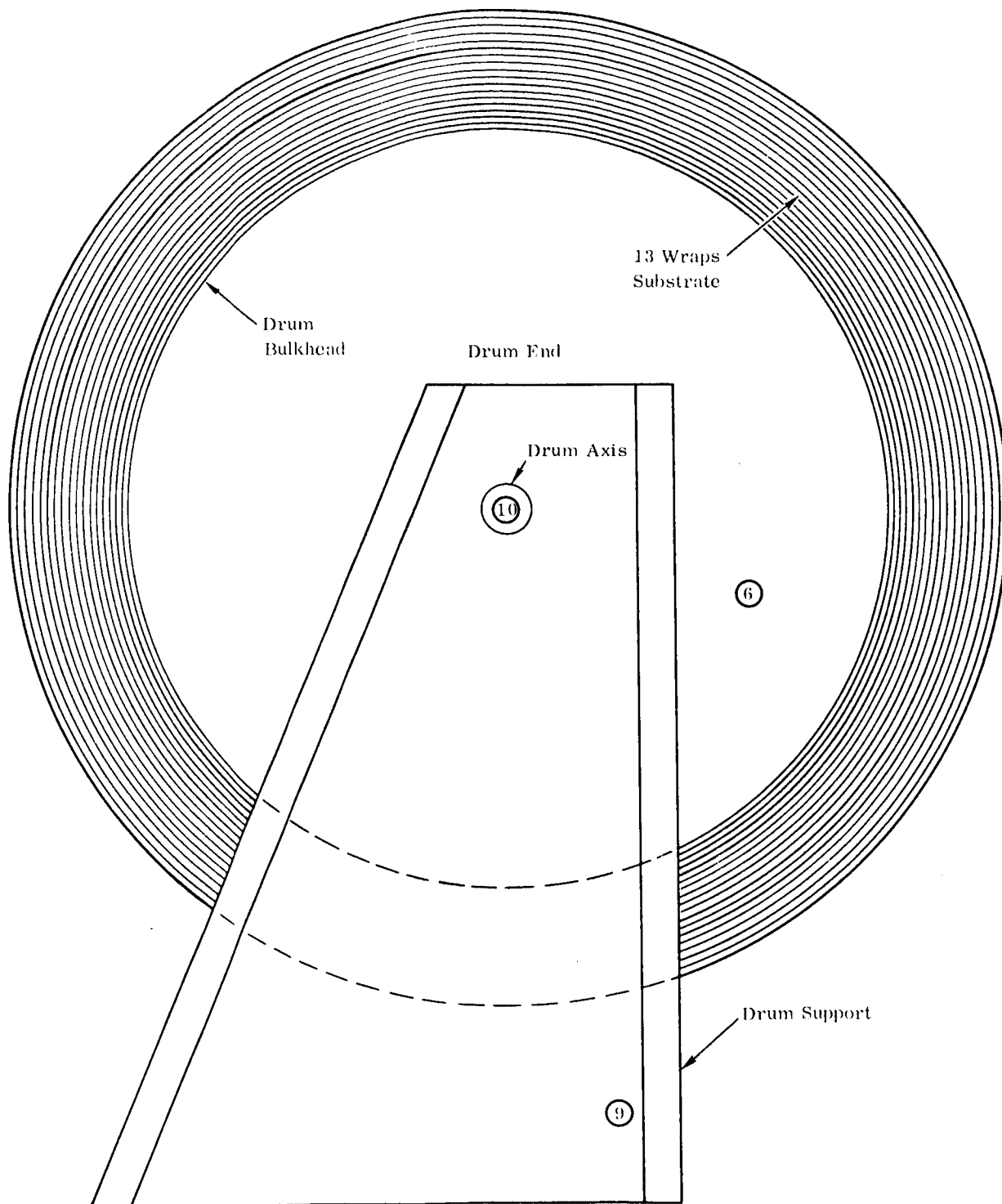


Figure A-3. End-On Solar Flux Considerations, Cold End Nodal Points

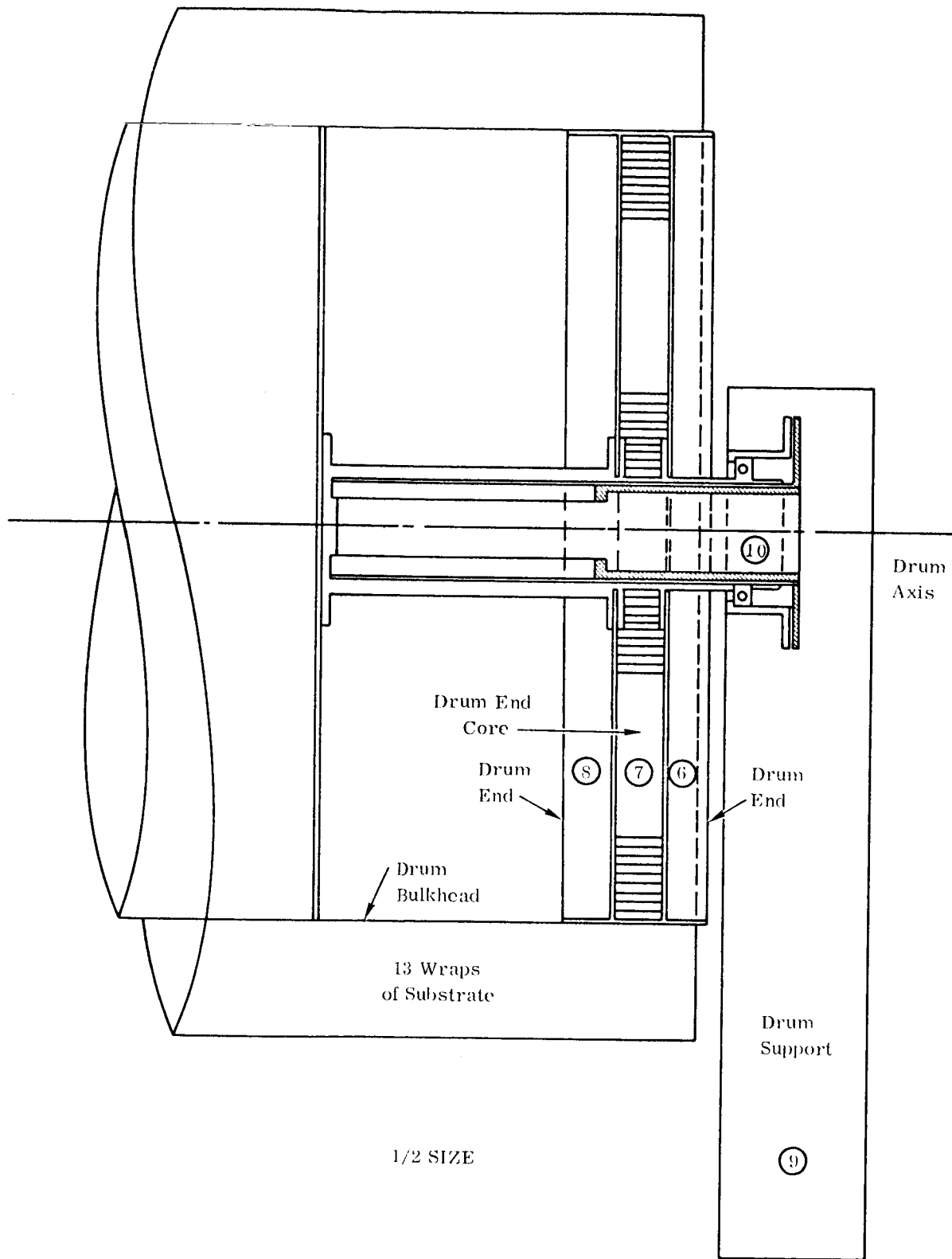


Figure A-4. End-On Solar Flux Considerations, Cold End of Drum and Support, Nodal Points

Assumptions and Material Properties

No assumptions were made as to coatings on the exposed surfaces of the drum since the purpose of this analysis was to determine the temperature gradients that would cause deformation of the beams. The materials used in the drum and some of their properties are shown below:

Node #	Node Description	Material	Specific Heat $\frac{\text{BTU}}{\text{LB}^\circ\text{R}}$	α	ϵ
1, 3, 6, 8	Drum End	Aluminum	.23	.25	.08
4, 9	Support	Magnesium	.245	.25	.08
2, 7	Drum End Core	Aluminum Honeycomb	.23		
5, 10	End Axis	Aluminum	.23		
11 - 20	Drum Bulkhead	Magnesium	.245		
21 - 30	Fiberglass Substrate	Fiberglass, Glass Solar Cells	.261	1.	1.

INTEGRATION OF THERMAL TRANSIENTS

JOB 1179

3 OCTOBER, 1967

BOB TRAYLOR

EXTENDABLE WRAP DRUM THERMAL ANALYSIS

31 NODES	INITIAL TIME (HOURS)	0.0
40 PATHS, CONDUCTIVE	COMPUTATION INCREMENT	0.0
14 PATHS, RADIATIVE	PRINT INCREMENT	1.0000E-01
3 NODES AFFECTED BY ENVIRONMENT	FINAL	6.000

	NODE	TEMP	W	A	C	Q	ALPHA	EPSILON
						DIS		
DR E OUT H	1	70.0	.4420	81.86	.2300		.2500	.08000
DR E COR H	2	70.0	.3450		.2300			
DR E IN H	3	70.0	.4420	122.9	.2300			
SUPPORT H	4	70.0	.2480	95.40	.2450		.2500	.08000
END AXIS H	5	70.0	.6100		.2300			
DR E OUT C	6	70.0	.4420	81.86	.2300			.08000
DR E COR C	7	70.0	.3450		.2300			
DR E IN C	8	70.0	.4420	122.9	.2300			
SUPPORT C	9	70.0	.2480	95.40	.2450			.08000
END AXIS C	10	70.0	.6100		.2300			
DR BL1	11	70.0	.4670		.2450			
DR BL2	12	70.0	.4670		.2450			
DR BL3	13	70.0	.4670		.2450			
DR BL4	14	70.0	.4670		.2450			
DR BL5	15	70.0	.4670		.2450			
DR BL6	16	70.0	.4670		.2450			
DR BL7	17	70.0	.4670		.2450			
DR BL8	18	70.0	.4670		.2450			
DR BL9	19	70.0	.4670		.2450			
DR BL10	20	70.0	.4670		.2450			
SUB 1	21	70.0	5.588	494.4	.2610		1.000	1.000
SUB 2	22	70.0	5.588	416.4	.2610		1.000	1.000
SUB 3	23	70.0	5.588	416.4	.2610		1.000	1.000
SUB 4	24	70.0	5.588	416.4	.2610		1.000	1.000
SUB 5	25	70.0	5.588	416.4	.2610		1.000	1.000
SUB 7	26	70.0	5.588	416.4	.2610		1.000	1.000
SUB 7	27	70.0	5.588	416.4	.2610		1.000	1.000
SUB 8	28	70.0	5.588	416.4	.2610		1.000	1.000
SUB 9	29	70.0	5.588	416.4	.2610		1.000	1.000
SUB 10	30	70.0	5.588	494.4	.2610		1.000	1.000
SPACE	31	-460.0						
		0			2 BTU/ 0			
		F	LBS	IN	/LB.F	WATTS		

RYAN AERONAUTICAL, SAN DIEGO

INTEGRATION OF THERMAL TRANSIENTS

JOB 1179

3 OCTOBER, 1967

BOB TRAYLOR

EXTENDABLE WRAP DRUM THERMAL ANALYSIS

CONDUCTIVE PATH	FROM	TO		L	A
1 DR E OUT H	1	2 DR E COR H	.1670	.3500	122.9
2 DR E COR H	2	3 DR E IN H	.1670	.3500	122.9
3 SUPPORT H	4	5 END AXIS H	72.00	5.500	.3960
4 END AXIS H	5	11 DR BL1	72.00	3.050	.8790
5 DR E OUT H	1	11 DR BL1	72.00	3.050	.8790
6 DR E IN H	3	11 DR BL1	72.00	3.050	.8790
7 DR BL1	11	12 DR BL2	72.00	8.500	1.520
8 DR BL2	12	13 DR BL3	72.00	8.500	1.520
9 DR BL3	13	14 DR BL4	72.00	8.500	1.520
10 DR BL4	14	15 DR BL5	72.00	8.500	1.520
11 DR BL5	15	16 DR BL6	72.00	8.500	1.520
12 DR BL6	16	17 DR BL7	72.00	8.500	1.520
13 DR BL7	17	18 DR BL8	72.00	8.500	1.520
14 DR BL8	18	19 DR BL9	72.00	8.500	1.520
15 DR BL9	19	20 DR BL10	72.00	8.500	1.520
16 DR BL1	11	21 K SUB 1	.02500	1.620	13.80
17 DR BL2	12	22 K SUB 2	.02500	1.620	13.80
18 DR BL3	13	23 K SUB 3	.02500	1.620	13.80
19 DR BL4	14	24 K SUB 4	.02500	1.620	13.80
20 DR BL5	15	25 K SUB 5	.02500	1.620	13.80
21 DR BL6	16	26 K SUB 7	.02500	1.620	13.80
22 DR BL7	17	27 K SUB 7	.02500	1.620	13.80
23 DR BL8	18	28 K SUB 8	.02500	1.620	13.80
24 DR BL9	19	29 K SUB 9	.02500	1.620	13.80
25 DR BL10	20	30 K SUB 10	.02500	1.620	13.80
26 SUB 1	21	22 K SUB 2	.08450	8.500	.4300
27 SUB 2	22	23 K SUB 3	.08450	8.500	.4300
28 SUB 3	23	24 K SUB 4	.08450	8.500	.4300
29 SUB 4	24	25 K SUB 5	.08450	8.500	.4300
30 SUB 5	25	26 K SUB 7	.08450	8.500	.4300
31 SUB 7	26	27 K SUB 7	.08450	8.500	.4300
32 SUB 7	27	28 K SUB 8	.08450	8.500	.4300
33 SUB 8	28	29 K SUB 9	.08450	8.500	.4300
34 SUB 9	29	30 K SUB 10	.08450	8.500	.4300
35 DR BL10	20	6 DR E OUT C	72.00	3.050	.8790
36 DR BL10	20	8 DR E IN C	72.00	3.050	.8790
37 DR BL10	20	10 END AXIS C	72.00	3.050	.8790
38 END AXIS C	10	9 SUPPORT C	72.00	5.500	.3960
39 DR E IN C	8	7 DR E COR C	.1670	.3500	122.9
40 DR E COR C	7	6 DR E OUT C	.1670	.3500	122.9

BTU/ 0 2
/HR.FT.F INCHES INCH

RYAN AERONAUTICAL, SAN DIEGO

INTEGRATION OF THERMAL TRANSIENTS

JOB 1179

3 OCTOBER, 1967

BOB TRAYLOR

EXTENDABLE WRAP DRUM THERMAL ANALYSIS

RADIATIVE PATH		FROM	TO		F
1	DR E OUT H	1	31	SPACE	.08000
2	SUPPORT H	4	31	SPACE	.08000
3	DR E OUT C	6	31	SPACE	.08000
4	SUPPORT C	9	31	SPACE	.08000
5	SUB 1	21	31	SPACE	1.000
6	SUB 2	22	31	SPACE	1.000
7	SUB 3	23	31	SPACE	1.000
8	SUB 4	24	31	SPACE	1.000
9	SUB 5	25	31	SPACE	1.000
10	SUB 7	26	31	SPACE	1.000
11	SUB 7	27	31	SPACE	1.000
12	SUB 8	28	31	SPACE	1.000
13	SUB 9	29	31	SPACE	1.000
14	SUB 10	30	31	SPACE	1.000

RYAN AERONAUTICAL, SAN DIEGO

INTEGRATION OF THERMAL TRANSIENTS

JOB 1179

3 OCTOBER, 1967

BOB TRAYLOR

EXTENDABLE WRAP DRUM THERMAL ANALYSIS

ENVIRONMENTAL EFFECTS

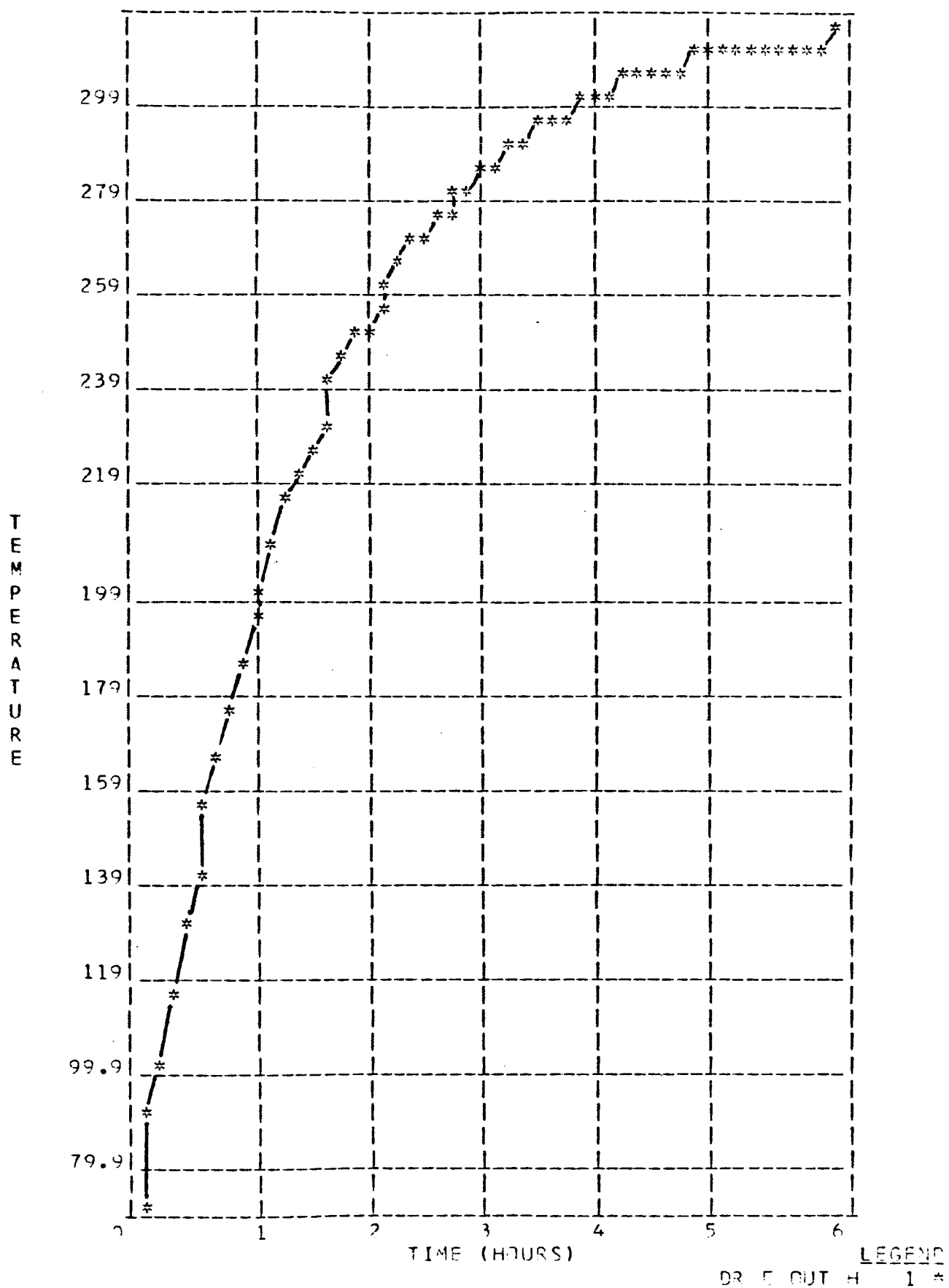
NODE	TIME	SOLAR	ALBEDO	THERMAL	POWER
1 DR E OUT	H0.0	255.77	0.0	0.0	
4 SUPPORT	H0.0	298.12	0.0	0.0	
21 SUB 1	0.0	243.74	0.0	0.0	
1 DR E OUT	H6.0	255.70	0.0	0.0	
4 SUPPORT	H6.0	298.12	0.0	0.0	
21 SUB 1	6.0	243.74	0.0	0.0	

RYAN AERONAUTICAL, SAN DIEGO

3 OCTOBER, 1967

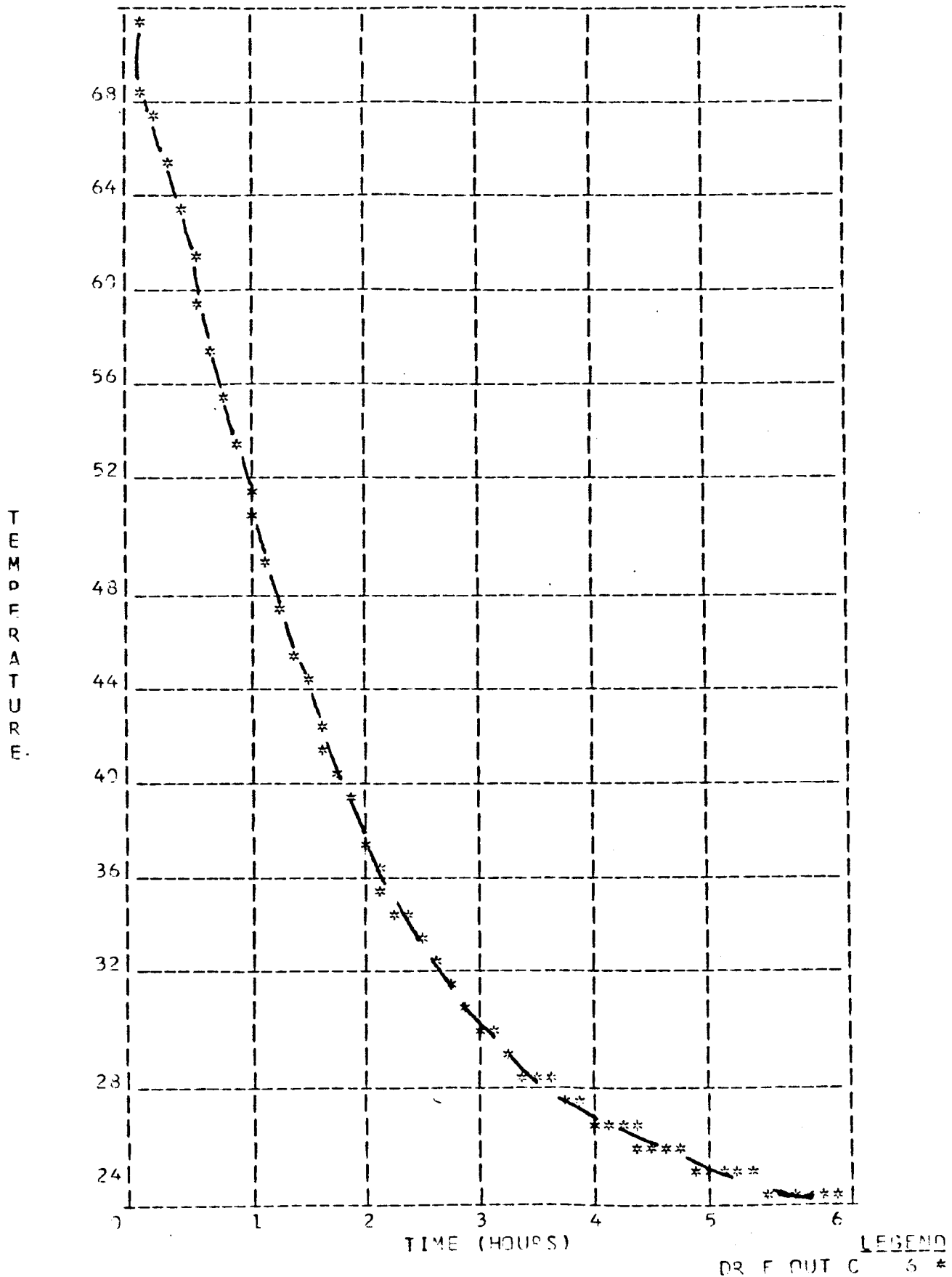
BOB TRAYLOR

EXTENDABLE WRAP DRUM THERMAL ANALYSIS



TYPICAL GRADIENT - HOT END, DRUM OUTER BULKHEAD

EXTENDABLE WRAP DRUM THERMAL ANALYSIS

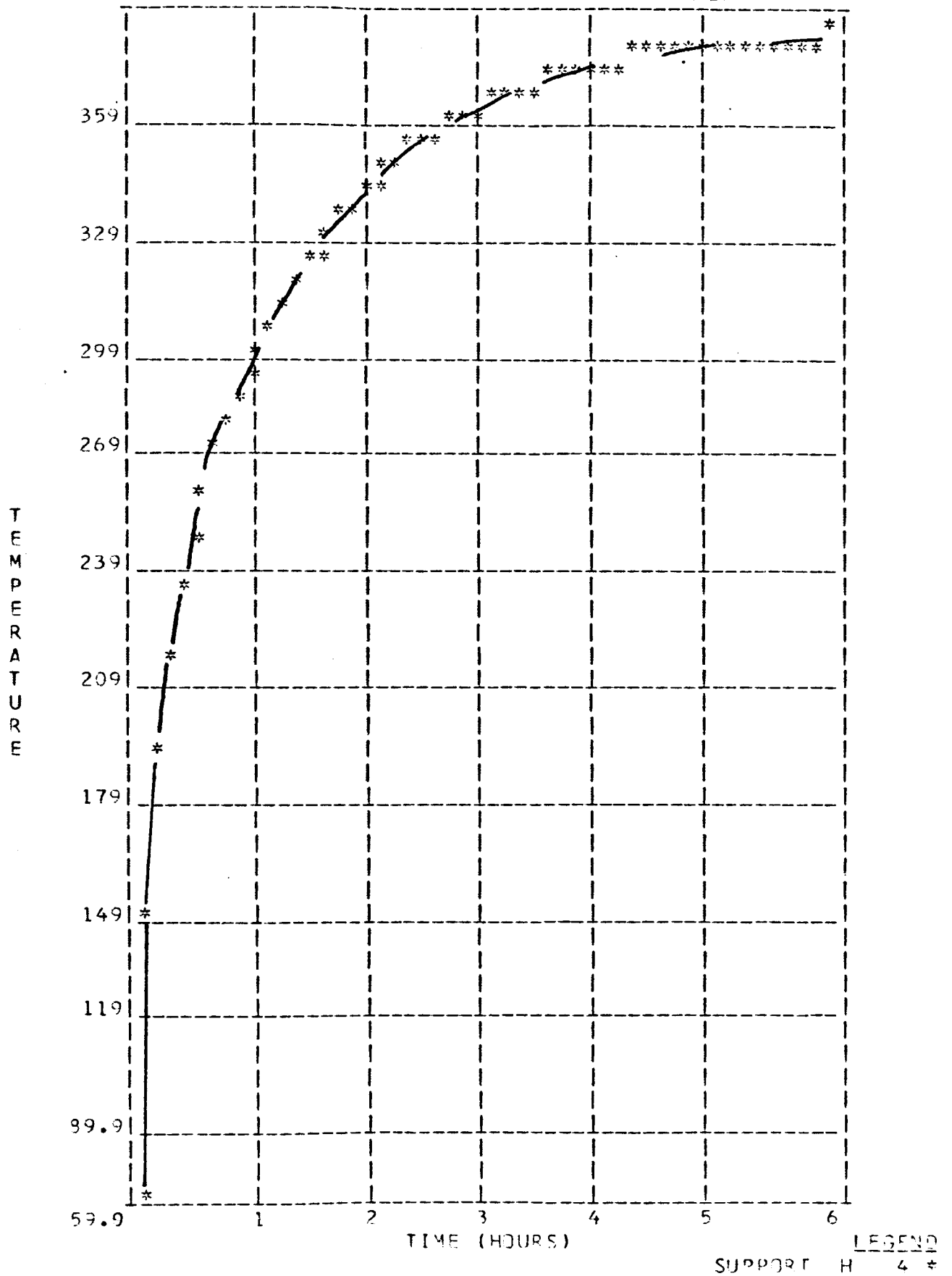


TYPICAL GRADIENT - COLD END, DRUM OUTER BULKHEAD

3 OCTOBER, 1967

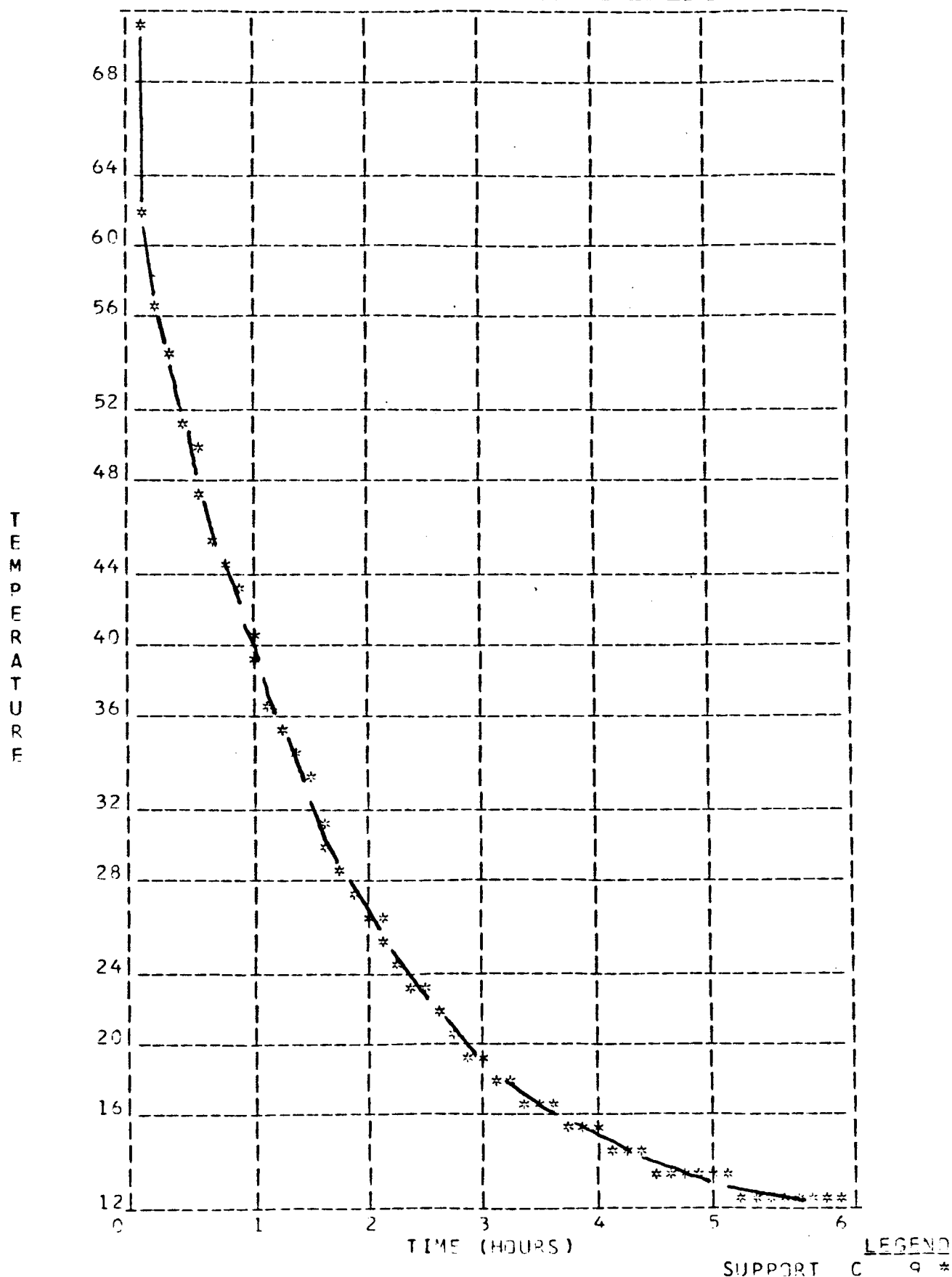
BOB TRAYLOR

EXTENDABLE WRAP DRUM THERMAL ANALYSIS



TYPICAL GRADIENT - HOT END, DRUM SUPPORT

EXTENDABLE WRAP DRUM THERMAL ANALYSIS

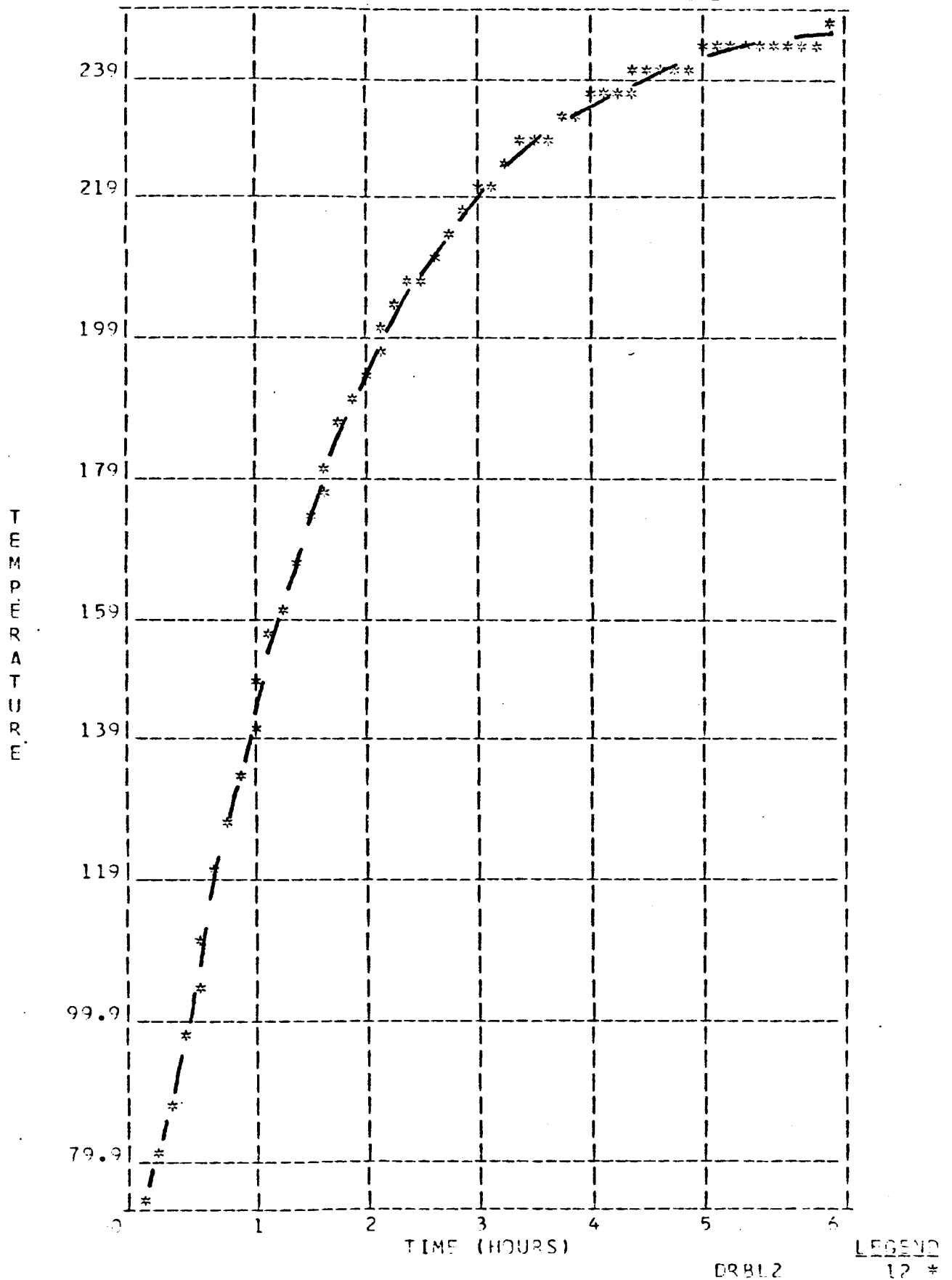


TYPICAL GRADIENT - COLD END, DRUM SUPPORT

3 OCTOBER, 1967

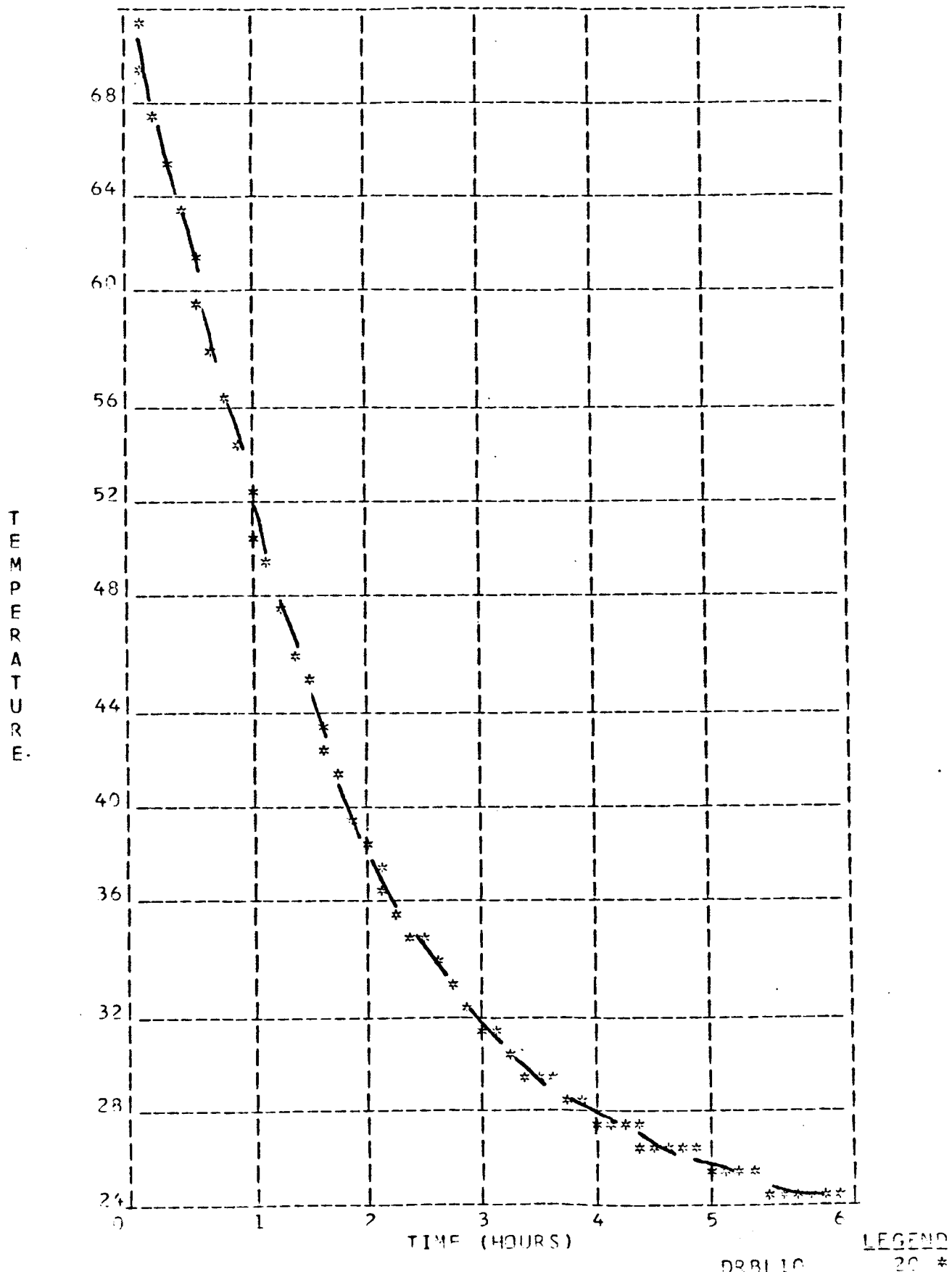
BOB TRAYLOR

EXTENDABLE WRAP DRUM THERMAL ANALYSIS



TYPICAL GRADIENT - HOT END, DRUM INNER BULKHEAD

EXTENDABLE WRAP DRUM THERMAL ANALYSIS

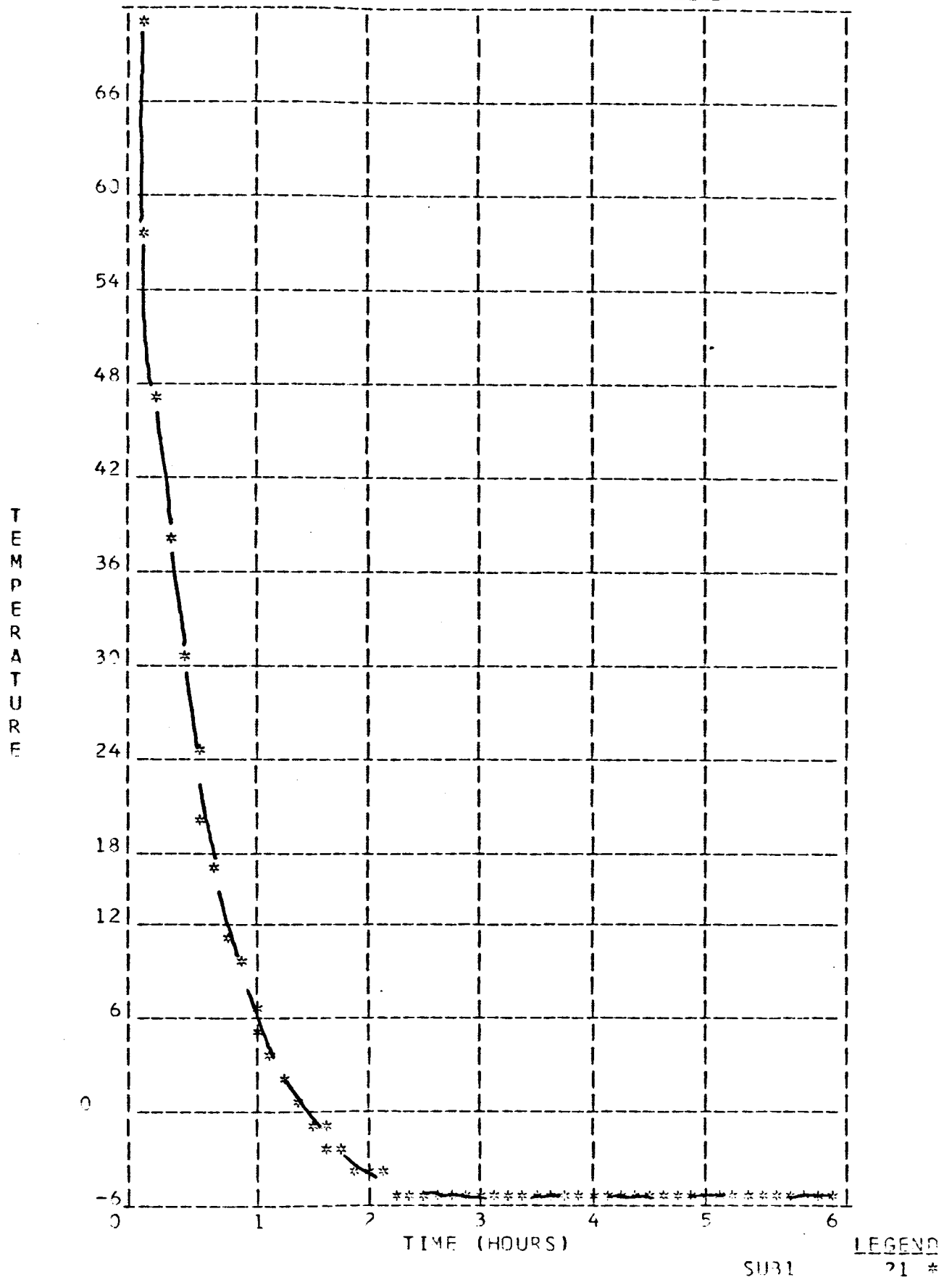


TYPICAL GRADIENT - COLD END, DRUM INNER BULKHEAD

3 OCTOBER, 1967

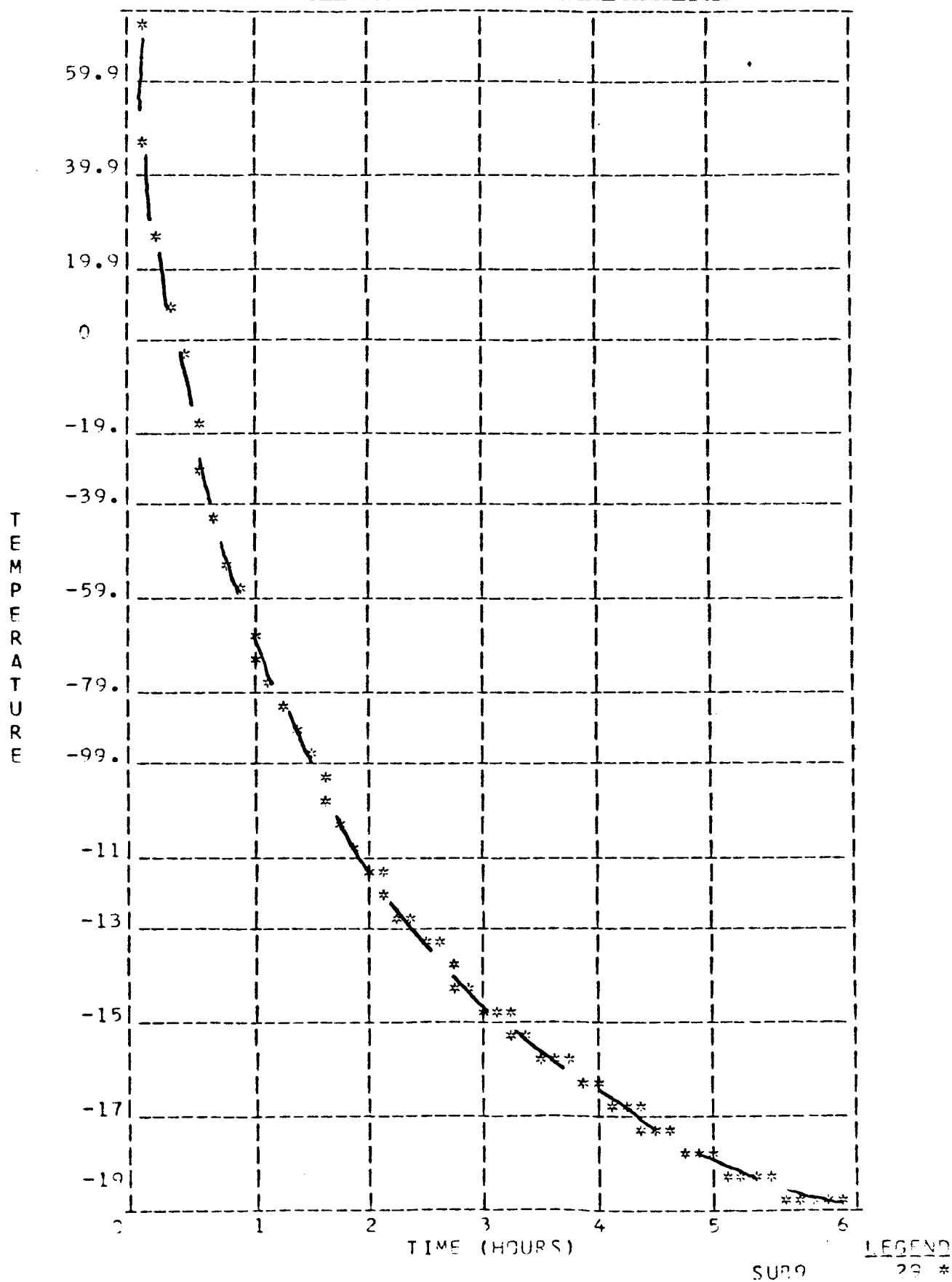
BOB TRAYLOR

EXTENDABLE WRAP DRUM THERMAL ANALYSIS



TYPICAL GRADIENT - HOT END, SUBSTRATE WRAP

EXTENDABLE WRAP DRUM THERMAL ANALYSIS



TYPICAL GRADIENT - COLD END, SUBSTRATE WRAP

Conclusions

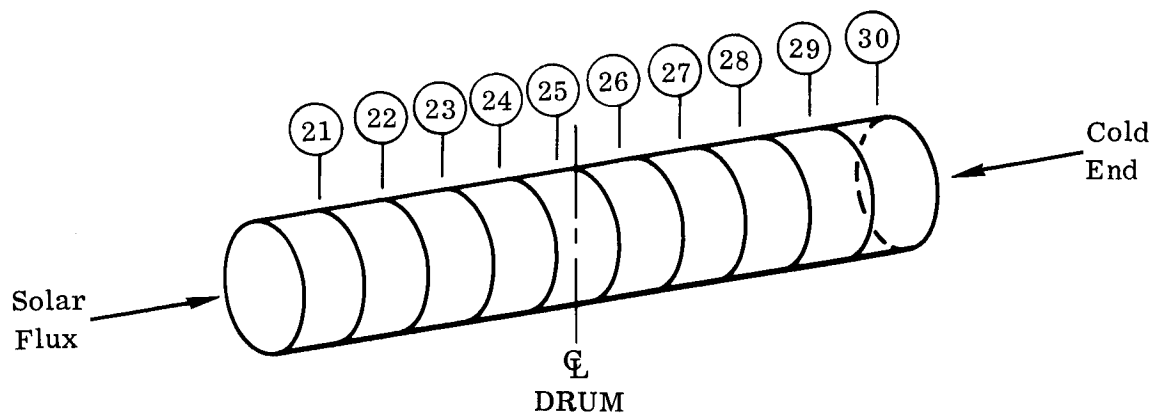
No conclusions are reached at this time regarding the effects of this End-On Solar Flux condition on deployment of the solar array assembly. Evaluation of the results of this analysis (see summary which follows) will be made later in the program.

The analysis shows that at the cold end of the wrapped drum and substrate, temperatures are well above -150°F , even after six hours exposure, (substrate temperature after six hours is estimated as -20°F). We therefore, might conclude that temperatures lower than -20°F , are unrealistic. However, for a condition where the stowed panel might be in complete shadow, a temperature of -150°F could be attained in approximately 90 minutes time.

Analysis Summary

The following table shows the temperature gradient between corresponding hot and cold nodes on the wrap drum.

Nodes		Node Description	ΔT Between Nodes ($^{\circ}\text{F}$)
Hot End	Cold End		
1,	6	Drum End Outside	289.1 $^{\circ}$
2,	7	Drum End Core	286.1 $^{\circ}$
3,	8	Drum End Inside	283.1 $^{\circ}$
4	9	Drum Support	370.5 $^{\circ}$
5,	10	Drum End Axis	283.6 $^{\circ}$
11,	20	Drum Bulkheads	274.7 $^{\circ}$
12,	19	Drum Bulkheads	209.7 $^{\circ}$
13,	18	Drum Bulkheads	146.5 $^{\circ}$
14,	17	Drum Bulkheads	86.9 $^{\circ}$
15,	16	Drum Bulkheads	28.7 $^{\circ}$
21,	30	Substrate	213.7 $^{\circ}$
22,	29	Substrate	6.2 $^{\circ}$
23,	28	Substrate	4.2 $^{\circ}$
24,	27	Substrate	2.5 $^{\circ}$
25,	26	Substrate	.8 $^{\circ}$



DEFINITION OF NODE POSITIONS
ON SUBSTRATE WRAPS

8.6 PERFORMANCE OF VERY THIN SILICON SOLAR CELLS

A copy of a research paper, B118A, as presented by Heliotek, a division of Textron Electronics, Inc., at the 6th Photovoltaic Specialists Conference Cocoa Beach, Florida, 28-31 March 1967, is enclosed as appendix data to this report.



PRECEDING PAGE BLANK NOT FILMED.

PERFORMANCE OF VERY THIN SILICON SOLAR CELLS

by

E. L. Ralph

Heliotek, Division of Textron Electronics, Inc.

ABSTRACT

Electrical performance characteristics of N on P solar cells in the range of two to sixteen mils thickness have been determined and summarized. The evaluation was based on experimental solar cells made from both 2 and 10 ohm cm boron-doped silicon. Engineering and design data was obtained for the cells over a temperature range of -170° to $+120^{\circ}\text{C}$. The effect of decreasing solar cell thickness on the power to weight ratio of the bare cells and composite assemblies was evaluated.

PERFORMANCE OF VERY THIN SILICON SOLAR CELLS

by

E. L. Ralph

Heliotek, Division of Textron Electronics, Inc., Sylmar, California

INTRODUCTION

As the size of the solar cell arrays are increased and the use of flexible roll-up techniques are introduced, the importance of system weight becomes apparent. Many of the power systems of the future will require enormous solar cell panels. Weight is of primary concern. Advanced designs will need to try to obtain the most efficient solar cell array structure. Any weight or output power penalty will be multiplied many times in the very large array situation. Studies to eliminate these penalties must be concerned with the whole array since all the components, namely solar cells, covers, substrates and structures, are interrelated and have an influence on the power-weight parameter.

This paper is concerned with the solar cell device characteristics as the cell thickness and temperature is varied. It attempts to provide engineering and design data on the power-weight parameter, and on the cell performance as the thickness is decreased. Earlier studies have provided the basic understanding of the effect of decreasing the thickness and have provided performance characteristics for specific cell thicknesses ¹⁾ ²⁾. This paper complements the previous work and provides a comprehensive cell performance summary for a wide range of cell thicknesses over a very wide range of temperatures.

DESCRIPTION OF THE STUDY

There were essentially two basic areas of concern in this study. One was to accurately determine the effect of reducing cell thickness on the electrical output, and to properly correlate this effect to the state-of-the-art so that the data could be used with confidence in future designs. The second area of concern was the effect of temperature on the cell performance for the various cell thicknesses.

The cell performance versus thickness data was compiled and summarized from the results of several different experiments. Experiments were done over the past several years using various selected thicknesses, and these results were used as a starting basis. These experiments involved differing numbers of sample cells, ranging from large quantities of several thousand to only a few, depending on the specific thickness.

To complement this data and obtain a more comprehensive and consistent study, a new series of cells of various thicknesses was analyzed. The cells were made from nominally 2 ohm cm (1 to 3 ohm cm) and nominally 10 ohm cm (7 to 14 ohm cm) boron-doped silicon. Cell thicknesses of 0.012, 0.008, 0.006, and 0.004 inches were evaluated for each of the two resistivity groups.

N on P 2x2 cm cells with evaporated Ti-Ag solderless contacts were made using existing fabrication fixtures and processes. No particular process or handling problems were encountered in making the various cell types, except in the case of the 0.004 inch cells, where special care in handling these fragile cells was required. Also, the 0.004 inch thick cells were very flexible and the mechanical stresses between the contracts and the silicon bowed the cells. This was no particular disadvantage, however, since they flattened out in testing or in mounting to a coverglass. In the case of a flexible array, cell flexibility will probably be a distinct advantage.

The temperature dependence data was obtained on cells made with the same four thicknesses and two resistivities discussed above. Measurements were made in an X-25L Spectrosun[®] solar simulator, using a test fixture located in an insulated box with a quartz window. Dry nitrogen was pumped into the box to remove water vapor. The cell test fixture had heaters imbedded in the base and had facilities for passing liquid nitrogen through it. The cell temperature could be adjusted to any value from -170°C up to +120°C. Temperatures were measured with a thermocouple attached to the fixture block near the cell. This thermocouple was calibrated by attaching a second thermocouple to the surface of a solar cell and correlating the two temperatures over the complete temperature range of interest.

EXPERIMENTAL RESULTS

The data obtained from the four thickness and two resistivity cell types were combined with the thickness data from previous experiments. Typical IV curves were drawn and are shown in Figure 1. The primary effect of decreasing thickness for both 2 and 10 ohm cm cells was a decrease in I_{sc} ; however, a decrease in V_{oc} was also observed. The 2 ohm cm cells had a V_{oc} that was about 45 mV higher than the equivalent thickness 10 ohm cm cells. The 0.012 inch thick 10 ohm cm cells had an I_{sc} about 10 mA higher than the 2 ohm cm cells, but this difference was reduced with thinner cells until the difference was only about 5 mA for the 0.004 inch cells. This indicates that the effective collection region was being limited predominately by the thickness for the 0.004 inch thick cells, rather than by the minority carrier diffusion length. Therefore, the longer diffusion length of the 10 ohm cm material did not provide much of an advantage over the 2 ohm cm material for the very thin cells. This fact has a significant influence on the maximum power of the two types of cells. Since the V_{oc} drops off at the same rate with thickness for both the 2 and 10 ohm cm cells, the increased I_{sc} loss for the 10 ohm cm cells means the power must also drop off faster. In addition to this disadvantage, the curve factor (a measure of the sharpness of the knee) also showed that thin 10 ohm cm cells had poorer curve factors than the thick cells. This was not true for the 2 ohm cm cells so the net results was a faster drop-off in power for the 10 ohm cm cells.

Figure 2 shows how the above effect affected cell efficiency. As the cell thickness decreased, the differential between 2 and 10 ohm cm cells became greater. The 2 ohm cm cell efficiencies were higher in all cases. This plot covers some thicknesses not included in the discussion above. The curve was extended to thicknesses up to 0.016 inches in order to give more complete design information. For the 2 ohm cm case, data for cells 0.002 inches thick was included.

The IV curve versus temperature for each of the four thicknesses and two resistivities are shown in Figures 3 through 10. These curves should be very useful for system design purposes where the complete IV characteristic is helpful in selecting the optimum operating voltage for a specific mission. The open circuit voltage decreased and the short circuit current increased with increasing temperatures in all cases. The maximum power output typically decreased with increasing temperatures over the most commonly encountered temperatures; however, there were some anomalies at very low temperatures. The effect of temperature on the IV characteristics was generally the same for all cells except for the very thin ones.

The very thin cells for both 2 and 10 ohm cm material often had a degradation in the curve factor which became prominent at very low temperatures. Figures 6 and 10 show this effect for the 0.004 inch thick cells made from 2 and 10 ohm cm material respectively. Not all thin cells showed this effect, so it probably was associated with a low temperature shunt caused by thermal stresses or process variations.

An examination of the temperature data indicated that the V_{oc} and I_{sc} did not vary linearly with temperature over the complete range investigated. Short circuit current was plotted versus temperature in Figure 11, and a linear function for all cells was obtained between -40° and $+120^{\circ}\text{C}$. Below -40° the I_{sc} became nonlinear with temperature, with the 2 ohm cm cells showing a greater anomaly than 10 ohm cm cells.

Since the spectral response of the cells shifts with temperature, a second investigation was initiated to see if this I_{sc} anomaly could possibly have been caused by a large spike or valley in the X-25 spectrum. In this case, an unfiltered 2800°K tungsten light source was used since the spectrum was known to be very smooth and peaked in the long (red) wavelength region, while the sunlight simulator spectrum was peaked in the short (blue) wavelengths and has a line spectrum superimposed on the continuum. For the tungsten source no I_{sc} anomalies could have occurred due to the cell response shifting into a spectral peak or valley. The I_{sc} versus temperature plot was obtained for 0.012 inch thick 2 and 10 ohm cm cells in these two light sources. The anomaly was present in both light sources for both cell types. The deviation from linearity was actually greater in the tungsten source. Based on this information the cause of the deviation was concluded to be associated with the cell, not the light source.

The open circuit voltage temperature dependence showed a similar effect and is shown in Figure 12. The deviation from the linear function occurred at about -40°C as in the I_{sc} case. The 10 ohm cell plot appeared to follow two linear functions, one at high temperatures and a second at low temperatures. The 2 ohm cm cells did not follow a linear function at low temperatures, but they did at high temperatures.

The short circuit current temperature coefficient (slope of the curves in Figure 11) for each cell type is shown in Figure 13. For the higher temperatures the I_{sc} coefficient for both 2 and 10 ohm cm cells, irrespective of thickness, was constant with the 10 ohm cm cells having a slightly higher coefficient. At low temperatures the I_{sc} coefficient increased to a peak at -90°C , then decreased to a very low value at -170°C . The 2 ohm cm cells showed the greatest variation. Figure 14 shows the V_{oc} temperature coefficient to be constant and about the same value of $-2.2 \text{ mV}/^{\circ}\text{C}$ for all cells at the higher temperatures. At a temperature of -90°C , the coefficient was decreased by at least a factor of two for all cells.

CONCLUSION

A very comprehensive experimental evaluation of the effects of decreasing thickness on solar cell performance has been completed and should provide new engineering data for designing advanced solar cell array systems. The performance of 2 and 10 ohm cm cells evaluated over a very wide range of temperatures should provide sufficient data for most system design studies. The effects of 1 MeV electron irradiation on these various cell types have not been included, but a companion paper covering this aspect has been prepared and will be presented separately 3).

The effect of decreasing solar cell thickness on the power to weight ratio is shown in Figure 15. The bare 2 ohm cm silicon solar cell curve shows that the power to weight ratio increases from about 100 w/lb for a 12 mil thick cell, to about 250 w/lb for a 4 mil cell, and 450 w/lb for a 2 mil cell. This thickness change results in a very significant change in the bare cell merit factor. The bare cell situation, of course, is not the complete story. Protective glass or quartz covers are required. Point No. 1 shows a typical power to weight ratio value of 29 w/lb obtained using a 14 mil cell with a 20 mil quartz cover attached with adhesives. Mounting this composite structure on a panel would typically reduce the power to weight ratio to 14 w/lb as shown by Point No. 2. Point No. 3 is a recent state-of-the-art situation where a power to weight ratio of 97 w/lb was obtained using 7 mil cells with a 3 mil coverglass attached with adhesives. This increase from 20 w/lb (Point 1) to 97 w/lb (Point 3) represents a good improvement. A higher ratio is still possible by using integral quartz covers instead of applying the cover with adhesives. Curves showing the effect of using 1 or 2 mil thick integral covers on 2 ohm cm cells are also shown in Figure 15.

For comparative purposes the power to weight ratio of the present day bare CdS thin film (4 mil thick) solar cell is 100 w/lb. Future projections have jumped the power to weight ratio value to 200 w/lb for the bare cell which is still below the values presently available with thin silicon cells.

The picture still isn't complete, however, until the cells are mounted on the supporting structure. When this structure weight is added, the gains in cell performance obtained by decreasing thickness are greatly diminished. A curve showing some typical finished panel or array power to weight ratios, is plotted at the bottom of Figure 15. Presently panels are in the 10 to 15 w/lb range, using 12 to 16 mil silicon solar cells. Advanced panels are presently being made using 8 mil cells, and 20 w/lb ratios are expected. Development of ultra-lightweight panels using 4 mil cells has started, and these are expected to provide 40 w/lb. A projection to 2 mil thick silicon cells combined with advanced lightweight flexible support structures certainly looks very interesting.

REFERENCES

- 1) Wolf, M. and Ralph, E. L., "Effect of Thickness on Short Circuit Current," Proc. 4th Annual Photovoltaic Specialists Conference, Vol. I, Cleveland, Ohio, 2 June 1964.
- 2) Ralph, E. L., "Some Considerations Regarding the Production of Improved Solar Cells," Proc. 5th Annual Photovoltaic Specialists Conference, Vol. I, Goddard Space Flight Center, Maryland, 18 October 1965.
- 3) Martin, J. H., Statler, R. L., Ralph, E. L., "Radiation Damage to Thin Silicon Solar Cells," to be presented at the Intersociety Energy Conversion Engineering Conference in Miami Beach, Florida, August 13-17, 1967.

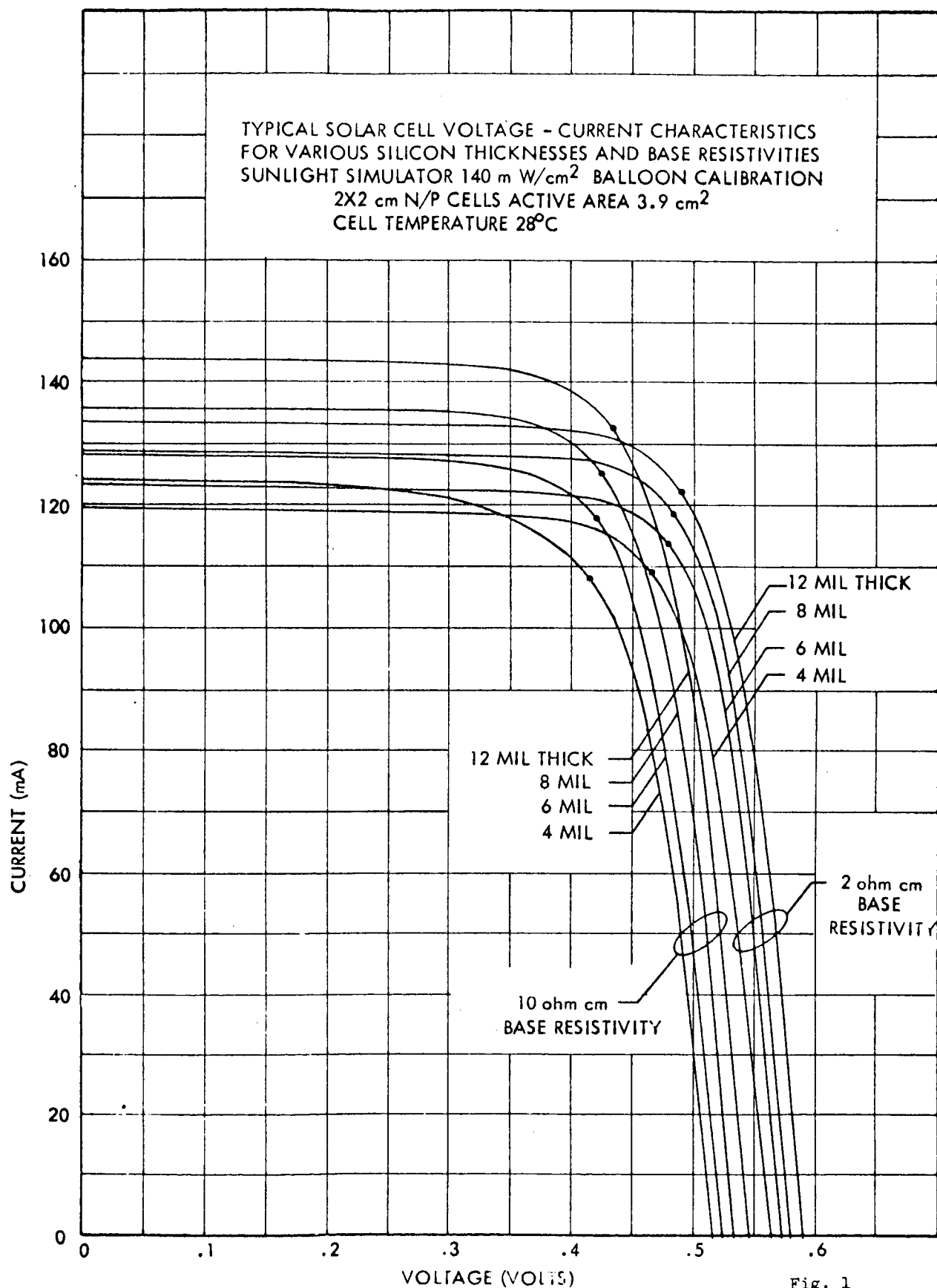


Fig. 1

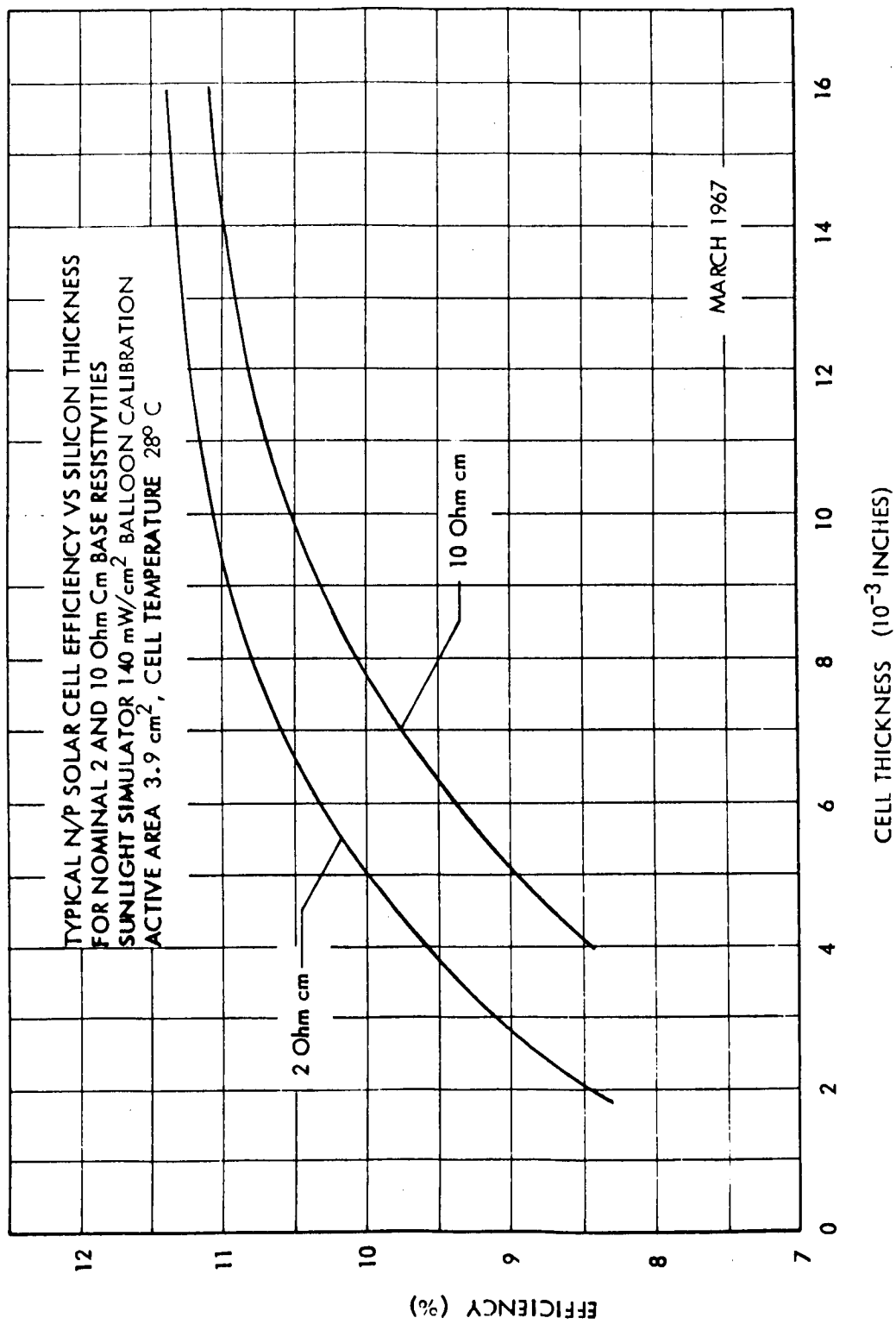


Fig. 2

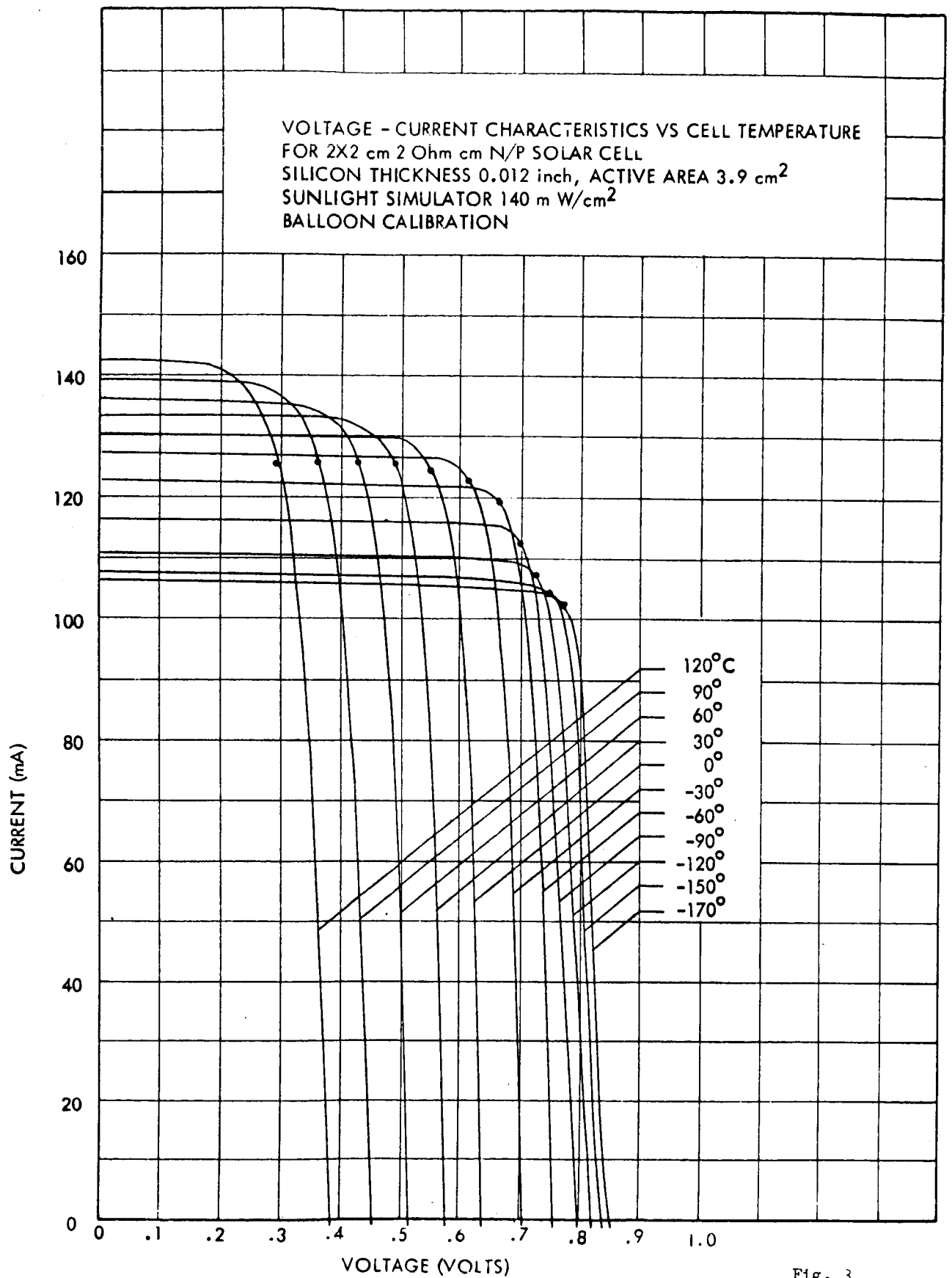


Fig. 3

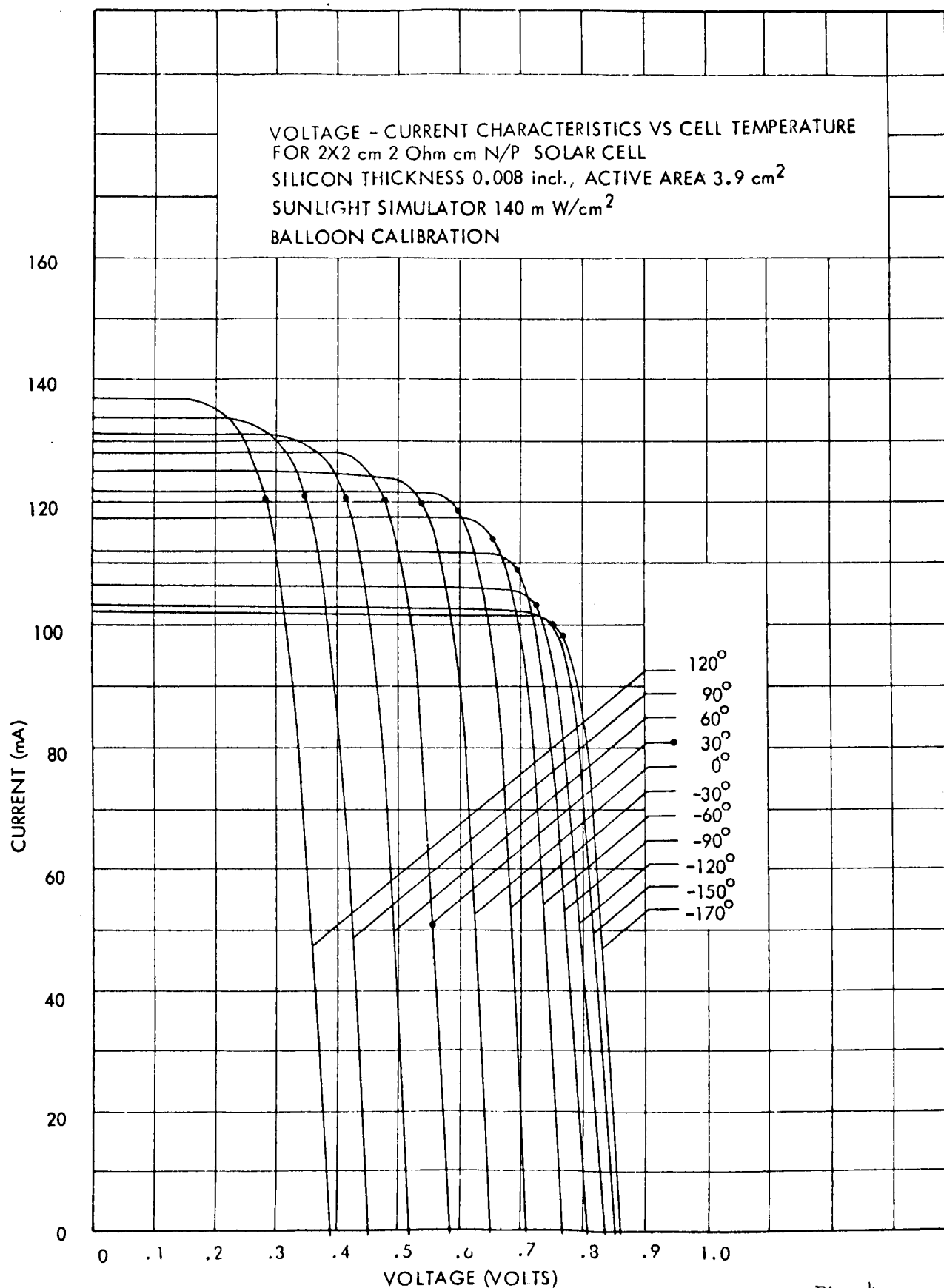


Fig. 4

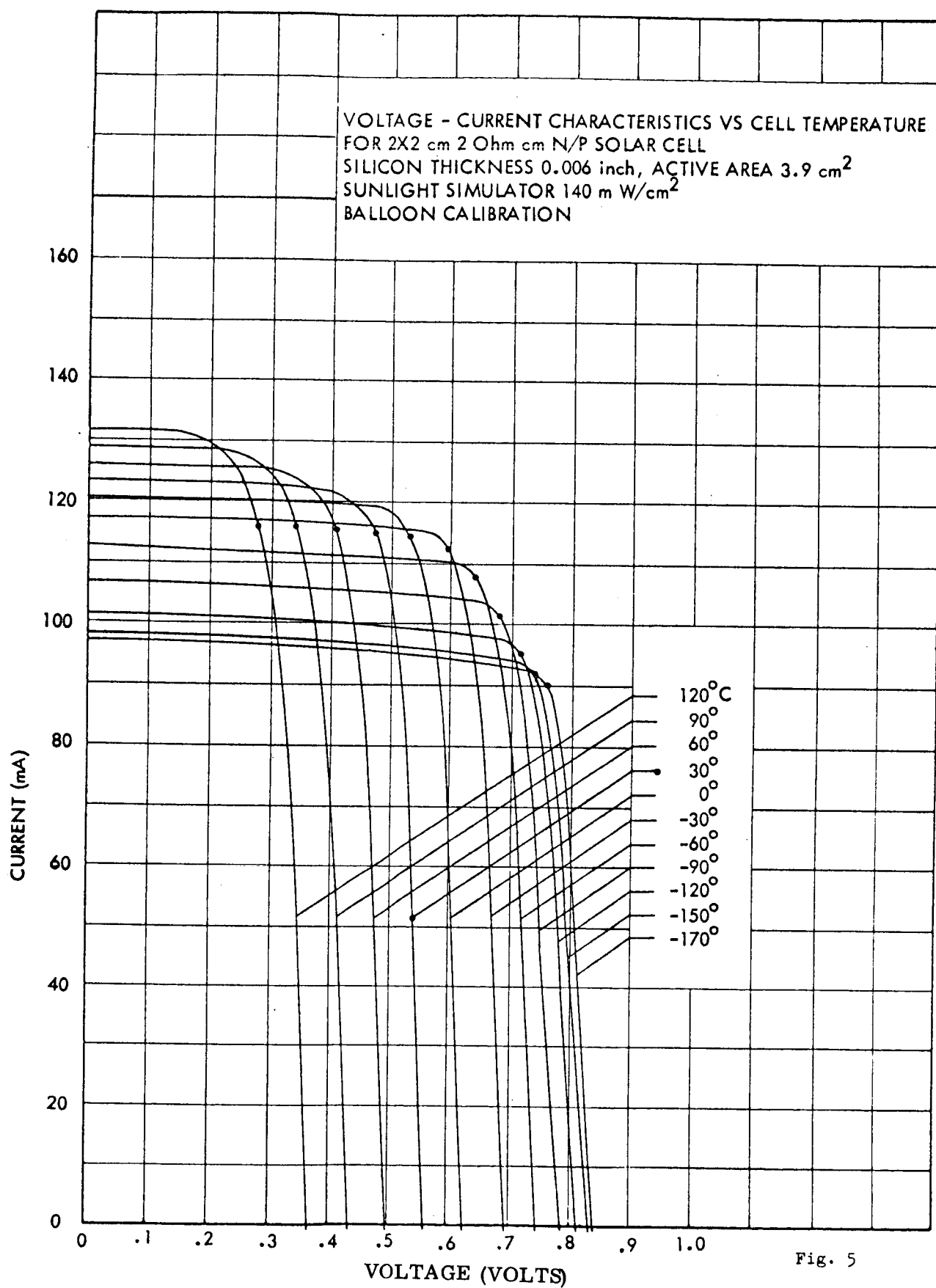


Fig. 5

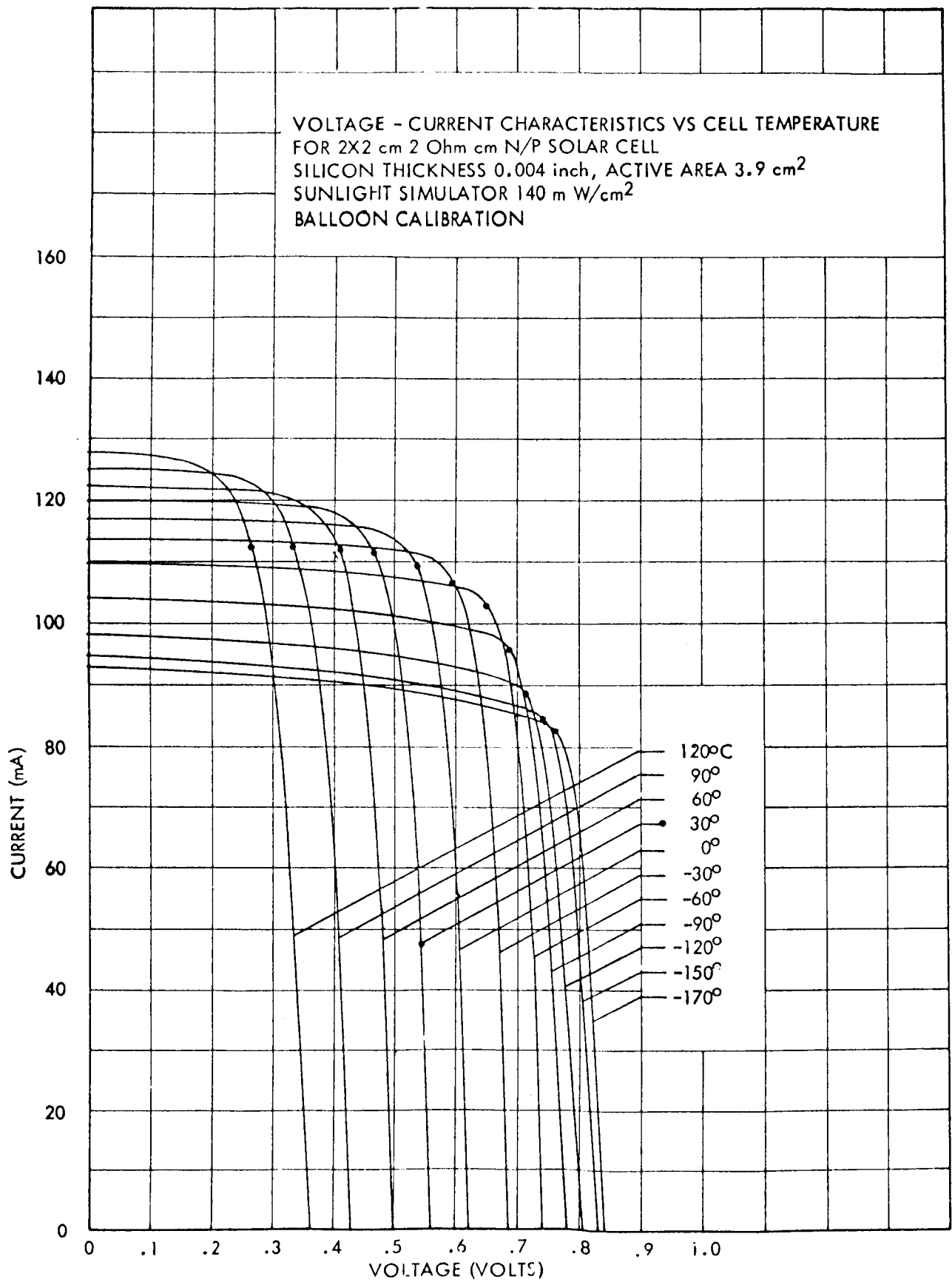


Fig. 6

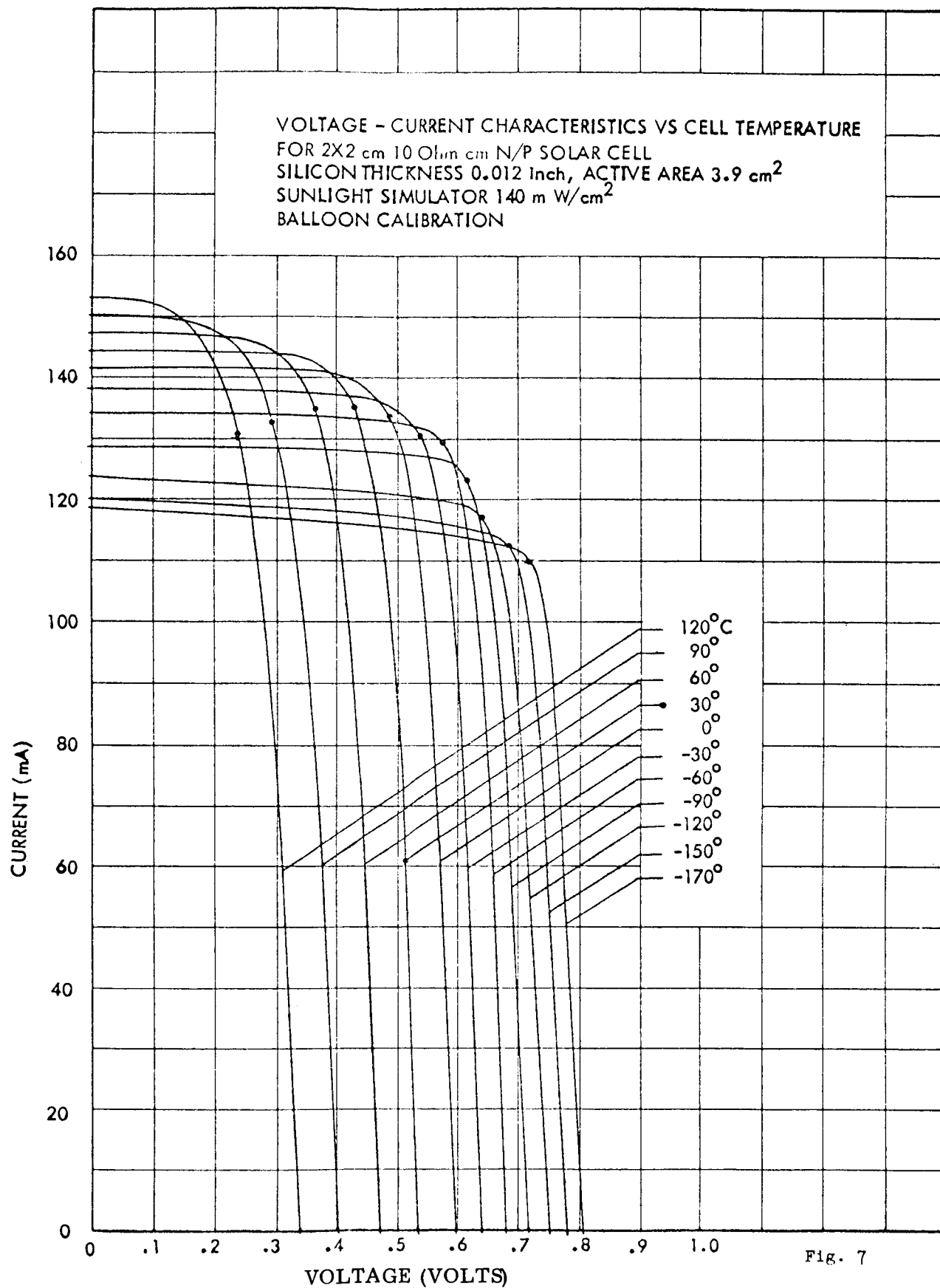


Fig. 7

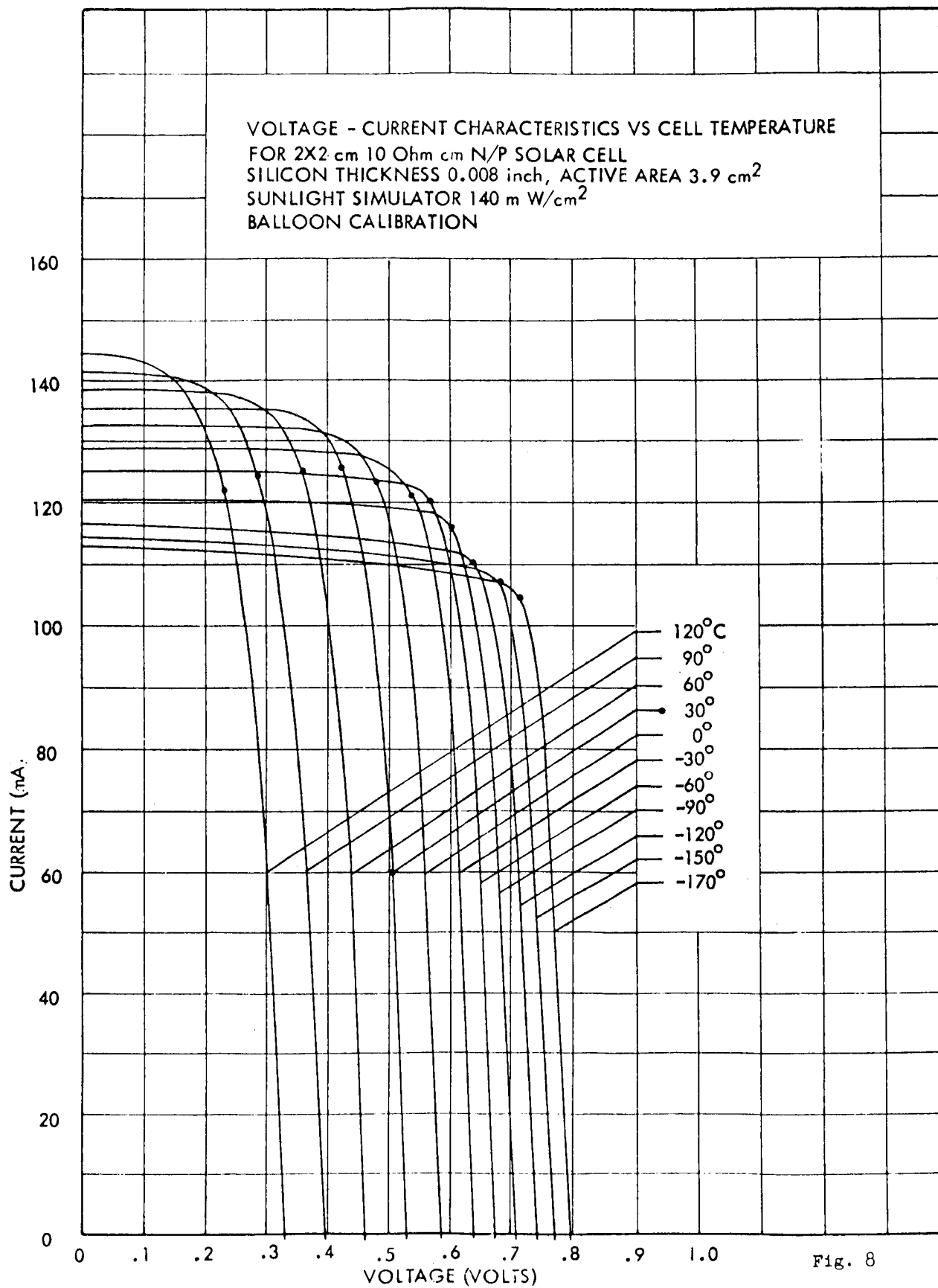


Fig. 8

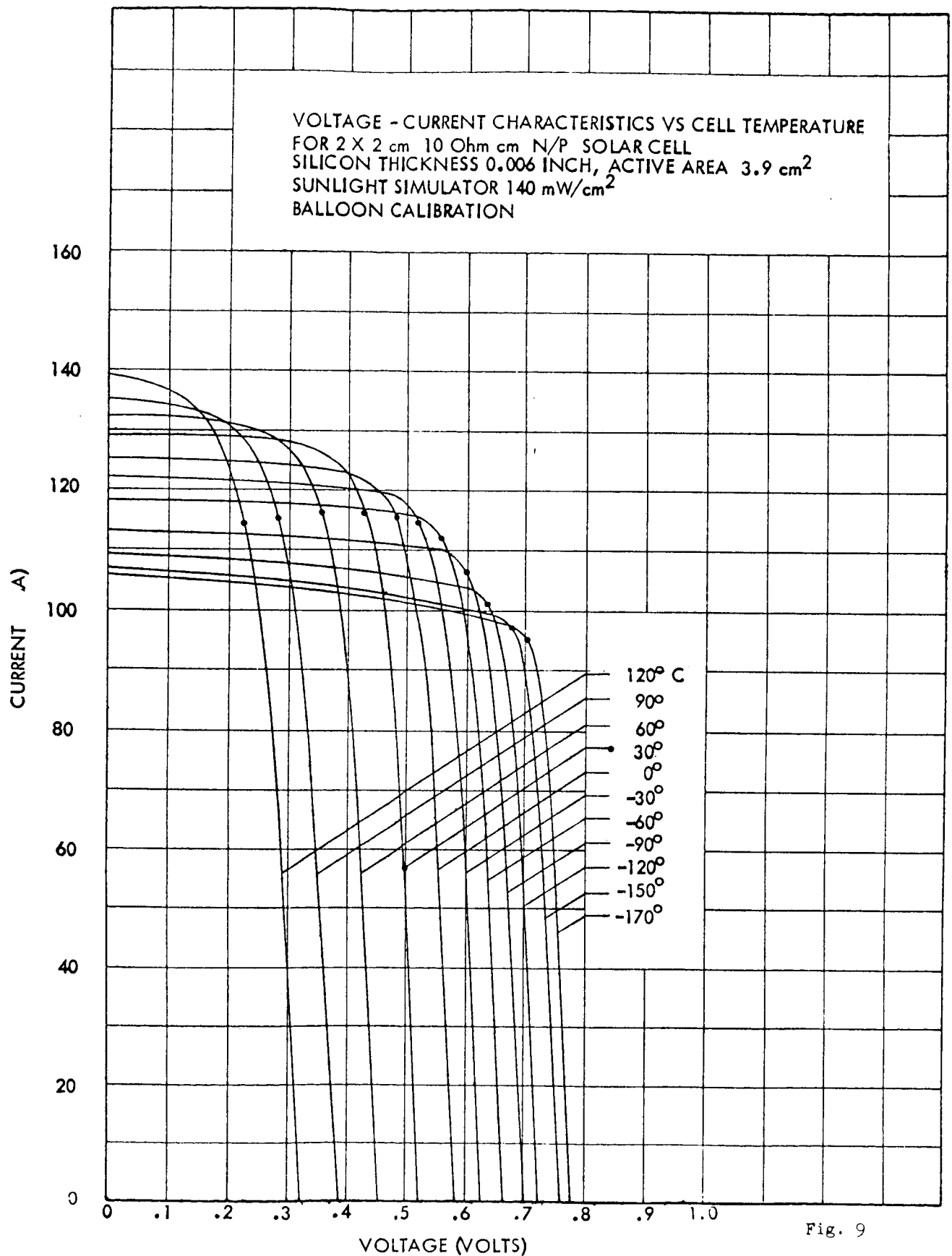
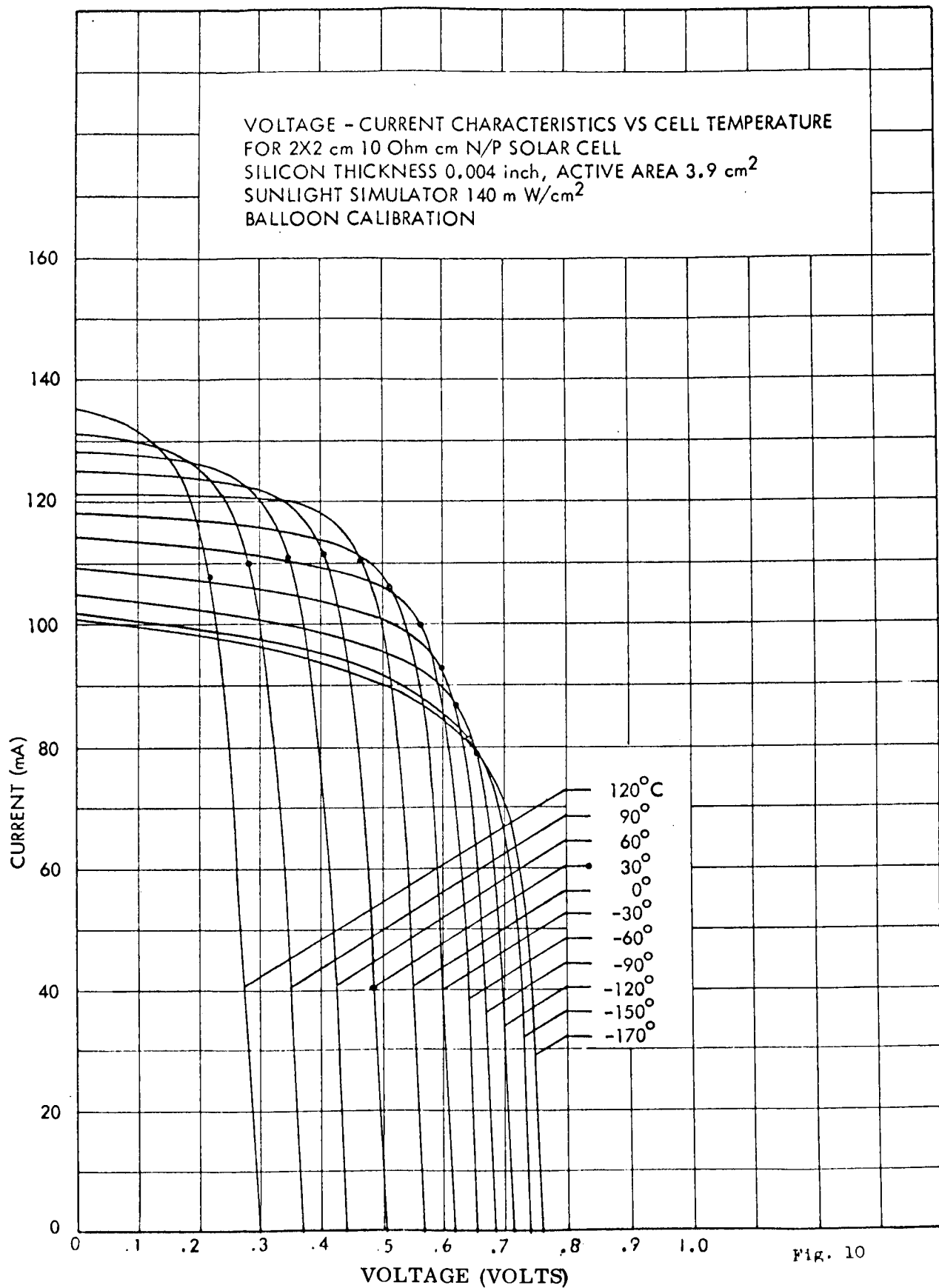


Fig. 9



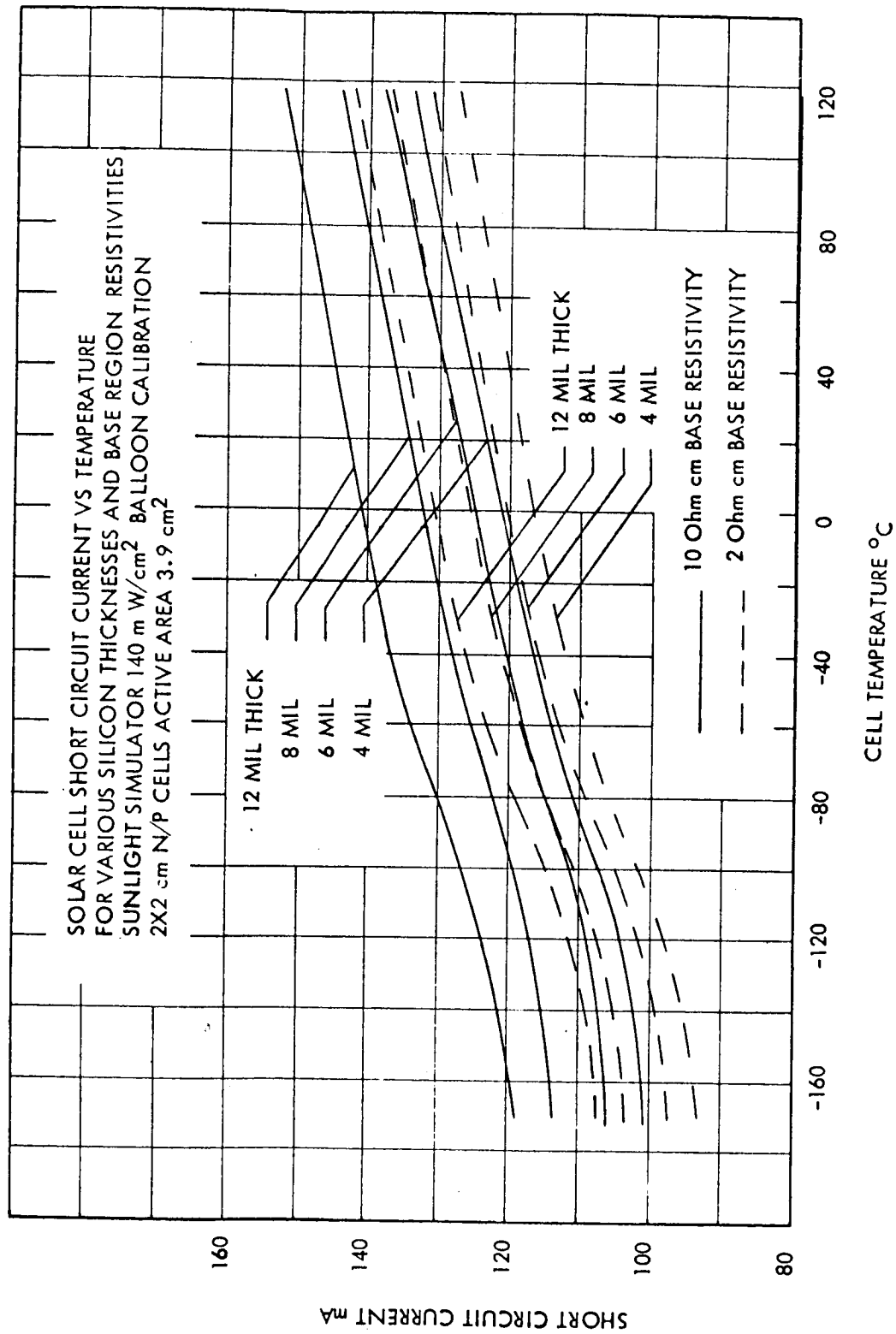


Fig. 11

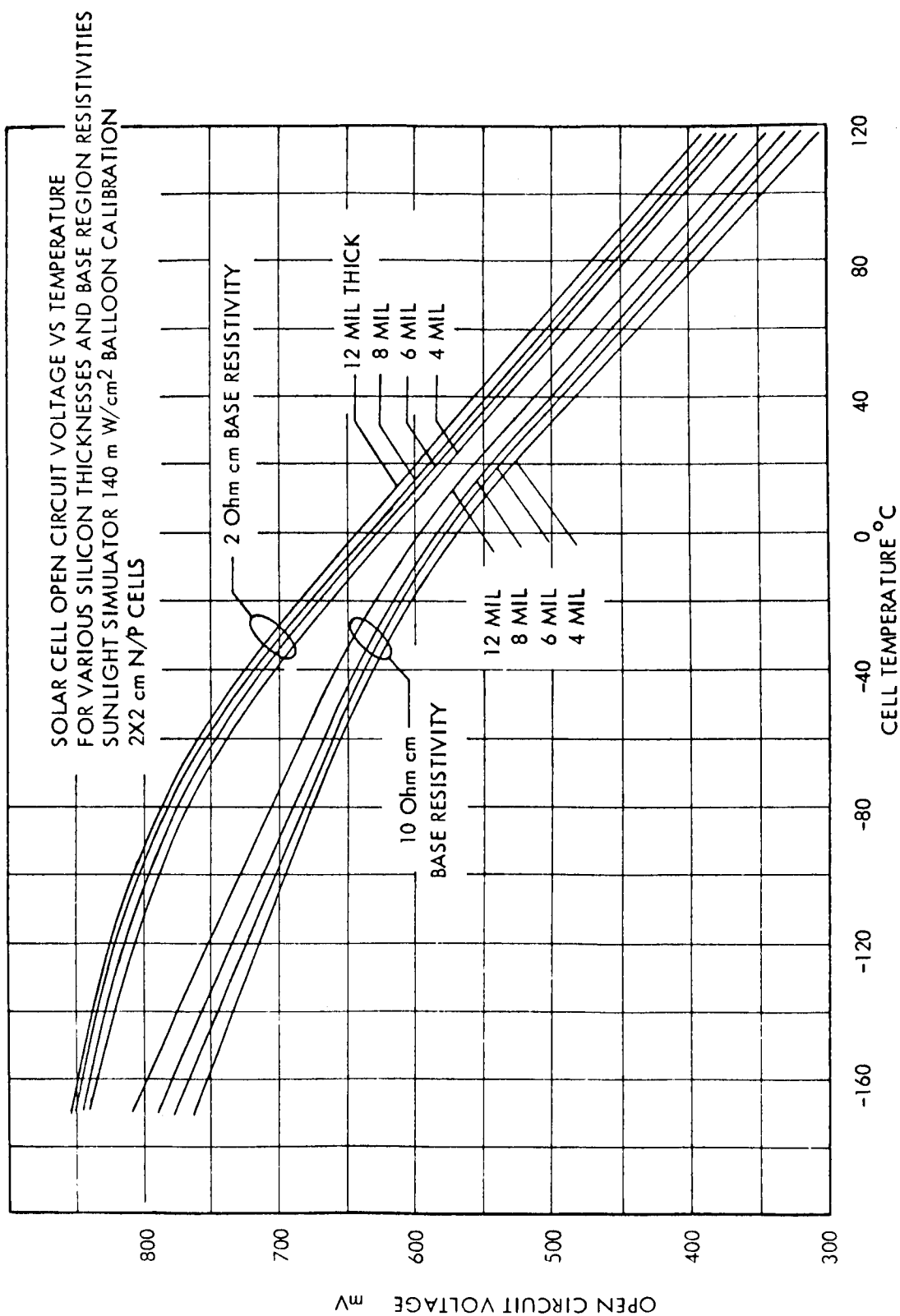


Fig. 12

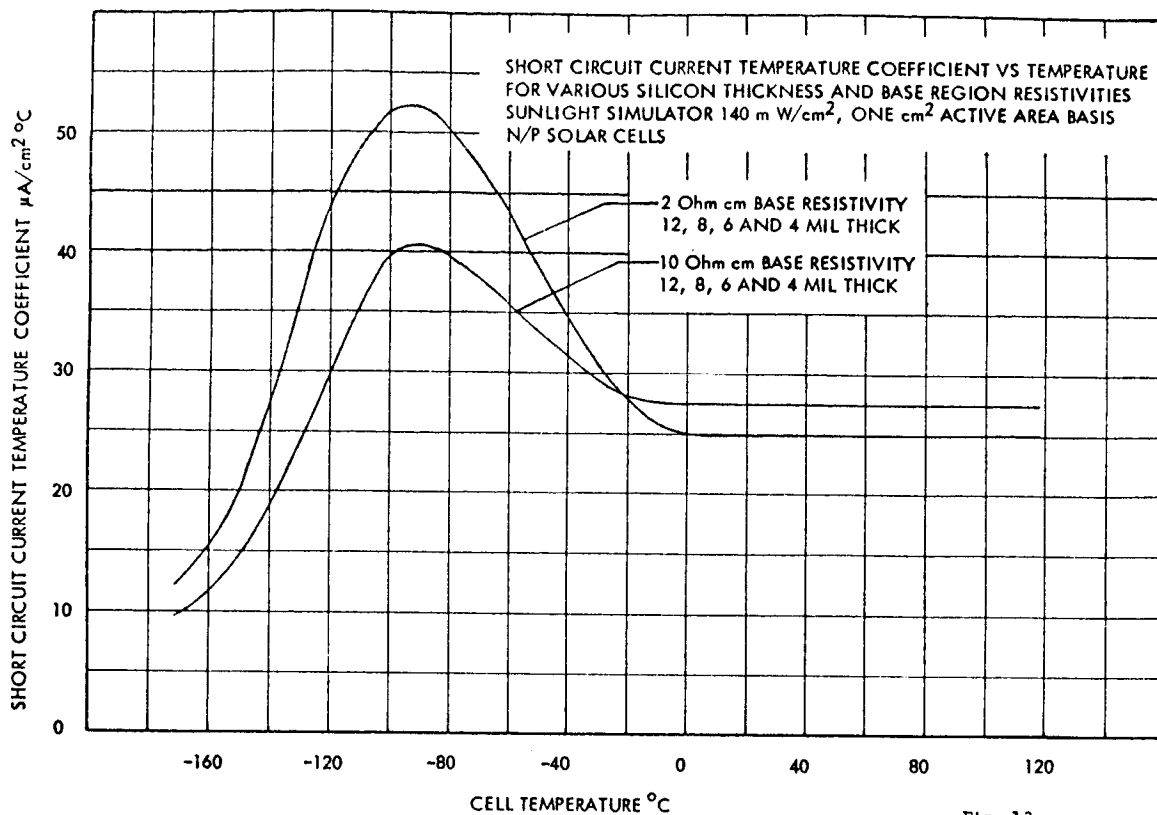


Fig. 13

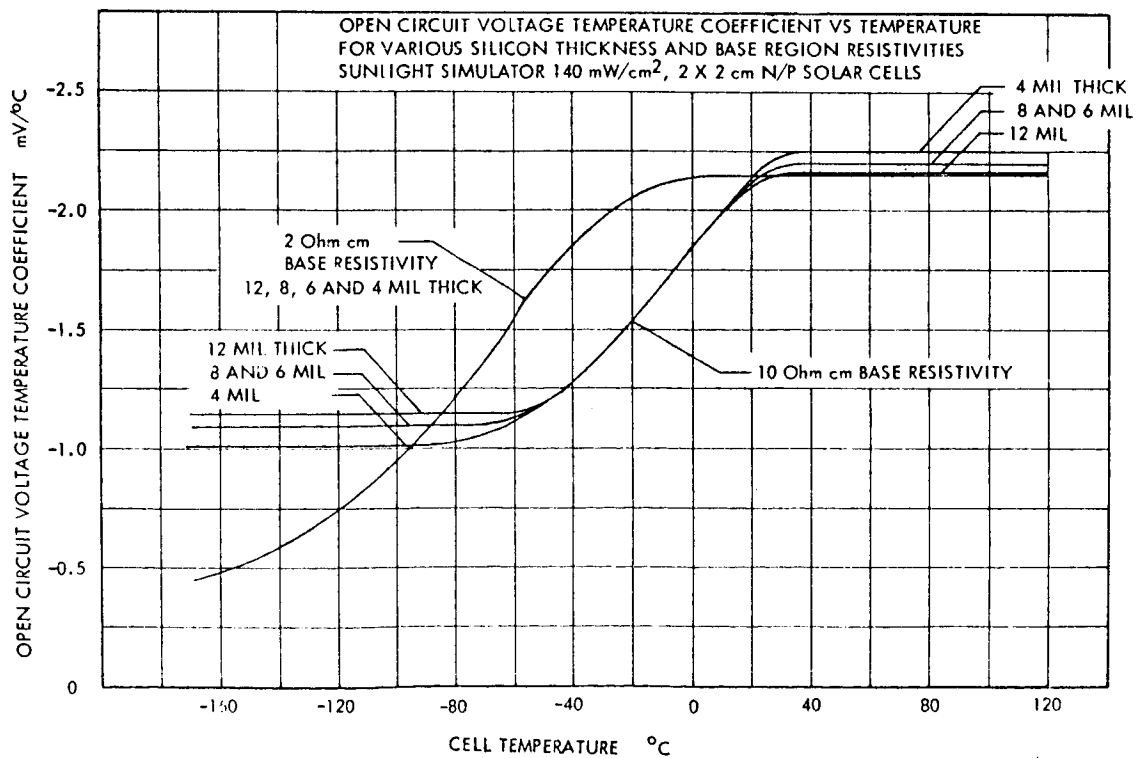


Fig. 14

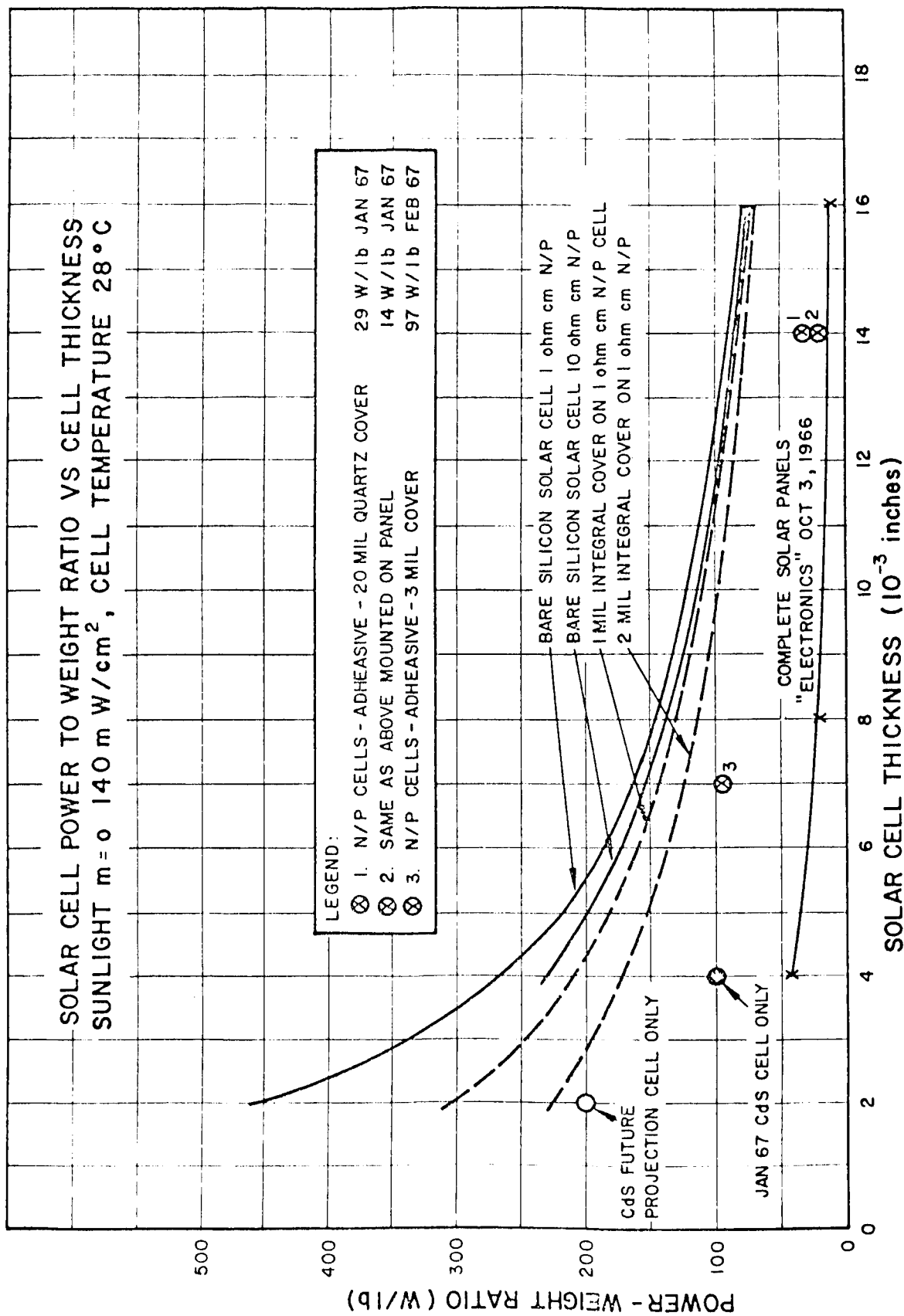


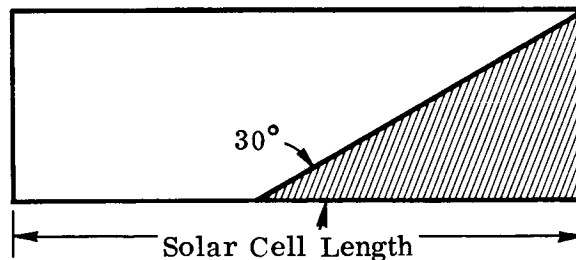
Fig. 15

8.7 FRACTURE OF SOLAR CELLS

Solar cell fractures may result from mechanical and thermal stress associated with the space environment, as well as by bombardment by meteoric particles.

The cracking of any individual solar cell does not represent a catastrophic failure, since part or complete output of the solar cell is maintained, even after the cell has been subjected to a crack. This feature is unique to Solaflex assemblies, and is a result of the extended solder tab connection. Empirical tests conducted on solar cells reveal that the cracking occurs in general at an angle of approximately 30° with respect to base of the solar cell. Empirical and geometric analyses indicate that to within this limit the cracking is random and will result in losses of cell area that can vary from a maximum of 60% of the area to no net loss of area, depending upon the position of the fracture and the size of the solar cell used. The loss of solar cell area will result in a current limiting effect for the affected circuit, with a resulting power degradation.

As shown in illustration below, an oblique solar cell fracture at an angle of 30° relative to the base of an extended length solar cell will result in essentially no loss of power provided it is not located in the shaded area. For the unshaded areas, electrical continuity is retained by the extended solder tabs on the rear, and by the multiple solder tabs on the top surface.



Extended Solar Cell Failure Region

Note that the maximum area lost by a solar cell of length greater than 3.5 cm will be 3.5 cm². For the 2x2 solar cell it has been determined experimentally that the maximum loss of area is 60% of the total area or 2.4 sq-cm. (Figure A-5). Since the crack may occur at random along the base of the extended length solar cell the average area loss for a crack in the shadowed area would be 1/3 of the maximum value or approximately 1.2 cm². In comparison, tests have shown that for the 2x2 solar cell an average of 30% of the total solar cell area is lost which is equivalent to 1.2 cm² in average lost area per fracture.

RELATIVE LOSS OF AREA FOR SOLAR CELL FRACTURES

Type Solar Cell	2x2 cm	2x6 cm
Total Area (A)	4 cm ²	12 cm ²
Max Area Loss per Fracture	2.4 cm ²	3.5 cm ²
Avg Area Loss Per Fracture	1.2 cm ²	1.2 cm ²
Avg Percentage Area Loss per Failure (%)	30%	10%

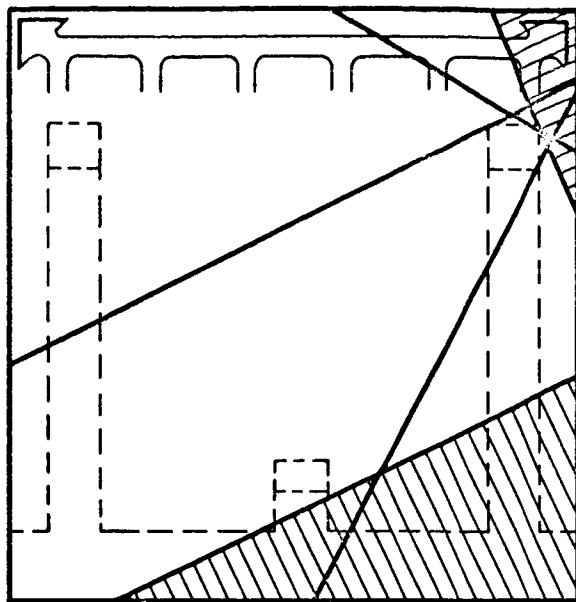
Table above shows a compilation of average percent area loss per solar cell per fracture, for those solar cell sizes proposed by Spectrolab.

If the probability of failure of an individual solar cell is considered to a first approximation to be proportional to the area of the solar cell, (A) a relative solar cell failure factor, which may be defined as the product of the solar cell area and the average percentage area loss per failure, (%) may be formed as follows:

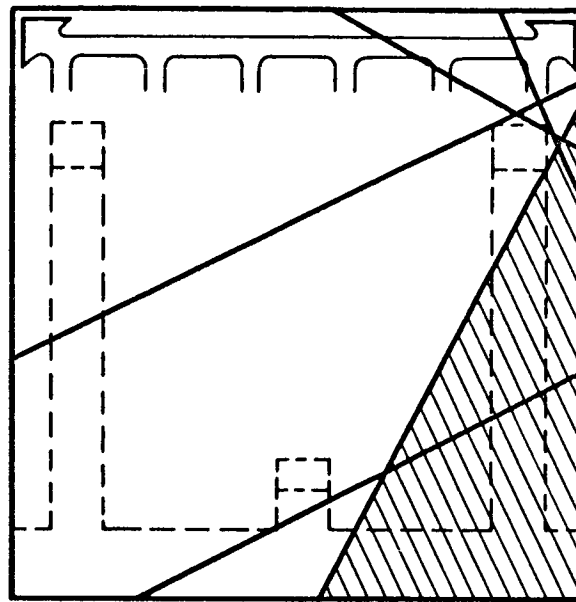
SOLAR CELL SIZE VS RELATIVE FAILURE FACTOR

$$P = (\text{Av. percent area lost}) (\text{Solar cell area}) = (\%) \cdot (A)$$

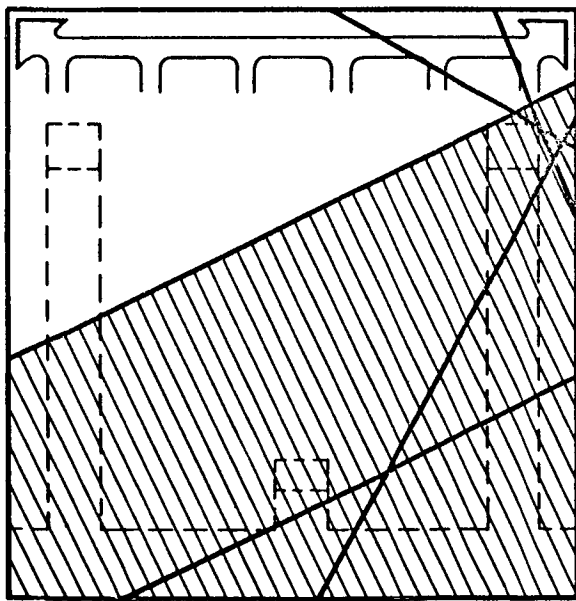
<u>SOLAR CELL</u>	<u>RELATIVE FAILURE FACTOR</u>
2x2	1.2
2x6	1.2



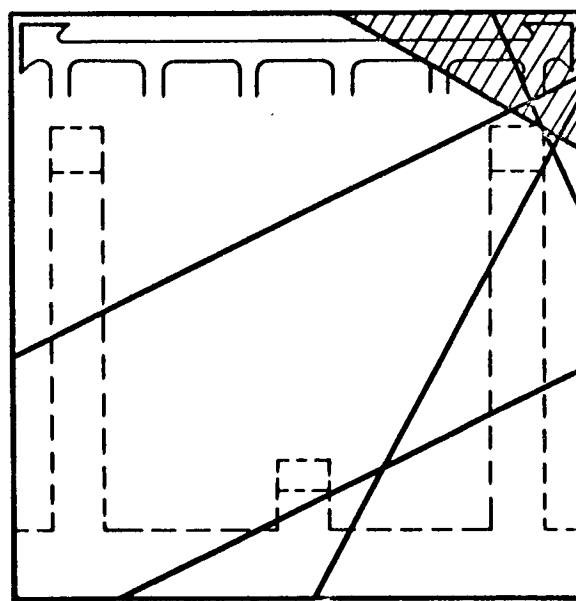
a



b



c



d

(2x2cm Solar Cells)
 30°, 60° Fractures Showing Maximum Losses in Area (Hatched).
 Lower Fracture in "a" is of same type as in "c".

Figure A-5. Solar Cells and Fracture Characteristics

Thus, based on the foregoing assumptions, there is no appreciable advantage gain in the use of one solar cell size in preference to another. It must be pointed out, however, that the assumption that failure rates for the larger solar cells will be proportional to the Solar cell area is too severe an assumption for it must be observed that preliminary testing in this area of extended solar cell failure modes and rates would suggest that the failure rate is proportional to the area raised to a power less than unity. Spectrolab is confident that comprehensive testing of extended length solar cells will confirm this observation, with the net result that the relative solar cell failure factors would exhibit lower and preferential values for the extended length solar cells, i.e.,

$$P_s = (\bar{\%}) \cdot (A)^n$$

where $0 < n < 1$

8.8 LOG SHEETS - THERMAL VACUUM TEST

A copy of the Environmental Laboratory Log Sheets of thermal vacuum testing of adhesives, performed by The Bunker-Ramo Corp., for Spectrolab, are enclosed as appendix data to this report.

ENVIRONMENTAL LABORATORY LOG SHEET

CUSTOMER SPECTRO LABS.

TEST THERMAL VACUUM

ITEM TESTED Bolt Assy S/N 6, 7, 20, 21, 5, 14, 15, 17

18, 12, 11, 8, 9.

EQUIPMENT LIST

[illegible]

TEST BY Y. D. Ruyana QAR. _____
ENGR. Y. D. Ruyana QAR. _____

THE DUNKIN-RAMO CORPORATION
CANOGA PARK, CALIFORNIA

PAGE 1 OF

ENVIRONMENTAL LABORATORY LOG SHEET

REPORT NO. 2459CUSTOMER SPECTRO LABS SPEC. PER CUSTOMER REQUESTTEST INTERNAL CYCLING IN VACUUM ITEM TESTED BOLT ASSY S/N 6, 8, 9, 10, 11, 12, 13, 14, 15, 17, 18, 19, 20, 21, 22, 23, 24, 25, 26, 27, 28, 29, 30, 31, 32, 33, 34, 35, 36, 37, 38, 39, 40, 41, 42, 43, 44, 45, 46, 47, 48, 49, 50, 51, 52, 53, 54, 55, 56, 57, 58, 59, 60, 61, 62, 63, 64, 65, 66, 67, 68, 69, 70, 71, 72, 73, 74, 75, 76, 77, 78, 79, 80, 81, 82, 83, 84, 85, 86, 87, 88, 89, 90, 91, 92, 93, 94, 95, 96, 97, 98, 99, 100DATE TIME

10-30-7 1700 HUNG SAMPLES S/N (2, 5, 6, 8, 9, 11, 12, 14, 15, 17, 18, 20, 21) ON THERMAL FIXTURE, LOWERED BELL JAR INTO PLACE. HOOKED UP LEAK DETECTOR AND CHECKED FOR LEAKS IN SYSTEM. S/N #3 WAS BROKEN APART WHILE STILL IN CASE. IT WAS NOT PUT IN CHAMBER.

2100 COMPLETED LEAK CHECKS. BEGAN EVACUATION OF SYSTEM.

2155 SYSTEM PRESSURE 5×10^{-6} TORR BEGAN INCREASING TEMPERATURE TO $+289^{\circ}\text{F}$

2212 REACHED $+289^{\circ}\text{F}$ BEGAN DECREASING TEMPERATURE TO -320°F . CYCLE #1 N.D.

2256 REACHED -320°F + HELD FOR BALANCE OF 90 MIN. CYCLE. SET TO $+284^{\circ}\text{F}$

2330 REACHED $+284^{\circ}\text{F}$. SET TO -320°F . PRESSURE $\approx 1 \times 10^{-6}$ TORR.

10-31-67 0110 REACHED -320°F . PRESSURE $\approx 1 \times 10^{-6}$ TORR.

0154 END OF CYCLE RESET FOR $+284^{\circ}\text{F}$. PRESSURE $= 2 \times 10^{-6}$ TORR.

0230 REACHED $+284^{\circ}\text{F}$ BEGAN REDUCING TEMP. TO -320°F .

0336 END OF CYCLE - RESET FOR $+284^{\circ}\text{F}$ - PRESSURE $= 1.6 \times 10^{-6}$ TORR.

0435 REACHED $+284^{\circ}\text{F}$ - BEGAN REDUCING TEMP. TO -320°F .

0539 END OF CYCLE - RESET FOR $+284^{\circ}\text{F}$ - PRESSURE $= 1 \times 10^{-6}$ TORR.

0634 REACHED $+284^{\circ}\text{F}$ - BEGAN REDUCING TEMP. TO -320°F .

0712 END OF CYCLE - RESET FOR $+284^{\circ}\text{F}$ - PRESSURE $= 2 \times 10^{-6}$ TORR.

0746 REACHED $+289^{\circ}\text{F}$ - BEGAN REDUCING TEMP. TO -320°F .

0945 END OF CYCLE - RESET FOR $+289^{\circ}\text{F}$ - PRESSURE $= 1.2 \times 10^{-6}$ TORR. N.D.R.

0930 REACHED $+284^{\circ}\text{F}$ - BEGAN REDUCING - TEMPERATURE -320°F AND HOLD.

0934 REACHED -100 ON STRIP CHART.

1020 END OF CYCLE - #7 RESET FOR $+284^{\circ}\text{F}$ - PRESSURE 9×10^{-7} TORR.

CONTINUED ON PAGE 3.

TEST BY Cymobile B-RC QARENGR CON'T QAR

THE BUNKER-RAMO CORPORATION

CANOGA PARK, CALIFORNIA

PAGE 2 OF OF

ENVIRONMENTAL LABORATORY LOG SHEET

REPORT NO. 2459

CUSTOMER SPECTRO LABS SPEC. PER CUSTOMER REQUEST P.O.

TEST THERMAL VACUUM ITEM TESTED BOLT ASSY SN 6, 7, 20, 21, 5, 19, 15, 17

DATE 10-31-77 TIME 1105

1205 REACHED +285°F. BEGAN REDUCING TEMPERATURE TO -320°F AND HOLD
 1205 END OF CYCLE #8 RESET FOR +284°F PRESSURE 8x10⁻⁷ TORR. CYCLE 9
 1240 REACHED +285°F BEGAN REDUCING TEMPERATURE TO -320°F AND HOLD.
 1340 END OF CYCLE #9 RESET FOR +284°F PRESSURE 8x10⁻⁷ TORR.
 1415 REACHED +284°F BEGAN REDUCING TEMPERATURE TO ROOM AMBIENT.
 1430 REACHED ROOM AMBIENT, INCREASED BELL JAR TO ROOM PRESSURE AMBIENT
 TEST COMPLETED. REMOVED SAMPLES FROM SYSTEM. NOTE: SAMPLE #9
 SEPARATED DURING TEST. ALL SAMPLES PLACED IN PLASTIC BOXES..

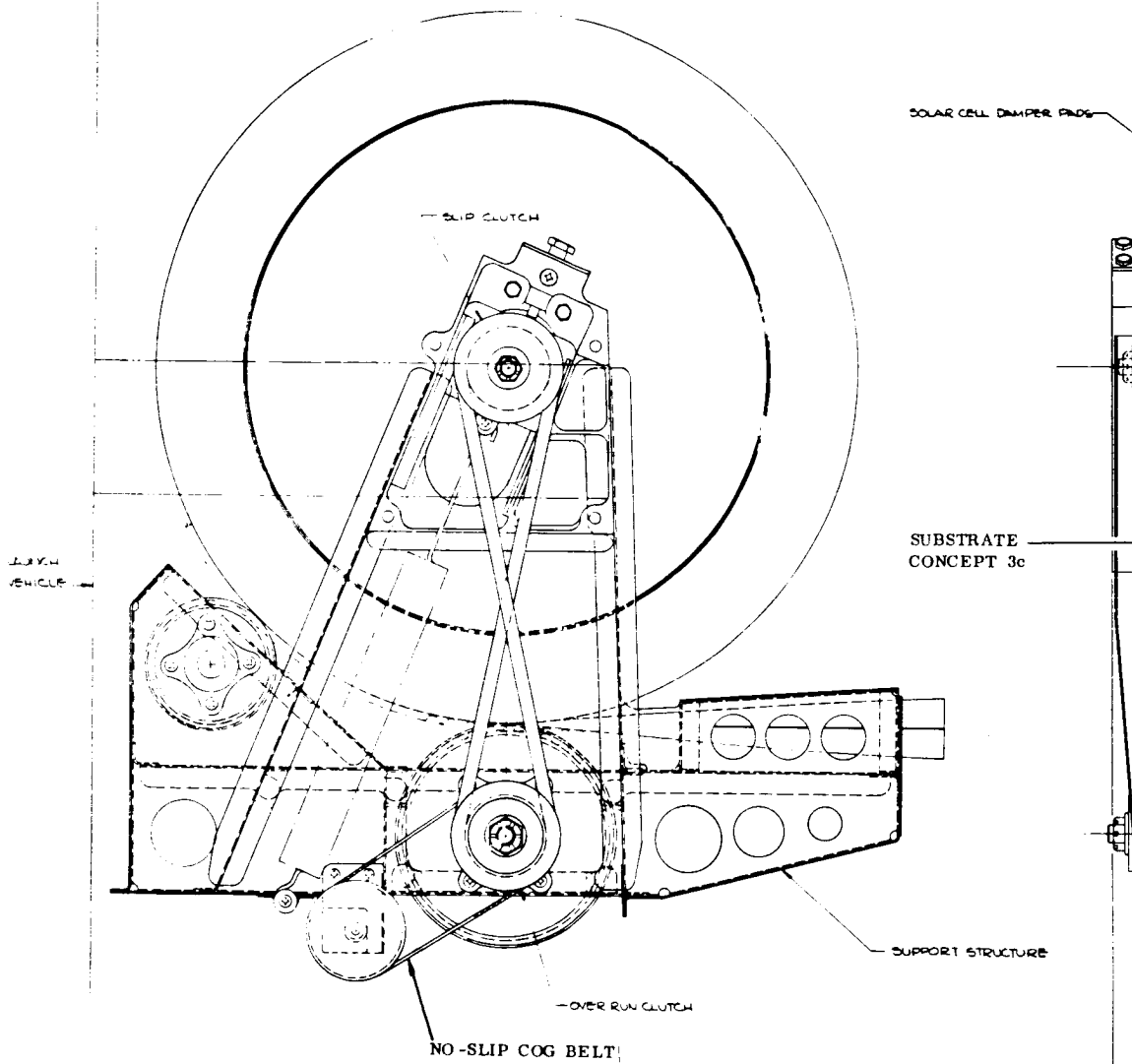
TEST BY H.D. Reynolds B-RC QAR
 ENGR By GOV'T QAR

THE BUNKER-RAMO CORPORATION
 CANOGA PARK, CALIFORNIA

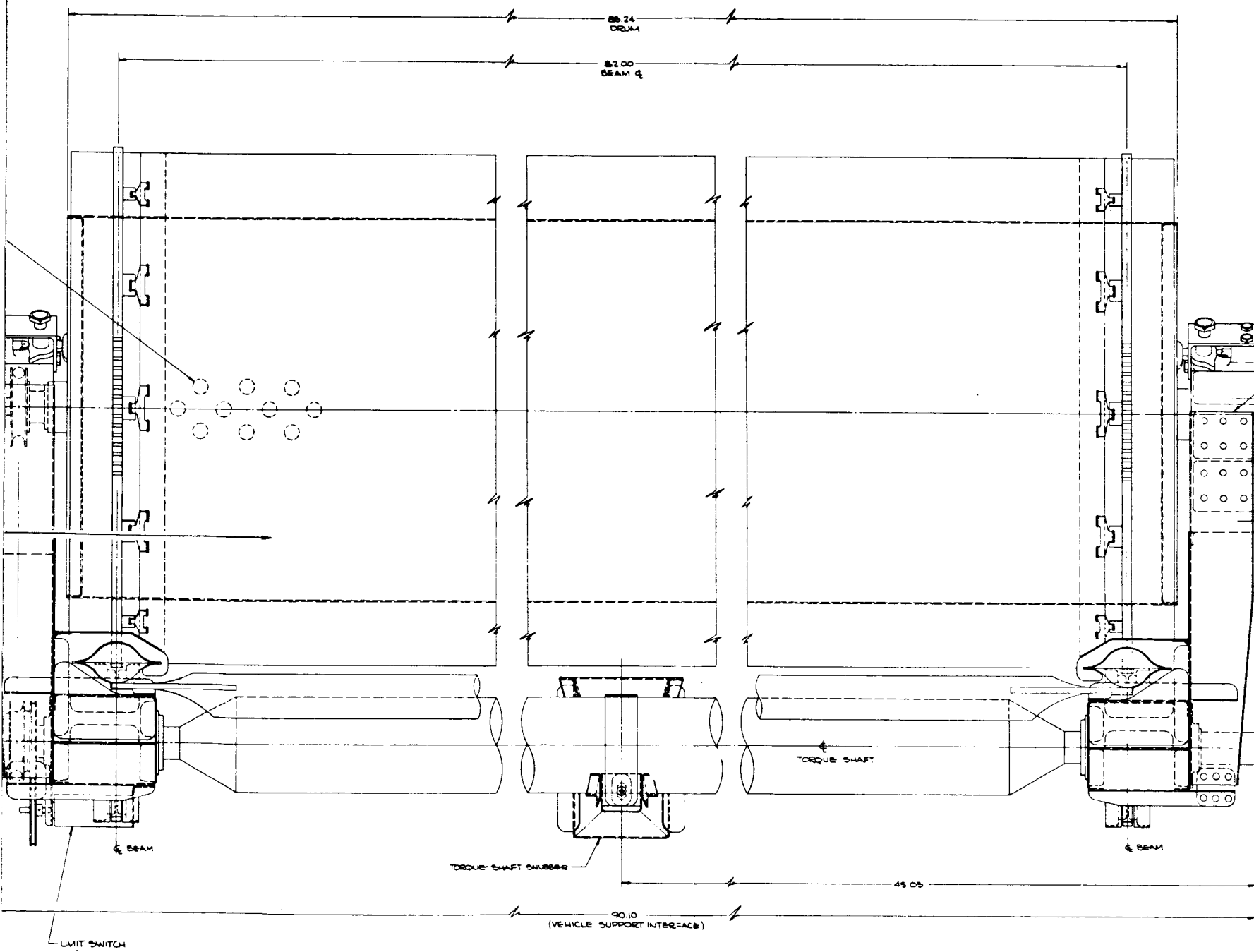
8.9 Drawings

Copies of the more significant drawings and layout studies, prepared during this first phase of the contract, are enclosed to acquaint the reader with details of conceptual ideas that were studied. Shown as figures, they relate for the most part to the concepts that are evaluated in Section 4.0, Conclusions. Comments and considerations expressed in Table 21, (Section 4.0) are illustrated in the subsequent pages.

Figure A-6, sheets 1 and 2, show the general arrangement of the solar array configuration selected for further design effort and development. Figure 31, is Spectrolab's recommended concept of the solar cell installation. The next thirteen illustrations, Figures A-7 through A-19, are the various subelement concepts which were studied.



301 - A



301 - B

NOTE:

This end view illustrates Concept 1 b.

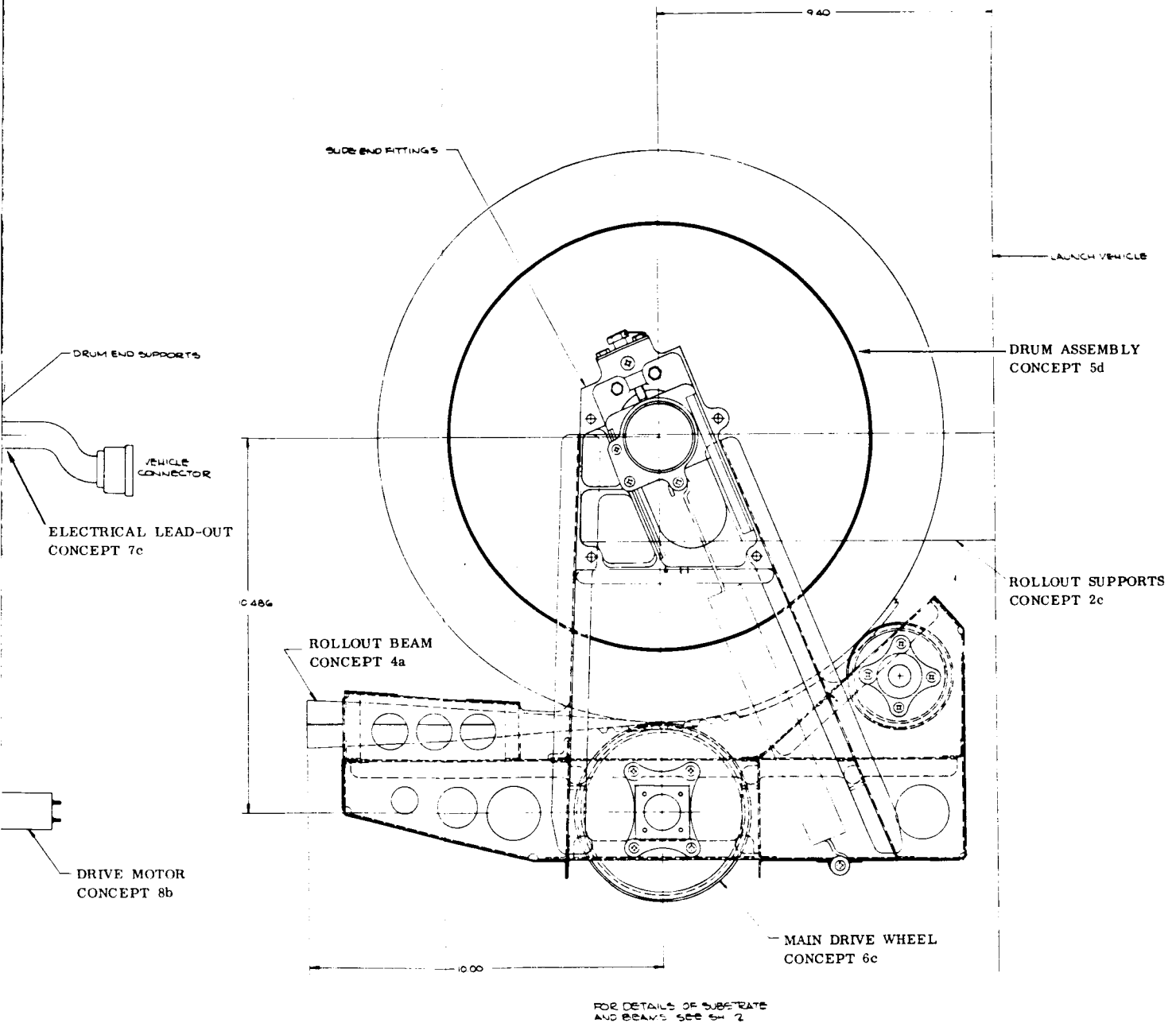
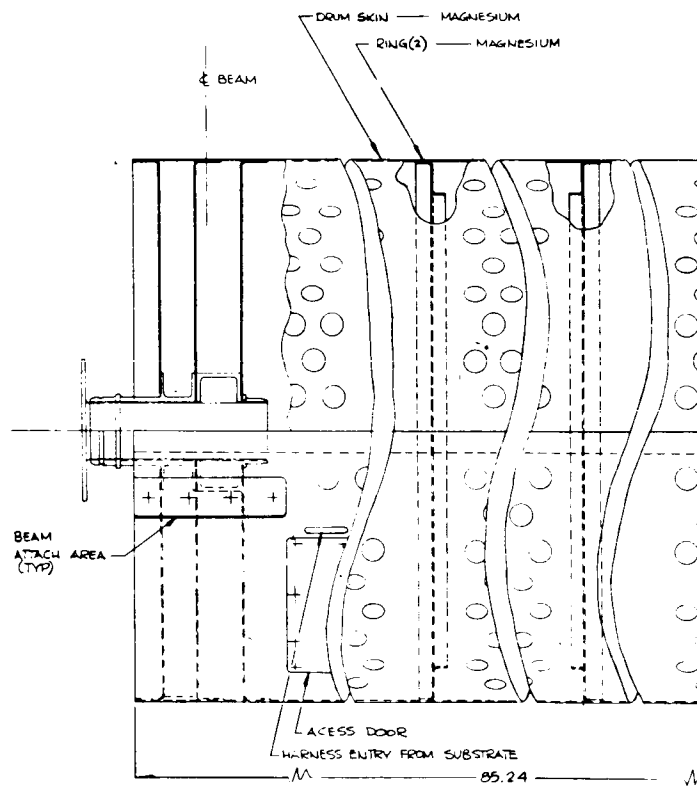
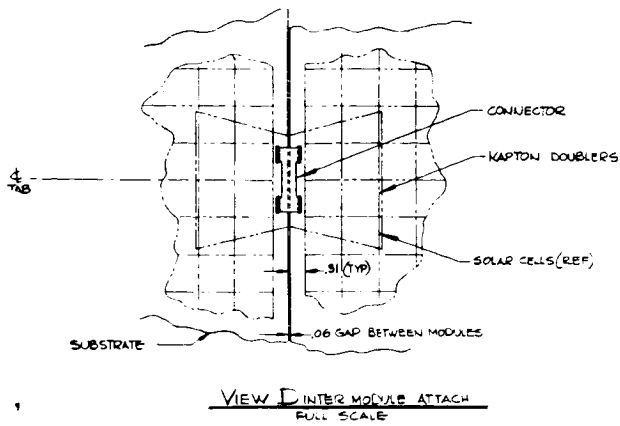
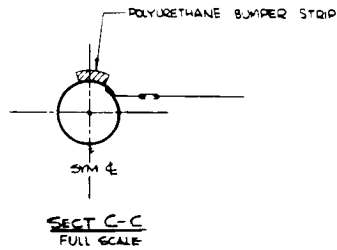


Figure A-6. Roll-Up Assembly - 250 Square Foot (Sheet 1 of 2)



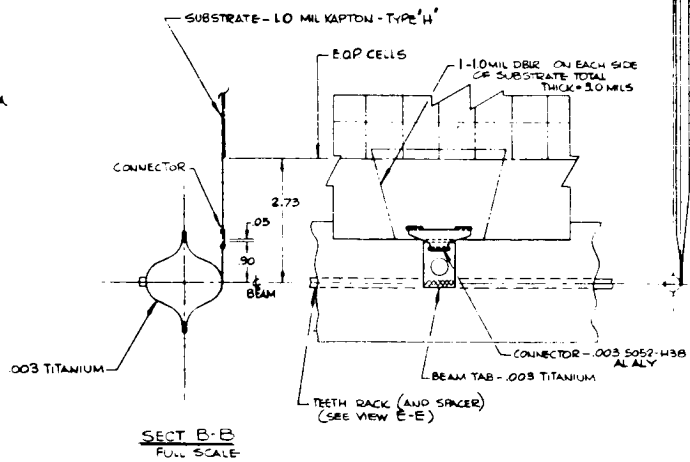
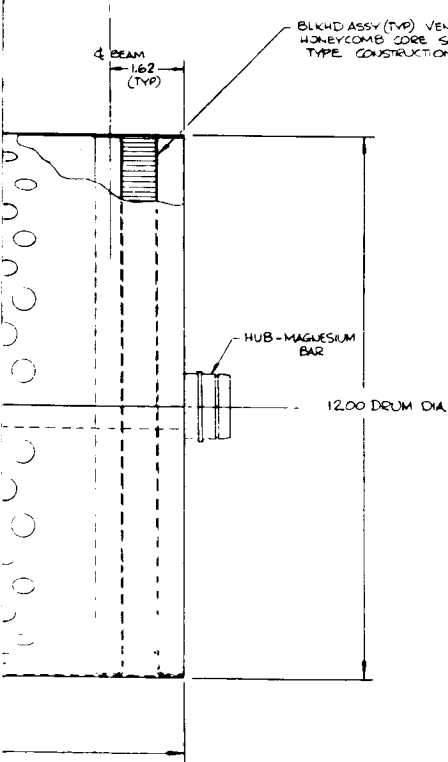


CROSS BEAM TAPERED IN THIS AREA TO PERMIT ENTRY THRU BEAM GUIDES



BLKHD ASSY (TYP) VENTED HONEYCOMB CORE SANDWICH TYPE CONSTRUCTION

BEAM 1.62 (TYP)



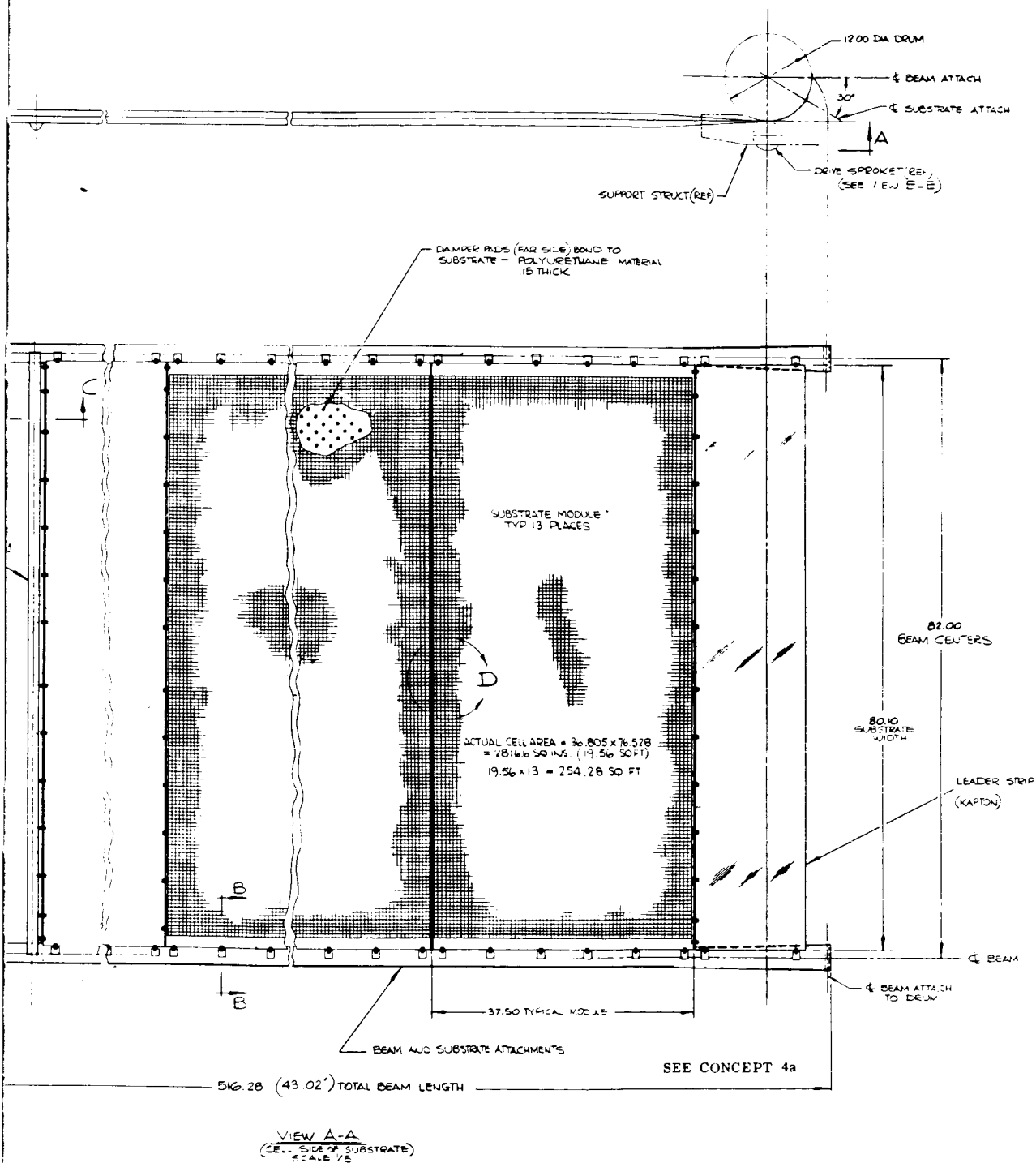
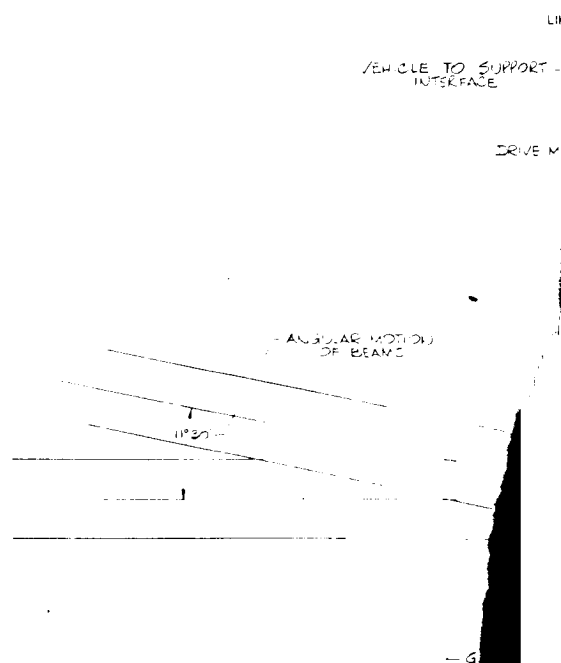
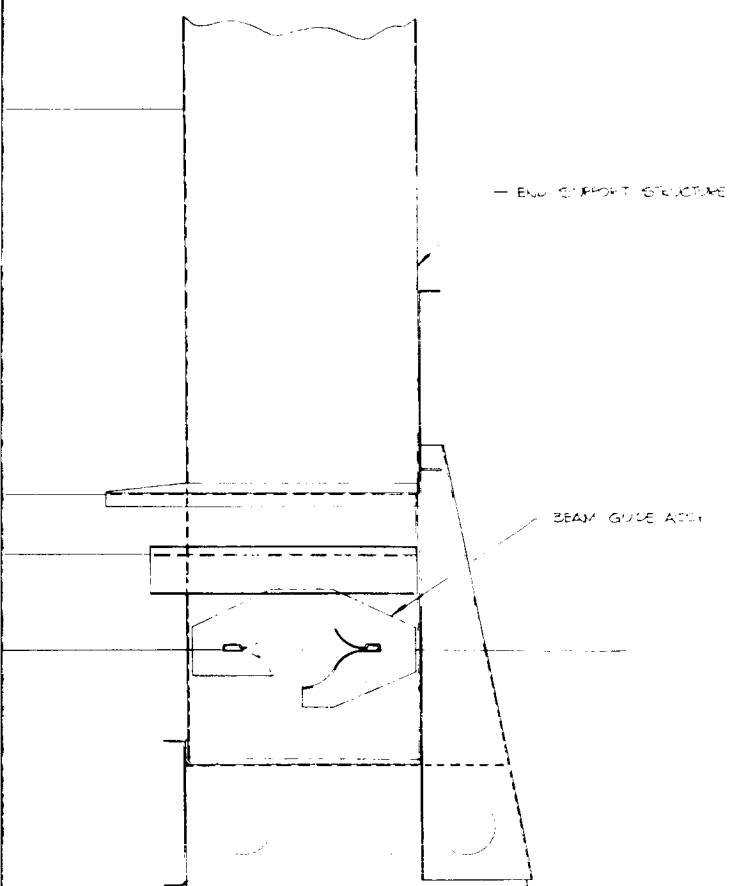


Figure A-6. Roll-Up Assembly - 250 Square Foot (Sheet 2 of 2)

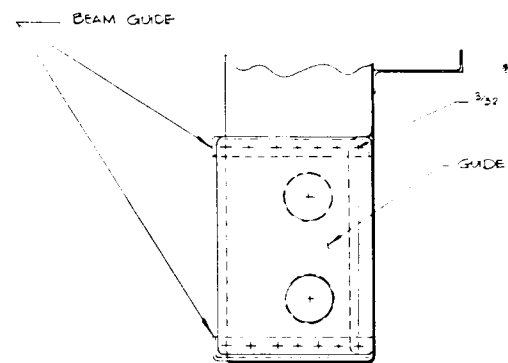
B

304



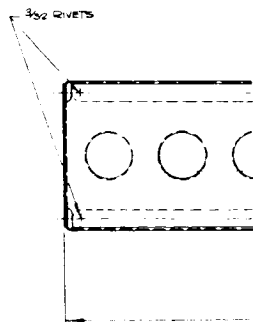
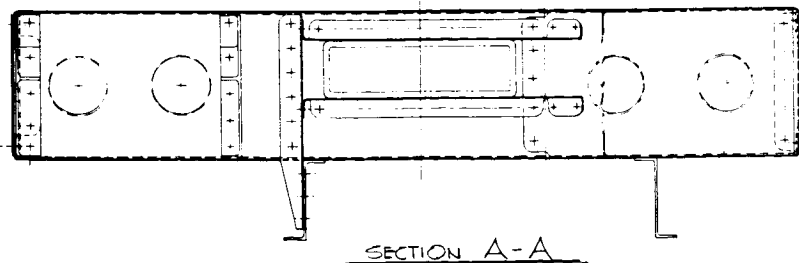
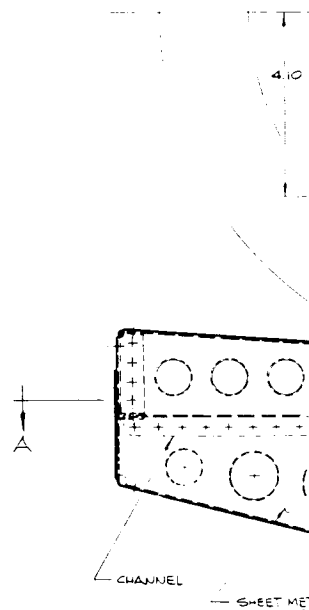
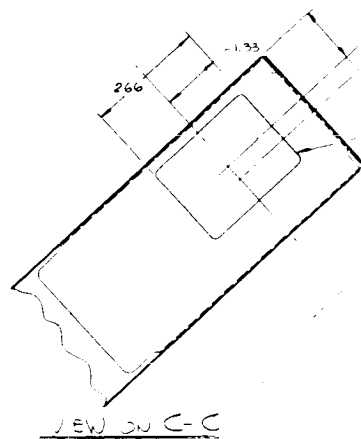
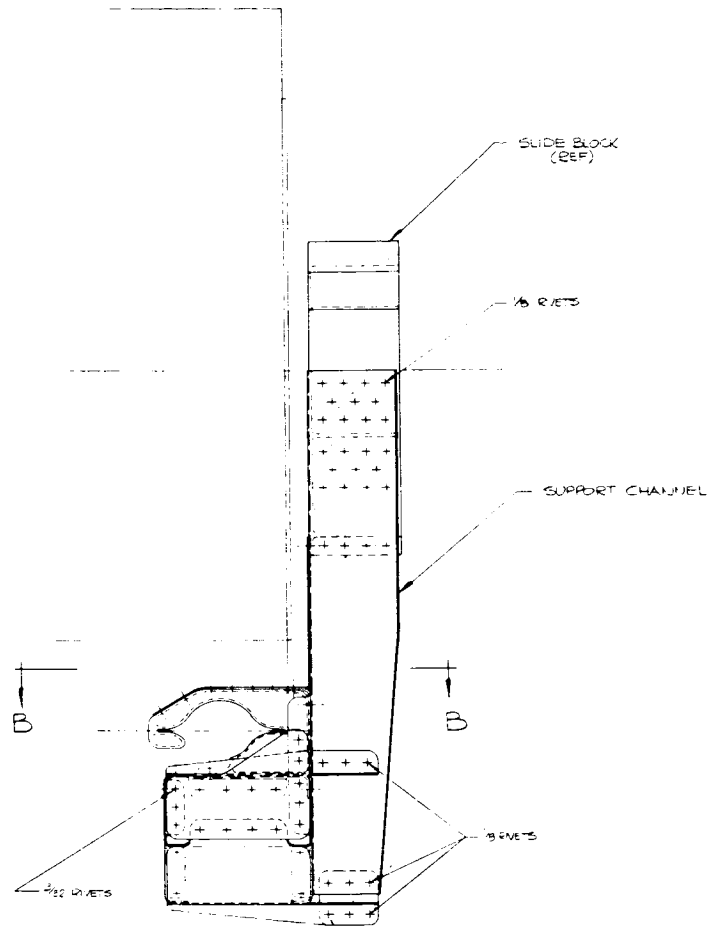


305

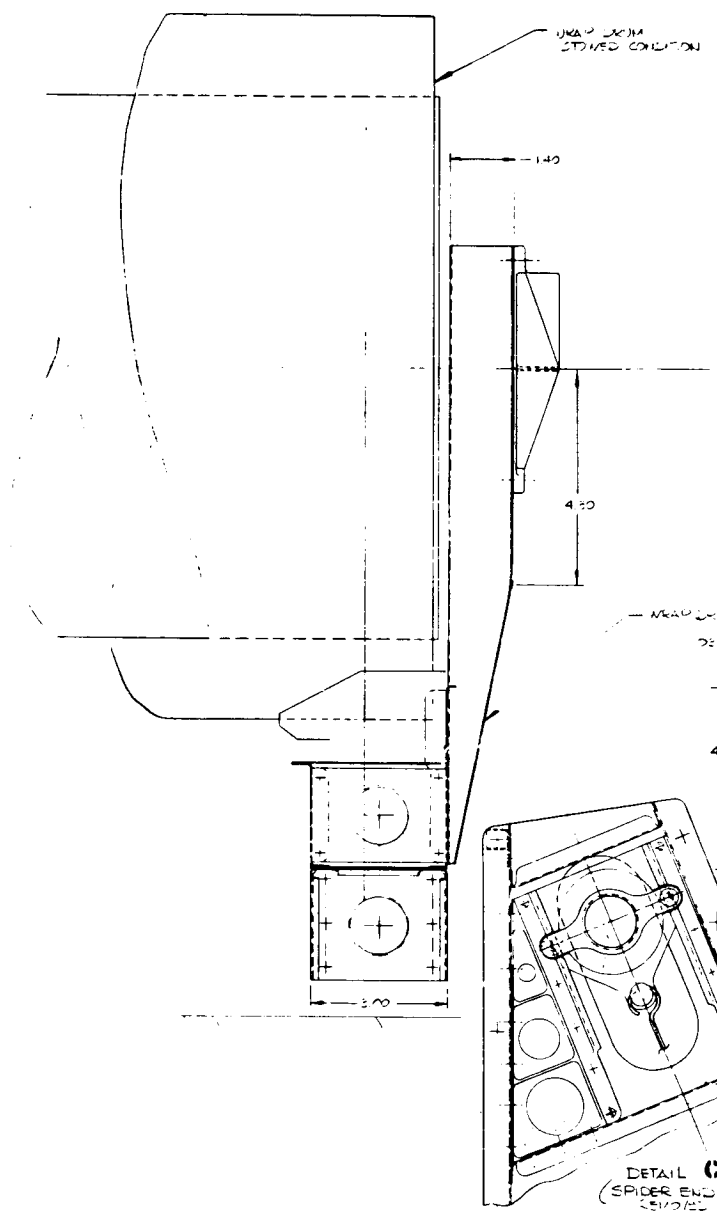
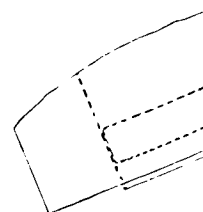


SECTION B-B

NETS
COVER



~~70~~ 307



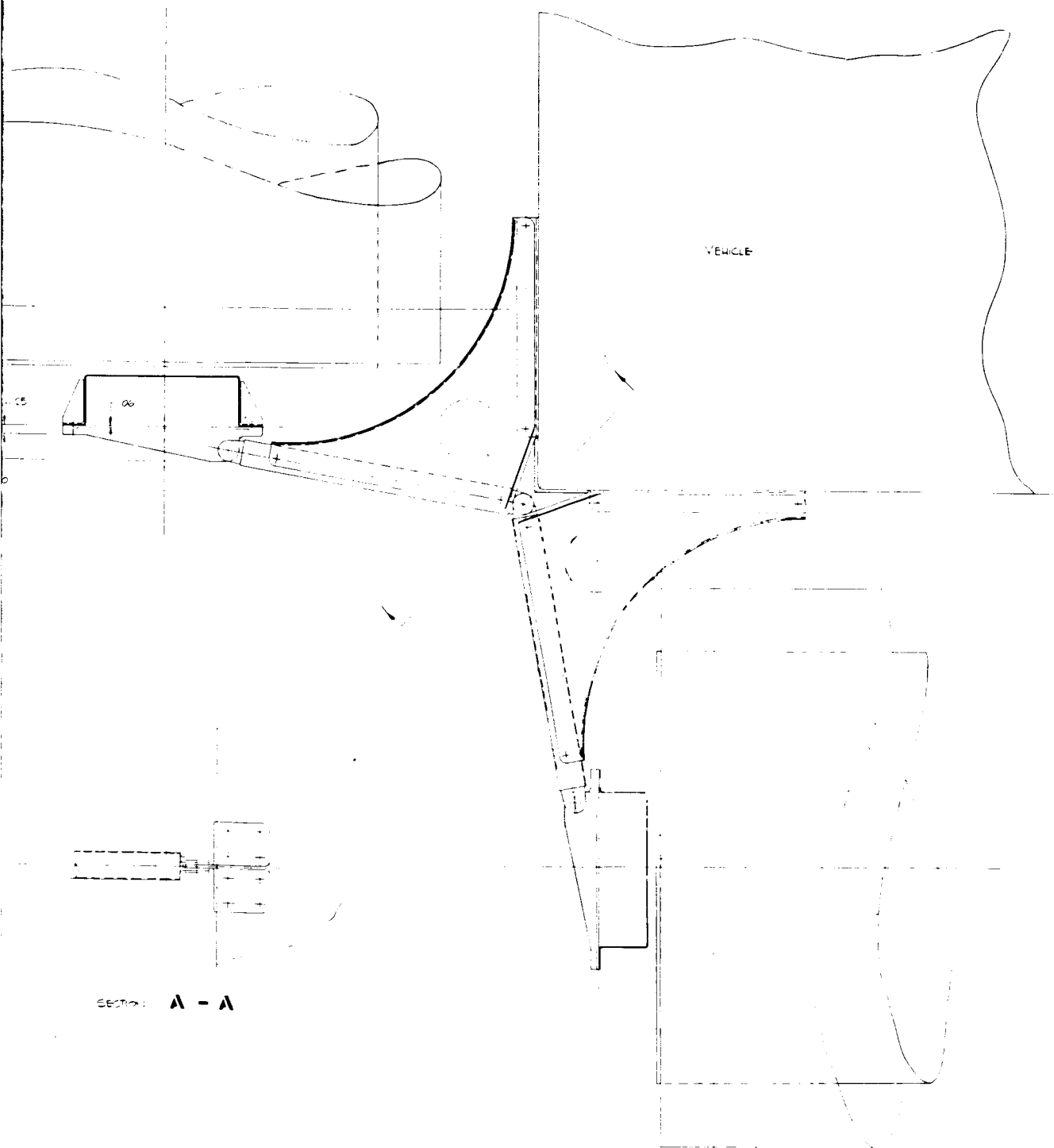


Figure A-9. Model 400 - Mounting To Vehicle,
Tubular Mounting, Concept 2a.

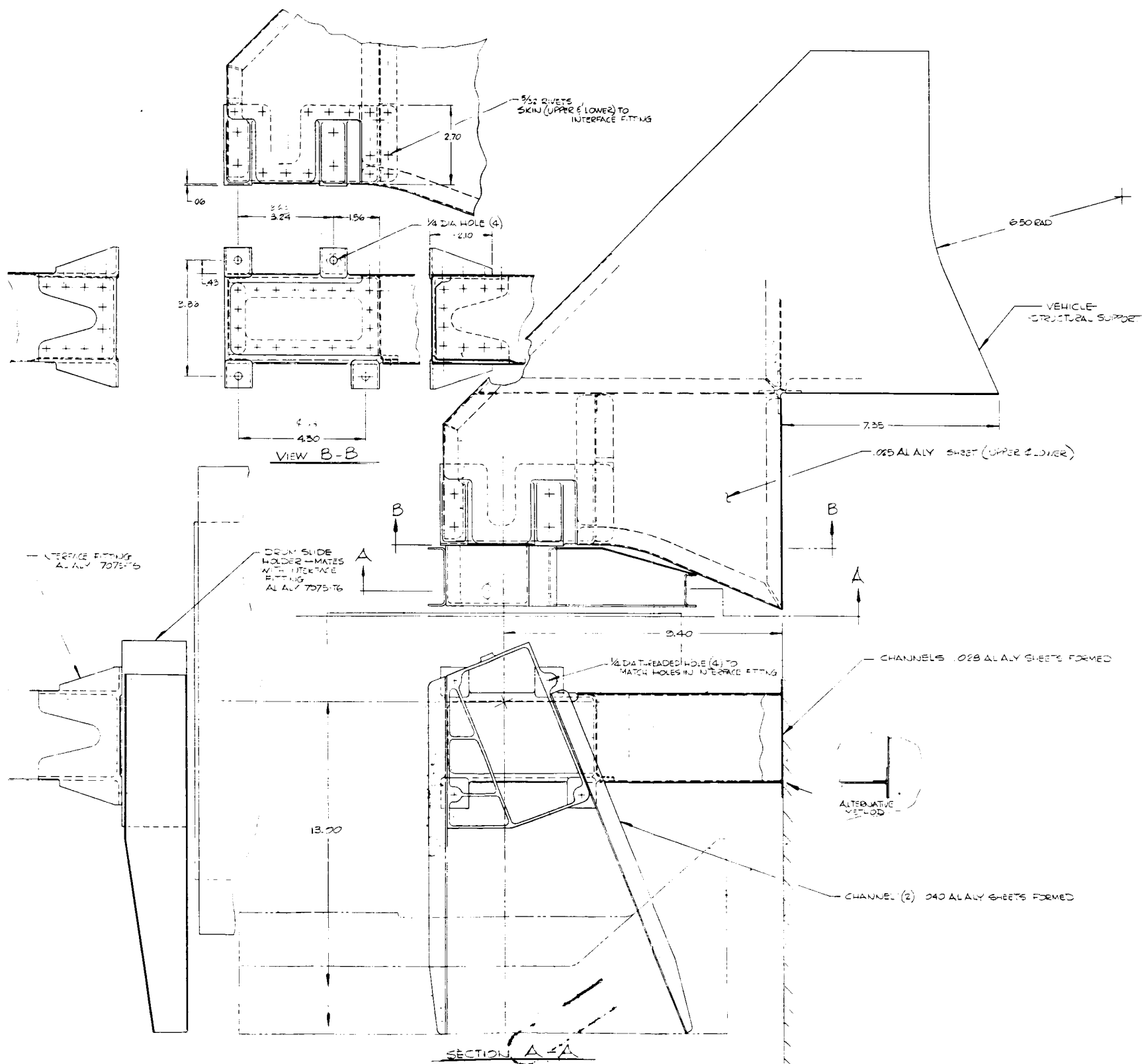


Figure A-10. Model 400 - Mounting to Vehicle, Box Mounting, Concept 2c.

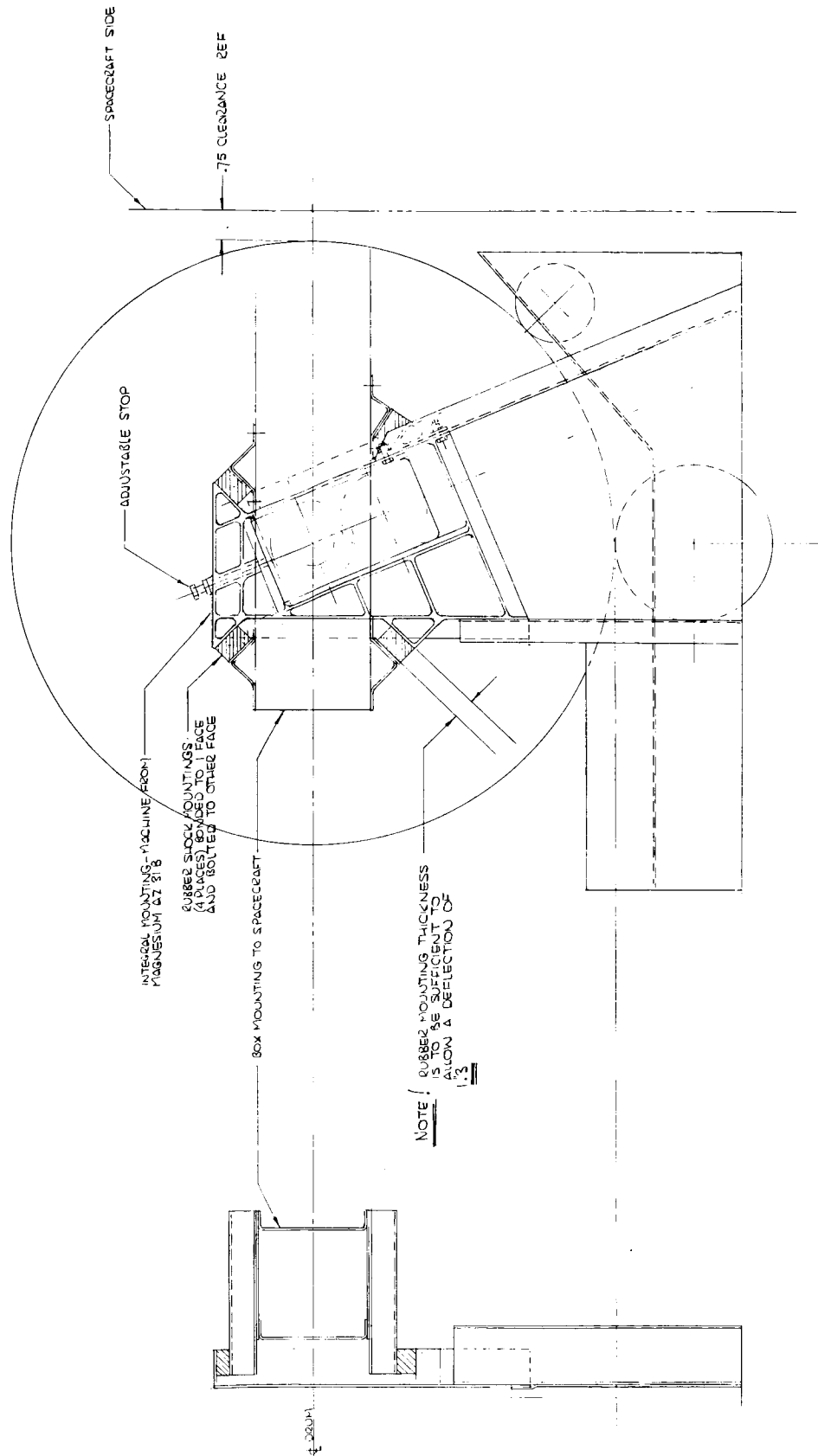
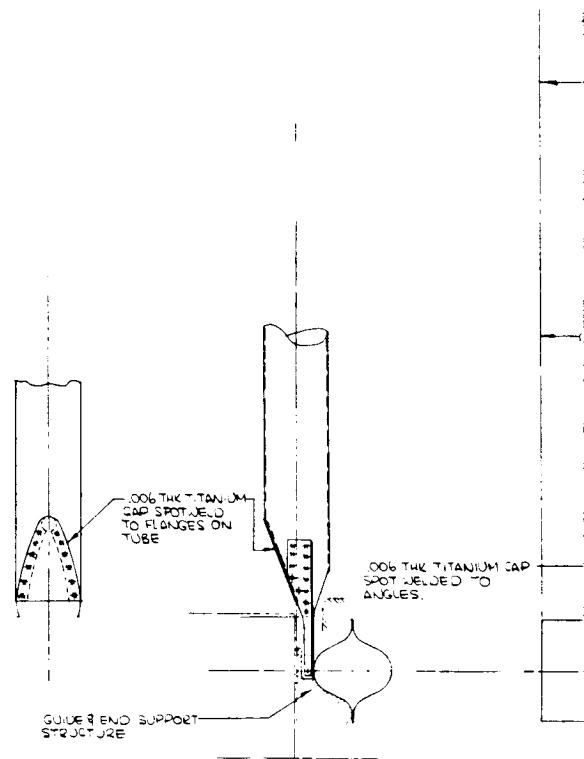
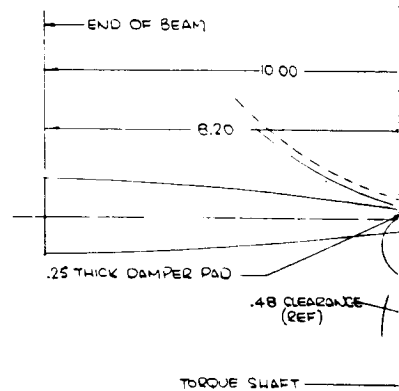
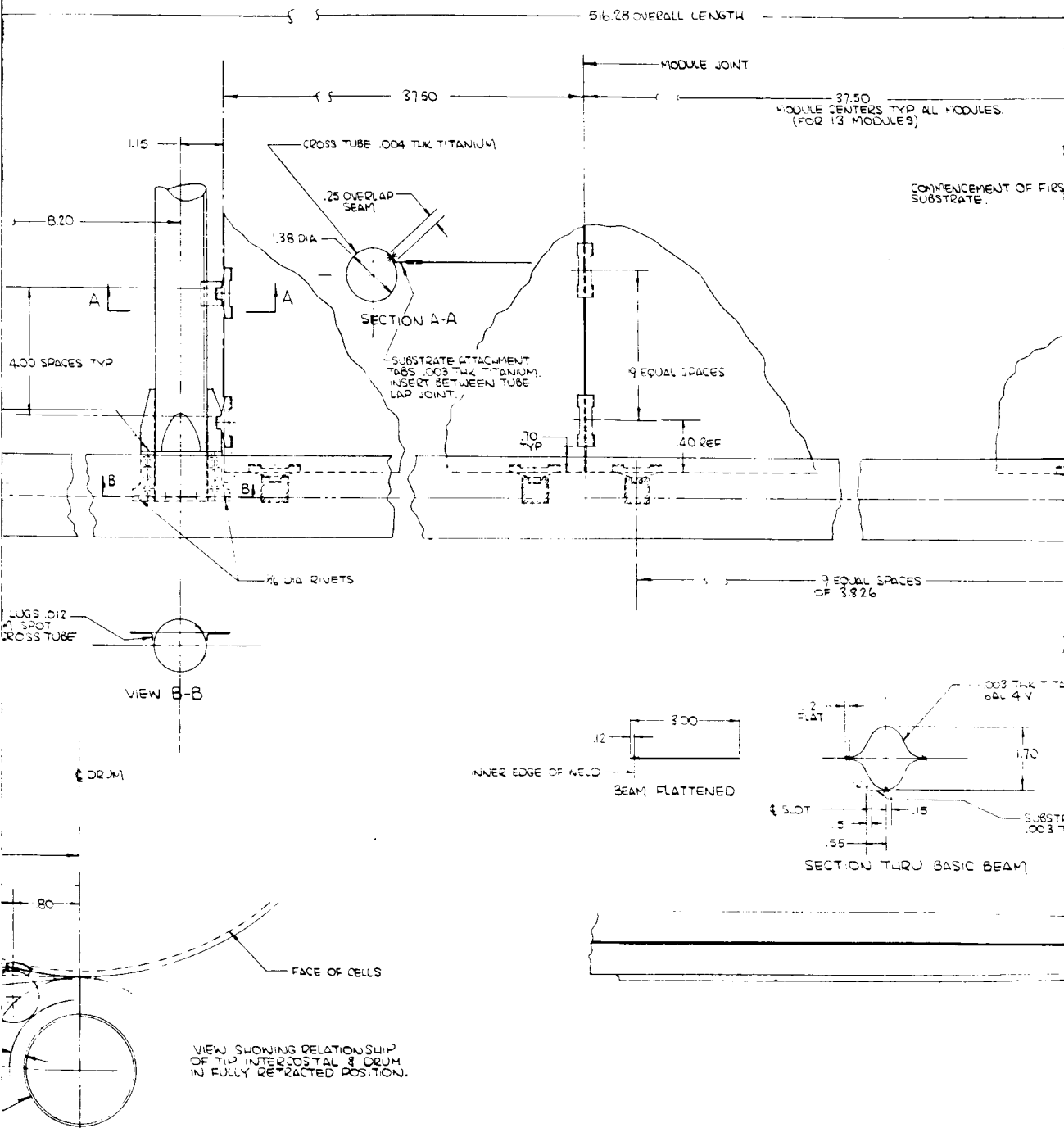


Figure A-11. Model 400 - Mounting to Vehicle, Mounting with Shock Mounts, Concept 2d.



ATTACHMENT
T.W. TITANIUM
WELDED TO





314-A

314

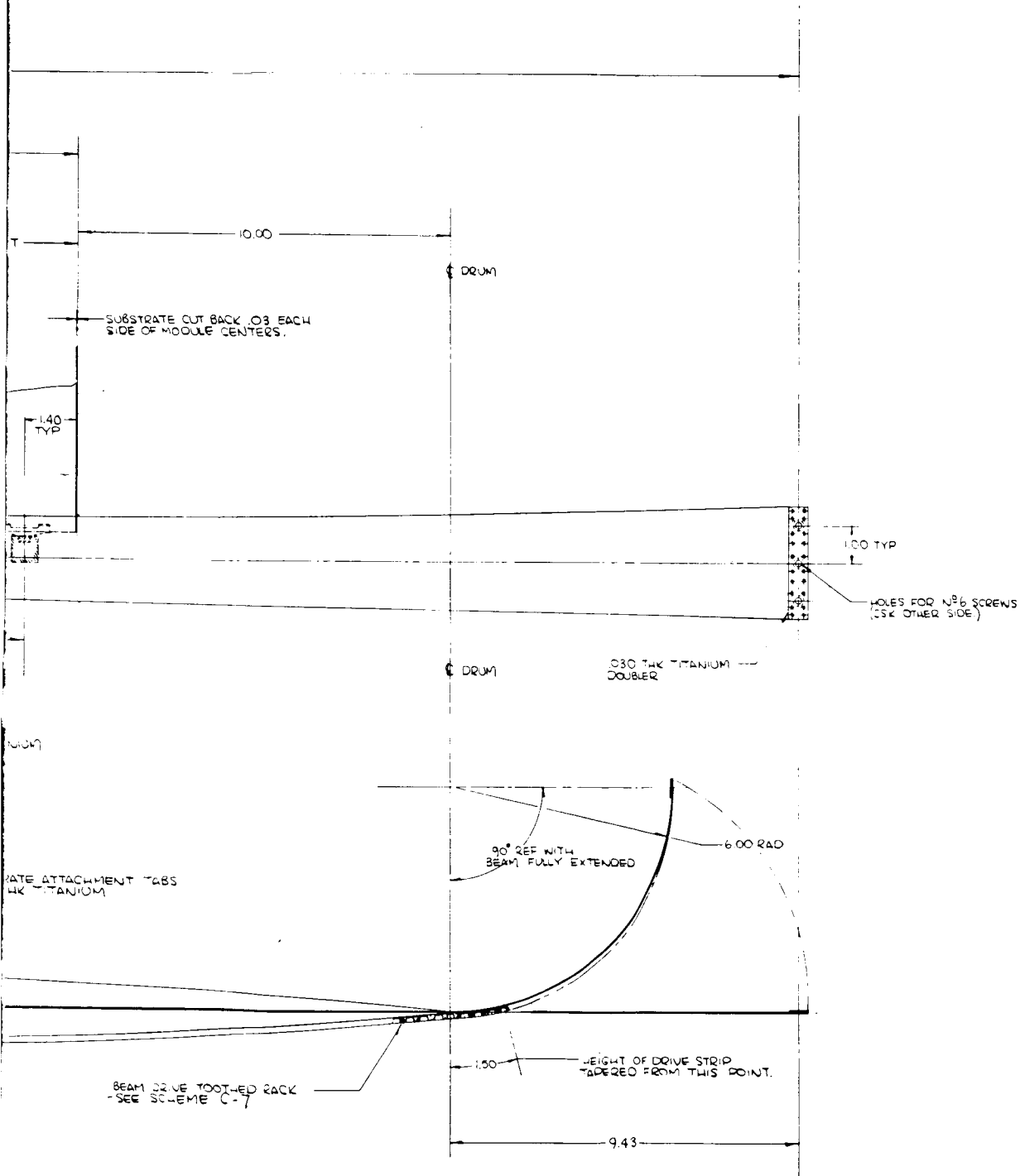


Figure A-12. Model 400 - Beam Design, Concept 4.

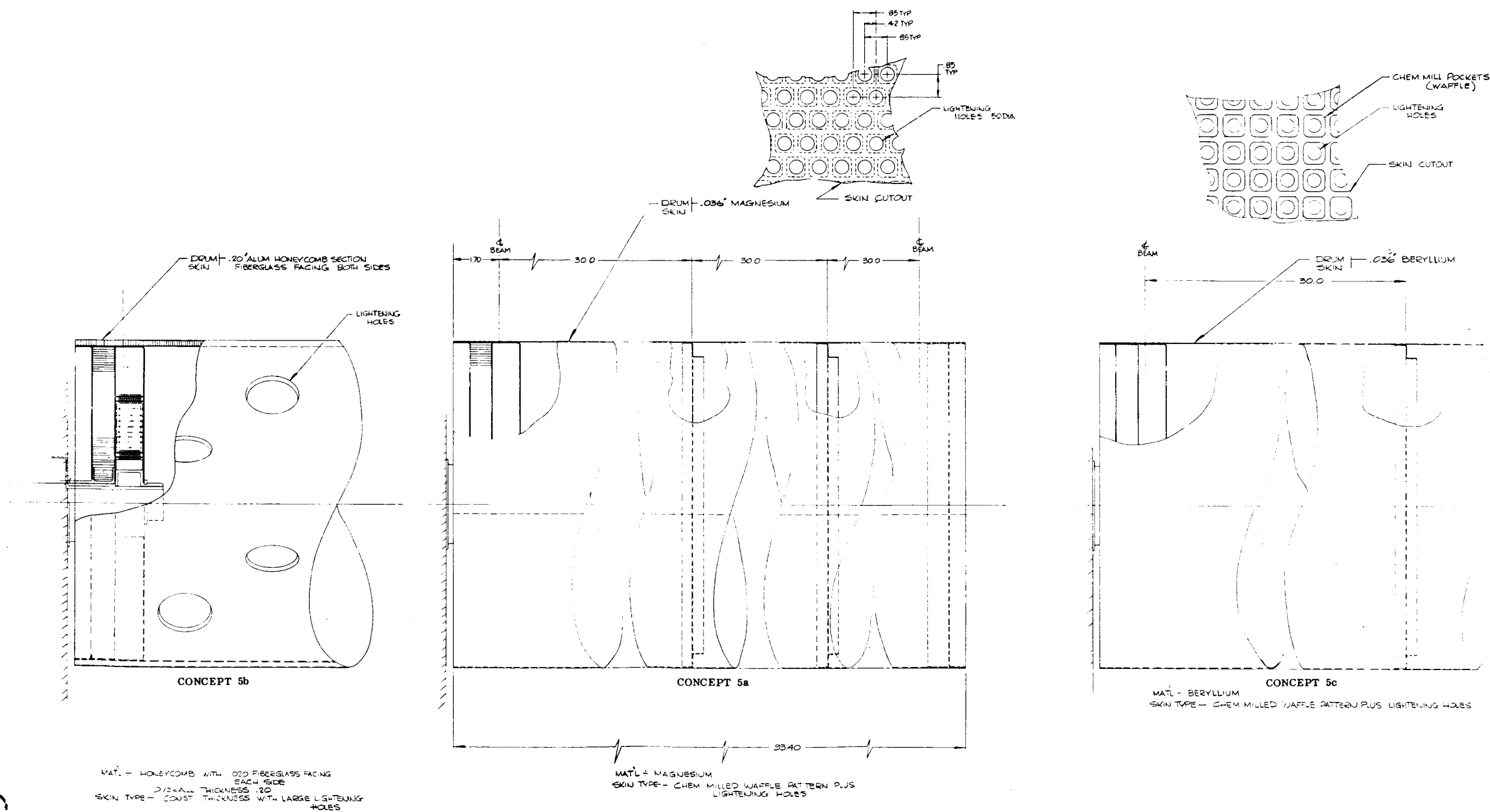
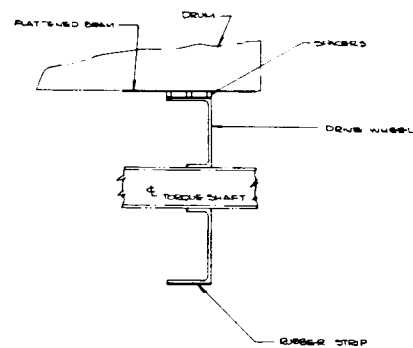
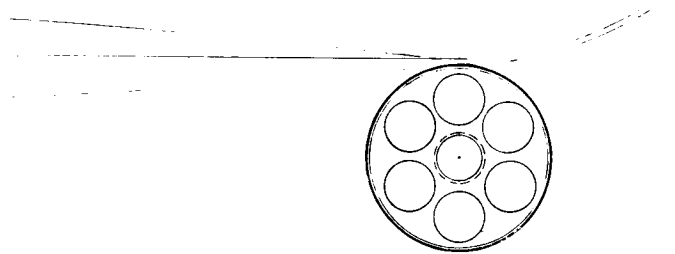


Figure A-13. Model 400 - Drum Assembly, Concept 5.



CONCEPT 6a DRIVE MECHANISM (RUBBER - P

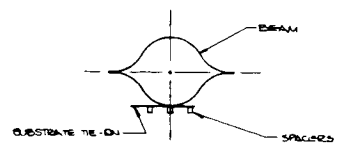
1 WEIGHT

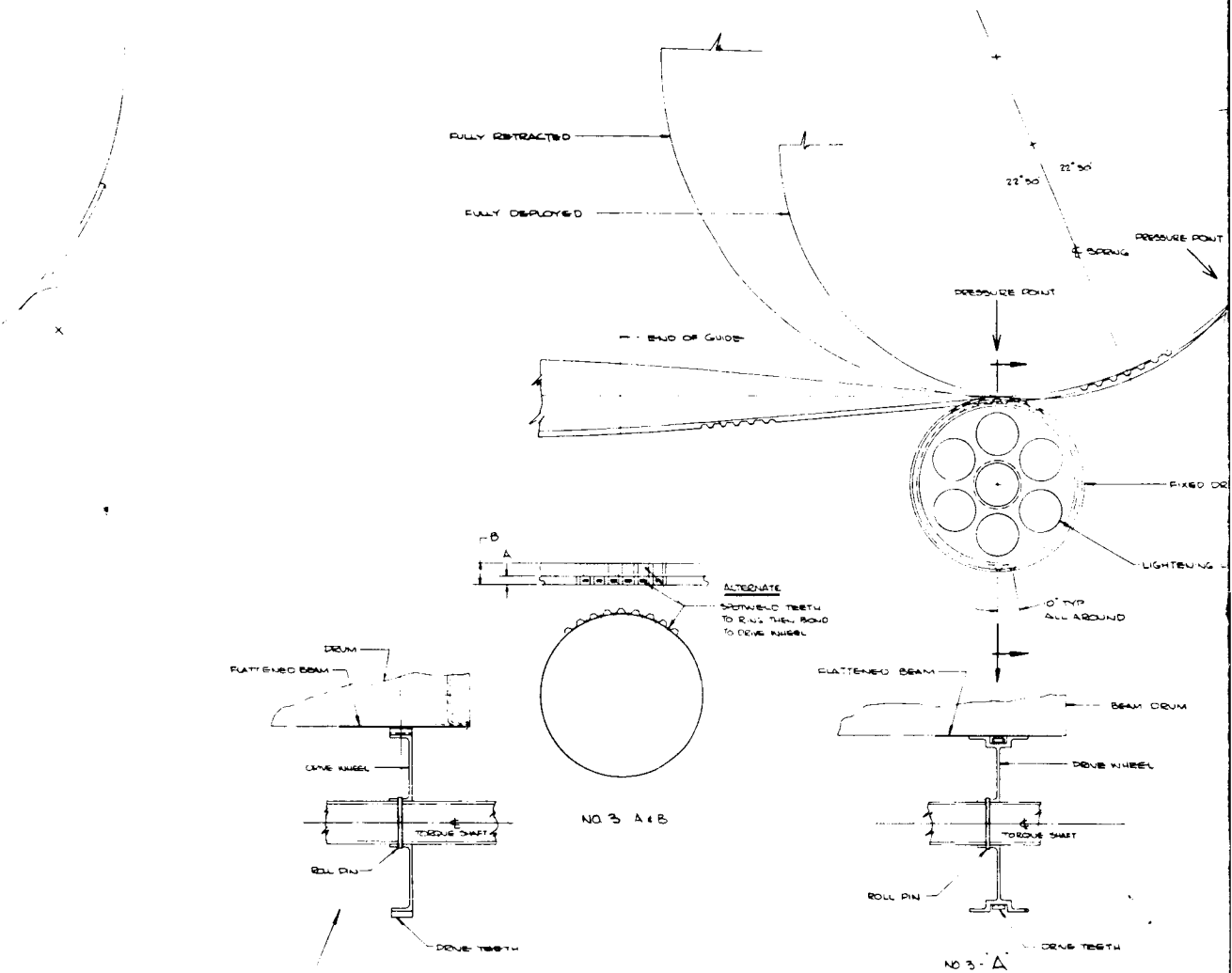
- 1 RUBBER SPACER STRAPS BOLDED TO SUBSTRATE
- 1 RUBBER STOP BOLDED TO DRIVE WHEEL
- 1 MAGNESIUM DRIVE WHEEL

TOTAL WEIGHT PER ROLL-OUT = 2.60 LBS

2 CONSIDERATIONS

- 1 (SAME AS NO 2)





RICTION)

(SHEET METAL)

(SAME AS 'A' EXCEPT AS SHOWN)

TOTAL WEIGHT PER ROLL-OUT = 160 LBS

50 PROVIDES ADEQUATE PRO (SUPPORT) DURING ROLL UP

(SHEET METAL)

CONCEPT 6c DRIVE MECHANISM ("A" & "B")

CONCEPT 6b DR

WEIGHT

1. METAL TEETH SPOTWELDED TO BEAM (200 LBS)

2. METAL TEETH BONDED TO DRIVE WHEEL (200 LBS)

3. MAGNETIC DRIVE WHEEL

TOTAL WEIGHT PER ROLL-OUT = 75 LBS

2 MATERIAL:

1. TITANIUM TEETH - GALVAN (BEAM)

2. TITANIUM TEETH - GALVAN (DRIVE WHEEL)

3. MAGNETIC DRIVE WHEEL

3 CONSIDERATIONS:

1. BEAMS MAY NOT ROLL UP EVENLY DUE TO PIVOT OR BOWING ABOUT SPANAL TEETH IN CENTER BEAM (MAY BE UNSTABLE)

2. SPOTWELDED TEETH TO BEAM UNIFORMLY & EVENLY SPACED & DEFLECTION IN METAL TEETH DUE TO LOAD (COULD POS)

3. CLOSE TOLERANCE REQUIRED FOR BOND ON BEAM TEETH

WEIGHT

1. TITANIUM

2. BOND

3. MAG

4. (SHEET METAL)

TOTAL WEIGHT

1. TITANIUM

2. BOND

3. MAG

4. (SHEET METAL)

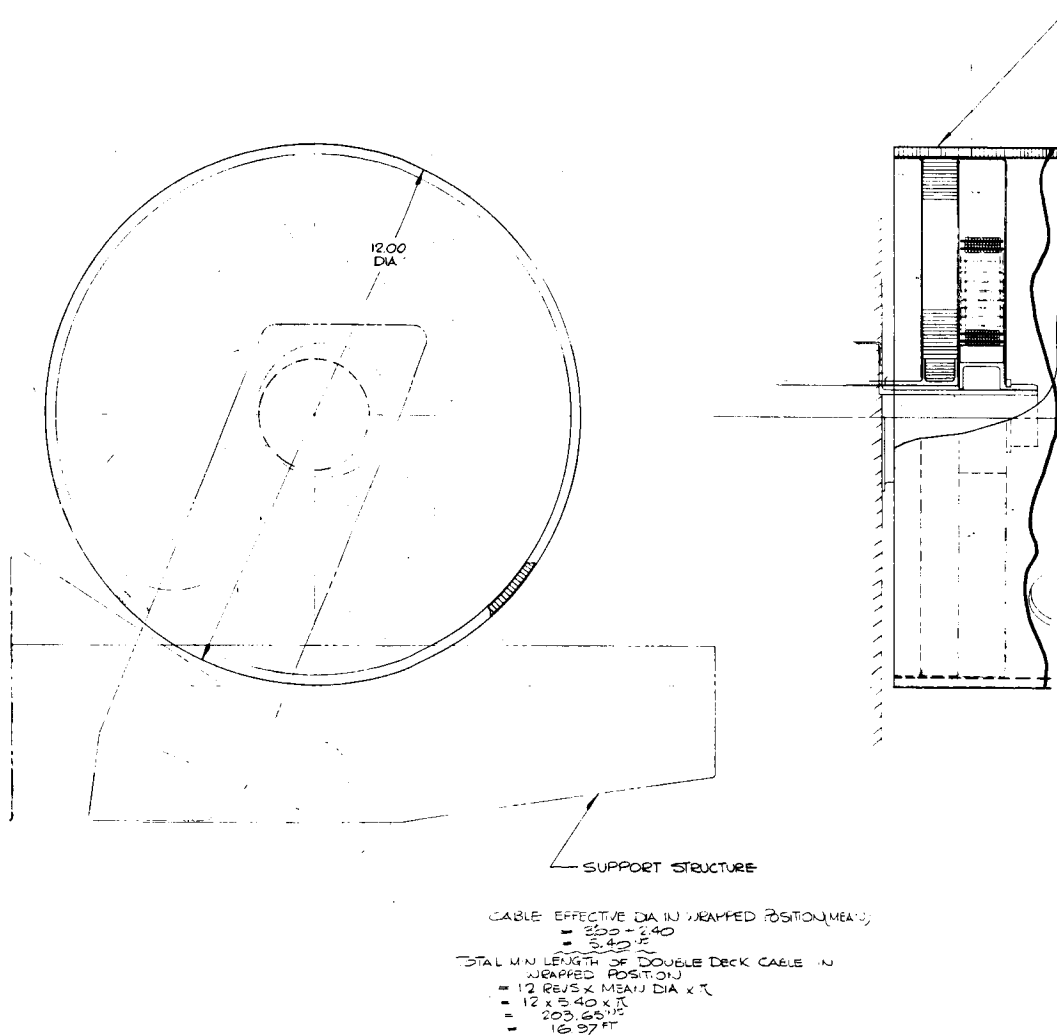


Figure A-15. Model 400 - Electrical Lead-Out, Coiled Continuous Harness, Concept 7a.

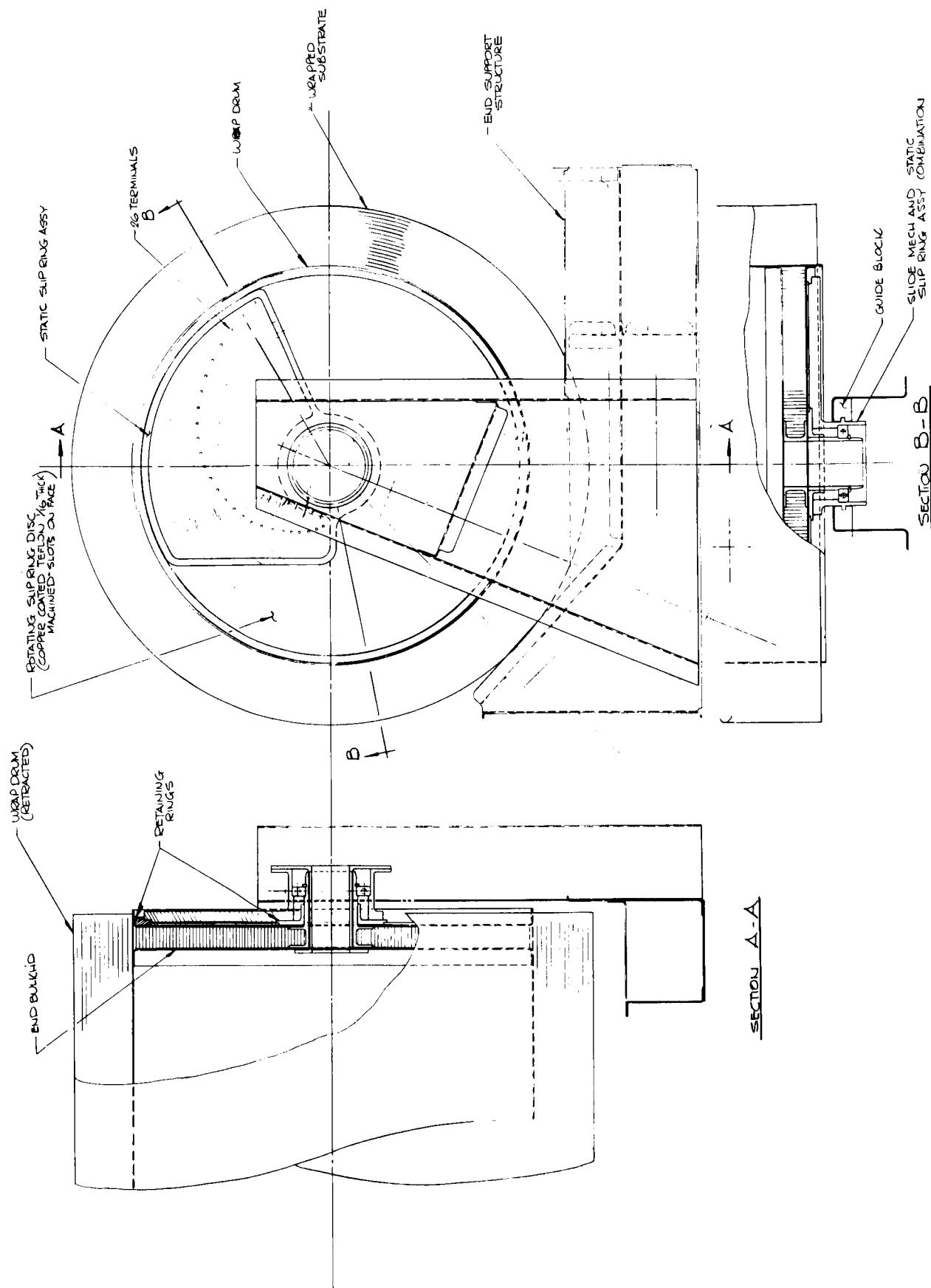


Figure A-16. Model 400 - Electrical Lead-Out, External Disc Slip Rings, Concept 7b.

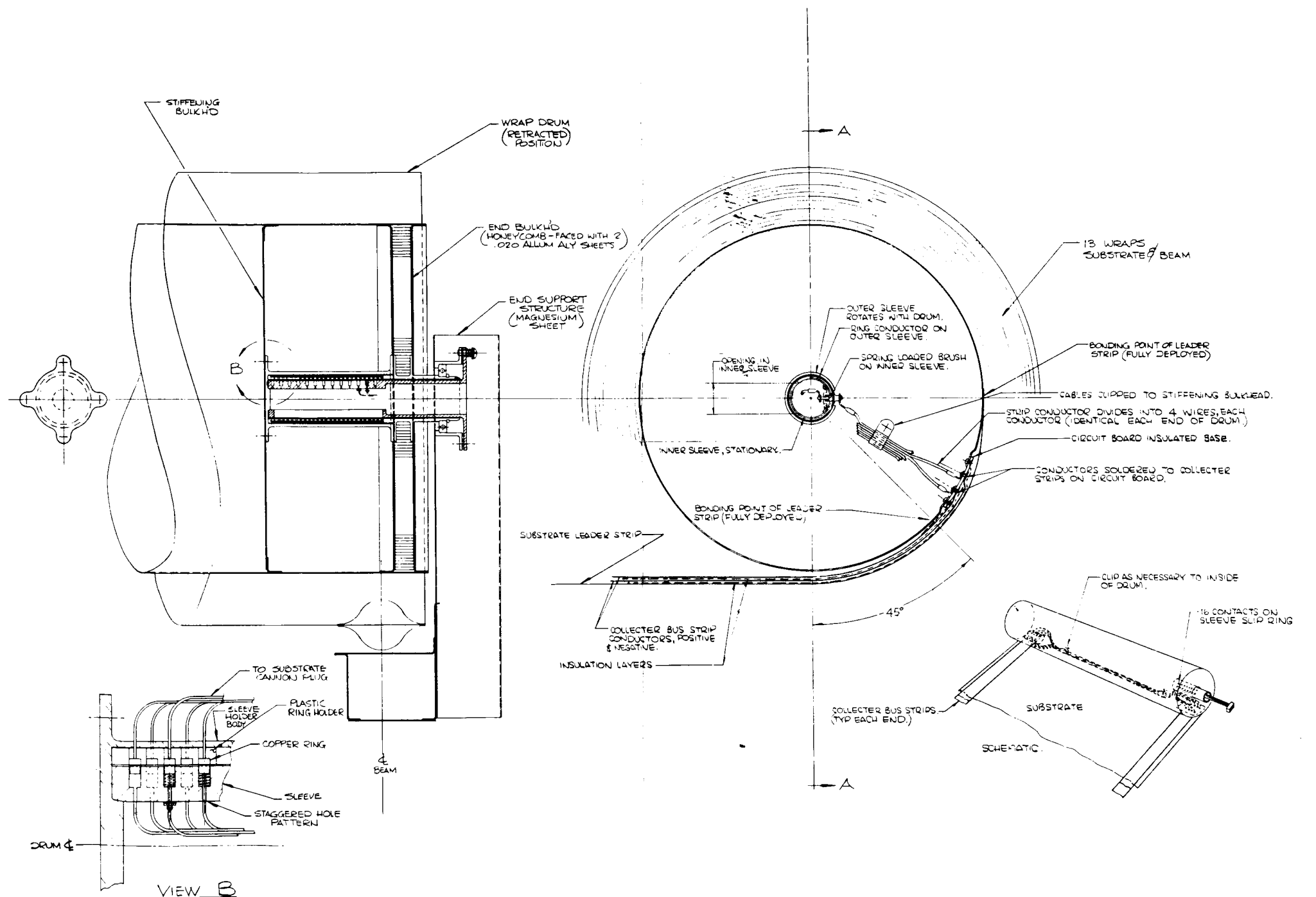
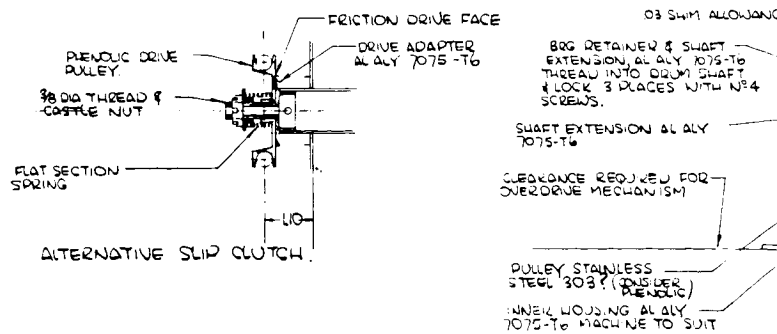
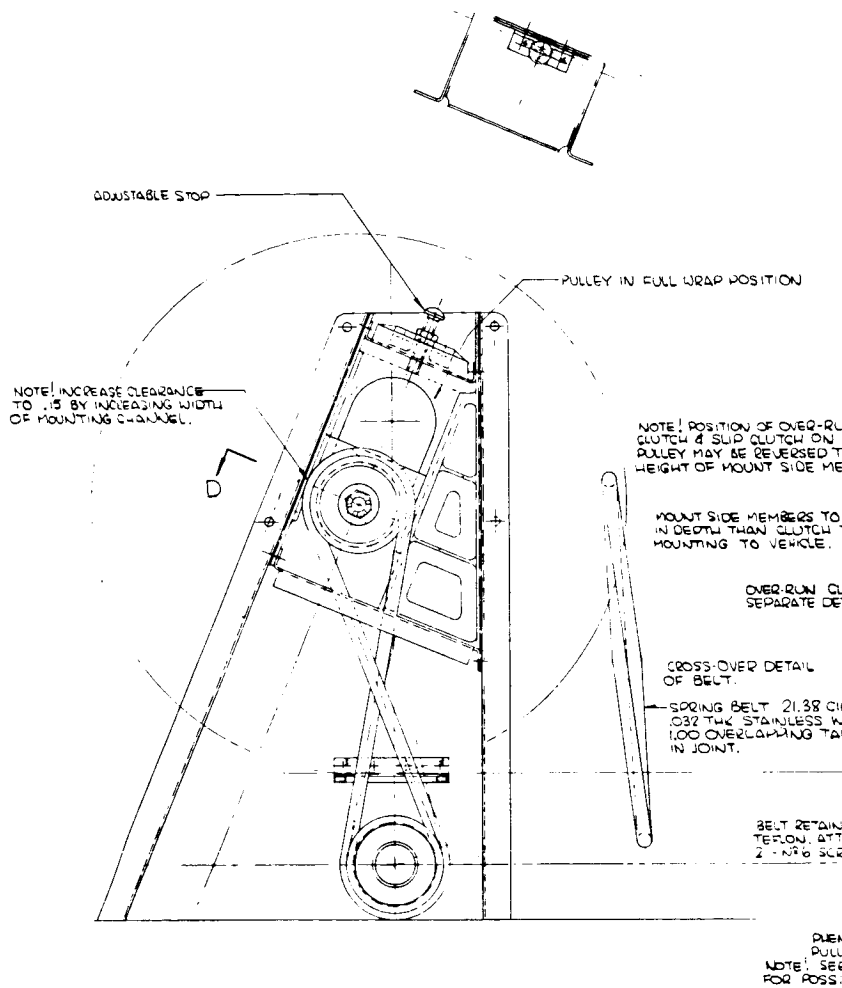


Figure A-17. Model 400 - Electrical Lead-Out, Internal Sleeve Slip Rings, Concept 7c.



HARNES FAIRLEAD

SECTION A

LOWER
REDUCE
VIBERS.

BE GREATER
TO CLEAR

ATCH - SEE
TAIL.

90.00 BEAM CENTERS

CONFERENCE
OF
SER. SCREW.

PER 1/8 THK
DISC WITH
SLEWS & NUTS.

OLIC DRIVE

SEPARATE DETAIL
SLE SLIP CLUTCH.

3/32 DIA

1.56 DIA
DRUM SHAFT AL ALY 7075-T6

WEB .040

AZ 3 B

E

2

B

1

4

5

6

7

8

9

10

11

12

13

14

15

16

17

18

19

20

21

22

23

24

25

26

27

28

29

30

31

32

33

34

35

36

37

38

39

40

41

42

43

44

45

46

47

48

49

50

51

52

53

54

55

56

57

58

59

60

61

62

63

64

65

66

67

68

69

70

71

72

73

74

75

76

77

78

79

80

81

82

83

84

85

86

87

88

89

90

91

92

93

94

95

96

97

98

99

100

101

102

103

104

105

106

107

108

109

110

111

112

113

114

115

116

117

118

119

120

121

122

123

124

125

126

127

128

129

130

131

132

133

134

135

136

137

138

139

140

141

142

143

144

145

146

147

148

149

150

151

152

153

154

155

156

157

158

159

160

161

162

163

164

165

166

167

168

169

170

171

172

173

174

175

176

177

178

179

180

181

182

183

184

185

186

187

188

189

190

191

192

193

194

195

196

197

198

199

200

201

202

203

204

205

206

207

208

209

210

211

212

213

214

215

216

217

218

219

220

221

222

223

224

225

226

227

228

229

230

231

232

233

234

235

236

237

238

239

240

241

242

243

244

245

246

247

248

249

250

251

252

253

254

255

256

257

258

259

260

261

262

263

264

265

266

267

268

269

270

271

272

273

274

275

276

277

278

279

280

281

282

283

284

285

286

287

288

289

290

291

292

293

294

295

FEATURES OF REDUNDANT DRIVE SYSTEM
FOR 250 SQ. FT. ROLL UP ARRAY.

NORMAL FUNCTION: - BOTH MOTORS OPERATE
THROUGH DIFFERENTIAL GEARBOX TO EXTEND
OR DETRACT ARRAY AT NORMAL SPEED.

FAILURE OF ANY ONE MOTOR WILL CAUSE THE
ARRAY TO BE OPERATED AT HALF NORMAL
SPEED.

MOTORS IN THE OFF CONDITION PROVIDE
THE NECESSARY 'LOCK' CONDITION TO
HOLD THE ARRAY IN ANY FIXED POSITION.

APPROX WEIGHT PENALTY FOR REDUNDANT
DRIVE 1.0 TO 1.25 LB.

ADDITIONAL COST: APPROX \$400

FOR OTHER DETAILS OF DRIVE SYSTEM SEE
CONCEPT 8a

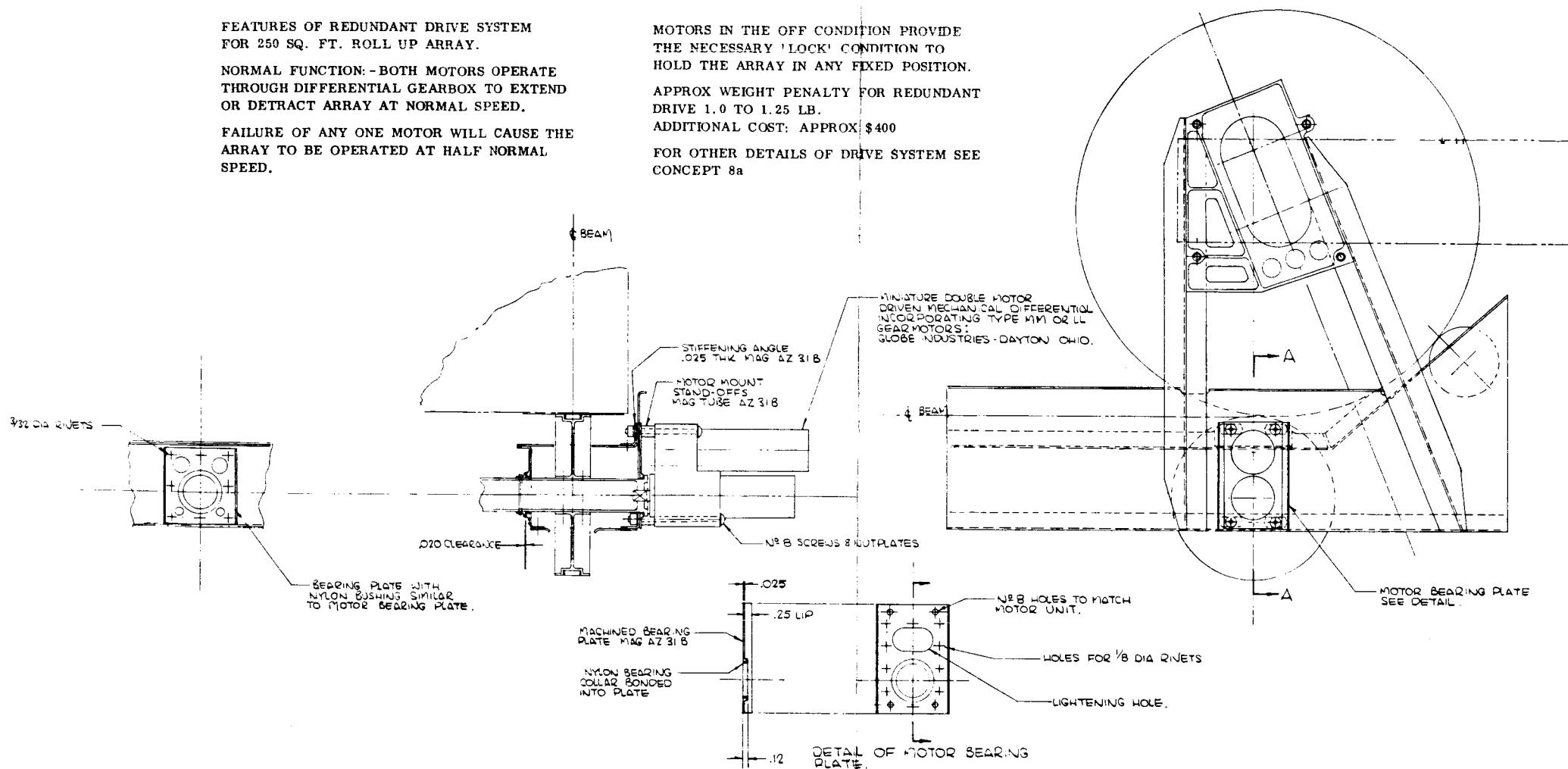


Figure A-19. Model 400 - Motor Drive, Double Gear Motor, Concept 8b.